UNIVERSITEIT GENT

High-throughput Polymer Synthesis for Supramolecular Materials

Lenny Voorhaar

Promotor: Prof. Richard Hoogenboom

Exam committee:
Prof. Bruno De Geest
Prof. Filip Du Prez
Prof. Dave Haddleton
Dr. Samarendra Maji
Dr. Anja Palmans
Dr. Jos Paulusse
Prof. Bruno Van Mele
Prof. Sandra Van Vlierberghe

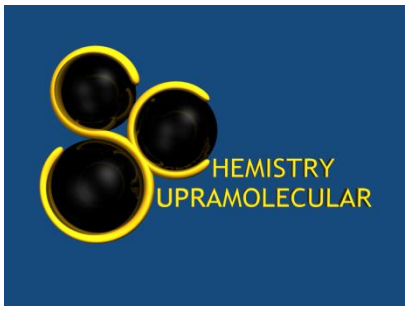

This research was funded by Bijzonder Onderzoeksfonds (Universiteit Gent) and Strategic Initiative Materials in Flanders.

Contents

Chapter 1: Introduction

1.1 Objectives and outline of the thesis

The work presented in this thesis is part of the Novel Active Protection system on Metals (NAPROM) project within the Engineered Self-Healing materials (SHE) program of Strategic Initiative Materials in Flanders (SIM). The aim of this work project within NAPROM was to create a new type of supramolecular self-healing coating with tunable properties for corrosion inhibition. Damage to a coating will generally lead to corrosion of the metal substrate due to exposure to moisture and oxygen. A self-healing coating could prevent this by combining the release of corrosion inhibiting ions when the coating is damaged with self-healing of the coating for long term protection, thereby greatly increasing the lifetime of the metal product.

The objective of this thesis was the synthesis of supramolecular self-healing materials with tunable properties based on electrostatic interactions between short polymers. Although several examples of supramolecular self-healing bulk material had been reported at the start of this project (see section 1.3.2), these all had their drawbacks.[1] For harder materials, heating or addition of solvent was necessary to provide enough chain dynamics to allow the material to heal. Softer materials that had enough chain mobility for self-healing had inferior mechanical properties and were therefore not suitable for use as a coating. To make a material with good mechanical properties that can still self-heal without external triggers, a combination of a harder and softer phase as well as careful tuning of the binding strength was envisioned.

Electrostatic interactions (Figure 1) were chosen as the most suitable type of supramolecular interaction for these materials for several reasons. Because one of the goals of the project was to create a self-healing coating for metal substrates, it was expected that ionic groups would be beneficial to improve adhesion of the coating to the substrate, as well as providing a miscible matrix for incorporation of corrosion-inhibiting ions. Additionally, phase-separated supramolecular self-healing bulk materials based on electrostatic interactions had never been shown before, although there were several examples of electrostatic self-healing hydrogels. Employing ionic monomers as the binding units would also allow for tuning the strength of the interaction by changing the block length of the polymers. For the initial design of the material we chose to use a mixture of ABA-triblock copolymers with an uncharged middle block and oppositely charged end blocks (Figure 2). This should allow for phase separation between an electrostatic phase that can be used for self-healing and an uncharged phase. The synthesis of these polymers will be performed via controlled radical polymerization, as this allows for good control over the polymer composition and molecular weight. High-throughput experimentation will be used for some of the polymerizations, as this will speed up the optimization of the synthesis and investigation of different block lengths of the polymers.

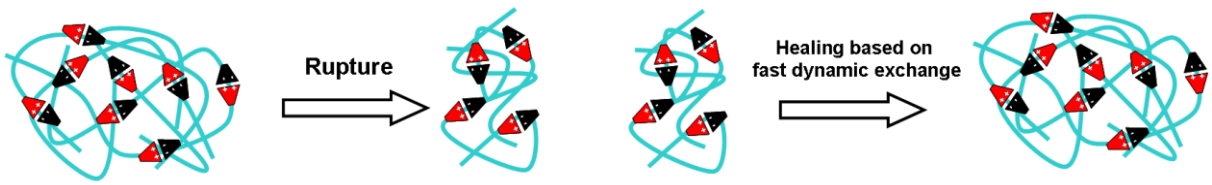

Figure 1. Concept of supramolecular self-healing material based on electrostatic interaction.

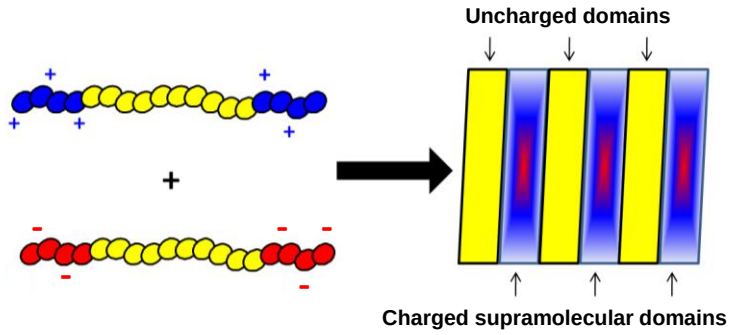

Figure 2. Expected phase separation between charged phases and uncharged phases in a supramolecular material.

The main part of the thesis is focused on the polymer synthesis via controlled radical polymerization, which will be discussed in more detail further in this introduction. The general aspects of controlled radical polymerization and a more detailed introduction to reversible addition–fragmentation chain-transfer (RAFT) polymerization, atom transfer radical polymerization (ATRP) and Cu(0)-mediated polymerization will be given, as well as a brief overview of published work on high-throughput polymerization. A review of different types of supramolecular network materials, which have been published so far in literature, will be provided in the second part of the introduction. This is split in two parts on supramolecular hydrogels and supramolecular bulk materials. Chapter 2 will discuss the optimization of high-throughput Cu(0)-mediated polymerization of *n*-butyl acrylate and 2-methoxyethyl acrylate, which was done by varying several reaction parameters. One-pot synthesis of diblock copolymers of these two monomers is also shown. As a follow-up to this work, Chapter 3 shows the automated one-pot synthesis of amphiphilic diblock and ABA-triblock copolymers containing *n*-butyl acrylate as hydrophobic block, and 2-(dimethylamino)ethyl acrylate, 1-ethoxyethyl acrylate, which forms acrylic acid when deprotected, or protected 2-carboxyethyl acrylate as charged hydrophilic blocks. Chapter 4 discusses the statistical copolymerizations of several oligo(ethylene glycol) acrylates, performed via automated RAFT polymerization, as well as their aqueous thermoresponsive behavior. In Chapter 5 the RAFT polymerization of several different types of charged ABA-triblock copolymers is reported. Mixing these oppositely charged polymers resulted in supramolecular materials with interesting properties that are tunable by polymer composition, which is discussed in Chapter 6. A detailed characterization of some of the synthesized materials is reported, which was done in collaboration with the Vrije Universiteit Brussel, University of Antwerp and ISIS-STFC Neutron Scattering Facility. Chapter 7 shows the automated synthesis of hydrophobic-hydrophilic-hydrophobic ABA-triblock copolymers, which were used to prepare supramolecular hydrogels based on hydrophobic interactions. Finally, Chapter 8 will present the conclusions of the thesis and an outlook into possible subsequent research directions and applications.

1.2 Controlled radical polymerization

The polymers in this thesis have all been synthesized via controlled radical polymerization (CRP). While the terms controlled and living polymerization are often used interchangeably, there are some differences between the two. A living polymerization shows a complete absence of chain transfer and termination, which can be obtained with for example anionic or cationic polymerization. In a controlled polymerization such as CRP chain transfer and termination do occur but are suppressed as much as possible. CRP is based on free radical polymerization (FRP), in which radicals are produced by heat- or light-sensitive radical initiators, which react with monomers to form a propagating chain. When two radicals meet, they will react with each other leading to termination by chain-chain

coupling, which can be prevented by lowering the radical concentration. Because two radicals are needed for termination, lowering the propagation radical concentration [P*] will suppress termination as it scales with $[P^*]^2$ while propagation scales with [P*].

CRP was developed to lower the active radical concentration while maintaining a high enough propagation rate. It usually shows fast initiation and comparatively slow propagation, with termination being kept as low as possible.[2] This is necessary to have good control over the molecular weight of the polymers being formed and to be able to make more complex polymer architectures, such as block copolymers. Different types of CRP exist, each with different advantages and drawbacks. The methods used in this thesis are reversible addition-fragmentation chain transfer (RAFT) polymerization and Cu(0)-mediated radical polymerization, which is also known as single electron transfer living radical polymerization (SET-LRP) or supplemental activator and reducing agent atom transfer radical polymerization (SARA ATRP).

A well-controlled CRP reaction should follow first order kinetic behavior with regard to monomer concentration [M], which means that the concentration of active chains is constant, i.e. no significant termination occurs. This can be derived from the equation of the polymerization rate (R_p), in which t is the time, k_p is the propagation rate constant and [P*] is the concentration of propagating radical species, that is polymer chains with a free radical chain end:

$$R_p = -\frac{d[M]}{dt} = k_p[P^*][M]$$

Integration of this gives the following equation:

$$ln\frac{[M]_0}{[M]} = k_p[P^*]t$$

To see if a polymerization follows such first order kinetics, the $ln\frac{[M]_0}{[M]}$, which can be determined by gas chromatography (GC) or proton nuclear magnetic resonance (^{1}H NMR) spectroscopy, is plotted against time, which is known as a first order kinetic plot. Non-linear behavior, such as a downward curvature, suggests termination while an upward curvature is generally due to slow initiation.

In addition to linear first-order kinetics, the degree of polymerization (DP) should be linear with respect to the monomer conversion during CRP, proving that the number of propagating chains is constant during the polymerization and that no chain transfer or chain coupling reactions occur.

$$DP_n = \frac{M_n}{M_0} = \frac{\Delta[M]}{[I]_0} = conversion\frac{[M]_0}{[I]_0}$$

Here, M_n is the number-average molecular weight, M_0 is the molecular weight of the monomer and [I] is the concentration of initiator. This linear relationship can be validated by plotting the M_n, which is usually measured by size exclusion chromatography (SEC), against the monomer conversion. A linear relationship shows the absence of chain transfer reactions or coupling between chains. However, it should be taken into account that the M_n is usually determined by SEC with respect to polymer standards that have different chemical properties from the measured polymer, which can lead to inaccurate values due to a smaller or larger hydrodynamic radius in the used solvent. The absence of chain transfer and termination reactions can also be shown by the preservation of end

groups, which can be observed by matrix-assisted lased desorption/ionization time of flight mass spectroscopy (MALDI-TOF MS) that can be used to determine the exact molecular weight of shorter polymers.

Generally CRP should also lead to polymers with a narrow molecular weight distribution, or low dispersity (Đ), which is the mass-average molecular weight (M_m) divided by M_n and can be determined by SEC.

$$Đ = \frac{M_m}{M_n}$$

In theory, a Đ of 1 would be obtained if all chains would have exactly the same chain length. However, even if all chains initiate at the same time, propagate at the same rate and no termination takes place during the polymerization a minor deviation of Đ from 1 will occur due to statistical variations. In practice even this is not possible using CRP, but dispersities around 1.05 to 1.1 can be obtained with different CRP techniques.

1.2.1 Reversible addition-fragmentation chain transfer polymerization

Reversible addition-fragmentation chain transfer (RAFT) polymerization[3, 4] is a type of controlled radical polymerization in which the equilibrium between active chains and dormant chains is regulated by a chain transfer agent (CTA), also known as RAFT agent. The polymerization is started when a radical initiator, such as AIBN, is activated by heat or light. The radicals will react with monomers and a short polymer chain is formed. When this growing chain encounters a CTA, it will bind to the double bonded S-atom and the radical will transfer to the R-group. To ensure fast initiation R should be a better leaving group than the polymer chain. This R-group will then react with monomers and form a new polymer chain, during which it will regularly switch between active and dormant. This propagation step is shown in Figure 3. This process will continue until all monomer has reacted or until all radicals are gone. The DP of the final polymer is determined by [M]/[CTA] as most of the monomer will be reacted with the R-group of the CTA and not the initiating radical. The intermediate in which both chains are attached to the CTA is a stable radical intermediate that does not react with itself or other radicals. Due to the propagating polymer chains reacting with a different CTA molecule each time it goes from the active to dormant state, only a small amount of initiating radical is needed to activate all R-groups. This causes the concentration of active radicals in the system to be very low as only a small fraction of the polymer chains carries a radical, which together with the stable radical intermediate minimizes termination reactions. Because no metal catalyst is required, RAFT polymerization is especially suitable for functional monomers containing chemical groups that can interfere with other types of CRP, such as acids or amines.

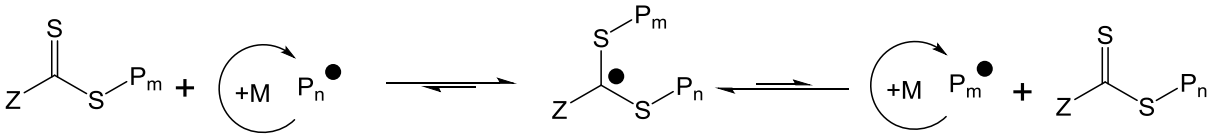

Figure 3. General mechanism of RAFT polymerization.

Chain transfer agents

Which CTA is more appropriate for a polymerization depends on the type of monomers used.[5] Each CTA consists of a thiocarbonylthio group, a leaving group R and stabilizing group Z. The transfer

constant of the CTA is dependent on the R and Z group. A CTA with high transfer constant, such as a dithiobenzoate or trithiocarbonate, is more suitable for more activated monomers (MAMs) like (meth)acrylates and styrenes. Dithiocarbamates and xanthates have a lower transfer constant and are more suitable for less activated monomers (LAMs) like vinyl esters. Recently, dithiocarbamates have been reported as acid/base 'switchable' CTAs.[6] In the protonated form they are suitable for the polymerization of MAMs, while they can be used for LAMs in the deprotonated form. These CTAs can be used to make block copolymers containing both LAMs and MAMs. Various functional groups can be part of the R and Z group, such as carboxylic acids and nitriles resulting in the formation of functional polymers. Multifunctional CTAs can be used to make star-shaped polymers.

1.2.2 Atom transfer radical polymerization

Atom transfer radical polymerization (ATRP) is a type of controlled radical polymerization in which the amount of radicals in the system is kept low through an equilibrium between dormant and active chains, which is regulated by a transition metal – ligand complex (Figure 4).[2, 7-11] In most cases the activator is Cu(I) while the deactivator is Cu(II), however other transition metals have also been used.[12] The oxidation of Cu(I) to Cu(II) by an alkyl halide will produce a radical on the growing polymer chain, which can propagate by addition of monomers until the radical is deactivated again through reduction of Cu(II). When two active radicals meet, they will recombine and the chains are terminated. For classical ATRP, relatively high concentrations (>1000 ppm) of catalyst are needed for a high polymerization rate. More recently, several types of ATRP have been developed in which much lower concentrations of catalyst are needed, either because the activator is continuously regenerated through reducing reactions or through formation of new radicals. Examples of this are activators regenerated by electron transfer (ARGET) ATRP,[13] initiators for continuous activator regeneration (ICAR) ATRP,[14, 15] electrochemically mediated ATRP[16] and photochemically mediated ATRP.[17]

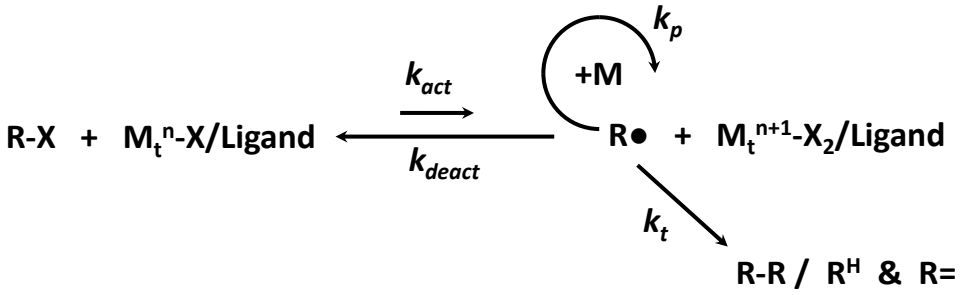

Figure 4. General mechanism of ATRP (reprinted from ref. 11).

Initiators

The initiator in ATRP is an alkyl halide, usually an alkyl bromide or alkyl chloride. Alkyl bromides are generally more active than alkyl chlorides, however in some cases, for example when using a monomer with a strongly nucleophilic group, it is better to use an alkyl chloride. Whether a primary, secondary or tertiary alkyl halide initiator is a better option depends on the monomer. In general, an initiator that has a similar structure to the monomer with an additional methyl group is recommended, for example methyl α-bromoisobutyrate for the ATRP of methyl methacrylate. Many different kinds of functional initiators have been synthesized and used to make functional polymers for different applications.[18]

Catalysts and ligands

The catalyst in ATRP is a transition metal. Usually copper is used, in combination with a nitrogen-containing ligand, such as *N*,*N*,*N*′,*N*′′,*N*′′-pentamethyldiethylenetriamine (PMDETA), 2,2′-bipyridine (bpy) or tris(2-(dimethylamino)ethyl)amine (Me_6TREN). Each ligand forms complexes with a different activity resulting in a higher K_{ATRP} in the order bpy < PMDETA < Me_6TREN, which will lead to a faster polymerization.[11] See also the equation below, in which K_{ATRP} is k_{act}/k_{deact} (Figure 4) and [I], [Cu(I)] and [X – Cu(II)] are the concentrations of initiator, Cu(I) and Cu(II), respectively. Other transition metals like ruthenium and iron have also been used, these are the so-called 'Sawamoto systems'.[12]

$$R_p = k_p[P^*][M] = k_p K_{ATRP}[M][I]_0 \frac{[Cu(I)]}{[X - Cu(II)]}$$

Supplemental activator and reducing agent ATRP (SARA ATRP)

In SARA ATRP, metallic copper (Cu(0)) is used as a supplemental activator and reducing agent for Cu(II) (Figure 5).[19-25] However, there is still some controversy about this mechanism versus single electron transfer living radical polymerization (SET-LRP), which will be discussed below. For SARA ATRP, Cu(I) is assumed to be the major activator, while Cu(0) is a supplemental activator. The activation occurs via inner sphere electron transfer. The produced Cu(II) is reduced again to Cu(I) through comproportionation, using Cu(0) as a reducing agent.

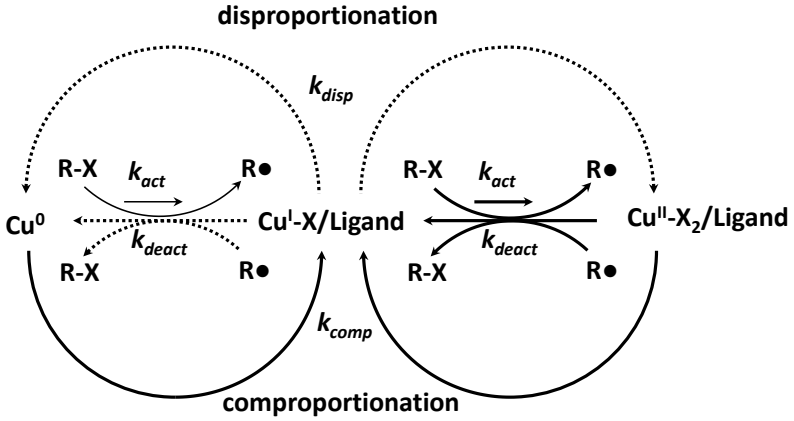

Figure 5. Mechanism of SARA-ATRP as proposed by Matyjaszewski (reprinted from ref. 20).

1.2.3 Cu(0)-mediated radical polymerization

One of the proposed mechanisms for Cu(0)-mediated radical polymerization is single electron transfer living radical polymerization (SET-LRP, Figure 5).[26] This model assumes that Cu(I) is instantly disproportionated to Cu(0) and Cu(II), in contrast with the SARA ATRP mechanism discussed earlier. For this disproportionation a polar solvent is needed. Cu(0) acts as the activator of alkyl halides through outer sphere electron transfer and Cu(II) is the deactivator. Advantages of this type of polymerization are the very low amounts of catalyst that are needed to achieve a controlled polymerization and the high end group fidelity. Usually the ligand Me_6TREN is used, which forms highly active complexes with copper.

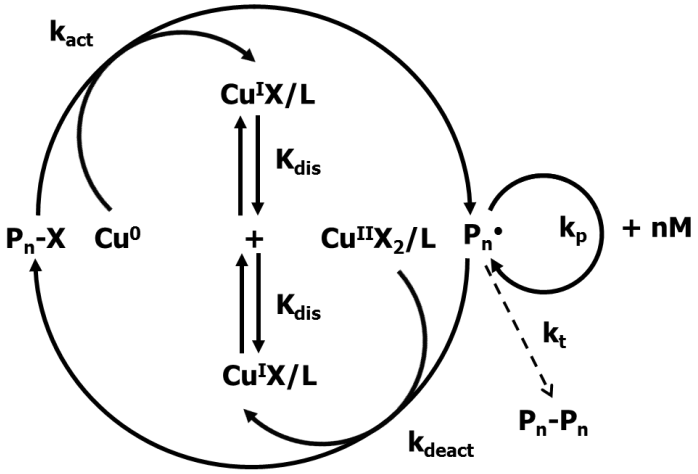

Figure 6. Mechanism of SET-LRP as proposed by Percec (reprinted from ref. 26).

1.2.4 High-throughput polymerization

High-throughput experimentation is often used in the pharmaceutical industry for fast synthesis and screening of many compounds for a certain activity. In polymer chemistry, high-throughput polymerization or automated parallel polymerization can be used to efficiently synthesize libraries of different polymers via controlled radical polymerization or to compare and optimize many different reaction conditions. The reactions can be performed using automated synthesizers such as the Chemspeed parallel synthesizer. This technique has previously been successfully used for high-throughput parallel synthesis of polymers using different polymerization mechanisms.[27, 28]

The group of Destarac has shown automated parallel synthesis of homo- and diblock copolymers of butyl acrylate (BA) and ethyl acrylate (EA) via Macromolecular Design via the Interchange of Xanthates (MADIX).[29] Automated RAFT polymerization was reported by Schubert, who showed the optimization of the polymerization of methyl methacrylate (MMA) by using different CTA/initiator ratios and different temperatures.[30] A later paper by the same group reports a more detailed protocol for the automated homopolymerization of different acrylates, acrylamides and *p*-methyl styrene.[31] Chiefari and Moad showed the synthesis of quasi-block copolymer libraries of butyl methacrylate (BMA) and MMA via automated sequential RAFT polymerization.[32, 33] Together with Schubert they also reported the synthesis of quasi-multiblock copolymers of MMA, BMA, di(ethylene glycol) methyl ether methacrylate and benzyl methacrylate using the same technique.[34] Automated ATRP of MMA was also reported by Schubert, [35, 36] as well as the statistical copolymerizations of hydroxypropyl acrylate (HPA) with *N*-acryloylmorpholine (NAM) or *N,N*-dimethylacrylamide (DMA) via nitroxide mediated polymerization (NMP).[37] Also by Schubert, the automated cationic ring-opening polymerization (CROP) of 2-ethyl-2-oxazoline was shown under different conditions.[38, 39]

1.2.5 Conclusions

CRP will be used in this thesis because this technique allows for the synthesis of functional polymers with complex architectures with good control. RAFT polymerization is chosen as the main method for its good compatibility with functional groups. As an alternative, Cu(0)-mediated polymerization will be used, because this is a relatively new technique which has not been used often for the polymerization of functional monomers, although protective groups may be necessary for this. Additionally, we will employ high-throughput experimentation for faster screening and optimization

of reaction conditions and to be able to synthesize libraries of functional polymers with variations in composition.

1.3 Supramolecular network materials

In a supramolecular material the building blocks, which can either be small molecules or polymers, are held together by non-covalent interactions, such as hydrogen bonding, ionic interactions, metal coordination, π-π stacking or hydrophobic interactions. Multiple interactions are often needed for strong binding and in some cases a combination of different binding mechanisms is used.[40] Most supramolecular networks are either formed by low molecular weight species, polymers that form crosslinks at the end groups, or polymers in which the crosslinking groups are randomly distributed across the polymer chain. In polymers, the crosslinks can be formed by discrete binding moieties, such as UPy or cyclodextrin, or by an array of monomers that interact or phase-separate. Supramolecular network materials can be divided into two main groups, namely supramolecular hydro- or organogels that are swollen networks containing water or solvent, and supramolecular bulk materials. Because the cross-linking interactions in supramolecular networks are generally reversible, many of these materials show self-healing behavior and can easily be processed. This introducing section will discuss supramolecular crosslinked hydrogels and bulk networks. Supramolecular linear polymers, which have been reviewed already many times, will not be discussed here.[41-44] A recently published book[45] as well as earlier reviews[46-48] also give an overview of different types of supramolecular networks and gels. In the following discussion, the different materials are organized by the main type of supramolecular interaction that is used. In view of the recent developments on supramolecular self-healing materials and the existence of earlier review articles, this overview is mainly focused on publications from the past few years.

1.3.1 Supramolecular hydrogels

As a general definition, a gel is a material that partly consists of a liquid, which is usually water (in case of a hydrogel) or solvent (in case of an organogel), that is held together with a network formed by polymers or other molecules. A gel behaves like a solid, which can be determined by rheology or other techniques as a solid has a higher storage modulus than loss modulus, or more simply using the vial inversion method, by which a vial containing the gel is inverted and the gel should stay at the bottom of the vial, showing no visible flow. Gels are usually formed by chemically crosslinked polymers surrounded by water or solvent. However, they can also be made by physically crosslinked polymers or smaller molecules, in which case they are supramolecular gels. In stimuli-responsive supramolecular gels, a sol-gel transition can occur dependent on the environment such as temperature, pH or the presence of certain compounds. A combination of covalent and physical crosslinking can also be used to improve the properties of hydrogels.[49-52] One of the main applications of supramolecular hydrogels is the use as injectable drug carrier,[53] although other applications such as tissue engineering[54] and oil recovery[55] have also been shown. Many different types of supramolecular interactions can be used to make physically crosslinked hydrogels, of which we will discuss the most important ones below. Several other reviews discuss different polymeric supramolecular gels,[56-58] supramolecular gels formed by low molecular weight species,[59-63] their biomedical applications[64-67] and other uses.[68]

Hydrophobic interactions

Hydrophobic interactions are especially suitable to form hydrogels. The main chain of the polymers is water soluble, while non-water soluble end groups, side chains or monomers can be used to form

physical crosslinks. The hydrophobic parts of the gel can also be formed by thermoresponsive polymers, in which case the gel can undergo a transition between a sol and a gel by changing the temperature. Polymers used to form hydrogels via hydrophobic interactions will usually form micelles with a hydrophobic core at lower concentrations, as they are essentially amphiphiles that can act as surfactants. While at low concentrations the hydrophilic parts of the polymers form loops, thereby allowing all hydrophobic groups to be contained in the same micellar core, at increased concentration they will start to form bridges between micelles resulting in a network (Figure 7).[69] The concentration at which this happens is dependent on the nature and ratio of the hydrophilic and hydrophobic groups, the length of the polymer and additional components in the water, such as salt or surfactants.

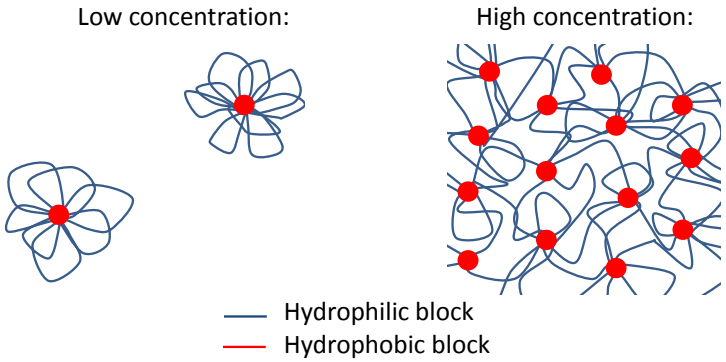

Figure 7. Behavior of ABA-triblock copolymers with a hydrophobic-hydrophilic-hydrophobic structure in water at different concentrations.

Several papers show the use of hydrophobically associating telechelic polymers to increase viscosity of aqueous solutions.[69-74] Some of the earliest hydrogels based on hydrophobic interactions were reported by Tsitsilianis and colleagues, who showed the formation of hydrogels from polystyrene-*b*-poly(sodium acrylate)-*b*-polystyrene (PSt-*b*-PNaA-*b*-PSt) triblock copolymers with around 3 wt% PSt.[75, 76] Micelles were formed below 0.2 % concentration, while weak gels were formed above 0.4 % concentration. The charged middle block makes backfolding of loops into the same micellar core unfavorable and favors extended bridging between hydrophobic cores compared to uncharged hydrophilic middle blocks. A similar hydrogel consisting of poly(methyl methacrylate)-*b*-poly(2-(dimethylamino)ethyl methacrylate)-*b*-poly(methyl methacrylate) (PMMA-*b*-PDMAEMA-*b*-PMMA) block copolymer was also reported.[77, 78] Similar behavior was found for poly(*tert*-butyl acrylate)-*b*-poly(2-vinyl pyridine)-*b*-poly(*tert*-butyl acrylate) (PtBA-*b*-P2VP-*b*-PtBA), while the hydrolyzed poly(acrylic acid)-*b*-P2VP-*b*-poly(acrylic acid) (PAA-*b*-P2VP-*b*-PAA) formed hydrogels through electrostatic interactions.[79]

Other hydrogels prepared from triblock copolymers with a hydrophobic-hydrophilic-hydrophobic structure, in which the hydrophilic block was formed by poly(sodium methacrylate) and the hydrophobic blocks by polybutadiene (10 wt%), were reported by Vlassopoulos.[80] The effect of cationic and anionic surfactants was studied, and it was found that the addition of surfactants induces gel formation by promoting bridge formation between micelles at a low polymer concentration of 0.5 wt%. Weiss reported physically crosslinked hydrogels made from the ABA-triblock copolymer with hydrophobic poly(2-(N-ethylperfluorooctanesulfonamido)ethylmethyl acrylate) as outer blocks and hydrophilic poly(N,N'-dimethylacrylamide) (PDMAM) as middle block.[81]

Laschewski reported thermoresponsive hydrogels prepared from PSt-*b*-poly(di(ethylene glycol) methyl ether acrylate)-*b*-PSt (PSt-*b*-PmDEGA-*b*-PSt) with different sizes of the thermoresponsive middle block.[82] Polymers with longer middle blocks formed hydrogels at lower concentrations than the shorter polymers, together with an increase in cloud point temperature (T_{cp}). An additional thermal transition from gel to liquid was observed well below the T_{cp}, thought to be caused by a decrease in bridging between micelles at increasing temperatures. A similar reported hydrogel consisted of poly(*N*-isopropyl acrylamide) (PNIPAM) as thermoresponsive middle block and PSt, poly(2-ethylhexyl acrylate) and poly(n-octadecyl acrylate) as hydrophobic outer blocks, although relatively high concentrations were needed to form gels from these polymers.[83] Winnik also showed hydrogels with a PNIPAM middle block and hydrophobic end groups, which were synthesized via RAFT using a CTA with two C18 chains.[84]

An interpenetrating multiresponsive hydrogel, formed by combining the two triblock copolymers poly(2-methacryloyloxyethyl acrylate)-*b*-poly(ethylene glycol)-*b*-poly(2-methacryloyloxyethyl acrylate) (PMAEA-*b*-PEG-*b*-PMAEA) and P(AA-*stat*-*n*-butyl acrylate)-*b*-PAA-*b*-P(AA-*stat*-*n*-butyl acrylate) (P(AA-*stat*-BA)-*b*-PAA-*b*-P(AA-*stat*-BA)) was reported by Nicolai (Figure 8).[85] Hydrogels prepared from only the PEG-containing polymers can be chemically crosslinked by UV,[86] while P(AA-*stat*-BA)-*b*-PAA-*b*-P(AA-*stat*-BA) forms pH-responsive gels.[87-89] Combining the two systems led to gels which combined both properties.

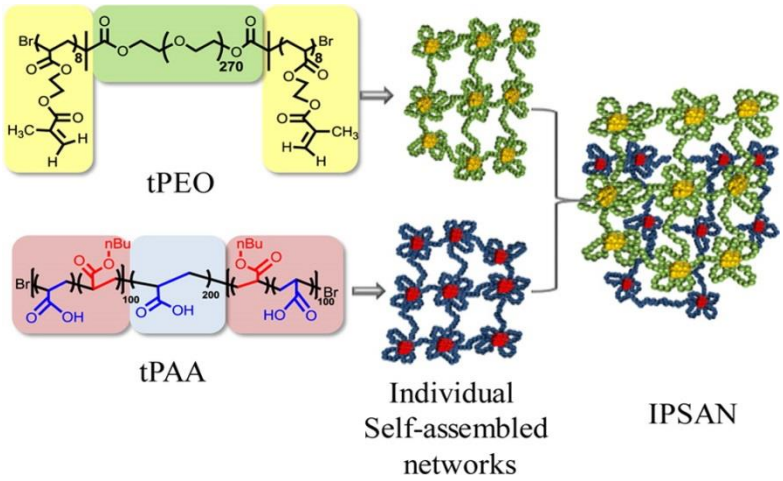

Figure 8. Interpenetrating supramolecular hydrogel formed by PMAEA-b-PEG-b-PMAEA and P(AA-stat-BA)-b-PAA-b-P(AA-stat-BA) (reprinted from ref. 85).

A physical hydrogel formed by poly(poly(ethylene glycol) methyl methacrylate))-*b*-poly(*n*-butyl methacrylate)-*b*-PDMAEMA (PPEGMA-*b*-PBMA-*b*-PDMAEMA) was shown by Georgiou.[90] Gels were formed at 20 wt% in PBS buffer above the PDMAEMA T_{cp} of 54 °C. Other polymers consisting of the same monomers in different architectures did not form a gel. Asymmetrical ABA-triblock copolymers with PDMAEMA as middle block and PBMA as outer blocks, as well as statistical copolymers, were also tested for their ability to form thermoresponsive gels.[91] Only the triblock copolymers formed hydrogels, with an increase in the gel point temperature with increasing symmetry and decreasing hydrophobic content, showing symmetry is beneficial for gel formation.

An example of a hydrogel with thermoresponsive outer blocks was reported by Armes.[92] ABA-type triblock copolymers were synthesized via ATRP with poly(2-methacryloyloxyethyl phosphorylcholine) as the middle block and PNIPAM as the thermoresponsive outer blocks. At temperatures above the

T_{cp} of PNIPAM of 37 °C a free-standing hydrogel was formed. A similar type of hydrogel was shown by Tsitsilianis.[93] These gels were formed by poly(*N,N*-diethylacrylamide)-*b*-PAA-*b*-poly(N,N-diethylacrylamide) (PDEAM-*b*-PAA-*b*-PDEAM) above 60 °C, which is about 20 °C higher than the T_{cp} of PDEAM. The gelation temperature could be lowered by increasing the salt concentration. Other similar types of hydrogels were formed by poly(*N*-(2-hydroxypropyl) methacrylamide lactate)-*b*-PEG-*b*-poly(*N*-(2-hydroxypropyl) methacrylamide lactate), with varying sizes of the middle and outer blocks.[94, 95] Stronger gels were formed by the copolymers with shorter thermoresponsive blocks, which was explained by a higher cross-linking density in the case of shorter blocks, while stronger phase separation between water-rich and polymer-rich phases occurred when using shorter middle blocks. Other hydrogels prepared from ABA-triblock copolymers with thermoresponsive outer blocks were reported by Armes,[96] Ruokolainen,[97] Liu,[98] Laschewsky,[99] Sumerlin[100] and Booth.[101-103] Zeng reported a hydrogel made from PNIPAM-*b*-PEG-*b*-PNIPAM, in which the NIPAM was partially modified with dopamine, which leads to additional stabilization by hydrogen bonding and π-π interactions of the catechol group.[104]

Liu reported hydrogels prepared from multiblock copolymers of PDMAM and PNIPAM.[105, 106] While one of the polymers formed a hydrogel from interconnected micelles at 10 wt% and 60 °C, other polymers only showed precipitation under these conditions, showing that careful tuning of the block sizes is necessary. The multiblock copolymer gels were compared to PNIPAM-*b*-PDMAM-*b*-PNIPAM triblock copolymers, revealing that the multiblocks had a higher storage modulus and lower gelation temperature. The critical gelation concentration could be further lowered by adding salts.

However, polymers do not necessarily need to contain the hydrophobic and hydrophilic parts as well-defined block copolymers. It is also possible to prepare supramolecular hydrogels from copolymers with short randomly distributed hydrophobic blocks, which was shown by the group of Okay (Figure 9).[107-110] The gels were synthesized by free-radical copolymerization of hydrophilic acrylamide (AM) with 2% of stearyl methacrylate (SMA) or dococyl acrylate within sodium dodecyl sulfate (SDS) micelles in water with a high NaCl concentration. In the presence of SDS the gels showed good mechanical properties with reversible cross-links and self-healing abilities, while gels from which the SDS was extracted after synthesis behaved more like a fragile covalently cross-linked gel.[107, 111] Similar hydrogels were synthesized using AA and SMA,[112, 113] and DMAM and SMA.[114]

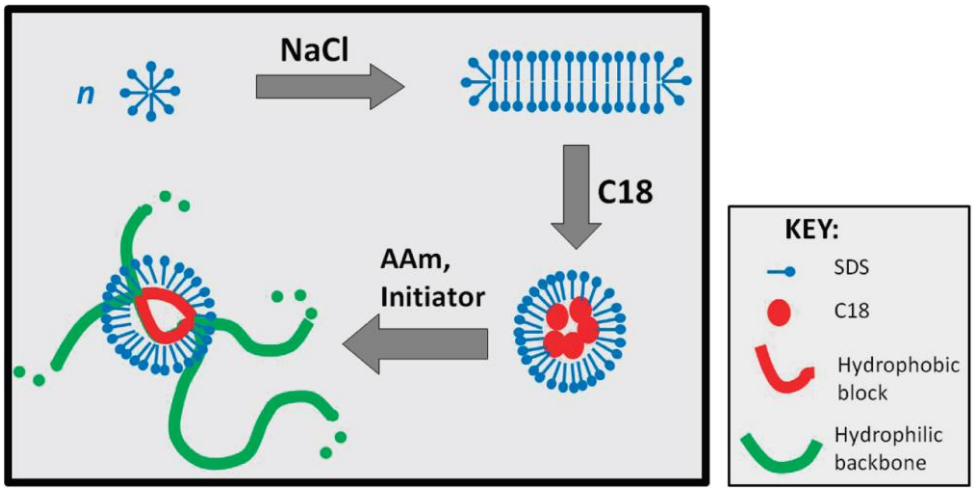

Figure 9. Hydrogels formed by hydrophobic interaction of stearyl methacrylate, which was copolymerized within SDS micelles together with acrylamide as hydrophobic blocks (reprinted from ref. 107).

Percec showed that supramolecular hydrogels can also be prepared from miscible blends of hydrophilic and hydrophobic polymers.[115] Different polymer blends were film casted and submerged in water, after which the water uptake was determined. It was explained that hydrogen bonding and other non-covalent interactions between the two polymers helped to form hydrophobic clusters that crosslinked the network of hydrophilic polymers.

Besides synthetic polymers, biopolymers such as chitosan and cellulose are also often used for preparing supramolecular hydrogels. Liu and Wang reported hydrogels made from chitosan that was modified with ferrocene.[116] The ferrocene groups aggregated by hydrophobic interactions to form crosslinks that were redox responsive and addition of different metal ions led to precipitation by chelation or transition to a sol.

An example of bio-inspired hydrophobic interactions was reported by Werner and Zhang, who used the receptor-ligand interaction between biotin and avidin, in which hydrophobic interactions play an important role, for hydrogel formation.[117] A linear PEG was end-functionalized with biotin, while four biotin units could bind to each avidin to form a network.

Nanocomposite hydrogels can be formed by the inclusion of inorganic particles in the network, for which different types of clay are regularly used. Nagahama reported hydrogel formation from a mixture of poly(D,L-lactide-*co*-glycolide)-*b*-PEG-*b*-poly(D,L-lactide-*co*-glycolide) and clay nanosheets.[118] The triblock copolymer formed micelles through hydrophobic interactions, while the clay interacted with the PEG chains. Addition of doxorubicin (DOX) at different concentrations showed DOX interacted with the clay, forming secondary crosslinks, and this injectable hydrogel could be used for controlled release of DOX in vivo (Figure 10).[119]

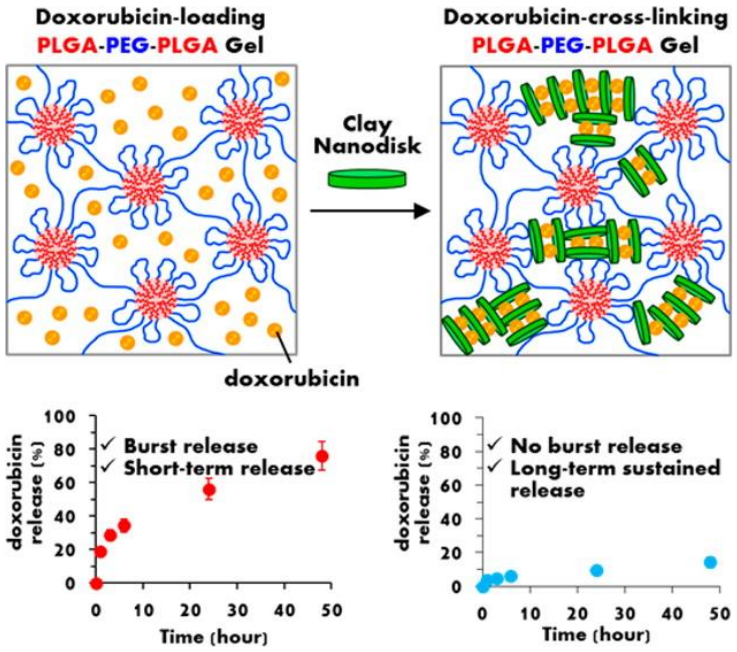

Figure 10. DOX release from a triblock copolymer/clay hydrogel (reprinted from ref 119)

Appel and Tibitt used the interaction between nanoparticles and hydrophobically modified cellulose to form a hydrogel.[120] The nanoparticles were composed of either PSt or PEG-*b*-poly(lactic acid) (PEG-*b*-PLA) with a diameter of around 50 nm, and the hydroxypropylmethylcellulose was modified with adamantyl, hexyl or dodecyl isocyanate. By adsorbing to the surface of multiple nanoparticles, the

cellulose linked the hydrogel together. The gels prepared with dodecyl-modified cellulose were significantly stronger than those with adamantyl or hexyl, showing that increased hydrophobicity of the polymer leads to stronger polymer-nanoparticle interaction.

Hydrogen bonding

Single hydrogen bonds are generally not strong enough in water to form hydrogels, but several examples of hydrogen-bonding organogels have been shown. For hydrogels, the use of multiple multivalent hydrogen bonds such as in ureidopyrimidinone (UPy), often in combination with water shielding by hydrophobic groups, is needed to form a strong network. In the case of biopolymers such as peptides or agarose, hydrogen bonding stabilizes the secondary structure that can form hydrogels by stacking into fibrils or fibers.

Del Campo showed self-healing hydrogels based on UPy-UPy interaction.[121] DMAEMA was copolymerized with UPy methacrylate (10 %) and the resulting polymer formed hydrogels above pH 8, while viscous solutions were formed at lower pH. Meijer reported hydrogels from PEG end-functionalized with UPy groups, hydrophobic spacers and urea groups, which formed fibers that could be modified by changing the length of the PEG or the hydrophobic spacer.[122] Multiblock copolymers with PEG and UPy, which formed tough hydrogels, were also shown.[123] Another UPy-based hydrogel was reported by Chirila, who copolymerized dimethylacrylamide with an adamantyl-functionalized UPy methacrylate at different ratios.[124] The resulting polymers formed injectable self-healing hydrogels, in which the adamantyl group stabilized the hydrogen bond through hydrophobic shielding.

Sijbesma showed hydrogels made from PEG-*b*-bisurea-*b*-PEG-*b*-bisurea-*b*-PEG pentablock copolymers (Figure 11).[125] This polymer formed supramolecular rods by hydrogen bonding between the bisureas, with the longer PEG middle block forming crosslinks between different rods. By using two different sizes of the hydrophobic linker between the urea groups of one polymer, the amount of crosslinking between the rods could be controlled as only ureas with the same linker are included in one rod. Using two sizes of linker instead of one highly increased the bridging between rods by suppressing loop formation into the same rod.

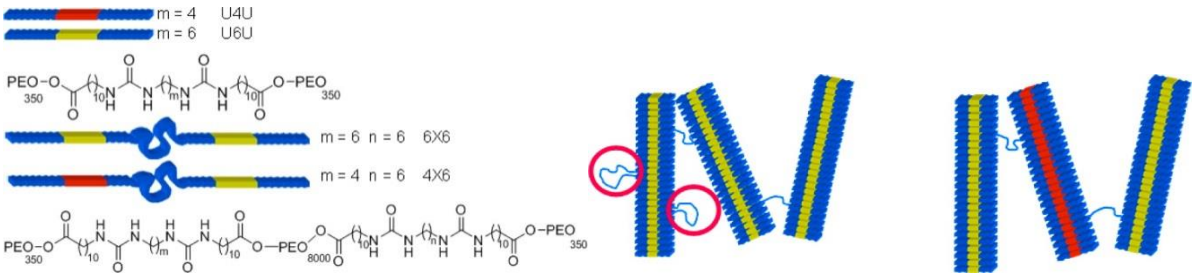

Figure 11. Left: structure of pentablock copolymers that assemble into rods by hydrophobically shielded hydrogen bonding. Right: using different sizes of hydrophobic linkers supresses loop formation (reprinted from ref. 125).

Burdick reported the formation of hydrogels by what the authors call a 'dock and lock' mechanism.[126] It is based on the dimerization of peptide sequences (docking) located on the ends of a linear peptide, which is then locked in place with another peptide sequence on the chain ends of a four-armed PEG star. Shear thinning and self-healing behavior was observed as well as cell compatibility.

Besides these examples of discrete units being used for assembly by hydrogen bonding, several research groups have used polymers that can form large amounts of weak hydrogen bonds for hydrogel preparation. For example, Liu and Zhang showed a material based on poly(2-acrylamido-2-methyl-1-propanesulfonic acid) (PAMPSA) that could form both supramolecular hydrogels and bulk material via multiple hydrogen bonding between the amide and sulfonic acid.[127] Hydrogels at 20 and 50 wt% showed self-healing after cutting without external stimulus, while the 90+ wt% material shaped into a cup could repeatedly heal in a 100 % humidity chamber and be used as a container for organic solvents before and after healing. A small amount of moisture to facilitate motion of the hydrogen bond donors and acceptors was, however, necessary for efficient healing.

Wu reported hydrogel formation from poly(amic acid) ammonium salt, that was based on a combination of hydrogen bonding, π-π stacking and electrostatic interaction between the polymer chains.[128] Cui reported a hydrogel prepared from poly(*N*-acryloyl glycinamide), in which the cooperative hydrogen bonding between the amides stabilized the gel at 10 wt% concentration.[129] The hydrogel could be molded and healed at 90 °C.

Fu reported hydrogels prepared from montmorillonite sheets mixed with polyacrylamide, in which polymer/clay interactions were primarily based on hydrogen bonding and provided a very tough and stretchable hydrogel.[130]

Langer, Traverso and colleagues reported a gel prepared form a mixture of poly(acryloyl 6-aminocaproic acid) and a copolymer of methacrylic acid and ethyl acrylate.[131] Under neutral conditions, the deprotonated polymers were water-soluble, while a gel with around 30 % water content was formed through inter-chain hydrogen bonding under acidic conditions. This material was intended to be used in gastric devices.

Electrostatic interactions

Because charged groups are generally very well water-soluble and form strong electrostatic interactions, they have been frequently explored as basis for supramolecular hydrogels. This can be done by using for example blocks of ionic monomers, which can form complex coacervate clusters that will act as supramolecular crosslinks, together with nonionic water-soluble blocks. Mixtures of homopolymers of certain weak polyions can also form hydrogels, as only part of the ionic groups will participate in crosslinking while others remain in solution. As the solubility of ionic groups in most organic solvents is generally low, organogels can be formed by relatively weak electrostatic interactions. A recent review discusses supramolecular materials based on electrostatic interactions for biomedical applications.[132]

An example of a hydrogel formed by electrostatic charges was shown by Hennink.[133] Oppositely charged dextran microspheres were formed by copolymerization of hydroxyethyl methacrylate-functionalized dextran with either methacrylic acid or dimethylaminoethyl methacrylate. Gelation occurred when equal volumes of positively and negatively charged microspheres were mixed together at pH 7. The physical network was broken at high stress and reformed when the stress was removed, so-called shear thinning behavior.

Gong showed hydrogels that were prepared by random copolymerization of cationic and anionic monomers in an almost 1:1 ratio.[134] The used monomers were sodium 3-(methacryloylamino)propyl-trimethylammonium chloride (MPTC), [2-(acryloyloxy)ethyl]trimethyl ammonium chloride (AETMAC),

p-styrenesulphonate (NaSS) and 2-acrylamido-2-methylpropanesulphonic acid (AMPS). The copolymers showed precipitation at lower concentration, but uniform hydrogels were formed when concentrations around 40-50 wt% were used. A follow-up paper describes hydrogels made by mixed charged homopolymers using the same monomers.[135]

Jiang reported hydrogels prepared by free radical polymerization of carboxybetaine methacrylate.[136] Electrostatic interaction between the zwitterionic groups formed the physical crosslinks in the materials, which could self-heal repeatedly.

Lapitsky reported a hydrogel formed by mixing poly(allylamine hydrochloride) and pyrophosphate or tripolyphosphate sodium salt, yielding very stiff hydrogels that would stick to both hydrophilic and hydrophobic surfaces.[137]

Hydrogels prepared from a short imidazolium acrylate homopolymer with a phosphonate end group were shown by Monnereau.[138] The relatively weak electrostatic interaction was strong enough to physically crosslink the polymer, but was strongly affected by pH and ionic strength.

Another hydrogel based on electrostatic interaction was reported by Aida (Figure 12).[139] These gels were formed by a PEG chain with cationic G3-dendrons on each end, mixed with negatively charged clay nanosheets that are dispersed by sodium polyacrylate. Multiple dendrons bind to each clay nanosheet, forming a free-standing gel that can self-heal and be remolded.

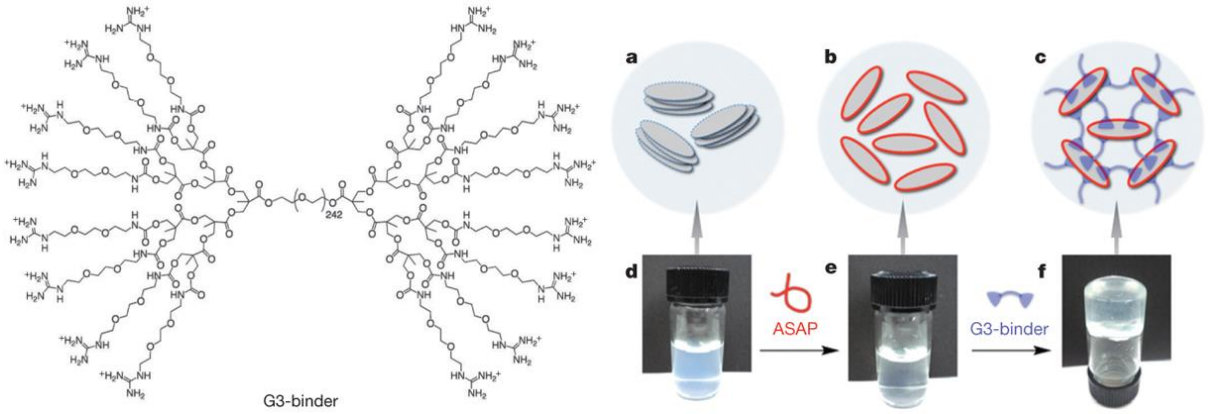

Figure 12. Left: structure of G3-binder. Right: hydrogel preparation by first dispersing clay nanosheets with sodium polyacrylate (ASAP), followed by addition of G3-binder to form electrostatic supramolecular crosslinks (reprinted from ref. [139]).

Kramer and Hawker showed hydrogels made by mixing ABA triblock copolymers containing a water-soluble middle block and end blocks with anionic and cationic groups (Figure 13).[140] The ionic groups form complex coacervate domains phase separated from the water phase, which are the crosslinks of the hydrogel. The guanidinium-based cationic polymer formed hydrogels with both the (weaker) carboxylate- and (stronger) sulfonate-based anionic polymers, while the weaker ammonium-based cationic polymer did not form hydrogels with either. Further characterization of these hydrogels and their weakening in response to salt was reported,[141] as well as comparison of structure of the ionic crosslinks with coacervates of charged homopolymers.[142]

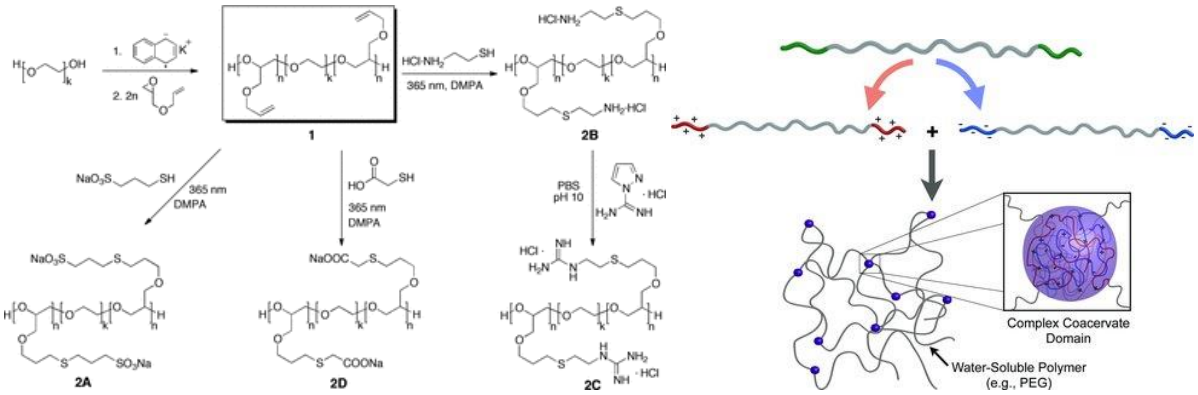

Figure 13. Left: synthesis of charged water soluble ABA-triblock copolymers from a single precursor. Right: Oppositely charged ABA triblock copolymers are mixed in equimolar amounts to form a hydrogel crosslinked by complex coacervate domains (reprinted from ref. [140]).

Similar hydrogels were reported by Lemmers, who mixed ABA-triblock copolymers containing charged end groups with oppositely charged homopolymers.[143] PEG was used as neutral middle block and poly(potassium 3-sulfopropylmethacrylate) as negatively charged end blocks, with poly(allylamine hydrochloride) as the positively charged homopolymer. At lower concentration these form flower-like micelles with a complex coacervate core, and at higher concentrations bridges between the micelles resulted in the formation of hydrogels that were responsive to pH and salt concentration.

Wan reported hydrogels based on the electrostatic interaction between guanidinium and polyoxometalates.[144] ABA-triblock copolymers containing a PEO middle block and poly(2-(2-guanidinoethoxy)ethyl methacrylate) (PG) were synthesized with different block lengths and mixed with $Na_9EuW_{10}O_{36}$ in water. Flower-like core-shell micelles were formed, linked by the triblock copolymers. Longer PG blocks resulted in larger core micelles with a higher crosslinking density. The hydrogels were shown to be self-healing after being cut and pressed together for three minutes.

Jiang showed hydrogels that were prepared from a mixture of linear hyaluronic acid and four-armed PEG-*b*-poly(2-aminoethyl methacrylate).[145] A hydrogel was formed at a 1:1 charge ratio and in vivo injection and biocompatibility was shown.

Yang showed hydrogels made from acrylamide and 3-((2-(methacryloyloxy)ethyl) dimethylammonio)propane-1-sulfonate copolymers, that crosslinked through electrostatic interaction and hydrogen bonding.[55]

Jiang reported a supramolecular network made from hyperbranched poly(ether amine) nanogels with carboxyl groups and chitosan, that interacted through hydrogen bonding and electrostatic interactions, which could be used both as hydrogel or bulk material.[146] It could be used for selective absorption of dyes, which interacted through hydrophobic interaction.

Metal coordination

Metal coordination has often been used in the preparation of linear supramolecular polymers in non-competing organic solvents,[43, 147-149] and gels can be formed using similar approaches.[150] Many research groups also use the interaction between metal ions and polymer chains for crosslinking. Some metal-ligand complexes can form fibers through secondary interactions like π-π stacking and hydrophobic aggregation.

An early example of hydrogels prepared from side-chain bipyridyl-functionalized poly(2-oxazoline)s that could be crosslinked with Fe(II), Ru(II), Ni(II) or Co(III) was reported by Chujo and colleagues.[151-153] The amount of swelling in water was dependent of the degree of functionalization of the polymer. Gels with Fe(II) and Co(III) were relatively stable at room temperature but turned soluble when heated to 30 °C or higher due to exchange from intermolecular to intramolecular crosslinks, while gels with Ru(II) were very stable even in boiling water. After evaporation to dryness, all gels could be reformed again in water. Gels with Co(III) could also be dissolved by reduction to the labile complex-forming Co(II).

Several metal coordination hydrogels made from star-shaped PEG have been reported. Because metal-ligand interactions usually only bind two polymer chains together, the covalent crosslink between the polymer arms is needed for network formation. Feijen showed eight-armed star polymers containing a long PEG core block and short poly(L-lactide) end blocks end-functionalized with pyridine that could form hydrogels.[154] Thermoreversible gels were formed by adding different transition metal ions, such as Cu(II), Co(II) or Mn(II), to a solution of the polymer, with the sol-gel transition temperature dependent on the polymer concentration and type of ion. Kikuchi reported hydrogels based on three-armed PEG end-functionalized with terpyridine and crosslinked by cobalt ions.[155] Kinetically labile networks that behave as a sol were formed by adding Co(II), which turned into a gel by oxidation of the cobalt by exposure to air. This mechanism was exploited by adding small amounts of Ni(II) to the system, leading to self-healable gels. Seiffert reported supramolecular networks made from four-armed PEG with terpyridine end groups and different transition metal ions in both organic solvents and water.[156] The purpose of these materials was to serve as a model network in which the effect of different strength crosslinks could be studied.

Gohy reported hydrogels formed by poly(triethyleneglycol methylether methacrylate)-*b*-PSt (PmTEGMA-*b*-PSt) with terpyridine groups randomly distributed in the PmTEGMA block.[157] The polymer self-assembled into micelles in aqueous solution by hydrophobic association, which could be crosslinked by adding Ni(II). While terpyridine-functionalized mTEGMA homopolymers could also form hydrogels with Ni(II), much higher concentrations were needed and weaker gels were formed than for the diblock copolymer, showing that the additional crosslinking by the micellar core greatly improves the properties of the hydrogel. A thermoresponsive hydrogel was also formed by PSt-*b*-PNIPAM end-functionalized with terpyridine, with strain-dependent behavior depending of the PSt block length.[158-160]

Nanocomposite hydrogels consisting of silica nanoparticles, telechelic terpyridine-functionalized PEG and Co(II) were reported by Sprakel.[161] Some of the PEG chains adsorbed onto the silica surface by hydrogen bonding, which, together with the metal-terpyridine interaction with free PEG, led to formation of a self-healing network.

Johnson reported gels made from bipyridyl tetrazine end-functionalized PEG with Fe(II) or Ni(II) as crosslinker in MeCN or water.[162] These gels could also be covalenty crosslinked using Diels-Alder reactions.

A mussel-inspired hydrogel was first reported by Messersmith.[163] Linear and branched PEG was end-functionalized with one to four 3,4-dihydroxyphenylalanine (dopa) groups, and hydrogels were formed upon mixing with oxidizing agents. Dopa-based metal-ligand hydrogels were also reported by Messersmith and colleagues (Figure 14).[164, 165] A four-armed PEG was end-functionalized with dopa,

which has a structure similar to catechol and can bind to Fe(III) ions. This metal-ligand interaction forms monocomplexes at pH<5, biscomplexes at pH~8 and triscomplexes at pH>8, making it possible to control the gelation and crosslink density by variation of pH. Birkedal reported the synthesis of hydrogels from random functionalization of polyallylamine with dopa mixed with Fe(III).[166] The combined effect of the pH-dependent complex formation and reduction in polymer charge leading to collapse at higher pH resulted in a maximum in storage modulus around pH 9. In a follow-up paper tannic acid was mixed with polyallylamine and Fe(III), which led to complex formation at lower pH and covalent crosslinking between the tannic acid and polyallylamine above pH 8 via Schiff base reaction and Michael addition.[167]

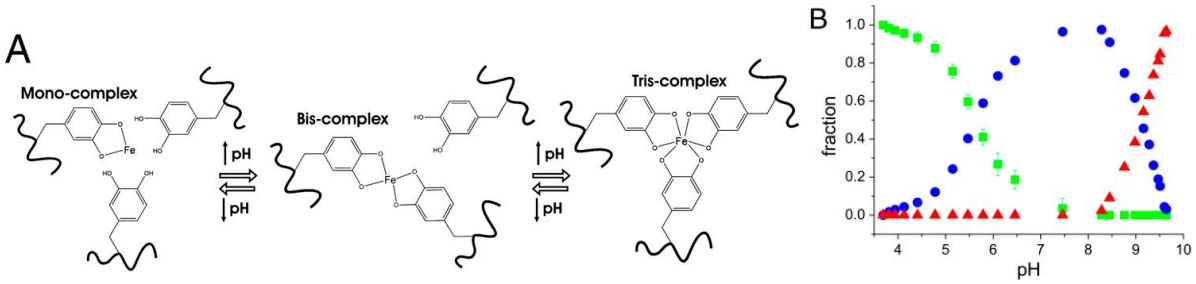

Figure 14. A: pH-dependent complex formation between Fe(III) and dopa. B: Fractions of mono-, bis- and triscomplexes at different pH in green, blue and red, respectively (reprinted from ref. [164]).

Besides dopa, histidine is another mussel-inspired metal coordinating group.[168, 169] Messersmith studied the hydrogel formation of histidine end-functionalized four-armed PEG with different divalent cations.[170] The histidine-metal interaction was found to be pH-dependent, with 2:1 complexes being formed at a higher pH which was also dependent on the metal ion used.

Several polymers can coordinate with metal ions without the need for a specific ligand, for example by carboxylic acids or amines. Tong reported a light-switchable hydrogel made from PAA complexed with Fe(III) ions.[171] Irradiation leads to reduction of Fe(III) to Fe(II), thereby dissolving the gel. This could be reversed by oxidation from bubbling the solution with oxygen. Zhang and Lu showed multiresponsive hydrogels made from chitosan with a variety of different metal ions as crosslinkers.[172] Xie reported silica nanoparticles grafted with PAA and mixed with Fe(III) to form nanocomposite hydrogels.[173] Also shown was a graphene oxide-PAA nanocomposite hydrogel with Fe(III) as crosslinks.[174]

Host-guest interactions

Supramolecular gels based on host-guest interactions have the characteristics of not only strong binding affinity, but also a fixed geometry and directionality and often responsiveness to pH[175] or other stimuli.[176, 177] This makes them very useful for biomedical applications such as drug delivery. Cyclodextrins (CD) are often used as the host molecule, as they are hydrophilic on the outside and relatively hydrophobic on the inside and different types of guest molecules can be used. Additionally they are commercially available and can be modified relatively easily. Other hosts that have been used for gels are cucurbituril for hydrogels, and crown ether[178-180] and pillarene[181] for organogels. Other recent reviews discuss cyclodextrin-based supramolecular materials in more detail,[182] as well as host-guest based materials in general.[183, 184]

Many examples have been shown of PEG forming inclusion complexes with α-cyclodextrin (α-CD), which in turn form larger aggregates that act as crosslinks. One of the earliest examples of a hydrogel

formed in this way was shown by Harada and Kamachi.[185] PEG with different molecular weights was mixed with α-CD at different concentrations and left standing for several days, during which inclusion complexes of PEG chains in α-CD were formed. The time and concentration of PEG and α-CD needed to form a gel were dependent on the molecular weight of the PEG, and gel formation was reversible when heated or agitated. The authors suggested that physical crosslinks were formed by aggregation of PEG chain ends with multiple α-CDs on them into microcrystals. Based on this work, Yui reported hydrogels of dextran-*graft*-PEG mixed with α-CD.[186]

Li showed hydrogels prepared for PEG-*b*-poly[(R)-3-hydroxybutyrate]-*b*-PEG mixed with α-CD (Figure 15).[187] The combination of inclusion complexes between α-CD and PEG end groups with hydrophobic interaction between poly[(R)-3-hydroxybutyrate] blocks gave a strong supramolecular network that could be used for controlled drug release.

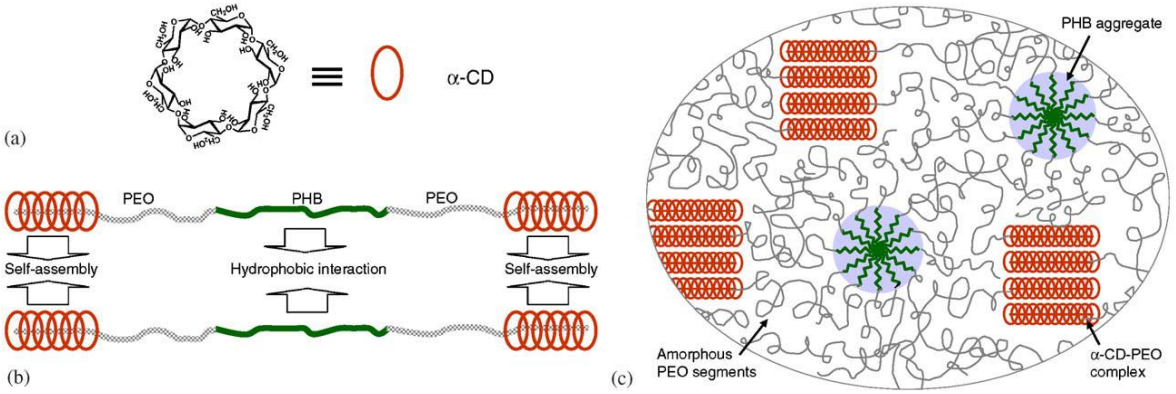

Figure 15. Supramolecular hydrogels formed by a combination of hydrophobic interaction and host-guest interaction (reprinted from ref. [187]).

Dufresne reported a hydrogel prepared from cellulose nanocrystals functionalized with β-CD and mixed with pluronic polymers and α-CD.[188] The poly(propylene oxide) middle block would be enclosed inside the β-CD, while α-CD was added to complexate with the PEG outer blocks and self-assemble into crosslinks.

Dai and Pan reported hydrogel formation of star shaped poly(ε-caprolactone)-*b*-PEG with a porphyrin core and α-CD.[189] The α-CD-PEG complexes, together with π-π stacking of the porphyrins and hydrophobic interaction of PCL provided supramolecular crosslinking of the gel, while the porphyrin core could be used to produce singlet oxygen by visible light irradiation for photodynamic therapy.

CD can also form host-guest complexes with many other guests, for which both α-CD and β-CD have been used. By attaching both the CD and the guest molecule to water-soluble polymers, stimuli-responsive supramolecular hydrogels can be formed. Harada reported statistical copolymers of acrylic acid and β-CD, which were mixed with statistical copolymers of acrylic acid and ferrocene (Figure 16).[190] The material was switchable from gel to sol by a reversible oxidation reaction, as only the uncharged ferrocene can form host-guest complexes with β-CD. A follow-up paper showed hydrogels prepared by copolymerization of acrylamide with either α-CD methacrylate complexed with BA, or β-CD methacrylate complexed with adamantane acrylamide in water.[191] Another paper

by the same group shows an acrylamide and NIPAM copolymers with adamantane, ferrocene and β-CD.[192] The resulting hydrogels showed shape memory in response to redox stimuli.

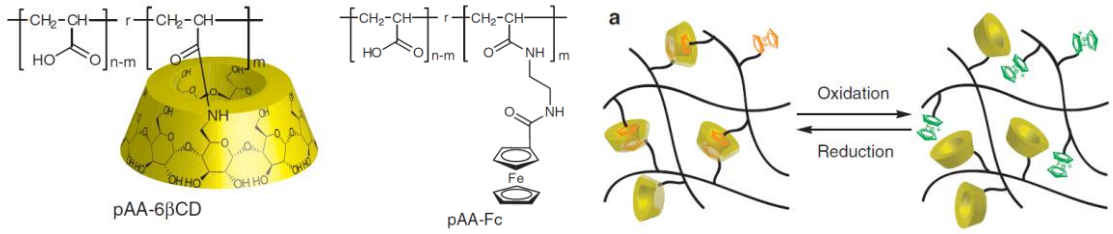

Figure 16. Left: structure of β-CD- and ferrocene-functionalized PAA. Right: redox-responsive supramolecular hydrogel formation (reprinted from ref. [190]).

Burdick used hyaluronic acid that was functionalized with either β-cyclodextrin or adamantane that formed shear-thinning hydrogels when mixed together.[193] Increasing the number of crosslinks by using more host and guest increased the storage modulus of the gels. Thiols and Michael acceptors were grafted to the polymers to facilitate in vivo covalent crosslinking by Michael addition after injecting the gel,[194] while using a peptide linker to attach the adamantane allowed for in vivo cleavage and degradation of the hydrogels.[195] Tian showed phosphorescent self-healing hydrogels consisting of a β-CD-acrylamide copolymer and an α-bromonaphthalene-acrylamide copolymer.[196] The phosphorescence could be tuned by addition of an azobenzene-acrylamide copolymer. Zhu mixed β-CD-functionalized PDMA and cholic acid-functionalized PDMA together to form hydrogels.[197] Yuan reported a redox responsive hydrogel made from a mixture of β-CD-functionalized PDMA and ferrocene-functionalized PDMA.[198]

Ravoo showed self-healing hydrogels prepared from hydroxyethyl cellulose that was modified with adamantane and mixed with β-CD that had *n*-dodecyl chains attached on one side and oligo(ethylene glycol) chains on the other side.[199] Bilayer vesicles were formed with the β-CD available on the surface for binding with the adamantane, resulting in hydrogel network formation.

Scherman reported hydrogels based on the complexation between cucurbit[8]uril (CB[8]) and different guest molecules.[200] Naphtalene-functionalized hydroxyethyl cellulose and methyl viologen-functionalized poly(vinyl alcohol) (PVA-MV) were mixed with CB[8], which would complex both the naphthalene and methyl viologen inside one CB[8]. The hydrogels could be dissociated by addition of an excess of a competing guest molecule or by reduction of the electron-deficient methyl viologen. A follow-up paper to this work describes the use of cellulose nanocrystals (CNC) as reinforcements in the supramolecular hydrogel (Figure 17).[201] The cellulose was grafted with a copolymer of protonated DMAEMA and naphtyl methacrylate, and mixed with PVA-MV and CB[8] to form the hydrogel via host-guest interaction. Inclusion of the CNC led to a much stiffer hydrogel that still showed rapid self-healing and sol-gel transition. A similar hydrogel that was reinforced with nanofibrillated cellulose, to which naphtalene-functionalized hydroxyethyl cellulose adsorbed via hydrogen bonding, was also reported.[202] A double network hydrogel was prepared from phenylalanine-functionalized carboxymethyl cellulose with CB[8] and three-armed DNA with hybridizing sticky ends, which combined properties of each separate network type.[203] A positively charged anthracene-functionalized hydroxyethyl cellulose, which also formed 2:1 complexes with CB[8], was used to form hydrogel microcapsules in an emulsion.[204]

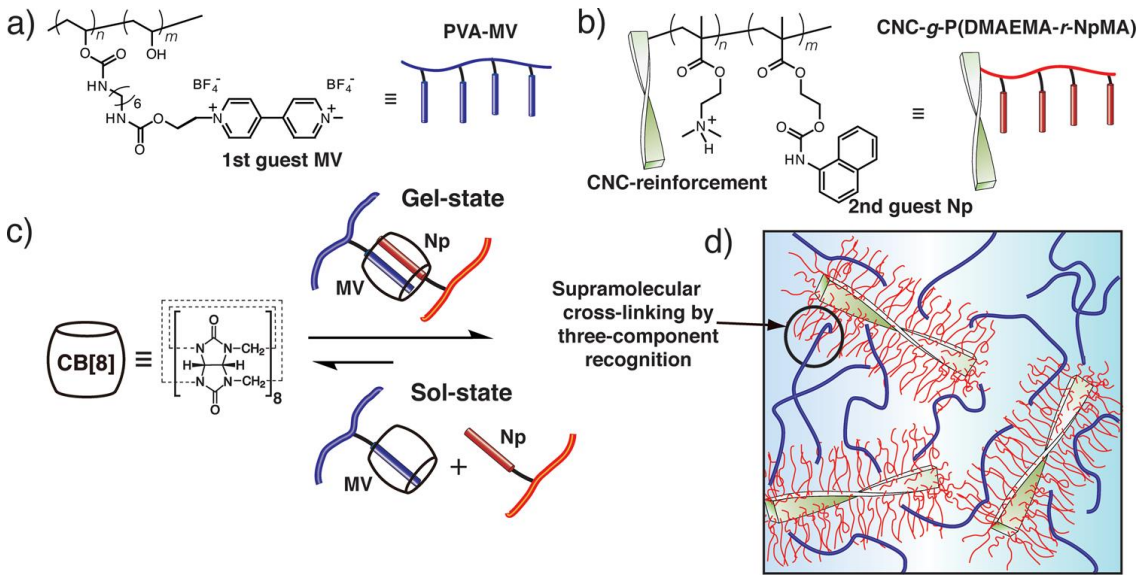

Figure 17. Supramolecular host-guest hydrogel reinforced with cellulose nanocrystals (CNC) (reprinted from ref. [201]). a) copolymer of methyl viologen (MV) and poly(vinyl alcohol), b) copolymer of protonated DMAEMA and naphtyl methacrylate (NpMA) grafted to CNC, c) host-guest interaction between CB[8] and MV and NpMA, d) structure of the supramolecular hydrogel.

1.3.2 Supramolecular bulk materials

While supramolecular gels are relatively easy to define, this can be more difficult for supramolecular bulk materials. Many non-chemically crosslinked materials behave as hard solids or rubbers, for example because they are used below their glass transition temperature (T_g), form crystalline domains or the polymer chains are sufficiently long to form a network solely by chain entanglements. However, these are not seen as supramolecular materials as they do not have defined non-covalent physical crosslinks. Low molecular weight polymers and oligomers with a T_g well below room temperature generally behave as liquids when they are not chemically crosslinked. However, in some materials the supramolecular interaction between the molecules is strong enough to make the material behave like a solid, which we call supramolecular materials. The supramolecular interactions may be formed by discrete chemical groups, such as the hydrogen bonding UPy, or by interaction or phase-separation between arrays of monomers or multiple functional groups. Several recent reviews give another overview of supramolecular self-healing materials.[205-208] Here we will discuss supramolecular crosslinked materials, both with and without self-healing properties.

Hydrogen bonding

UPy and urea are often used in supramolecular materials, as they can form strong interactions by multiple hydrogen bonds. Meijer showed one of the earliest supramolecular networks based on the hydrogen bonding of UPy and urea.[209] Three-armed block copolymers of propylene oxide and ethylene oxide, end-functionalized with UPy, urea and reference structures, were synthesized and all materials had a low T_g around -53 °C. The urea-functionalized material showed a higher bulk viscosity than the UPy-functionalized material, which was explained by the urea forming extended H-bonding arrays phase-separated from the polymer, while UPy can only form dimers that are miscible with the polymer. Both materials had viscoelastic properties, with the UPy network showing more defined transitions compared to the urea network.

Another paper by Meijer reports a mixture of low molecular weight bis-UPy-oligocaprolactones with two short synergistic UPy end-functionalized peptides, which formed supramolecular polymers

containing the peptides as end-groups.[210] The material was used for specific binding of fibroblast cells, which needed both peptides to adhere to the surface.

A supramolecular elastomer made from polyolefins was reported by Coates.[211] Small amounts of UPy derivative were incorporated into the main chain of poly(1-hexene) homopolymer. The UPy units formed reversible crosslinks in the material, which could be broken by adding an excess of non-olefinic UPy. Tensile tests showed that the bulk material behaved like an elastomer.

Moore and coworkers reported a copolymer of phthalaldehyde and benzaldehyde, in which the benzaldehyde was functionalized with UPy.[212] This polymer formed a supramolecularly crosslinked network, which could be depolymerized by the addition of TFA.

A paper by Anthamatten reports random copolymers of BA with different monomers with H-bonding capabilities, namely the weakly bonding acrylamidopyridine, acrylic acid, 2-carboxyethyl acrylate and the strongly bonding UPy acrylate.[213] While the polymers containing weakly bonding groups behaved like polymer melts and mainly showed an increase in T_g that scaled with their concentration, the UPy acrylate-containing polymers behaved more like an elastic solid.

Bouteiller reported a supramolecular thermoplastic elastomer based on poly(dimethylsiloxane)s.[214] Amino-functional PDMS, which is liquid at room temperature, was modified with different bis-ureas to form either graft-like or telechelic bis-urea functional PDMS. Most of the synthesized materials had rubber properties from physical crosslinking of the bis-ureas, with the strength depending on the bis-urea content and length of the polymer chains.

Chang showed a material made from maleated polyethylene-octene elastomer in which the maleic anhydride groups were reacted with 3-amino-1,2,4-triazole, introducing groups capable of forming hydrogen bonds.[215] A higher amount of the triazole led to an increase in storage modulus, and scratches could be healed at elevated temperatures. Octadecylamine-modified graphene oxide was added to the material to improve the mechanical properties.[216]

Guo reported a material consisting of poly(vinyl alcohol) crosslinked via hydrogen bonds with pyrimidine derivatives containing multiple amines and melamine.[217] T_gs of the material increased with loading level from 0 to 2 wt% when compounds with three or four amines were used, explained by forming a more crosslinked material, while crystallinity was decreased. An improvement in strength, modulus and toughness was also observed with higher H-bond densities.

Different types of self-healing supramolecular bulk materials based on hydrogen bonding were shown by Guan. One of his systems is built up of graft copolymers with a polystyrene backbone and amide-containing polyacrylate side chains (Figure 18).[218] In bulk, the polystyrene forms phase-separated domains, while the amide groups in the matrix are reversibly bound to each other via hydrogen bonds. A similar material, consisting of triblock copolymers with a PMMA middle block and the same amide-containing polyacrylate outer blocks, was also reported.[219] It was shown that a larger weight fraction of PMMA increases the strength of the phase-separated materials and decreases elastomeric properties. Another system by Guan is formed by PSt-*b*-PBA diblock copolymers end-functionalized with UPy, leading to PSt-*b*-PBA-*b*-PSt ABA triblock copolymers.[220] The PSt forms phase-separated domains which are hard physical crosslinks in the softer PBA matrix. Damage will break the UPy-UPy hydrogen bonds, which can be reformed again.

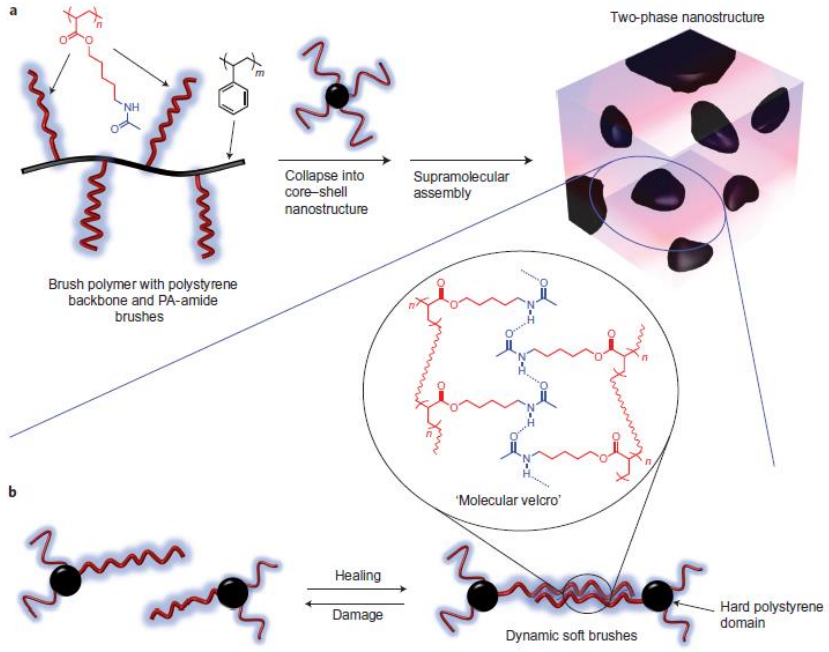

Figure 18. Design of a multiphase self-healing brush polymer (reprinted from ref. [218]). a: The brush polymer self-assembles into a two-phase nanostructure morphology with hard polystyrene domains and a soft polyacrylic amide matrix. B: Self-healing through breaking and reforming the hydrogen bonds of the polyacrylic amide.

While all of the previous examples are based on associating polymer building blocks, multiple hydrogen bonding can also be used to make functional materials of smaller molecules. A supramolecular self-healing rubber made from hydrogen-bonding oligomers was shown by the group of Leibler.[221] It was synthesized by reacting a mixture of fatty acids with urea, resulting in a mixture of oligomers that can form multiple hydrogen bonds (Figure 19). These hydrogen bonds can break and be formed again in different places, resulting in a rubber-like material that can heal repeatedly after damage. The use of a variation of oligomers with different shapes, sizes and associating groups was done to prevent crystallization and ensure an optimum compromise between elastic and self-healing behavior.[222] It was shown that different reaction conditions can lead to supramolecular polymeric materials with very different properties.[223] A paper by Saalwächter and coworkers describes the hydrogen-bonding dynamics and aging of this material, showing that water will act as a plasticizer and significant aging takes place above 110 °C.[224]

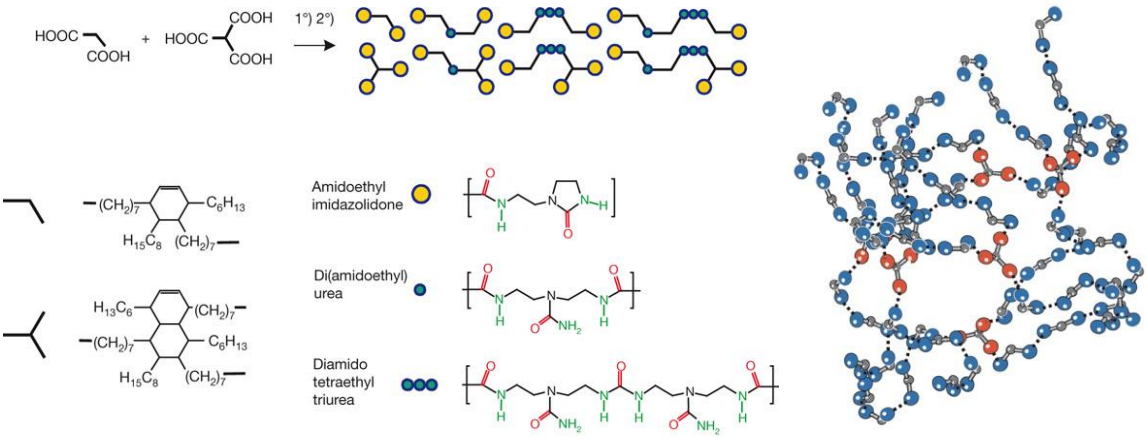

Figure 19. Left: synthesis of oligomers by reacting a mixture of fatty diacid and triacid with diethylene triamine and urea. Right: supramolecular network formation through multiple hydrogen bonding interactions (reprinted from ref. [221]).

Zhang reported a self-healing thermoplastic elastomer made from PDMS with the end groups modified with diethylenetriamine and urea, inspired by the work of Leibler.[225, 226] Polymers and oligomers with different molecular weights were prepared and each showed low T_gs and elastomeric behavior up to around 140 °C, indicating network formation, as well as self-healing behavior.

In another paper by Leibler and coworkers, a supramolecular thermoplastic material was reported based on low molecular weight polyamides.[227] The oligomers consisted of a noncrystallizable soft block derived from vegetable oil and a rigid block that was able to crystallize, present in different amounts, terminated with hydrogen bonding groups. Bridges between the oligomers are formed both by hydrogen bonding and the formation of crystalline segments. All compounds showed a low T_g and a melting temperature above 140°C, with higher melting enthalpy and much higher stress at break for the oligomers that contained more crystalline blocks, showing that the crystalline blocks greatly enhance the strength of the material. The materials could be recycled without much change in mechanical properties, and was easily processable because of the low melt viscosity.

Biomolecules like peptides and nucleic acids are also excellent sources for hydrogen-bonded materials, because these can form stabilized secondary structures as they are found in nature, such as in DNA or proteins. Rowan reported low molecular weight polytetrahydrofuran (PTHF) end-functionalized with modified nucleobases.[228] The PTHF containing thymine, adenine or cytosine end groups each showed different material properties, which were attributed to the different hydrogen bonding strengths of the end groups in combination with phase separation between the nucleobases and the PTHF.

Another supramolecular material based on the hydrogen-bonding between nucleobases was reported by Long.[229, 230] Triblock copolymers of BA containing either adenine or thymine end blocks were synthesized via nitroxide-mediated polymerization. The polymers were mixed in solution, film cast, dried and annealed, yielding a material with rubbery properties up to 150-160°C and a cylindrical morphology in which the high T_g adenine-thymine blend was phase-separated from the low T_g PBA.

Frauenrath reported supramolecular materials in which the self-assembly of oligopeptides, which originates from hydrogen bonding, resulted in materials with different properties (Figure 20).[231] Low molecular weight polyisobutylene was modified with between zero and five L-alanines (Ala) on one or both ends of the polymer, resulting in diblock and triblock copolymers with different size end groups. The diblock copolymers would self-organize into viscous small hydrogen-bonded aggregates (0-1 Ala), single β-sheet tapes (2-3 Ala), or stacked β-sheet nanofibrils (4-5 Ala) with rubbery material properties. The individual triblocks containing more than one Ala already formed hard and brittle solids. Blends of diblocks and triblocks containing 2 Ala end groups formed thermoplastic elastomers reinforced by shorter β-sheets, while a blend of 1 Ala diblock and 2 Ala triblock would result in an interpenetrating supramolecular network containing both longer β-sheets and small aggregates.

Jia reported star shaped polyisobutylene with oligo(β-alanine) end blocks.[232] The β-alanine segments formed H-bonded crystalline β-sheets that were phase-separated from the matrix, and acted both as physical crosslinks and fillers for the elastomeric material.

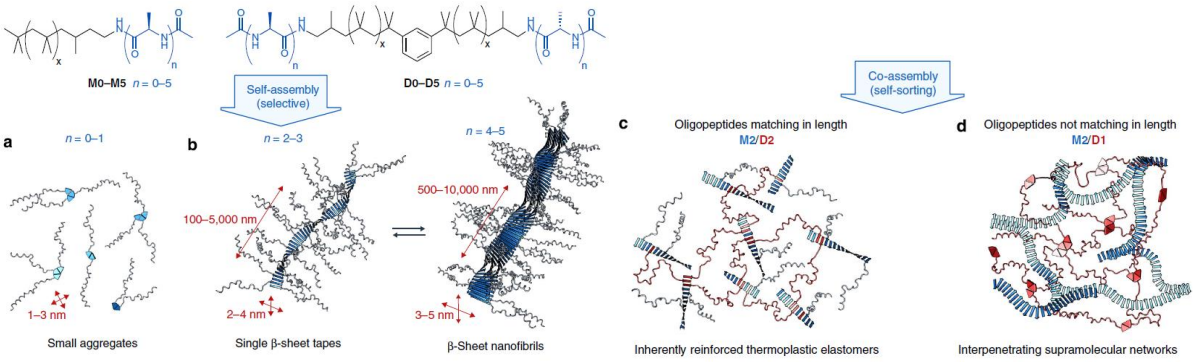

Figure 20. Self-assembly of oligopeptide-modified polyisobutylene into (a) small hydrogen-bonded aggregates or (b) stacked β-sheet fibrils and tapes, which in blends of molecules with different oligopeptide termini leads to the formation of (c) inherently reinforced thermoplastic elastomers or (d) interpenetrating supramolecular networks. (reprinted from ref. [231]).

Electrostatic interactions

Several examples of materials held together by electrostatic interactions are reported based on mixtures of ionomers with randomly distributed positively and negatively charged groups. Different types of ionomers and their self-healing behavior were reported by Van der Zwaag and Varley.[233-236] Commercially available poly(ethylene-*co*-methacrylic acid) was mixed with zinc stearate, resulting in a material with ionic clusters that could self-heal after ballistic penetration through a combination of elastic and viscous behavior. Lyon prepared self-healing films of sodium poly(styrenesulfonate) and poly(allylamine hydrochloride).[237] Frisch and coworkers showed polyelectrolyte complexes made from mixing poly(allylamine hydrochloride) and poly(acrylic acid sodium salt).[238, 239]

Matsushita reported polymer blends made from carboxylic acid-terminated PDMS and hyperbranched polyethyleneimine (PEI).[240] Mixing the two liquid polymers together resulted in a large increase in viscosity, due to the charge interaction, and SAXS revealed a nanophase-separated morphology.

Valentin reported an elastomer based on carboxylated nitrile rubber mixed with magnesium oxide.[241] Ionic clusters were formed that behaved as dynamic crosslinks in the material, and an increase in the amount of MgO to beyond stoichiometric led to a larger amount of smaller ionic clusters compared to stoichiometric ratio and an increase in the transition temperature of the ionic clusters. A small amount of covalent crosslinks was used to improve the properties of the material at higher temperatures.[242]

Rozes reported a PBA-based material, in which BA was copolymerized with a sulfonate acrylamide-functionalized butyltin oxo-cluster macrocation.[243] Ionic interactions between the cation and sulfonate groups provided supramolecular crosslinks that gave elastomeric properties to the material, similar to covalently crosslinked PBA. Slow healing of the sample after damage was observed at room temperature, and could be sped up with increasing temperature.

A supramolecular material consisting of α,ω-sulfonated polystyrene and α,ω-amino-polyisobutylene was shown by Weiss and coworkers.[244] Ionic interaction between the end groups led to the formation of a supramolecular multiblock copolymer from which free-standing flexible films could be made.

Xu showed a material prepared from polybutadiene, in which polymers functionalized with carboxylic acid and primary amine groups via thiol-ene reactions were mixed together in stoichiometric amounts.[245] This material was studied both with and without the addition of a covalent trifunctional crosslinker. Covalent crosslinking improved the mechanical properties of the material and increased the T_g, while decreasing the self-healing ability. Shape memory of the covalently linked materials was also shown and proposed to arise from thermal locking of the ionic bonds in their new position, while breaking them at higher temperatures to restore the original shape.

Furusho reported a material formed by blending telechelic carboxylic acid-terminated polybutadiene and polyamidine with multiple *N,N*-di-substituted acetamidine groups.[246] Charge interaction between the carboxylic acid and amidine groups led to solid network formation, which was not seen when the polyamidine was exchanged for PEI.

Grinstaff reported supramolecular ionic networks made from low molecular weight species, specifically a phosphonium dication and EDTA as tetraanion.[247] Addition of EDTA to the dication formed an ionic liquid with a 12x increase in viscosity, which was not observed when using structural analogs of the compounds with fewer charges. A mixture of phosphonium dication with *p*-tetracarboxy tetraphenyl porphine also gave a higher viscosity material, from which fibers could be formed and studied with SEM.

An oligomer-based self-healing material based on ionic interactions was shown by Mecerreyes.[248, 249] The material was made by mixing low molecular weight (di-/tri-)carboxylic acids and (di-/tri-)alkyl amines, which are held together by a combination of ionic interactions and hydrogen bonds. The viscoelastic gel-like material could be healed fast by heating to 50 °C or slowly at room temperature.

Heinrich and colleagues recently reported bromobutyl rubber that was functionalized with imidazolium groups.[250] The resulting ionically crosslinked rubber showed a higher elastic modulus, indicating a higher degree of cross-linking, than conventionally sulfur-cured bromobutyl rubber, with a higher stretchability and tensile strength. The ionic crosslinks were broken at temperatures above 130 °C, and cut samples could be healed over several days at room temperature, which was shortened by increasing the temperature to 100 °C for the first ten minutes of the healing.

Metal coordination

Polymer networks based on terpyridine complexes were reported by Schubert.[251] A terpyridine methacrylate was copolymerized via RAFT with methyl methacrylate (MMA), butyl methacrylate (BMA) and lauryl methacrylate (LMA) in a 1:9 ratio, chosen for their different T_gs. The polymers were crosslinked by adding iron(II) to the polymer solution and drying it to form a film. Scratches in the films could be healed by heating the PBMA or PLMA material to 100 °C, while the PMMA did not show self-healing. These polymers were also crosslinked with cadmium(II) and different counterions.[252] An effect of the size of the counterions on the self-healing was not found, but cadmium(II) acetate-containing networks showed better self-healing than the other investigated cadmium salts. LMA physically crosslinked with triazole pyridine ligands and iron(II) and Co(II) salts was also reported.[253] Self-healing was studied at elevated temperatures, with $FeCl_2$ and $CoCl_2$ showing the best results.

Also by the group of Schubert, histidine-based monomers were copolymerized with BMA and LMA and crosslinked with zinc ions.[254] Polymers crosslinked with $Zn(NO_3)_2$ showed self-healing at lower temperatures than those cross-linked with $ZnCl_2$, with $Zn(OAc)_2$ needing the highest temperatures, which was explained by a stronger binding between zinc and acetate compared to chloride or nitrate.

Xiong reported a thermoplastic elastomer formed by PSt-*b*-polyisoprene (PSt-*b*-PI), which was synthesized via anionic polymerization and terminated with terpyridine.[255] Complexes were formed with Fe(II), Zn(II) and Co(II) in solution and purified by precipitation and drying under vacuum. The metal-ligand complexes phase-separated from the polymer matrix into clusters, which could be observed by TEM, in addition to the phase separation between the hard PSt and softer PI. Stress-strain curves showed the differences in mechanical properties between the different materials, of which the Zn(II)-crosslinked material was clearly weaker than the other two due to weaker supramolecular interactions.

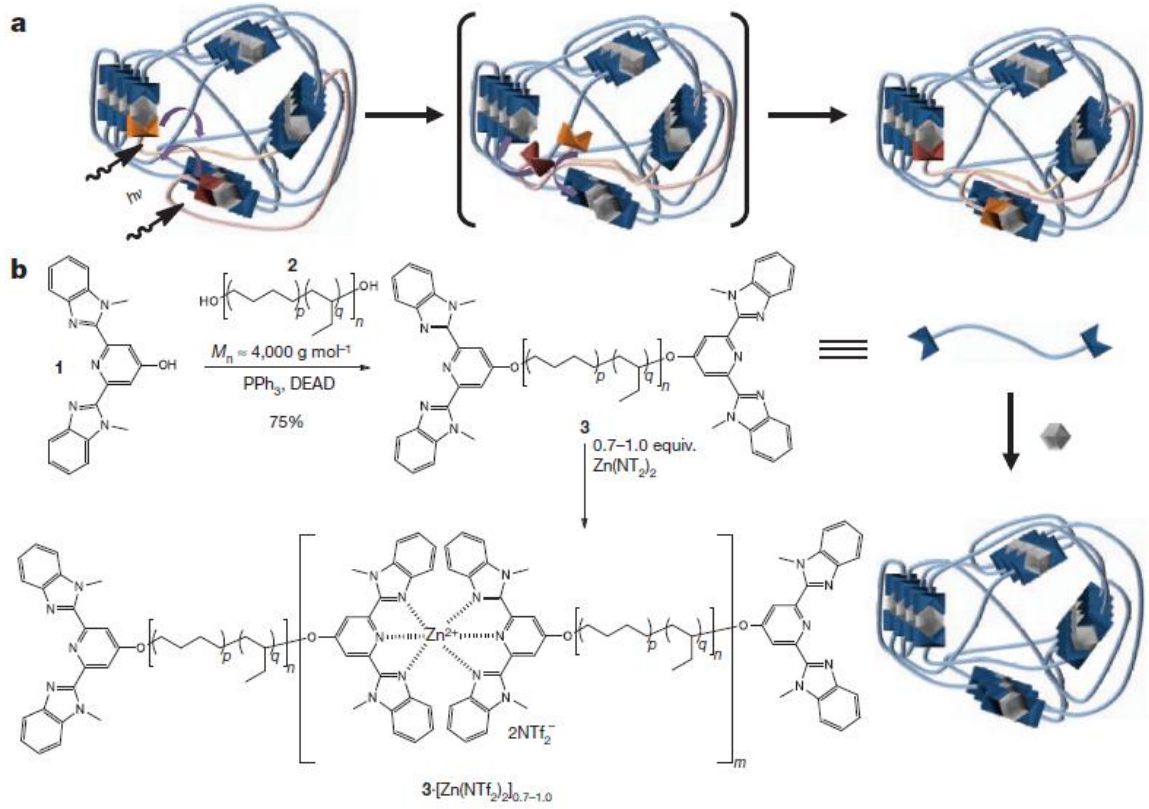

Figure 21. a: Optical healing of metallosupramolecular network, b: polymer synthesis and crosslinking by Zn(II) (reprinted from ref. [256]).

A metallosupramolecular polymer material that can self-heal under the influence of light was shown by Rowan and Weder (Figure 21).[256] The polymers consisted of a poly(ethylene-*co*-butylene) with 2,6-bis(19-methylbenzimidazolyl)pyridine (Mebip), which can coordinate with different metal ions, at both ends. The polymer was mixed with $Zn(NTf_2)_2$ in solution and upon evaporation resulted in elastic films, in which the hydrophobic low T_g polymer core was phase separated from the higher T_g Mebip domains in a lamellar morphology. Irradiation with UV light provided enough local heat to break the Mebip-Zn(II) complexes, resulting in mobility in the material that could heal damage. Crosslinking the polymers with $La(NTf_2)_3$ yielded more labile and dynamic complexes and better self-healing efficiency.

Guan has shown a self-healing thermoplastic elastomer in which a zinc-imidazole interaction provided dynamic crosslinks in a phase-separated material.[257] The material consisted of brush copolymers with a polystyrene backbone and poly(butyl acrylate-*stat*-imidazole acrylate) brushes. The bulk material microphase separated into hard PSt spheres in a softer PBA matrix, in which the polymers were connected by multiple zinc-imidazole interactions. The mechanical properties of the material could be tuned by changing the ratios of the three monomers and the amount of zinc, and full healing of a cut sample was obtained in three hours at room temperature.

Li has shown a material consisting of PTHF containing multiple 2,6-bis(1,2,3-triazol-4-yl)pyridine (BTP) units in the backbone of the polymer.[258] Two BTP ligands interact with one zinc(II) ion, while three BTPs are needed for europium(III) or terbium(III) to form kinetically labile metal-ligand complexes. Gels were formed when metal ions were added to a solution containing the polymer, which were then dried to form solid films, which showed weakly crosslinked behavior and self-healing.

Urban reported a supramolecular network formed by PEI crosslinked with Cu(II).[259] A scratch or cut in the material could be healed by exposing it to UV light for 3 hours. This healing was attributed to a square-planar to tetrahedral rearrangement of the metal-ligand coordination. Weak networks were formed by mixing PEG and $NiCl_2$ in MeOH, which were studied by Bailly and coworkers.[260, 261]

Host-guest interaction

While host-guest interactions are often used in supramolecular gels, it is less suitable for bulk materials. This is likely because of limited chain mobility in bulk compared to in solution, which limits the ability of host and guest molecules to approach each other close enough to from a complex as well as a decrease in the predominantly hydrophobic driving force. Lui reported a material consisting of poly(glycidyl methacrylate) modified with ferrocene groups, which was crosslinked with a difunctional β-cyclodextrin derivative.[262] The two components were mixed in DMF and complexation yielded an insoluble material. The complex between ferrocene and cyclodextrin could be broken by treating the material with an electrical current and the crosslinks reformed slowly over time. The ability to break and reform the crosslinks was shown to lead to electrically driven self-healing, which was increased with thermal treatment.

π-π stacking

π-π stacking is also scarcely used in supramolecular bulk materials. Colquhoun, Hayes and coworkers reported several supramolecular materials crosslinked by π-π stacking interactions. Their first paper on this topic reports a material in which pyrenyl end-functionalized polyamide was mixed with polyimide that contained chain-folding triethylenedioxy–diimide motifs.[263] Stacks of the pyrenyl groups in between the imide groups were formed by π-π interactions, evident by a color change, which formed the crosslinked network. Self-healing was shown at 87 °C by reversible dissociation of the stacks. Mixtures of chain-folding polyimide with pyrenyl-functionalized polyurethane resulted in a healable elastomer with a nanophase-separated morphology.[264] Divalent and trivalent PEG-based polymers with pyrenyl end groups were blended with a copolymer containing chain-folding naphthalene–diimide residues and a 2,2'-(ethylenedioxy)bis(ethylamine) derived linker, forming tough elastomeric solids (Figure 22).[265, 266] The material prepared with the trivalent polymers showed a higher tensile modulus compared to the divalent polymers, attributed to the higher crosslinking density. Self-healing of a polymer film was shown at 100 °C, with completely homogeneous healing of the damage site at 200 °C.

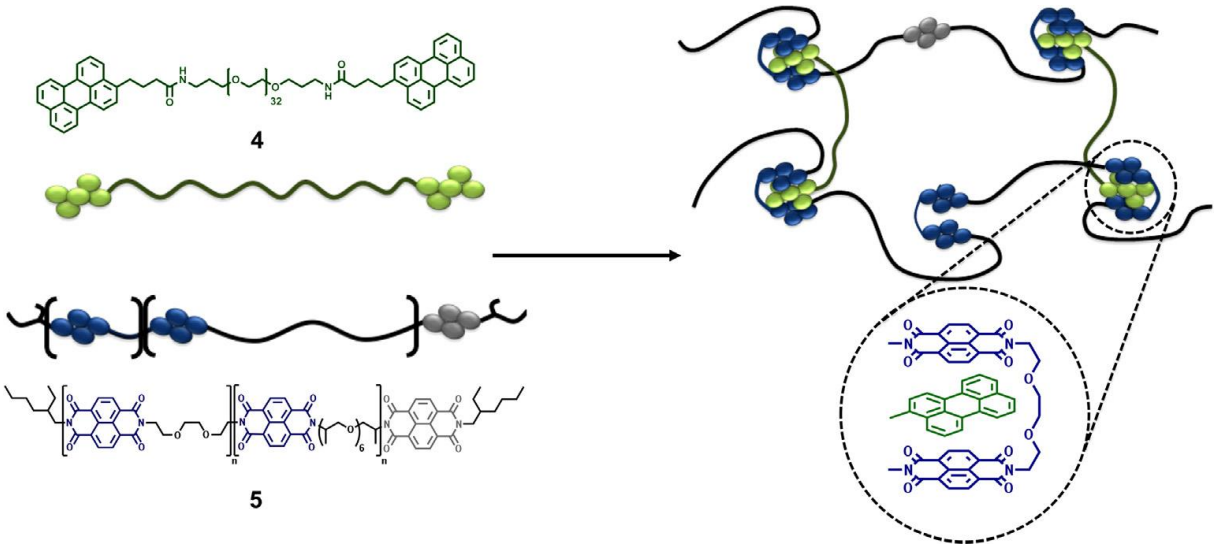

Figure 22. Perylene-terminated polymer (4), chain-folding polydiimide (5) and their supramolecular blend, showing the π-π stacking interactions (reprinted from ref [266]).

Phase separation

Most materials that are kept together solely by phase separation between different blocks are thermoplastic elastomers with a hard block – soft block – hard block copolymer structure in which the hard and soft blocks are immiscible, inducing microphase separation and physical crosslinking. Commercially available examples of this are styrene-butadiene-styrene block copolymers[267, 268] and thermoplastic polyurethane.[269] As many materials are based on these, the examples discussed here only present a small part of the recent work on these types of materials.

Several different thermoplastic elastomers, consisting of polyvinyl ether based ABA-triblock copolymers with hard outer segments and soft inner segments, were shown by Sakaguchi and colleages.[270-272] The hard segments were formed by either poly(tricyclodecyl vinyl ether) or poly(2-adamantyl vinyl ether), while the soft segments were formed by poly(*n*-butyl vinyl ether)- poly(6-acetoxyhexyl vinyl ether), poly(6-hydroxyhexyl vinyl ether), or poly(2-(2-methoxyethoxy)ethyl vinyl ether), all synthesized via cationic polymerization. In all materials a phase-separated microstructure was shown with TEM, and two separate T_gs for the harder and softer segments and elastomeric properties at temperatures in between the two T_gs were observed with DSC and DMA.

Zentel showed a functionalized SBS rubber, in which RAFT-synthesized PNIPAM was coupled to the butadiene groups via a thiol-ene reaction.[273] The polar PNIPAM formed microdomains within the apolar polybutadiene matrix, and the temperature-responsiveness of PNIPAM led to a hydrophilic material at lower temperatures with an increase in the contact angle of water at higher temperatures.

Ricci reported a new type of polymer synthesis for thermoplastic elastomers catalyzed by α-diimine Ni(II)/Et_2AlCl, to synthesize semi-crystalline polymers with a low T_g of 1-dodecene, 1-hexene and 1-octene.[274] An ABA-triblock copolymer of poly(1-dodecene) as A block and the amorphous polyethylene as B block, as well as AB diblock copolymers, all showed thermoplastic elastomer behavior.

A thermoplastic elastomer made from an ABA-triblock copolymer with a polyisobutylene middle block and alloocimene end blocks was reported by Roland.[275] The alloocimene formed glassy phase-separated domains at room temperature, which beside crosslinking the material also acted as reinforcing fillers. Mixing of the phases was observed above the T_g of the alloocimene.

Kramer reported a series of thermoplastic elastomers based on asymmetrical linear and star block copolymers of PSt and polyisopreen.[276] Different morphologies were obtained depending on the volume fraction of PSt and the polymer structure, with lamellar morphology for linear block copolymers with f_{PSt} = 0.4 and 0.5 and miktoarm block copolymers with f_{PSt} = 0.7, and cylindrical morphology at f_{PSt} = 0.4 and 0.5 for the miktoarms. Tensile testing revealed that the miktoarms with cylindrical morphology had very good elastic recovery, even with such a high fraction of PSt, showing that these star polymer structures can be useful for creating tougher and stronger elastomers compared to the linear analogues.

A PBA-based supramolecular elastomer was shown by Bazuin.[277] An ABA-triblock copolymer with PBA as middle block and quarternized poly(dimethylaminoethyl methacrylate) was synthesized and complexated with methyl orange, inducing a phase separation between soft PBA and hard Q-PDMAEAMA/MO phases which was observed by two T_gs in DSC. Samples with 18 to 29 wt% of hard block content showed elasticity and AFM and TEM suggested a mixed spherical/cylindrical morphology for samples with 18-22 % hard blocks, mixed cylindrical/lamellar morphology for 29 % hard blocks and continuous phases for higher content of hard blocks. UV-vis showed a reversible cis-trans photoisomerization of methyl orange.

1.3.3 Conclusions

Many types of supramolecular interactions are available for the preparation of supramolecular network materials. Hydrophobic and electrostatic interactions between groups of monomers can be used for preparing hydrogels with tunable strength by varying the polymer composition and architecture. Of these two, hydrophobic interactions seems to be the simplest approach because many different monomer combinations and polymer architectures can lead to hydrogel formation, while more careful tuning of the binding strength is needed for electrostatic interactions to prevent precipitation or full dissolution of the polymers. Metal coordination and host-guest interactions provide stimuli-responsive crosslinking for which incorporating a specific binding group on the polymer, being a ligand or host and guest molecule, is often necessary. Which type of interaction and design is most suitable depends largely on the envisioned application. Furthermore, the strength and responsiveness of the hydrogel are largely dependent on concentration, cross-linking density, chain length and polymer composition, as well as other variables such as salt concentration or presence of other compounds. Almost all supramolecular hydrogels show self-healing ability due to the reversibility of the crosslinking and high chain mobility in water.

For supramolecular bulk materials, most reported examples make use of hydrogen bonding interactions, although electrostatic interactions and metal coordination have also been used by various groups. While some examples of supramolecular bulk materials employing host-guest interactions and π-π stacking have been reported, these are highly specific and therefore not very suitable for most applications. While many of these materials show self-healing abilities, this is not always the case and the definition of what constitutes as self-healing is not always clear. Again, the most promising type of interaction is dependent on the desired properties. Multiple weak

interactions between low T_g polymers or oligomers often lead to soft or rubbery materials with self-healing ability. For harder materials, it is usually necessary to obtain a phase-separated morphology containing harder and softer phases, in which the softer phase contains the reversible supramolecular crosslinks. Often heating the material above the T_g is necessary to obtain enough chain mobility for self-healing.

However, not many examples of hard or high T_g supramolecular self-healing materials have been reported. Especially creating a hard material that possesses self-healing properties for which no external stimulus such as heat is necessary remains a challenge. In this thesis, we will try to prepare such a material based on the electrostatic interactions between oppositely charged triblock copolymers.

References

1. R. Hoogenboom, *Angew. Chem. Int. Ed.* **2012**, *51*, 11942.
2. W. A. Braunecker, K. Matyjaszewski, *Prog. Polym. Sci.* **2007**, *32*, 93.
3. J. Chiefari, Y. K. Chong, F. Ercole, J. Krstina, J. Jeffery, T. P. T. Le, R. T. A. Mayadunne, G. F. Meijs, C. L. Moad, G. Moad, E. Rizzardo, S. H. Thang, *Macromolecules* **1998**, *31*, 5559.
4. G. Moad, E. Rizzardo, S. H. Thang, *Aust. J. Chem.* **2012**, *65*, 985.
5. D. J. Keddie, G. Moad, E. Rizzardo, S. H. Thang, *Macromolecules* **2012**, *45*, 5321.
6. M. Benaglia, J. Chiefari, Y. K. Chong, G. Moad, E. Rizzardo, S. H. Thang, *J. Am. Chem. Soc.* **2009**, *131*, 6914.
7. J.-S. Wang, K. Matyjaszewski, *J. Am. Chem. Soc.* **1995**, *117*, 5614.
8. K. Matyjaszewski, T. E. Patten, J. Xia, *J. Am. Chem. Soc.* **1997**, *119*, 674.
9. K. Matyjaszewski, J. Xia, *Chem. Rev.* **2001**, *101*, 2921.
10. M. Ouchi, T. Terashima, M. Sawamoto, *Chem. Rev.* **2009**, *109*, 4963.
11. W. Tang, N. V. Tsarevsky, K. Matyjaszewski, *J. Am. Chem. Soc.* **2006**, *128*, 1598.
12. M. Kamigaito, T. Ando, M. Sawamoto, *Chem. Rev.* **2001**, *101*, 3689.
13. W. Jakubowski, K. Min, K. Matyjaszewski, *Macromolecules* **2006**, *39*, 39.
14. K. Matyjaszewski, W. Jakubowski, K. Min, W. Tang, J. Huang, W. A. Braunecker, N. V. Tsarevsky, *Proc. Natl. Acad. Sci. U. S. A.* **2006**, *103*, 15309.
15. L. Mueller, W. Jakubowski, W. Tang, K. Matyjaszewski, *Macromolecules* **2007**, *40*, 6464.
16. A. J. D. Magenau, N. C. Strandwitz, A. Gennaro, K. Matyjaszewski, *Science* **2011**, *332*, 81.
17. J. Mosnáček, M. Ilčíková, *Macromolecules* **2012**, *45*, 5859.
18. K. Matyjaszewski, N. V. Tsarevsky, *J. Am. Chem. Soc.* **2014**, *136*, 6513.
19. K. Matyjaszewski, N. V. Tsarevsky, W. A. Braunecker, H. Dong, J. Huang, W. Jakubowski, Y. Kwak, R. Nicolay, W. Tang, J. A. Yoon, *Macromolecules* **2007**, *40*, 7795.
20. D. Konkolewicz, Y. Wang, M. Zhong, P. Krys, A. A. Isse, A. Gennaro, K. Matyjaszewski, *Macromolecules* **2013**, *46*, 8749.
21. D. Konkolewicz, Y. Wang, P. Krys, M. Zhong, A. A. Isse, A. Gennaro, K. Matyjaszewski, *Polym. Chem.* **2014**, *5*, 4396.
22. C.-H. Peng, M. Zhong, Y. Wang, Y. Kwak, Y. Zhang, W. Zhu, M. Tonge, J. Buback, S. Park, P. Krys, D. Konkolewicz, A. Gennaro, K. Matyjaszewski, *Macromolecules* **2013**, *46*, 3803.
23. Y. Wang, M. Zhong, W. Zhu, C.-H. Peng, Y. Zhang, D. Konkolewicz, N. Bortolamei, A. A. Isse, A. Gennaro, K. Matyjaszewski, *Macromolecules* **2013**, *46*, 3793.
24. Y. Gao, T. Zhao, W. Wang, *RSC Adv.* **2014**, *4*, 61687.
25. F. Lorandi, M. Fantin, A. A. Isse, A. Gennaro, *Polymer* **2015**, *72*, 238.
26. V. Percec, T. Guliashvili, J. S. Ladislaw, A. Wistrand, A. Stjerndahl, M. J. Sienkowska, M. J. Monteiro, S. Sahoo, *J. Am. Chem. Soc.* **2006**, *128*, 14156.
27. R. Hoogenboom, M. A. R. Meier, U. S. Schubert, *Macromol. Rapid Commun.* **2003**, *24*, 15.
28. R. Hoogenboom, U. S. Schubert, *J. Polym. Sci., Part A: Polym. Chem.* **2003**, *41*, 2425.
29. P. Chapon, C. Mignaud, G. Lizarraga, M. Destarac, *Macromol. Rapid Commun.* **2003**, *24*, 87.

30. M. W. M. Fijten, M. A. R. Meier, R. Hoogenboom, U. S. Schubert, *J. Polym. Sci., Part A: Polym. Chem.* **2004**, *42*, 5775.
31. C. R. Becer, A. M. Groth, R. Hoogenboom, R. M. Paulus, U. S. Schubert, *QSAR Comb. Sci.* **2008**, *27*, 977.
32. C. Guerrero-Sanchez, L. O'Brien, C. Brackley, D. J. Keddie, S. Saubern, J. Chiefari, *Polym. Chem.* **2013**, *4*, 1857.
33. J. J. Haven, C. Guerrero-Sanchez, D. J. Keddie, G. Moad, *Macromol. Rapid Commun.* **2014**, *35*, 492.
34. J. Haven, C. Guerrero-Sanchez, D. Keddie, G. Moad, S. Thang, U. S. Schubert, *Polym. Chem.* **2014**, *5*, 5236.
35. H. Zhang, M. W. M. Fijten, R. Hoogenboom, R. Reinierkens, U. S. Schubert, *Macromol. Rapid Commun.* **2003**, *24*, 81.
36. H. Zhang, H. Abeln Caroline, W. M. Fijten Martin, S. Schubert Ulrich, *e-Polym.* **2006**, *6*, 90.
37. T. M. Eggenhuisen, C. R. Becer, M. W. M. Fijten, R. Eckardt, R. Hoogenboom, U. S. Schubert, *Macromolecules* **2008**, *41*, 5132.
38. R. Hoogenboom, M. W. M. Fijten, M. A. R. Meier, U. S. Schubert, *Macromol. Rapid Commun.* **2003**, *24*, 92.
39. R. Hoogenboom, M. W. M. Fijten, C. Brändli, J. Schroer, U. S. Schubert, *Macromol. Rapid Commun.* **2003**, *24*, 98.
40. P. Wei, X. Yan, F. Huang, *Chem. Soc. Rev.* **2015**, *44*, 815.
41. S. K. Yang, A. V. Ambade, M. Weck, *Chem. Soc. Rev.* **2011**, *40*, 129.
42. T. Aida, E. W. Meijer, S. I. Stupp, *Science* **2012**, *335*, 813.
43. L. Yang, X. Tan, Z. Wang, X. Zhang, *Chem. Rev.* **2015**, *115*, 7196.
44. S. L. Li, T. Xiao, C. Lin, L. Wang, *Chem. Soc. Rev.* **2012**, *41*, 5950.
45. S. Seiffert (Ed.), *Adv. Polym. Sci. 268: Supramolecular Polymer Networks and Gels* (Springer, 2015).
46. B. Rybtchinski, *ACS Nano* **2011**, *5*, 6791.
47. S. Seiffert, J. Sprakel, *Chem. Soc. Rev.* **2012**, *41*, 909.
48. X. Yan, F. Wang, B. Zheng, F. Huang, *Chem. Soc. Rev.* **2012**, *41*, 6042.
49. J.-Y. Sun, X. Zhao, W. R. K. Illeperuma, O. Chaudhuri, K. H. Oh, D. J. Mooney, J. J. Vlassak, Z. Suo, *Nature* **2012**, *489*, 133.
50. A. B. South, L. A. Lyon, *Angew. Chem. Int. Ed.* **2010**, *49*, 767.
51. D. C. Tuncaboylu, A. Argun, M. P. Algi, O. Okay, *Polymer* **2013**, *54*, 6381.
52. J. T. Auletta, G. J. LeDonne, K. C. Gronborg, C. D. Ladd, H. Liu, W. W. Clark, T. Y. Meyer, *Macromolecules* **2015**, *48*, 1736.
53. L. Yu, J. Ding, *Chem. Soc. Rev.* **2008**, *37*, 1473.
54. J. Boekhoven, S. I. Stupp, *Adv. Mater.* **2014**, *26*, 1642.
55. H. Liu, C. Xiong, Z. Tao, Y. Fan, X. Tang, H. Yang, *RSC Adv.* **2015**, *5*, 33083.
56. E. A. Appel, J. del Barrio, X. J. Loh, O. A. Scherman, *Chem. Soc. Rev.* **2012**, *41*, 6195.
57. A. Noro, M. Hayashi, Y. Matsushita, *Soft Matter* **2012**, *8*, 6416.
58. C. Tsitsilianis, *Soft Matter* **2010**, *6*, 2372.
59. M. de Loos, B. L. Feringa, J. H. van Esch, *Eur. J. Org. Chem.* **2005**, *2005*, 3615.
60. L. E. Buerkle, S. J. Rowan, *Chem. Soc. Rev.* **2012**, *41*, 6089.
61. R. G. Weiss, *J. Am. Chem. Soc.* **2014**, *136*, 7519.
62. X. Yu, L. Chen, M. Zhang, T. Yi, *Chem. Soc. Rev.* **2014**, *43*, 5346.
63. E. Krieg, B. Rybtchinski, *Chem. - Eur. J.* **2011**, *17*, 9016.
64. C. T. Huynh, M. K. Nguyen, D. S. Lee, *Macromolecules* **2011**, *44*, 6629.
65. R. Dong, Y. Pang, Y. Su, X. Zhu, *Biomater. Sci.* **2015**, *3*, 937.
66. H. Wang, S. C. Heilshorn, *Adv. Mater.* **2015**, *27*, 3717.
67. D. Wang, G. Tong, R. Dong, Y. Zhou, J. Shen, X. Zhu, *Chem. Commun.* **2014**, *50*, 11994.
68. N. M. Sangeetha, U. Maitra, *Chem. Soc. Rev.* **2005**, *34*, 821.
69. T. Annable, R. Buscall, R. Ettelaie, D. Whittlestone, *J. Rheol.* **1993**, *37*, 695.

70. V. Tirtaatmadja, K. C. Tam, R. D. Jenkins, *Macromolecules* **1997**, *30*, 3271.
71. R. D. Jenkins, C. A. Silebi, M. S. El-Aasser, in *Polymers as Rheology Modifiers*. (American Chemical Society, 1991), vol. 462, chap. 13, pp. 222.
72. J. Sprakel, E. Spruijt, M. A. Cohen Stuart, N. A. M. Besseling, M. P. Lettinga, J. van der Gucht, *Soft Matter* **2008**, *4*, 1696.
73. L. E. Bromberg, D. P. Barr, *Macromolecules* **1999**, *32*, 3649.
74. A. C. Lara-Ceniceros, C. Rivera-Vallejo, E. J. Jiménez-Regalado, *Polym. Bull.* **2007**, *58*, 425.
75. C. Tsitsilianis, I. Iliopoulos, G. Ducouret, *Macromolecules* **2000**, *33*, 2936.
76. C. Tsitsilianis, I. Iliopoulos, *Macromolecules* **2002**, *35*, 3662.
77. F. Bossard, T. Aubry, G. Gotzamanis, C. Tsitsilianis, *Soft Matter* **2006**, *2*, 510.
78. G. T. Gotzamanis, C. Tsitsilianis, S. C. Hadjiyannakou, C. S. Patrickios, R. Lupitskyy, S. Minko, *Macromolecules* **2006**, *39*, 678.
79. N. Stavrouli, T. Aubry, C. Tsitsilianis, *Polymer* **2008**, *49*, 1249.
80. S. Pispas, D. Vlassopoulos, G. Fytas, B. Loppinet, N. Hadjichristidis, *Polymer* **2006**, *47*, 7302.
81. H. Niu, F. Wang, R. A. Weiss, *Macromolecules* **2015**, *48*, 645.
82. A. Miasnikova, A. Laschewsky, G. De Paoli, C. M. Papadakis, P. Müller-Buschbaum, S. S. Funari, *Langmuir* **2012**, *28*, 4479.
83. A. Bivigou-Koumba, E. Görnitz, A. Laschewsky, P. Müller-Buschbaum, C. Papadakis, *Colloid Polym. Sci.* **2010**, *288*, 499.
84. P. Kujawa, H. Watanabe, F. Tanaka, F. M. Winnik, *Eur. Phys. J. E* **2005**, *17*, 129.
85. A. Klymenko, T. Nicolai, L. Benyahia, C. Chassenieux, O. Colombani, E. Nicol, *Macromolecules* **2014**, *47*, 8386.
86. V. Kadam, T. Nicolai, E. Nicol, L. Benyahia, *Macromolecules* **2011**, *44*, 8225.
87. C. Charbonneau, C. Chassenieux, O. Colombani, T. Nicolai, *Macromolecules* **2011**, *44*, 4487.
88. C. Charbonneau, T. Nicolai, C. Chassenieux, O. Colombani, M. Miriam de Souza Lima, *React. Funct. Polym.* **2013**, *73*, 965.
89. A. Shedge, O. Colombani, T. Nicolai, C. Chassenieux, *Macromolecules* **2014**, *47*, 2439.
90. M. A. Ward, T. K. Georgiou, *J. Polym. Sci., Part A: Polym. Chem.* **2010**, *48*, 775.
91. M. A. Ward, T. K. Georgiou, *J. Polym. Sci., Part A: Polym. Chem.* **2013**, *51*, 2850.
92. C. Li, Y. Tang, S. P. Armes, C. J. Morris, S. F. Rose, A. W. Lloyd, A. L. Lewis, *Biomacromolecules* **2005**, *6*, 994.
93. S. A. Angelopoulos, C. Tsitsilianis, *Macromol. Chem. Phys.* **2006**, *207*, 2188.
94. T. Vermonden, N. A. M. Besseling, M. J. van Steenbergen, W. E. Hennink, *Langmuir* **2006**, *22*, 10180.
95. T. Vermonden, S. S. Jena, D. Barriet, R. Censi, J. van der Gucht, W. E. Hennink, R. A. Siegel, *Macromolecules* **2010**, *43*, 782.
96. J. Madsen, S. P. Armes, A. L. Lewis, *Macromolecules* **2006**, *39*, 7455.
97. A. Nykänen, M. Nuopponen, A. Laukkanen, S.-P. Hirvonen, M. Rytelä, O. Turunen, H. Tenhu, R. Mezzenga, O. Ikkala, J. Ruokolainen, *Macromolecules* **2007**, *40*, 5827.
98. X. Zhao, W. Liu, D. Chen, X. Lin, W. W. Lu, *Macromol. Chem. Phys.* **2007**, *208*, 1773.
99. K. Skrabania, W. Li, A. Laschewsky, *Macromol. Chem. Phys.* **2008**, *209*, 1389.
100. A. P. Vogt, B. S. Sumerlin, *Soft Matter* **2009**, *5*, 2347.
101. A. Kelarakis, V. Havredaki, X.-F. Yuan, Y.-W. Yang, C. Booth, *J. Mater. Chem.* **2003**, *13*, 2779.
102. A. Kelarakis, V. Havredaki, X.-F. Yuan, C. Chaibundit, C. Booth, *Macromol. Chem. Phys.* **2006**, *207*, 903.
103. V. Castelletto, I. W. Hamley, X. F. Yuan, A. Kelarakis, C. Booth, *Soft Matter* **2005**, *1*, 138.
104. L. Li, B. Yan, J. Yang, L. Chen, H. Zeng, *Adv. Mater.* **2015**, *27*, 1294.
105. Y. Zhou, K. Jiang, Q. Song, S. Liu, *Langmuir* **2007**, *23*, 13076.
106. Z. Ge, Y. Zhou, Z. Tong, S. Liu, *Langmuir* **2011**, *27*, 1143.
107. D. C. Tuncaboylu, M. Sahin, A. Argun, W. Oppermann, O. Okay, *Macromolecules* **2012**, *45*, 1991.
108. D. C. Tuncaboylu, M. Sari, W. Oppermann, O. Okay, *Macromolecules* **2011**, *44*, 4997.

109. D. C. Tuncaboylu, A. Argun, M. Sahin, M. Sari, O. Okay, *Polymer* **2012**, *53*, 5513.
110. G. Akay, A. Hassan-Raeisi, D. C. Tuncaboylu, N. Orakdogen, S. Abdurrahmanoglu, W. Oppermann, O. Okay, *Soft Matter* **2013**, *9*, 2254.
111. A. Argun, M. Algi, D. Tuncaboylu, O. Okay, *Colloid Polym. Sci.* **2013**, 1.
112. U. Gulyuz, O. Okay, *Soft Matter* **2013**, *9*, 10287.
113. U. Gulyuz, O. Okay, *Macromolecules* **2014**, *47*, 6889.
114. M. P. Algi, O. Okay, *Eur. Polym. J.* **2014**, *59*, 113.
115. V. Percec, T. K. Bera, R. J. Butera, *Biomacromolecules* **2002**, *3*, 272.
116. Y.-K. Li, C.-G. Guo, L. Wang, Y. Xu, C.-y. Liu, C.-Q. Wang, *RSC Adv.* **2014**, *4*, 55133.
117. M. S. Thompson, M. V. Tsurkan, K. Chwalek, M. Bornhauser, M. Schlierf, C. Werner, Y. Zhang, *Chem. - Eur. J.* **2015**, *21*, 3178.
118. N. Oyama, H. Minami, D. Kawano, M. Miyazaki, T. Maeda, K. Toma, A. Hotta, K. Nagahama, *Biomater. Sci.* **2014**, *2*, 1057.
119. K. Nagahama, D. Kawano, N. Oyama, A. Takemoto, T. Kumano, J. Kawakami, *Biomacromolecules* **2015**, *16*, 880.
120. E. A. Appel, M. W. Tibbitt, M. J. Webber, B. A. Mattix, O. Veiseh, R. Langer, *Nat. Commun.* **2015**, *6*.
121. J. Cui, A. d. Campo, *Chem. Commun.* **2012**, *48*, 9302.
122. P. Y. W. Dankers, T. M. Hermans, T. W. Baughman, Y. Kamikawa, R. E. Kieltyka, M. M. C. Bastings, H. M. Janssen, N. A. J. M. Sommerdijk, A. Larsen, M. J. A. van Luyn, A. W. Bosman, E. R. Popa, G. Fytas, E. W. Meijer, *Adv. Mater.* **2012**, *24*, 2703.
123. M. Guo, L. M. Pitet, H. M. Wyss, M. Vos, P. Y. W. Dankers, E. W. Meijer, *J. Am. Chem. Soc.* **2014**, *136*, 6969.
124. T. V. Chirila, H. H. Lee, M. Oddon, M. M. L. Nieuwenhuizen, I. Blakey, T. M. Nicholson, *J. Appl. Polym. Sci.* **2014**, *131*.
125. M. M. E. Koenigs, A. Pal, H. Mortazavi, G. M. Pawar, C. Storm, R. P. Sijbesma, *Macromolecules* **2014**, *47*, 2712.
126. H. D. Lu, M. B. Charati, I. L. Kim, J. A. Burdick, *Biomaterials* **2012**, *33*, 2145.
127. X. Xing, L. Li, T. Wang, Y. Ding, G. Liu, G. Zhang, *J. Mater. Chem. A* **2014**, *2*, 11049.
128. L. Zhang, J. Wu, N. Sun, X. Zhang, L. Jiang, *J. Mater. Chem. A* **2014**, *2*, 7666.
129. X. Dai, Y. Zhang, L. Gao, T. Bai, W. Wang, Y. Cui, W. Liu, *Adv. Mater.* **2015**, *27*, 3566.
130. G. Gao, G. Du, Y. Sun, J. Fu, *ACS Appl. Mater. Interfaces* **2015**, *7*, 5029.
131. S. Zhang, A. M. Bellinger, D. L. Glettig, R. Barman, Y.-A. L. Lee, J. Zhu, C. Cleveland, V. A. Montgomery, L. Gu, L. D. Nash, D. J. Maitland, R. Langer, G. Traverso, *Nat. Mater.* **2015**.
132. H. Yoon, E. J. Dell, J. Freyer, L. M. Campos, W.-D. Jang, *Polymer* **2014**, *55*, 453.
133. S. R. Van Tomme, M. J. van Steenbergen, S. C. De Smedt, C. F. van Nostrum, W. E. Hennink, *Biomaterials* **2005**, *26*, 2129.
134. T. L. Sun, T. Kurokawa, S. Kuroda, A. B. Ihsan, T. Akasaki, K. Sato, M. A. Haque, T. Nakajima, J. P. Gong, *Nat. Mater.* **2013**, *12*, 932.
135. F. Luo, T. L. Sun, T. Nakajima, T. Kurokawa, Y. Zhao, K. Sato, A. B. Ihsan, X. Li, H. Guo, J. P. Gong, *Adv. Mater.* **2015**, *27*, 2722.
136. T. Bai, S. Liu, F. Sun, A. Sinclair, L. Zhang, Q. Shao, S. Jiang, *Biomaterials* **2014**, *35*, 3926.
137. Y. Huang, P. G. Lawrence, Y. Lapitsky, *Langmuir* **2014**, *30*, 7771.
138. H. Srour, O. Ratel, M. Leocmach, E. A. Adams, S. Denis-Quanquin, V. Appukuttan, N. Taberlet, S. Manneville, J.-C. Majesté, C. Carrot, C. Andraud, C. Monnereau, *Macromol. Rapid Commun.* **2015**, *36*, 55.
139. Q. Wang, J. L. Mynar, M. Yoshida, E. Lee, M. Lee, K. Okuro, K. Kinbara, T. Aida, *Nature* **2010**, *463*, 339.
140. J. N. Hunt, K. E. Feldman, N. A. Lynd, J. Deek, L. M. Campos, J. M. Spruell, B. M. Hernandez, E. J. Kramer, C. J. Hawker, *Adv. Mater.* **2011**, *23*, 2327.
141. D. V. Krogstad, N. A. Lynd, S.-H. Choi, J. M. Spruell, C. J. Hawker, E. J. Kramer, M. V. Tirrell, *Macromolecules* **2013**, *46*, 1512.

142. J. H. Ortony, S.-H. Choi, J. M. Spruell, J. N. Hunt, N. A. Lynd, D. V. Krogstad, V. S. Urban, C. J. Hawker, E. J. Kramer, S. Han, *Chem. Sci.* **2014**, *5*, 58.
143. M. Lemmers, J. Sprakel, I. K. Voets, J. van der Gucht, M. A. Cohen Stuart, *Angew. Chem.* **2010**, *122*, 720.
144. H. Wei, S. Du, Y. Liu, H. Zhao, C. Chen, Z. Li, J. Lin, Y. Zhang, J. Zhang, X. Wan, *Chem. Commun.* **2014**, *50*, 1447.
145. D. Cross, X. Jiang, W. Ji, W. Han, C. Wang, *Macromol. Biosci.* **2015**, *15*, 668.
146. J. Li, Z. Su, H. Xu, X. Ma, J. Yin, X. Jiang, *Macromolecules* **2015**, *48*, 2022.
147. U. S. Schubert, C. Eschbaumer, *Angew. Chem. Int. Ed.* **2002**, *41*, 2892.
148. R. Dobrawa, F. Würthner, *J. Polym. Sci., Part A: Polym. Chem.* **2005**, *43*, 4981.
149. C. A. Fustin, P. Guillet, U. S. Schubert, J. F. Gohy, *Adv. Mater.* **2007**, *19*, 1665.
150. J. Brassinne, C.-A. Fustin, J.-F. Gohy, *J. Inorg. Organomet. Polym. Mater.* **2013**, *23*, 24.
151. Y. Chujo, K. Sada, T. Saegusa, *Macromolecules* **1993**, *26*, 6315.
152. Y. Chujo, K. Sada, T. Saegusa, *Macromolecules* **1993**, *26*, 6320.
153. Y. Chujo, K. Sada, T. Saegusa, *Polym. J.* **1993**, *25*, 599.
154. S. J. Buwalda, P. J. Dijkstra, J. Feijen, *J. Polym. Sci., Part A: Polym. Chem.* **2012**, *50*, 1783.
155. T.-A. Asoh, H. Yoshitake, Y. Takano, A. Kikuchi, *Macromol. Chem. Phys.* **2013**, *214*, 2534.
156. T. Rossow, S. Seiffert, *Polym. Chem.* **2014**, *5*, 3018.
157. F. D. Jochum, J. Brassinne, C.-A. Fustin, J.-F. Gohy, *Soft Matter* **2013**, *9*, 2314.
158. J. Brassinne, A. M. Stevens, E. Van Ruymbeke, J.-F. Gohy, C.-A. Fustin, *Macromolecules* **2013**, *46*, 9134.
159. J. Brassinne, J.-P. Bourgeois, C.-A. Fustin, J.-F. Gohy, *Soft Matter* **2014**, *10*, 3086.
160. J. Brassinne, J.-F. Gohy, C.-A. Fustin, *Macromolecules* **2014**, *47*, 4514.
161. M. Gerth, M. Bohdan, R. Fokkink, I. Voets, J. van der Gucht, J. Sprakel, *Macromol. Rapid Commun.* **2014**, *35*, 2065.
162. K. Kawamoto, S. C. Grindy, J. Liu, N. Holten-Andersen, J. A. Johnson, *ACS Macro Lett.* **2015**, 458.
163. B. P. Lee, J. L. Dalsin, P. B. Messersmith, *Biomacromolecules* **2002**, *3*, 1038.
164. N. Holten-Andersen, M. J. Harrington, H. Birkedal, B. P. Lee, P. B. Messersmith, K. Y. C. Lee, J. H. Waite, *Proc. Natl. Acad. Sci. U. S. A.* **2011**, *108*, 2651.
165. M. J. Harrington, A. Masic, N. Holten-Andersen, J. H. Waite, P. Fratzl, *Science* **2010**, *328*, 216.
166. M. Krogsgaard, M. A. Behrens, J. S. Pedersen, H. Birkedal, *Biomacromolecules* **2013**, *14*, 297.
167. M. Krogsgaard, A. Andersen, H. Birkedal, *Chem. Commun.* **2014**, *50*, 13278.
168. R. J. Sundberg, R. B. Martin, *Chem. Rev.* **1974**, *74*, 471.
169. M. J. Harrington, J. H. Waite, *Biomacromolecules* **2008**, *9*, 1480.
170. D. E. Fullenkamp, L. He, D. G. Barrett, W. R. Burghardt, P. B. Messersmith, *Macromolecules* **2013**, *46*, 1167.
171. F. Peng, G. Li, X. Liu, S. Wu, Z. Tong, *J. Am. Chem. Soc.* **2008**, *130*, 16166.
172. Z. Sun, F. Lv, L. Cao, L. Liu, Y. Zhang, Z. Lu, *Angew. Chem. Int. Ed.* **2015**, *54*, 7944.
173. M. Zhong, X.-Y. Liu, F. Shi, L. Zhang, X. Wang, A. G. Cheetham, H. Cui, X.-M. Xie, *Soft Matter* **2015**, *11*, 4235.
174. M. Zhong, Y.-T. Liu, X.-M. Xie, *J. Mater. Chem. B* **2015**, *3*, 4001.
175. H. Frisch, P. Besenius, *Macromol. Rapid Commun.* **2015**, *36*, 346.
176. X. Ma, H. Tian, *Acc. Chem. Res.* **2014**, *47*, 1971.
177. Z. Qi, C. A. Schalley, *Acc. Chem. Res.* **2014**, *47*, 2222.
178. M. Zhang, D. Xu, X. Yan, J. Chen, S. Dong, B. Zheng, F. Huang, *Angew. Chem. Int. Ed.* **2012**, *51*, 7011.
179. S. Li, H.-Y. Lu, Y. Shen, C.-F. Chen, *Macromol. Chem. Phys.* **2013**, *214*, 1596.
180. D. Liu, D. Wang, M. Wang, Y. Zheng, K. Koynov, G. K. Auernhammer, H.-J. Butt, T. Ikeda, *Macromolecules* **2013**, *46*, 4617.
181. W. Xia, M. Ni, C. Yao, X. Wang, D. Chen, C. Lin, X.-Y. Hu, L. Wang, *Macromolecules* **2015**.
182. A. Harada, Y. Takashima, M. Nakahata, *Acc. Chem. Res.* **2014**, *47*, 2128.

183. X. J. Loh, *Mater. Horiz.* **2014**, *1*, 185.
184. X. Yang, H. Yu, L. Wang, R. Tong, M. Akram, Y. Chen, X. Zhai, *Soft Matter* **2015**, *11*, 1242.
185. J. Li, A. Harada, M. Kamachi, *Polym. J.* **1994**, *26*, 1019.
186. K. M. Huh, T. Ooya, W. K. Lee, S. Sasaki, I. C. Kwon, S. Y. Jeong, N. Yui, *Macromolecules* **2001**, *34*, 8657.
187. J. Li, X. Li, X. Ni, X. Wang, H. Li, K. W. Leong, *Biomaterials* **2006**, *27*, 4132.
188. N. Lin, A. Dufresne, *Biomacromolecules* **2013**, *14*, 871.
189. H. Jin, X.-H. Dai, C. Wu, J.-M. Pan, X.-H. Wang, Y.-S. Yan, D.-M. Liu, L. Sun, *Eur. Polym. J.* **2015**, *66*, 149.
190. M. Nakahata, Y. Takashima, H. Yamaguchi, A. Harada, *Nat. Commun.* **2011**, *2*.
191. T. Kakuta, Y. Takashima, M. Nakahata, M. Otsubo, H. Yamaguchi, A. Harada, *Adv. Mater.* **2013**, *25*, 2849.
192. K. Miyamae, M. Nakahata, Y. Takashima, A. Harada, *Angew. Chem. Int. Ed.* **2015**, *54*, 8984.
193. C. B. Rodell, A. L. Kaminski, J. A. Burdick, *Biomacromolecules* **2013**, *14*, 4125.
194. C. B. Rodell, J. W. MacArthur, S. M. Dorsey, R. J. Wade, L. L. Wang, Y. J. Woo, J. A. Burdick, *Adv. Funct. Mater.* **2015**, *25*, 636.
195. C. Rodell, R. Wade, B. Purcell, N. Dusaj, J. A. Burdick, *ACS Biomater. Sci. Eng.* **2015**, *1*, 277.
196. H. Chen, X. Ma, S. Wu, H. Tian, *Angew. Chem. Int. Ed.* **2014**, *53*, 14149.
197. Y.-G. Jia, X. X. Zhu, *Chem. Mater.* **2014**, *27*, 387.
198. L. Peng, H. Zhang, A. Feng, M. Huo, Z. Wang, J. Hu, W. Gao, J. Yuan, *Polym. Chem.* **2015**, *6*, 3652.
199. S. Himmelein, V. Lewe, M. C. A. Stuart, B. J. Ravoo, *Chem. Sci.* **2014**, *5*, 1054.
200. E. A. Appel, X. J. Loh, S. T. Jones, F. Biedermann, C. A. Dreiss, O. A. Scherman, *J. Am. Chem. Soc.* **2012**, *134*, 11767.
201. J. R. McKee, E. A. Appel, J. Seitsonen, E. Kontturi, O. A. Scherman, O. Ikkala, *Adv. Funct. Mater.* **2014**, *24*, 2706.
202. E.-R. Janeček, J. R. McKee, C. S. Y. Tan, A. Nykänen, M. Kettunen, J. Laine, O. Ikkala, O. A. Scherman, *Angew. Chem. Int. Ed.* **2015**, *54*, 5383.
203. C. Li, M. J. Rowland, Y. Shao, T. Cao, C. Chen, H. Jia, X. Zhou, Z. Yang, O. A. Scherman, D. Liu, *Adv. Mater.* **2015**, *27*, 3298.
204. Z. Yu, J. Zhang, R. J. Coulston, R. M. Parker, F. Biedermann, X. Liu, O. A. Scherman, C. Abell, *Chem. Sci.* **2015**, *6*, 4929.
205. L. M. de Espinosa, G. L. Fiore, C. Weder, E. J. Foster, Y. C. Simon, *Prog. Polym. Sci.* **2015**.
206. L. R. Hart, J. L. Harries, B. W. Greenland, H. M. Colquhoun, W. Hayes, *Polym. Chem.* **2013**, *4*, 4860.
207. F. Herbst, D. Döhler, P. Michael, W. H. Binder, *Macromol. Rapid Commun.* **2013**, *34*, 203.
208. G. M. L. van Gemert, J. W. Peeters, S. H. M. Söntjens, H. M. Janssen, A. W. Bosman, *Macromol. Chem. Phys.* **2012**, *213*, 234.
209. R. F. M. Lange, M. Van Gurp, E. W. Meijer, *J. Polym. Sci., Part A: Polym. Chem.* **1999**, *37*, 3657.
210. P. Y. W. Dankers, M. C. Harmsen, L. A. Brouwer, M. J. A. Van Luyn, E. W. Meijer, *Nat. Mater.* **2005**, *4*, 568.
211. L. R. Rieth, R. F. Eaton, G. W. Coates, *Angew. Chem. Int. Ed.* **2001**, *40*, 2153.
212. J. A. Kaitz, C. M. Possanza, Y. Song, C. E. Diesendruck, A. J. H. Spiering, E. W. Meijer, J. S. Moore, *Polym. Chem.* **2014**, *5*, 3788.
213. C. L. Lewis, K. Stewart, M. Anthamatten, *Macromolecules* **2014**, *47*, 729.
214. O. Colombani, C. Barioz, L. Bouteiller, C. Chanéac, L. Fompérie, F. Lortie, H. Montès, *Macromolecules* **2005**, *38*, 1752.
215. M. Kashif, Y.-W. Chang, *Polym. Int.* **2014**, *63*, 1936.
216. M. Kashif, Y.-W. Chang, *Eur. Polym. J.* **2015**, *66*, 273.
217. P. Song, Z. Xu, Y. Lu, Q. Guo, *Macromolecules* **2015**, *48*, 3957.
218. Y. Chen, A. M. Kushner, G. A. Williams, Z. Guan, *Nat. Chem.* **2012**, *4*, 467.
219. Y. Chen, Z. Guan, *Chem. Commun.* **2014**, *50*, 10868.

220. J. Hentschel, A. M. Kushner, J. Ziller, Z. Guan, *Angew. Chem. Int. Ed.* **2012**, *51*, 10561.
221. P. Cordier, F. Tournilhac, C. Soulie-Ziakovic, L. Leibler, *Nature* **2008**, *451*, 977.
222. D. Montarnal, P. Cordier, C. Soulie-Ziakovic, F. Tournilhac, L. Leibler, *J. Polym. Sci., Part A: Polym. Chem.* **2008**, *46*, 7925.
223. D. Montarnal, F. Tournilhac, M. Hidalgo, J. L. Couturier, L. Leibler, *J. Am. Chem. Soc.* **2009**, *131*, 7966.
224. R. Zhang, T. Yan, B.-D. Lechner, K. Schröter, Y. Liang, B. Li, F. Furtado, P. Sun, K. Saalwächter, *Macromolecules* **2013**, *46*, 1841.
225. A. Zhang, L. Yang, Y. Lin, L. Yan, H. Lu, L. Wang, *J. Appl. Polym. Sci.* **2013**, *129*, 2435.
226. L. Yang, Y. Lin, L. Wang, A. Zhang, *Polym. Chem.* **2014**, *5*, 153.
227. R. Agnaou, M. Capelot, S. Tencé-Girault, F. Tournilhac, L. Leibler, *J. Am. Chem. Soc.* **2014**, *136*, 11268.
228. S. Sivakova, D. A. Bohnsack, M. E. Mackay, P. Suwanmala, S. J. Rowan, *J. Am. Chem. Soc.* **2005**, *127*, 18202.
229. B. D. Mather, M. B. Baker, F. L. Beyer, M. A. G. Berg, M. D. Green, T. E. Long, *Macromolecules* **2007**, *40*, 6834.
230. K. Zhang, M. Aiba, G. Fahs, A. G. Hudson, W. Chiang, R. B. Moore, M. Ueda, T. Long, *Polym. Chem.* **2015**, *6*, 2434.
231. E. Croisier, S. Liang, T. Schweizer, S. Balog, M. Mionić, R. Snellings, J. Cugnoni, V. Michaud, H. Frauenrath, *Nat. Commun.* **2014**, *5*.
232. J. Scavuzzo, S. Tomita, S. Cheng, H. Liu, M. Gao, J. P. Kennedy, S. Sakurai, S. Z. D. Cheng, L. Jia, *Macromolecules* **2015**, *48*, 1077.
233. R. J. Varley, S. van der Zwaag, *Acta Mater.* **2008**, *56*, 5737.
234. R. J. Varley, S. van der Zwaag, *Polym. Int.* **2010**, *59*, 1031.
235. S. J. Kalista, J. R. Pflug, R. J. Varley, *Polym. Chem.* **2013**, *4*, 4910.
236. J. M. Vega, A. M. Grande, S. van der Zwaag, S. J. Garcia, *Eur. Polym. J.* **2014**, *57*, 121.
237. M. W. Spears, E. S. Herman, J. C. Gaulding, L. A. Lyon, *Langmuir* **2014**, *30*, 6314.
238. A. Reisch, P. Tirado, E. Roger, F. Boulmedais, D. Collin, J.-C. Voegel, B. Frisch, P. Schaaf, J. B. Schlenoff, *Adv. Funct. Mater.* **2013**, *23*, 673.
239. A. Reisch, E. Roger, T. Phoeung, C. Antheaume, C. Orthlieb, F. Boulmedais, P. Lavalle, J. B. Schlenoff, B. Frisch, P. Schaaf, *Adv. Mater.* **2014**, *26*, 2547.
240. A. Noro, K. Ishihara, Y. Matsushita, *Macromolecules* **2011**, *44*, 6241.
241. M. A. Malmierca, A. González-Jiménez, I. Mora-Barrantes, P. Posadas, A. Rodríguez, L. Ibarra, A. Nogales, K. Saalwächter, J. L. Valentín, *Macromolecules* **2014**, *47*, 5655.
242. I. Mora-Barrantes, M. A. Malmierca, J. L. Valentin, A. Rodriguez, L. Ibarra, *Soft Matter* **2012**, *8*, 5201.
243. F. Potier, A. Guinault, S. Delalande, C. Sanchez, F. Ribot, L. Rozes, *Polym. Chem.* **2014**, *5*, 4474.
244. L. Zhang, L. R. Kucera, S. Ummadisetty, J. R. Nykaza, Y. A. Elabd, R. F. Storey, K. A. Cavicchi, R. A. Weiss, *Macromolecules* **2014**, *47*, 4387.
245. D. Wang, J. Guo, H. Zhang, B. Cheng, H. Shen, N. Zhao, J. Xu, *J. Mater. Chem. A* **2015**, *3*, 12864.
246. Y. Furusho, T. Endo, *J. Polym. Sci., Part A: Polym. Chem.* **2014**, *52*, 1815.
247. M. Wathier, M. W. Grinstaff, *J. Am. Chem. Soc.* **2008**, *130*, 9648.
248. M. A. Aboudzadeh, M. E. Muñoz, A. Santamaría, R. Marcilla, D. Mecerreyes, *Macromol. Rapid Commun.* **2012**, *33*, 314.
249. A. Aboudzadeh, M. Fernandez, M. E. Muñoz, A. Santamaría, D. Mecerreyes, *Macromol. Rapid Commun.* **2014**, *35*, 460.
250. A. Das, A. Sallat, F. Böhme, M. Suckow, D. Basu, S. Wiessner, K. W. Stoeckelhuber, B. Voit, G. Heinrich, *ACS Appl. Mater. Interfaces* **2015**.
251. S. Bode, L. Zedler, F. H. Schacher, B. Dietzek, M. Schmitt, J. Popp, M. D. Hager, U. S. Schubert, *Adv. Mater.* **2013**, *25*, 1634.

252. S. Bode, R. K. Bose, S. Matthes, M. Ehrhardt, A. Seifert, F. H. Schacher, R. M. Paulus, S. Stumpf, B. Sandmann, J. Vitz, A. Winter, S. Hoeppener, S. J. Garcia, S. Spange, S. van der Zwaag, M. D. Hager, U. S. Schubert, *Polym. Chem.* **2013**, *4*, 4966.
253. B. Sandmann, B. Happ, S. Kupfer, F. H. Schacher, M. D. Hager, U. S. Schubert, *Macromol. Rapid Commun.* **2014**, *36*, 604.
254. M. Enke, S. Bode, J. Vitz, F. H. Schacher, M. J. Harrington, M. D. Hager, U. S. Schubert, *Polymer* **2015**, *69*, 274.
255. H. Li, W. Wei, H. Xiong, *Polymer* **2014**, *55*, 5739.
256. M. Burnworth, L. Tang, J. R. Kumpfer, A. J. Duncan, F. L. Beyer, G. L. Fiore, S. J. Rowan, C. Weder, *Nature* **2011**, *472*, 334.
257. D. Mozhdehi, S. Ayala, O. R. Cromwell, Z. Guan, *J. Am. Chem. Soc.* **2014**, *136*, 16128.
258. B. Yang, H. Zhang, H. Peng, Y. Xu, B. Wu, W. Weng, L. Li, *Polym. Chem.* **2014**, *5*, 1945.
259. Z. Wang, M. W. Urban, *Polym. Chem.* **2013**, *4*, 4897.
260. H. Goldansaz, E. van Ruymbeke, J.-F. Gohy, C.-A. Fustin, M. E. Ries, C. Bailly, *Macromolecules* **2015**, *48*, 2290.
261. H. Goldansaz, D. Auhl, B. Goderis, Q. Voleppe, C.-A. Fustin, J.-F. Gohy, C. Bailly, E. van Ruymbeke, *Macromolecules* **2015**, *48*, 3746.
262. T.-W. Chuo, T.-C. Wei, Y.-L. Liu, *J. Polym. Sci., Part A: Polym. Chem.* **2013**, *51*, 3395.
263. S. Burattini, H. M. Colquhoun, J. D. Fox, D. Friedmann, B. W. Greenland, P. J. F. Harris, W. Hayes, M. E. Mackay, S. J. Rowan, *Chem. Commun.* **2009**, 6717.
264. S. Burattini, B. W. Greenland, D. H. Merino, W. G. Weng, J. Seppala, H. M. Colquhoun, W. Hayes, M. E. Mackay, I. W. Hamley, S. J. Rowan, *J. Am. Chem. Soc.* **2010**, *132*, 12051.
265. L. R. Hart, J. H. Hunter, N. A. Nguyen, J. L. Harries, B. W. Greenland, M. E. Mackay, H. M. Colquhoun, W. Hayes, *Polym. Chem.* **2014**, *5*, 3680.
266. L. R. Hart, N. A. Nguyen, J. L. Harries, M. E. Mackay, H. M. Colquhoun, W. Hayes, *Polymer* **2015**, *69*, 293.
267. J. F. Masson, S. Bundalo-Perc, A. Delgado, *J. Polym. Sci., Part B: Polym. Phys.* **2005**, *43*, 276.
268. J. M. Widin, A. K. Schmitt, A. L. Schmitt, K. Im, M. K. Mahanthappa, *J. Am. Chem. Soc.* **2012**, *134*, 3834.
269. H. J. Qi, M. C. Boyce, *Mech. Mater.* **2005**, *37*, 817.
270. T. Hashimoto, T. Imaeda, S. Irie, M. Urushisaki, T. Sakaguchi, *J. Polym. Sci., Part A: Polym. Chem.* **2015**, *53*, 1114.
271. T. Imaeda, T. Hashimoto, S. Irie, M. Urushisaki, T. Sakaguchi, *J. Polym. Sci., Part A: Polym. Chem.* **2013**, *51*, 1796.
272. T. Hashimoto, T. Namikoshi, S. Irie, M. Urushisaki, T. Sakaguchi, T. Nemoto, S. Isoda, *J. Polym. Sci., Part A: Polym. Chem.* **2008**, *46*, 1902.
273. A. Hermann, R. Mruk, R. F. Roskamp, M. Scherer, L. Ma, R. Zentel, *Macromol. Chem. Phys.* **2014**, *215*, 32.
274. G. Leone, M. Mauri, F. Bertini, M. Canetti, D. Piovani, G. Ricci, *Macromolecules* **2015**, *48*, 1304.
275. J. H. Roh, D. Roy, W. K. Lee, A. L. Gergely, J. E. Puskas, C. M. Roland, *Polymer* **2015**, *56*, 280.
276. W. Shi, N. A. Lynd, D. Montarnal, Y. Luo, G. H. Fredrickson, E. J. Kramer, C. Ntaras, A. Avgeropoulos, A. Hexemer, *Macromolecules* **2014**, *47*, 2037.
277. X. Wang, J. Vapaavuori, Y. Zhao, C. G. Bazuin, *Macromolecules* **2014**, *47*, 7099.

Chapter 2: Cu(0)-mediated polymerization of hydrophobic acrylates using high-throughput experimentation

Abstract

In this chapter the optimization of the Cu(0)-mediated polymerization of *n*-butyl acrylate and 2-methoxyethyl acrylate using an automated parallel synthesizer is reported. Using this robot, up to 16 kinetic reactions could be performed in parallel, resulting in a fast screening of different reaction conditions. Several parameters were optimized to determine the optimal reaction conditions with regard to control over the polymerizations and reaction rate. These optimal reaction conditions were then used for the one-pot two-step synthesis of diblock copolymers by sequential monomer addition.

2.1 Introduction

Over the past decades, several types of controlled radical polymerization methods have been developed. The most popular methods are atom transfer radical polymerization (ATRP),[1-3] reversible addition-fragmentation chain transfer (RAFT) polymerization[4, 5] and nitroxide mediated polymerization (NMP).[6] One of the more recently developed techniques, that appears to be very promising, is Cu(0)-mediated polymerization, also known as single electron transfer living radical polymerization (SET-LRP).[7, 8] With this method, polymers with low dispersity can readily be synthesized at room temperature and below with high end group fidelity at high conversions.[9, 10] In contrast to ATRP, which also uses the change in oxidation state of a transition metal catalyst, Cu(0)-mediated polymerization can only be performed in polar solvents, sometimes in combination with apolar solvents. In these solvents and in combination with an appropriate nitrogen containing ligand, it is theorized that Cu(I)X species will disproportionate into Cu(0) and Cu(II)X_2 species.[11] Atomic Cu(0) species will activate the process and Cu(II)X_2 will mediate the deactivation, resulting in a single electron transfer (SET) mechanism, which facilitates an ultrafast controlled radical polymerization.[7] However, the exact mechanism through which Cu(0)-mediated polymerization occurs is still under debate.[12-17]

Recent publications have shown significant progress in the area of Cu(0)-mediated polymerization. Among the monomers that have been polymerized in a controlled manner via Cu(0)-mediated polymerization are acrylates,[7, 18-20] methacrylates,[7, 21] vinyl chloride[7] and (meth)acrylamides.[22-24] Also the synthesis of more complex polymeric architectures, such as multiblock copolymers,[25-32] star[33, 34] and graft[35] polymers, has been shown. However, for each monomer the polymerization conditions should be optimized, which is in general a very time consuming task.

To the best of our knowledge, Cu(0)-mediated polymerization has never been reported using an automated parallel synthesizer before, albeit it seems to be ideally suited for fast optimization of reaction conditions. In the past, such a parallel synthesis robot has already been used for controlled radical polymerizations via RAFT,[36-39] ATRP,[40, 41] MADIX[42] and NMP.[43, 44] Because many reactions can be performed simultaneously, it is much more time efficient than manually performing a large number of individual reactions. The reproducibility of the automated parallel polymerizations is also improved because of the similar conditions within the parallel reactors, as opposed to performing many reactions separately.

In this chapter, the optimization of the Cu(0)-mediated polymerization of *n*-butyl acrylate (BA) and 2-methoxyethyl acrylate (MEA) using an automated parallel synthesizer is described, which was done in collaboration with Sofie Wallyn from the Polymer Chemistry Research Group at Ghent University. These two monomers serve as examples for regularly applied acrylates. At first we will demonstrate that these Cu(0)-mediated polymerization reactions can be performed in a controlled and reproducible fashion in the robot system. Subsequently, we will vary different reaction parameters to evaluate their effect on the polymerization kinetics and to find the optimal reaction conditions. The parameters that are varied include the type of ligand and initiator, the amount of Cu(0), Cu(II) and ligand, and the monomer to initiator (M/I) ratio. The initiators ethyl α-bromoisobutyrate (EBiB) and ethyl 2-bromopropionate (EBP) (Figure 23) are used to compare the effect of a tertiary and secondary bromide, while both tris[2-(dimethylamino)ethyl]amine (Me_6TREN), which is commonly used in Cu(0)-mediated polymerization, and *N,N,N′,N″,N‴*-pentamethyldiethylenetriamine (PMDETA), which is mainly used in ATRP, are tested as ligands. The optimal reaction conditions were then used for the one-pot two-step synthesis of diblock copolymers by sequential monomer addition.

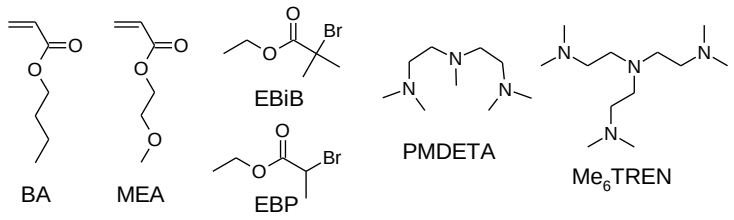

Figure 23. Structures of the compounds used in this chapter. *n*-Butyl acrylate (BA), 2-methoxyethyl acrylate (MEA), ethyl α-bromoisobutyrate (EBiB), ethyl 2-bromopropionate (EBP), *N,N,N′,N″,N‴*-pentamethyldiethylenetriamine (PMDETA) and tris[2-(dimethylamino)ethyl]amine (Me_6TREN).

2.2 Experimental section

Materials

N,N-Dimethylformamide (DMF) was purchased from Biosolve. Copper(II)bromide ($CuBr_2$, 99%) was purchased from Fluka and used as received. Copper powder (spheroidal, 10 µm, 99%), ethyl α-bromoisobutyrate (EBiB, 98%), ethyl 2-bromopropionate (EBP, 99%), and *N,N,N′,N″,N‴*-pentamethyldiethylenetriamine (PMDETA, 99%) were purchased from Sigma-Aldrich and used as received. *n*-Butyl acrylate (BA, 99%) and 2-methoxyethyl acrylate (MEA, 98%) were purchased from Sigma-Aldrich and purified by passing over a basic aluminum oxide column to remove the inhibitor. Pre-cut copper wire (Sigma-Aldrich, 99.9%) and copper wire (from the core of an electrical wire, hardware store) were stirred in sulphuric acid, milliQ water and acetone before use. The surface area of the copper was calculated from the measured length and diameter of the copper wire and from the particle size and weight of the copper powder.

Synthesis of tris[2-(dimethylamino)ethyl]amine (Me_6TREN)

Me_6TREN was synthesized according to a previously published procedure.[45] Formaldehyde (15.0 mL, 201 mmol) and formic acid (22.0 mL, 583 mmol) were cooled in an ice bath and a solution of tris(2-aminoethyl)amine (5.0 mL, 33 mmol) in water (3.0 mL) was added dropwise. The reaction mixture was stirred for one hour while slowly warming up to room temperature and subsequently refluxed at 120 °C overnight, during which the mixture slowly turned orange. It was put on the rotavap to remove residual CO_2 and then stirred in an ice bath. NaOH pellets were slowly added until the

mixture was basic, which was checked with pH paper. It was then extracted with dichloromethane (3 x 30 mL) and dried with $MgSO_4$. The product was distilled at 107 °C (3 mbar) to yield 5.6 g (73%) of clear liquid.

^{1}H NMR ($CDCl_3$, 300 MHz) δ: 2.57 ppm (6H, m, N-(CH_2-CH_2)$_3$), 2.33 ppm (6H, m, N-(CH_2-CH_2)$_3$), 2.18 ppm (18H, s, N-(CH_3)$_2$)

Automated Cu(0)-mediated polymerization

Reactions were performed using a Chemspeed ASW2000 automated synthesizer equipped with 16 parallel reactors of 13 mL, a Huber Petite Fleur thermostat for heating/cooling, a Huber Ministat 125 for reflux and a Vacuubrand PC 3000 vacuum pump. Stock solutions of all components were prepared and bubbled with argon for at least 30 minutes before being introduced into the robot system and then kept under argon atmosphere. The hood of the automated synthesizer was continuously flushed with nitrogen (20 L/min) and the reactors and stock solutions were flushed with argon (2 L/min) to ensure an inert atmosphere. Before starting the polymerizations, the reactors were degassed through ten vacuum-argon cycles. Stock solutions were transferred to the reactors using the syringe of the automated synthesizer to a total reaction volume of 4 mL. During the reactions, 50 µL samples were taken at preset time intervals and directly injected into 1.5 mL sample vials, each containing a 0.1 mg/mL solution of phenothiazine in ~1 mL of either THF or acetone to quench the reaction. A more detailed description of a representative experiment in which the concentration of ligand was varied is given below.

Table 1. Reagent ratios used for each reaction in this experiment. All reactions were performed with 3.0 M monomer concentration in DMF at 25°C, using 12.5 mm^2/mL Cu(0) wire.

reactor #	BA	EBP	Me_6TREN	$CuBr_2$
1	100	1	0.5	0.05
2	100	1	0.3	0.05
3	100	1	0.2	0.05
4	100	1	0.15	0.05
5	100	1	0.1	0.05
6	100	1	0.05	0.05
7	100	1	0.025	0.05
8	100	1	0	0.05
9	100	1	0.5	0.05
10	100	1	0.3	0.05
11	100	1	0.2	0.05
12	100	1	0.15	0.05
13	100	1	0.1	0.05
14	100	1	0.05	0.05
15	100	1	0.025	0.05
16	100	1	0	0.05

Table 2. Prepared stock solutions for variation of ligand concentration experiment.

stock solution #	compound	g	mL	g/mL in solution
1	BA	28.79	32.06	0.858
	1,2-dichlorobenzene	1.92	1.48	0.057
2	Me_6TREN	0.0857	0.0994	0.00815
	DMF	9.84	10.42	0.935
3	$CuBr_2$	0.0251	0	0.00523
	DMF	4.53	4.80	0.944
4	EBP	0.4067	0.2917	0.0846
	DMF	4.26	4.51	0.887

Besides the reactants for the polymerizations (Table 1), a small amount of 1,2-dichlorobenzene (0.1 mL in a total reaction volume of 4 mL) was added to each reaction to act as an internal standard for the calculation of monomer conversion from GC. Stock solutions were prepared as given in Table 2, sealed with a septum and bubbled with argon on a schlenkline for 30-60 minutes. In the meantime, the Chemspeed was prepared by manually adding the copper wire (5 pieces, or 50 mm^2 per reactor) to the reactors, placing the reflux condensers and reactor block on top of the reactors and installing them in the Chemspeed, as well as placing the sample vials prefilled with the quenching solution in the system (see Figure 25). The Chemspeed, thermostat, cryostat and vacuum pump are switched on and the software is started. The stock solutions were then taken inside the robot and, after ensuring adequate argon flow (4 L/min, which is reduced to 2 L/min after placing the vials), the septa were carefully removed and the stock solutions were placed on the stock solution rack while avoiding oxygen contamination. Then the hood of the Chemspeed was closed, nitrogen flow to the hood was switched on and the program, shown in Figure 24, was started.

First the solvent lines of the system are rinsed several times with DMF at 30 mL/min to remove bubbles and avoid contaminations. During the inertization the reactors and reflux condensers are heated to 25 °C, placed under vacuum (~20 mbar) for two minutes, argon for one minute and this cycle is repeated ten times. The temperature of the reflux condensers is then set to 10 °C. After two hours, which is the time needed to ensure inert conditions inside the hood at a nitrogen flow of 20 L/min, transfer of the stock solutions to the reactor is started using the 10 mL syringe of the Chemspeed. The amounts used in this experiment are given in Table 3. Note that additional DMF is added to all reactions to ensure a monomer concentration of 3.0 M. For all liquid transfers a speed of 5 mL/min is used with 2 seconds equilibration time and a 10 µL air gap. After adding all components except the initiator, the mixtures are stirred for one minute at 700 RPM and t0 samples are taken. When the initiator is added, the reactions start immediately.

Table 3. Amount of each stock solution that is added to the reactors for the variation of ligand concentration experiment. Additionally, 5 pieces of pre-cut copper wire (average surface area 10 mm^2) are added manually to the reactors.

reactor #	stock 1 (mL)	stock 2 (mL)	stock 3 (mL)	stock 4 (mL)	DMF (mL)
1	1.75	1.66	0.25	0.25	0
2	1.75	0.99	0.25	0.25	0.66
3	1.75	0.66	0.25	0.25	0.99
4	1.75	0.50	0.25	0.25	1.16
5	1.75	0.33	0.25	0.25	1.32
6	1.75	0.17	0.25	0.25	1.49
7	1.75	0.08	0.25	0.25	1.57
8	1.75	0	0.25	0.25	1.65
9	1.75	1.66	0.25	0.25	0
10	1.75	0.99	0.25	0.25	0.66
11	1.75	0.66	0.25	0.25	0.99
12	1.75	0.50	0.25	0.25	1.16
13	1.75	0.33	0.25	0.25	1.32
14	1.75	0.17	0.25	0.25	1.49
15	1.75	0.08	0.25	0.25	1.57
16	1.75	0	0.25	0.25	1.65

During the experiment, 50 µL samples are taken at times shown in Figure 24, using the 1 mL syringe. After each sample, the syringe is washed inside and outside with 1 mL of DMF at 20 mL/min, a process that takes about 54 seconds per sample, which should be taken into account for fast reactions. After the end of the program is reached, the software and hardware are switched off,

samples are measured with GC and SEC, final reaction mixtures are manually transferred into sample vials, and the reactors and reflux condensers are cleaned manually.

Task	Name	Parameter	Description	Estimated Time
1	Set Timer	Set the timer start inertization		00 sec
2	Prime lines	Macro Task	Prime lines in cycles	08 min 54 sec
1	Transfer Volumetrically	Transfer liquid from Reservoir 2 to variable 'Rinse_station'		01 min 19 sec
2	Transfer Volumetrically	Transfer liquid from variable 'Reservoir_solvent' to variable 'Rinse_statior		01 min 39 sec
	<insert sub tasks here>			
3	Inertization	Macro Task	Inertization	41 min 50 sec
1	Heat / Cool	Thermostat ON on zone all reactors		10 min 00 sec
2	Reflux	Reflux On on zone reactors 1-8		02 sec
3	Macro Task	Macro Task	Cycle for inertization	31 min 40 sec
S1	Drawer Valve	Set Reactionblock state to Closed Under Vacuum on zone all reactors		04 sec
S2	Vacuum	Vacuum On on zone reactors 1-8		02 sec
W3	it	Waiting for 2:00 minutes		02 min 00 sec
S4	Drawer Valve	Set Reactionblock state to Closed Under Inert Gas on zone all reactors		04 sec
W5	it	Waiting for 1:00 minutes		01 min 00 sec
	<insert sub tasks here>			
4	Set Drawer Valve	Set Reactionblock state to Closed Under Inert Gas on zone all reactors		04 sec
5	Set Vacuum	Vacuum Off on zone all reactors		02 sec
6	Reflux	Reflux On on zone reactors 1-8		02 sec
	<insert sub tasks here>			
4	Wait	Waiting for 2:00:00 hours after timer start inertization		00 sec
5	Prime lines	Macro Task	Prime lines in cycles	02 min 58 sec
1	Transfer Volumetrically	Transfer liquid from Reservoir 2 to variable 'Rinse_station'		01 min 19 sec
2	Transfer Volumetrically	Transfer liquid from variable 'Reservoir_solvent' to variable 'Rinse_statior		01 min 39 sec
	<insert sub tasks here>			
6	Stir	Agitation ON on zone all reactors		02 sec
7	Transfer Volumetrically	Transfer liquid from stock 1 to reactors 1-8	BA + DCB	13 min 18 sec
8	Transfer Volumetrically	Transfer liquid from stock 1 to reactors 9-16	BA + DCB	13 min 51 sec
9	Transfer Volumetrically	Transfer liquid from stock 2 to reactors 1-8	Me6TREN	08 min 30 sec
10	Transfer Volumetrically	Transfer liquid from stock 2 to reactors 9-16	Me6TREN	09 min 03 sec
11	Transfer Volumetrically	Transfer liquid from stock 3 to reactors 1-8	CuBr2	08 min 30 sec
12	Transfer Volumetrically	Transfer liquid from stock 3 to reactors 9-16	CuBr2	09 min 03 sec
13	Transfer Volumetrically	Transfer liquid from Reservoir 1 to reactors 1-8		10 min 17 sec
14	Transfer Volumetrically	Transfer liquid from Reservoir 1 to reactors 9-16		10 min 32 sec
15	Wait	Waiting for 1:00 minutes		01 min 00 sec
16	Transfer Volumetrically	Transfer liquid from reactors 1-8 to samples r1-8 t0		09 min 10 sec
17	Transfer Volumetrically	Transfer liquid from reactors 9-16 to samples r9-16 t0		09 min 10 sec
18	Set Timer	Set the timer start reaction		00 sec
19	Transfer Volumetrically	Transfer liquid from stock 4 to reactors 1-8	EBP	08 min 30 sec
20	Transfer Volumetrically	Transfer liquid from stock 4 to reactors 9-16	EBP	09 min 03 sec
21	Wait	Waiting for 10:00 minutes after timer start reaction		00 sec
22	Transfer Volumetrically	Transfer liquid from reactors 1-8 to samples r1-8 t1		09 min 10 sec
23	Transfer Volumetrically	Transfer liquid from reactors 9-16 to samples r9-16 t1		09 min 10 sec
24	Wait	Waiting for 30:00 minutes after timer start reaction		00 sec
25	Transfer Volumetrically	Transfer liquid from reactors 1-8 to samples r1-8 t2		09 min 10 sec
26	Transfer Volumetrically	Transfer liquid from reactors 9-16 to samples r9-16 t2		09 min 10 sec
27	Wait	Waiting for 50:00 minutes after timer start reaction		00 sec
28	Transfer Volumetrically	Transfer liquid from reactors 1-8 to samples r1-8 t3		09 min 10 sec
29	Transfer Volumetrically	Transfer liquid from reactors 9-16 to samples r9-16 t3		09 min 10 sec
30	Wait	Waiting for 1:10:00 hours after timer start reaction		00 sec
31	Transfer Volumetrically	Transfer liquid from reactors 1-8 to samples r1-8 t4		09 min 10 sec
32	Transfer Volumetrically	Transfer liquid from reactors 9-16 to samples r9-16 t4		09 min 10 sec
33	Wait	Waiting for 1:30:00 hours after timer start reaction		00 sec
34	Transfer Volumetrically	Transfer liquid from reactors 1-8 to samples r1-8 t5		09 min 10 sec
35	Transfer Volumetrically	Transfer liquid from reactors 9-16 to samples r9-16 t5		09 min 10 sec
36	Wait	Waiting for 2:00:00 hours after timer start reaction		00 sec
37	Transfer Volumetrically	Transfer liquid from reactors 1-8 to samples r1-8 t6		09 min 10 sec
38	Transfer Volumetrically	Transfer liquid from reactors 9-16 to samples r9-16 t6		09 min 10 sec
39	Wait	Waiting for 3:00:00 hours after timer start reaction		00 sec
40	Transfer Volumetrically	Transfer liquid from reactors 1-4 to samples r1-4 t7		04 min 37 sec
41	Transfer Volumetrically	Transfer liquid from reactors 5-8 to samples r5-8 t7		04 min 37 sec
42	Transfer Volumetrically	Transfer liquid from reactors 9-12 to samples r9-12 t7		04 min 37 sec
43	Transfer Volumetrically	Transfer liquid from reactors 13-16 to samples r13-16 t7		04 min 37 sec
44	Wait	Waiting for 4:00:00 hours after timer start reaction		00 sec
45	Transfer Volumetrically	Transfer liquid from reactors 1-4 to samples r1-4 t8		04 min 37 sec
46	Transfer Volumetrically	Transfer liquid from reactors 5-8 to samples r5-8 t8		04 min 37 sec
47	Transfer Volumetrically	Transfer liquid from reactors 9-12 to samples r9-12 t8		04 min 37 sec
48	Transfer Volumetrically	Transfer liquid from reactors 13-16 to samples r13-16 t8		04 min 37 sec
49	Wait	Waiting for 8:00:00 hours after timer start reaction		00 sec
50	Transfer Volumetrically	Transfer liquid from reactors 1-4 to samples r1-4 t9		04 min 37 sec
51	Transfer Volumetrically	Transfer liquid from reactors 5-8 to samples r5-8 t9		04 min 37 sec
52	Transfer Volumetrically	Transfer liquid from reactors 9-12 to samples r9-12 t9		04 min 37 sec
53	Transfer Volumetrically	Transfer liquid from reactors 13-16 to samples r13-16 t9		04 min 37 sec
54	Wait	Waiting for 12:00:00 hours after timer start reaction		00 sec
55	Transfer Volumetrically	Transfer liquid from reactors 1-4 to samples r1-4 t10		04 min 37 sec
56	Transfer Volumetrically	Transfer liquid from reactors 5-8 to samples r5-8 t10		04 min 37 sec
57	Transfer Volumetrically	Transfer liquid from reactors 9-12 to samples r9-12 t10		04 min 37 sec
58	Transfer Volumetrically	Transfer liquid from reactors 13-16 to samples r13-16 t10		04 min 37 sec
59	Heat / Cool	Thermostat OFF on zone all reactors		00 sec
60	Reflux	Reflux Off on zone reactors 1-8		02 sec
61	Stir	Agitation OFF on zone all reactors		02 sec

Figure 24. Program used for the variation of ligand concentration experiment.

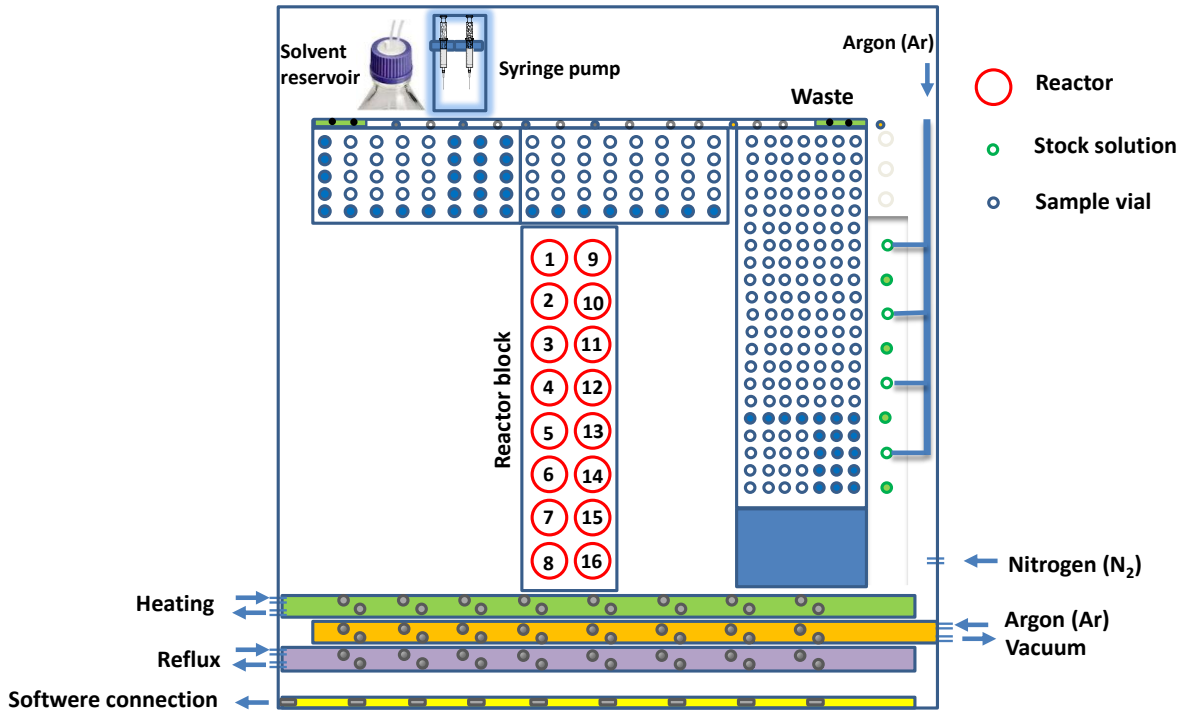

Figure 25. Schematic layout of the automated parallel synthesizer.

Gas Chromatography (GC)

Samples were measured with GC to determine the monomer conversion from the ratio of the integrals from the monomer and the internal standard (1,2-dichlorobenzene). GC was performed on an Agilent 7890A system equipped with a VWR Carrier-160 hydrogen generator and an Agilent HP-5 column of 30 m length and 0.320 mm diameter. An FID detector was used and the inlet was set to 240 °C with a split injection of ratio 25:1. Hydrogen was used as carrier gas at a flow rate of 2 mL/min. The oven temperature was increased with 20°C/min from 50°C to 120°C, followed by a ramp of 50°C/min to 150°C.

Size Exclusion Chromatography (SEC)

The samples were run over a short aluminum oxide column to remove residual copper before the SEC measurements. SEC was performed on a Varian PL-GPC 50 Plus system using THF at 1 mL/min as eluent, and equipped with two PLgel 5 µm MIXED-D columns, a PL-AS RT autosampler and five detectors: RI, light scattering at 15° and 90°, a viscometer and a UV Knauer Wellchrom Spectro-Photometer K-2501. Molecular weights were determined with the RI detector using polystyrene standards as many of the polymers were too small for accurate detection by light scattering or viscometry.

Matrix assisted laser desorption/ionization time of flight mass spectroscopy (MALDI-TOF MS)

MALDI-TOF MS was performed on an Applied Biosystems Voyager De STR MALDI-TOF mass spectrometer equipped with 2 m linear and 3 m reflector flight tubes. All mass spectra were obtained with an accelerating potential of 20 kV in positive ion mode and in reflectron mode. Dithranol (25 mg/mL in THF) was used as a matrix, NaI (20 mg/mL in THF) was used as a cationizing agent, and polymer samples were dissolved in THF (5 mg/mL). Analyte solutions were prepared by mixing 20 µL

of the matrix, 10 µL of the polymer and 10 µL of the salt solution. Subsequently, 0.5 µL of this mixture was spotted on the sample plate, and the spots were dried in air at room temperature. A poly(ethylene oxide) standard (M_n = 2000 g/mol) was used for calibration. All data were processed using the Data Explorer 4.0.0.0 (Applied Biosystems) software package.

2.3 Results and discussion

2.3.1 Reproducibility of automated Cu(0)-mediated polymerization

Before utilization of the synthesis robot for screening and optimization of Cu(0)-mediated polymerization reaction conditions, several experiments were performed to optimize the settings of the automated synthesizer to get reproducible results. One of the problems that turned up quickly was the inaccuracy of the liquid transfers by the syringe and liquid pumps of the automated synthesizer at higher transfer speeds, especially for liquids with higher viscosities. While a higher viscosity requires a slower transfer speed, a too low transfer speed can cause the stock solutions to mix with the rinsing solvent, leading to inaccurate concentrations. For DMF it was found that a liquid transfer speed of 5 mL/min with a waiting period of two seconds after the transfer leads to accurate results. For more viscous liquids, such as monomers like 2-hydroxyethyl acrylate or concentrated solutions of *N*-isopropylacrylamide, transfer speeds as low as 1 or 2 mL/min should be used.

Another problem that was encountered while using the automated synthesizer is that the relatively thick needle can push the septa of the sample vials through the cap and into the vial. As this leaves the vial open, the sample solvent, monomer and internal standard can evaporate, leading to inaccurate results when the sample is analysed. To prevent this, the best solution seems to be to tightly close the caps of the sample vials and ensure that the vials are aligned correctly through the software.

In many polymerizations, the reaction solvent has been used as an internal standard to calculate the monomer conversion. However, for Cu(0)-mediated polymerization reactions in the automated synthesizer this was not possible. When all components of the reaction are added together, the polymerization immediately starts, leaving no time to take an accurate sample at zero conversion. Therefore, a small amount of 1,2-dichlorobenzene was added together with the monomer into the reactors to serve as an internal standard. Then, most of the other stock solutions were added and a sample for zero conversion was taken. Subsequently the final component, in most cases the initiator, was added to start the reaction. Using both visual observation and the log of the automated synthesizer, the exact times that the stock solutions are added and at which time each sample is taken can be exactly determined, enabling accurate kinetic studies.

Due to the robustness and relatively high reaction rate of Cu(0)-mediated polymerization, it was found that in some cases the reaction still continued within the sample vials after sampling, leading to irreproducible kinetic plots. To prevent this, the radical inhibitor phenothiazine was added to the solvent in the sample vials, which ensures that no further polymerization can take place after sampling.

Because Cu(0)-mediated polymerization is an exothermic reaction, the heat that is produced during the reaction may have a significant influence on the temperature inside the reactors and the polymerization kinetics. This was verified, and while there is a 0.5°C increase in temperature in the

first few minutes immediately after the start of the polymerization, this is not expected to have a significant effect on the polymerization kinetics.

To show that these optimized settings lead to reproducible polymerizations, eight reactions were performed with similar conditions (Figure 26). BA was polymerized using a ratio of [BA]:[EBiB]:[PMDETA]:[Cu(II)] equal to 100:1:0.24:0.05 at a monomer concentration of 2.2M in DMF at 25°C. Two types of Cu(0) were used, namely a 5 cm piece of electrical wire (with a surface area of 75.5 mm^2/mL), bent in such a shape that it fits in the reactor, and small pieces of pre-cut copper wire (with a surface area of 76.3 mm^2/mL). As shown in Figure 26, both the conversion plots and SEC traces almost exactly overlap and the molecular weight distribution is relatively narrow, with dispersities (Đ) ranging from 1.2 to 1.3, clearly demonstrating that reproducible Cu(0)-mediated polymerization reactions can be performed in the synthesis robot. Control over the polymerizations is evident from the low Đ as well as the close to linear first order kinetic plot up to a $\ln([M]_0/[M])$ value of 2, corresponding to a conversion of 87%. Unfortunately, for one reaction the zero conversion sample was not taken properly, consequently the conversions for that reaction could not be calculated accurately. However, the obtained results were enough evidence to demonstrate the reproducibility of the reactions, so the experiment was not repeated. For future reactions, it was decided to use the pre-cut copper wire, because it is much easier to handle and to vary the amounts compared to the electrical wire. These optimized experimental procedures were further used in this work to study the effect of various parameters on the Cu(0)-mediated polymerizations.

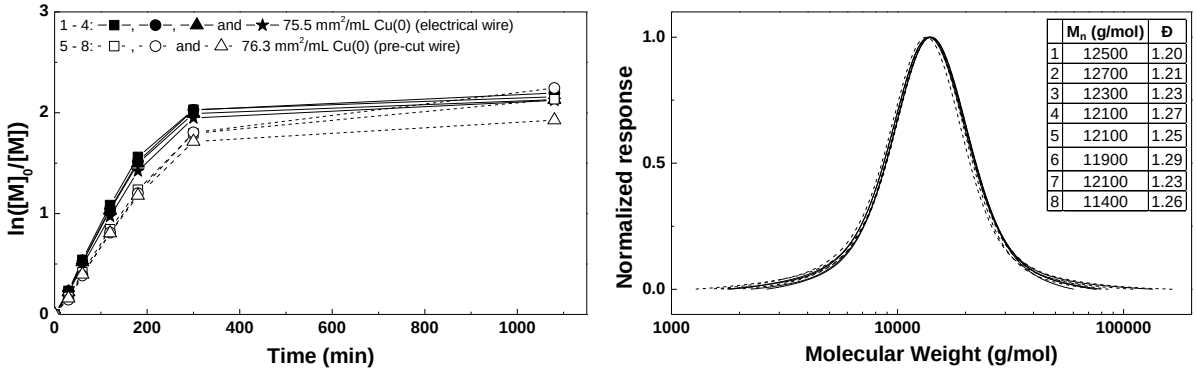

Figure 26. Left: first order kinetic plot for Cu(0)-mediated polymerization of BA using [BA]:[EBiB]:[PMDETA]:[Cu(II)] = 100:1:0.24:0.05, 2.2M monomer concentration in DMF at 25°C. Right: SEC traces of the eight individual PBA polymers at the end of the reaction.

2.3.2 Amount of Cu(0) and initiator type

As Cu(0) is the driving force behind the Cu(0)-mediated polymerization mechanism, it was expected that changing the amount of Cu(0), i.e. the available surface area, would have a significant influence on the reaction kinetics. Therefore, several series of reactions were performed with different amounts of Cu(0) to study this effect.

In the first series of reactions (Figure 27) a constant ratio of [BA]:[EBiB]:[PMDETA]:[$CuBr_2$] equal to 100:1:0.18:0.05, which has been shown previously to lead to good results,[26] was used with a monomer concentration of 2.2M in DMF. It is clear that an increase in the amount of Cu(0) increases the speed of the polymerization during the early stages of the reaction. However, after several hours the fastest reactions show more termination due to the higher radical concentration, as is evident from a decrease in the slope of the first order kinetic plot, resulting in a lower monomer conversion

towards the end of the reaction. Nonetheless, the measured M_ns for all polymerizations increase linearly with conversion and are in close agreement with the theoretical M_n. Dispersities are around 1.2 – 1.5 in the early stages of the reactions and decrease to around 1.15 with increasing monomer conversion.

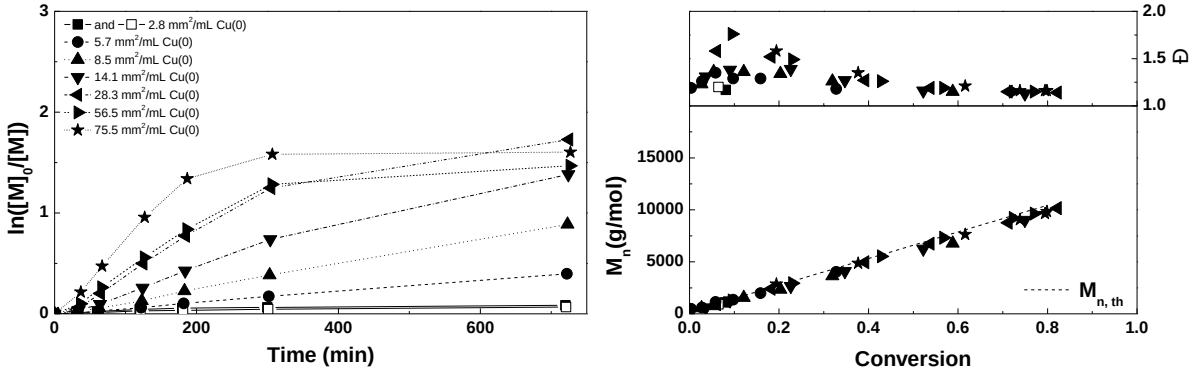

Figure 27. Left: first order kinetic plot for Cu(0)-mediated polymerization of BA using [BA]:[EBiB]:[PMDETA]:[Cu(II)] = 100:1:0.18:0.05, 2.2M monomer concentration in DMF at 25°C, using different amounts of Cu(0) expressed as surface area. Right: corresponding molecular weight and dispersity vs. conversion plot.

For the second series of reactions with different amounts of Cu(0) (Figure 28) we switched to Me_6TREN as ligand. This ligand is more generally used in Cu(0)-mediated polymerization reactions because of its higher k_{act}/k_{deact} ratio, which leads to faster polymerization rates and increased control. The [BA]:[EBiB]:[Me_6TREN]:[$CuBr_2$] ratio was 100:1:0.18:0.05 for all reactions and in addition to Cu(0) wire also Cu(0) powder was used. All reactions were performed in duplicate showing good reproducibility. While the surface area of the powder is close to that of the highest amount of Cu(0) wire, the polymerization is significantly faster during the first hour, likely caused by a difference in accessibility of the Cu(0) for the ligand. After a fast start, the reaction with powder terminates at a monomer conversion of 87%, which is probably due to the shape of the copper particles leading to a higher initial radical concentration and more termination, while the other reactions with Cu(0) wire show near linear first order kinetics up to full monomer conversion. The reactions with 12.5 and 25 mm^2/mL Cu(0) wire show similar reaction rates, indicating that this is the maximum reachable k_p, most probably limited by the solubility of copper in DMF. The M_ns are mostly in agreement with the theoretical M_n, except for the reactions containing 25 mm^2/mL Cu(0), which show higher M_n, possibly due to termination reactions from the higher concentration of radicals. Dispersities are around 1.5 at low conversion, and decrease to 1.05 above 40% conversion. In the case of 25 mm^2/mL Cu(0) the dispersity at full conversion is slightly higher (1.08), also demonstrating slightly lower control over the polymerization.

The third series of reactions (Figure 29), was performed with EBP as initiator and [BA]:[EBP]:[Me_6TREN]:[$CuBr_2$] equal to 100:1:0.18:0.05, revealing very similar results as obtained with EBiB. However, the initiation of the polymerizations was slightly faster, indicating that EBP is the more suitable initiator of the two tested ones, in agreement with the theory that the initiator structure should mimic the structure of dormant propagating macroradicals. Although a recent study oppositely suggested that EBiB is a better initiator for acrylates.[46] Nonetheless, EBP was chosen as initiator for further reactions based on our results.

As using PMDETA as ligand results in slower reactions and higher dispersities, it is clear that Me_6TREN is a better ligand for the polymerization of BA via Cu(0)-mediated polymerization. In both series with Me_6TREN the reactions containing the highest amount of Cu(0) show a deviation from the theoretical molecular weights and slightly higher dispersities. From all obtained results, it was decided to use a surface area of 12.5 mm^2/mL Cu(0) wire in further reactions in combination with EBP as initiator and Me_6TREN as ligand.

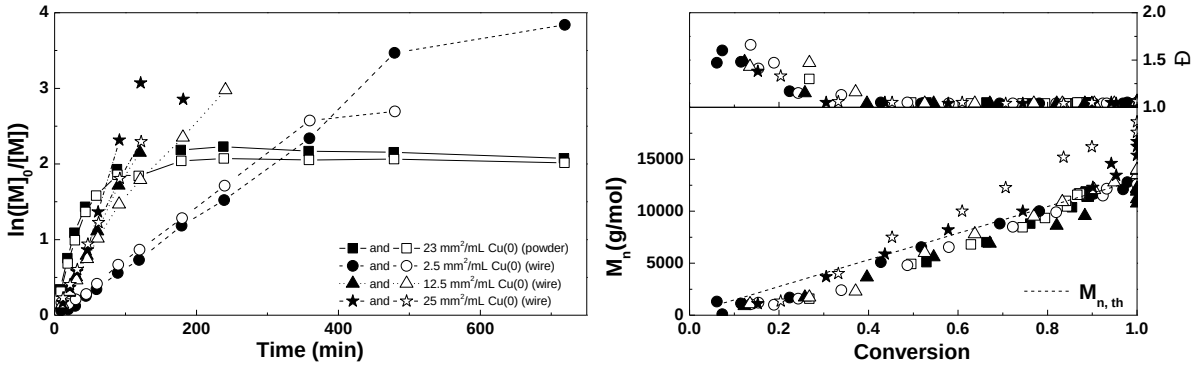

Figure 28. Left: first order kinetic plot for Cu(0)-mediated polymerization of BA using [BA]:[EBiB]:[Me_6TREN]:[Cu(II)] = 100:1:0.18:0.05, 3M monomer concentration in DMF at 25°C, using different amounts of Cu(0). Right: corresponding molecular weight and dispersity vs. conversion plot.

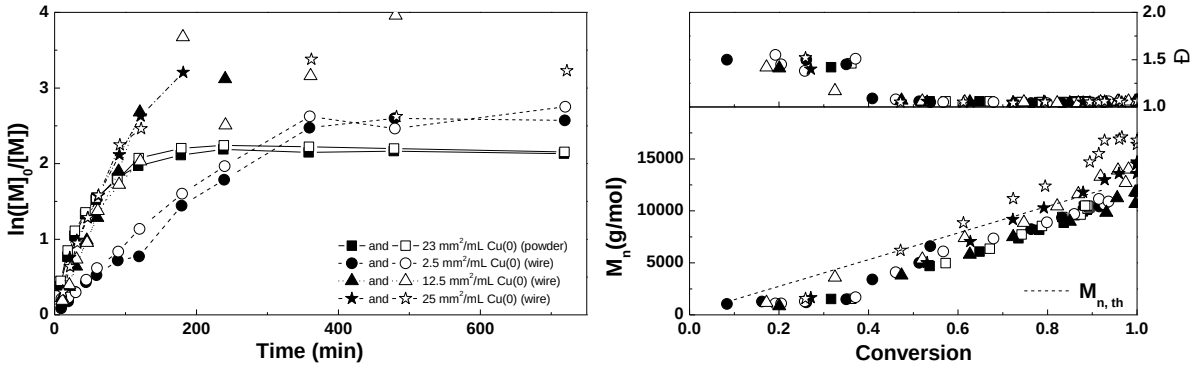

Figure 29. Left: first order kinetic plot for Cu(0)-mediated polymerization of BA using [BA]:[EBP]:[Me_6TREN]:[Cu(II)] = 100:1:0.18:0.05, 3M monomer concentration in DMF at 25°C, using different amounts of Cu(0). Right: corresponding molecular weight and dispersity vs. conversion plot.

2.3.3 Ligand concentration

The amount of Me_6TREN was subsequently varied from 0 to 0.5 equivalents with all other amounts kept constant at [BA]:[EBP]:[$CuBr_2$] equal to 100:1:0.05 (Figure 30). As expected, a larger amount of Me_6TREN results in a faster reaction because more copper can be dissolved. However, the reactions containing 0.5 eq. of Me_6TREN show a lower conversion in the last samples than those containing 0.3 or 0.2 eq. It is likely that more termination reactions occur with a higher amount of Me_6TREN as more Cu(0) will lead to a higher radical concentration. In contrast, the reactions containing 0.025 and 0 eq. Me_6TREN show almost no conversion due to almost no copper being dissolved under these conditions. Even though all reactions revealed a linear increase of M_n with conversion close to $M_{n,th}$, dispersities are somewhat higher for the reactions with higher amounts of Me_6TREN. This can also be seen in the SEC traces of these polymers (Figure 31), which show a shoulder at higher molecular weight that indicates coupling between chains, presumably due to termination by quarternization of the ligand with the terminal bromide group as recently shown by Haddleton.[47] At 0.15 eq. Me_6TREN

(and lower) this shoulder was not observed, indicating that a lower amount of ligand provides a better controlled reaction.

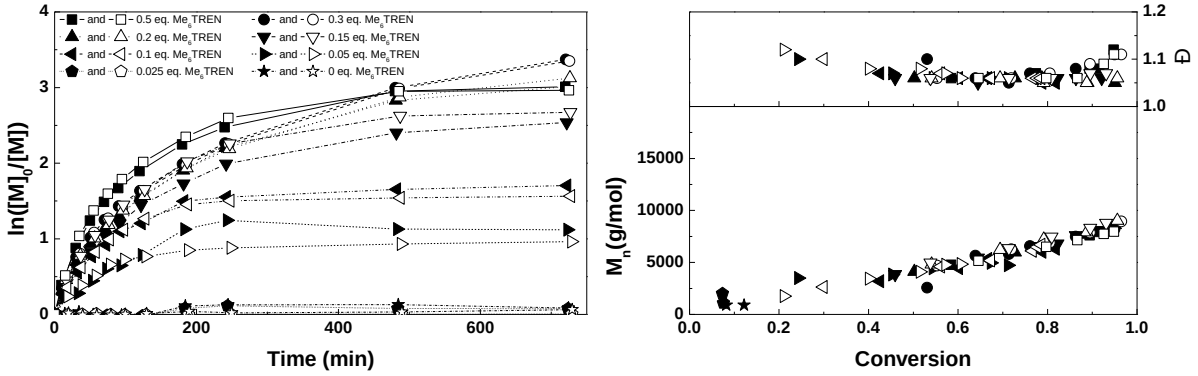

Figure 30. Left: first order kinetic plot for Cu(0)-mediated polymerization of BA using [BA]:[EBP]:[Cu(II)] = 100:1:0.05, 3M monomer concentration in DMF at 25°C, using 12.5 mm^2/mL Cu(0) wire and different amounts of Me_6TREN. Right: corresponding molecular weight and dispersity vs. conversion plot.

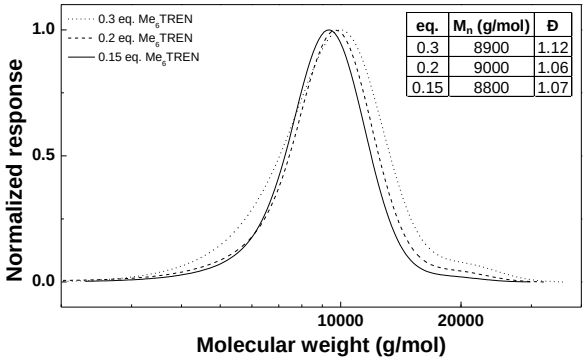

Figure 31. SEC traces of PBA polymers synthesized using [BA]:[EBP]:[Cu(II)] = 100:1:0.05, 3M monomer concentration in DMF at 25°C, using 12.5 mm^2/mL Cu(0) wire and different amounts of Me_6TREN.

2.3.4 Cu(II) concentration

The Cu(II) in the form of $CuBr_2$ is important in the Cu(0) – Cu(II) equilibrium that determines the control over the polymerization. Therefore it is expected that changing the amount of Cu(II) will not only have a large effect on the speed of the polymerization, but also on the molecular weight distribution. To investigate this, the [BA]:[EBP]:[Me_6TREN] ratio was kept constant at 100:1:0.18 while varying the amount of Cu(II). As seen in Figure 32, a larger amount of Cu(II) slows down monomer conversion, with no conversion with 0.5 eq. of Cu(II), relative to the initiator. This is probably because at this ratio the deactivation is too fast compared to the activation, thus no polymerization takes place. The polymerizations without Cu(II) or up to 0.05 eq. of Cu(II) proceed at similar rates. SEC results show that a higher amount of Cu(II) leads to more controlled molecular weights and lower dispersities. As can be seen in the SEC traces (Figure 33, left), a Cu(II) ratio of 0.05 eq. or lower leads to a small shoulder at higher molecular weights, indicative of chain termination by coupling resulting from a too high radical concentration, which is not observed at Cu(II) ratios of 0.1 and higher. From these results it was concluded that a Cu(II) ratio of 0.1 results in the most controlled polymerization while maintaining a fast polymerization speed. MALDI-TOF MS analysis of one of the samples confirmed high end-group fidelity (Figure 33, right). The zoom in Figure 33 (right) shows a peak spacing of 128 corresponding to the mass of BA while the exact mass corresponds to

the polymer with both the initiation fragment and bromide end-groups as well as a sodium ion, present to charge the polymer.

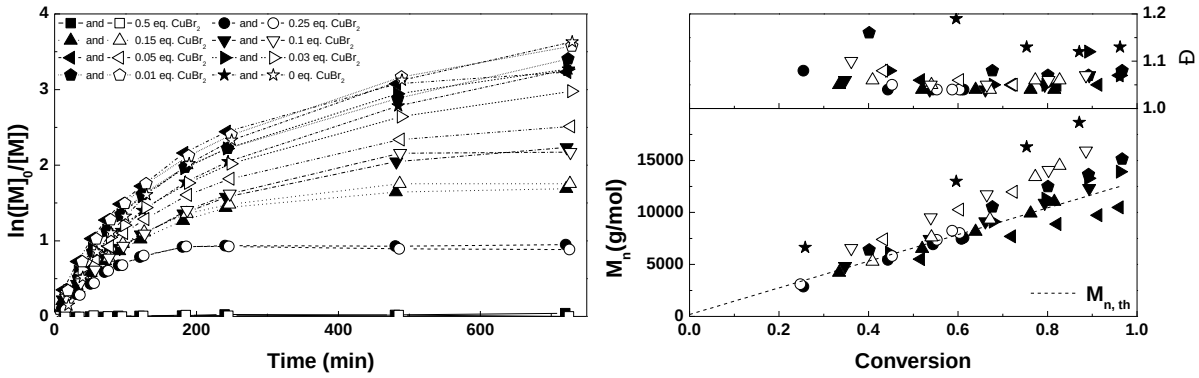

Figure 32. Left: first order kinetic plot for Cu(0)-mediated polymerization of BA using [BA]:[EBP]:[Me_6TREN] = 100:1:0.18, 3M monomer concentration in DMF at 25°C, using 12.5 mm^2/mL Cu(0) wire and different amounts of Cu(II). Right: corresponding molecular weight and dispersity vs. conversion plot.

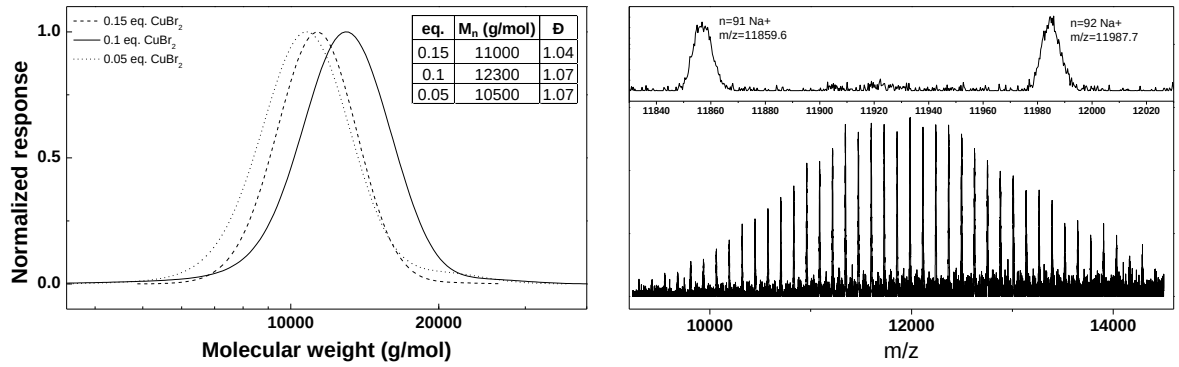

Figure 33. Left: SEC traces of PBA polymers synthesized using [BA]:[EBP]:[Me_6TREN] = 100:1:0.18, 3M monomer concentration in DMF at 25°C, using 12.5 mm^2/mL Cu(0) wire and different amounts of Cu(II). Right: MALDI-TOF MS spectrum of PBA synthesized using a [BA]:[EBP]:[Me_6TREN]:[$CuBr_2$] ratio of 100:1:0.18:0.1.

2.3.5 Variation of M/I ratio

Several experiments were performed to determine optimal conditions for polymerizations with different M/I ratios to find the limit in M_n reachable by Cu(0)-mediated polymerization. The reactions were performed with both BA and MEA as monomers to test whether the optimized conditions are applicable for other acrylates than BA. The investigated M/I ratios are 50, 100, 200 and 400. In the first experiment (Figure 34), the ratio of [M]:[EBP]:[Me_6TREN]:[Cu(II)] was kept constant at [M]:1:0.15:0.1, resulting in lower concentrations of Me_6TREN and Cu(II) with increasing M/I ratio. The amount of Cu(0) was 12.5 mm^2/mL in all reactions. As seen in Figure 34, this resulted in a slower reaction for higher M/I ratios and a lower monomer conversion after 48h, due to more termination earlier in the reaction. However, dispersities were in all cases around 1.05, indicating a well-controlled polymerization. The conversions of BA and MEA are very similar, indicating that these optimal reaction conditions are also applicable to other acrylates with similar hydrophobicity, that is solubility in DMF. The measured M_ns of MEA are higher than those of BA, which is especially clear at the highest M_ns. This is ascribed to a better solubility of pMEA in the eluent (THF), leading to a larger hydrodynamic volume and thus a higher M_n calculated relative to polystyrene standards. Overall the M_ns are in good agreement with the theoretical M_ns up to masses of about 30000 g/mol.

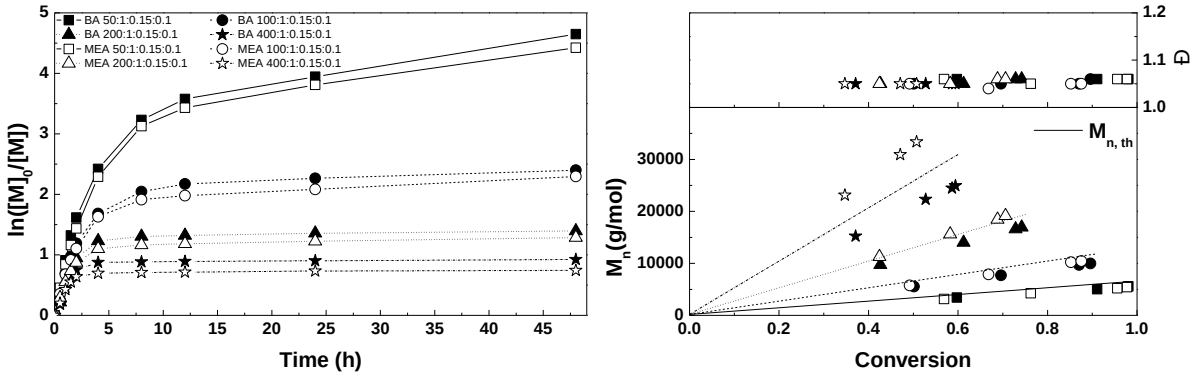

Figure 34. Left: first order kinetic plot for Cu(0)-mediated polymerization of BA and MEA using different [M]:[EBP]:[Me_6TREN]:[Cu(II)] ratios, 3M monomer concentration in DMF at 25°C, and 12.5 mm^2/mL Cu(0) wire. Right: corresponding molecular weight and dispersity vs. conversion plot.

For the second experiment, the amount of Cu(0) was adjusted to the amount of ligand (Figure 35). This resulted in similar polymerization rates as the previous experiment with a slightly longer inhibition period. Dispersities were somewhat higher, namely 1.09 for the higher M/I polymerizations. This indicates that a constant amount of 12.5 mm^2/mL Cu(0) wire, independent of the M/I ratio, gives the best results, even though all ligand is likely saturated with copper in either case.

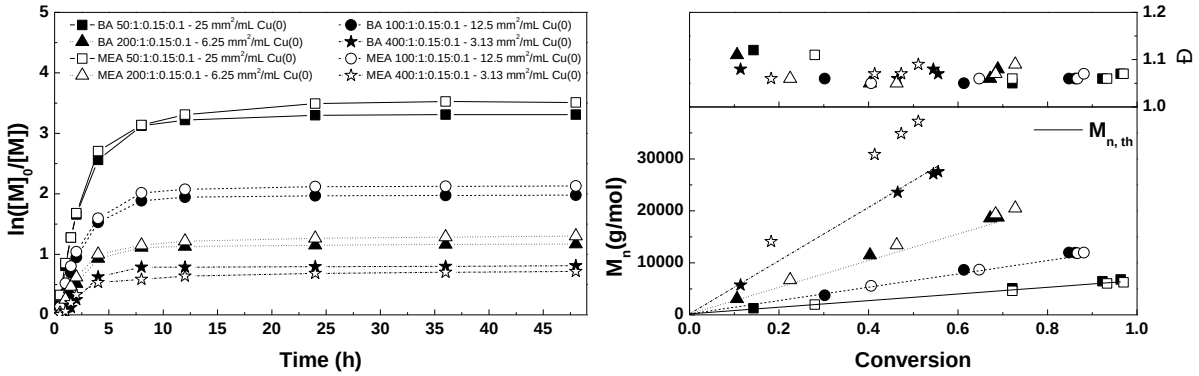

Figure 35. Left: first order kinetic plot for Cu(0)-mediated polymerization of BA and MEA using different [M]:[EBP]:[Me_6TREN]:[Cu(II)] ratios, 3M monomer concentration in DMF at 25°C. The amount of Cu(0) wire was adjusted to the amount of ligand. Right: corresponding molecular weight and dispersity vs. conversion plot.

For a third experiment the concentrations of monomer, Me_6TREN and Cu(II) and the amount of Cu(0) were kept constant, while only varying the EBP concentration to adjust the M/I ratio, leading to different [EBP]:[Me_6TREN]:[Cu(II)] ratios (Figure 36). This resulted in somewhat higher monomer conversion, but also a large increase in dispersity at higher conversions, indicating a loss of control over the polymerization.

According to these results, the best way to synthesize BA and MEA polymers of different lengths is to use a [M]:[EBP]:[Me_6TREN]:[Cu(II)] ratio of [M]:1:0.15:0.1, regardless of which M/I ratio is used. A constant Cu(0) wire amount of 12.5 mm^2/mL leads to slightly better results than adjusting the amount of Cu(0) to the amount of ligand.

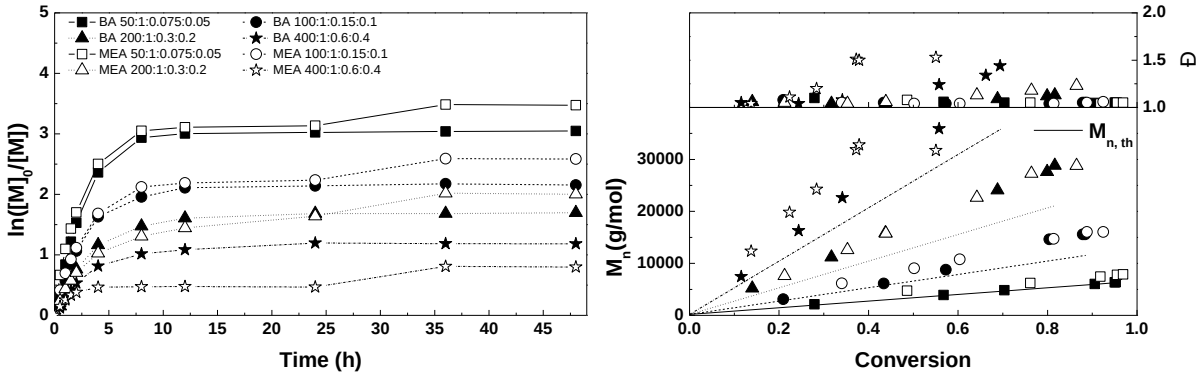

Figure 36. Left: first order kinetic plot for Cu(0)-mediated polymerization of BA and MEA using different [M]:[EBP]:[Me_6TREN]:[Cu(II)] ratios, 3M monomer concentration in DMF at 25°C, and 12.5 mm^2/mL Cu(0) wire. The total concentration of Me_6TREN and Cu(II) were kept constant for each reaction Right: corresponding molecular weight and dispersity vs. conversion plot.

2.3.6 Sequential addition of second monomer

To study the chain-end preservation of the polymerizations and the feasibility of one-pot two-step block copolymerizations by sequential monomer addition, a BA polymerization was performed for several hours, after which MEA was added as second monomer to the polymerization mixture (Figure 37). The initial [BA]:[EBP]:[Me_6TREN]:[$CuBr_2$] ratio was set to 50:1:0.15:0.1. After a certain time, either 3, 6, 12 or 24 hours, a 3M solution of MEA in DMF was added to the reactors, leading to a total M/I ratio of 100. A similar experiment was performed using [BA]:[EBP]:[Me_6TREN]:[$CuBr_2$] = 100:1:0.15:0.1 and a total M/I ratio of 200 after the addition of MEA, showing similar results (Figure 38).

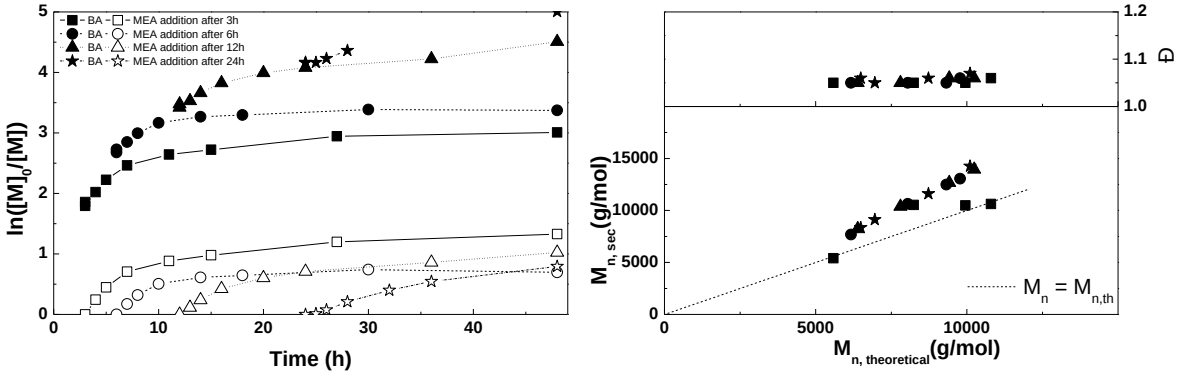

Figure 37. Left: first order kinetic plot for Cu(0)-mediated polymerization of BA with sequential addition of MEA using [BA]:[EBP]:[Me_6TREN]:[Cu(II)] = 50:1:0.15:0.1 and [MEA]:[EBP] = 50:1, 3M monomer concentration in DMF at 25°C and 12.5 mm^2/mL Cu(0) wire. Right: corresponding molecular weight and dispersity vs. theoretical molecular weight plot.

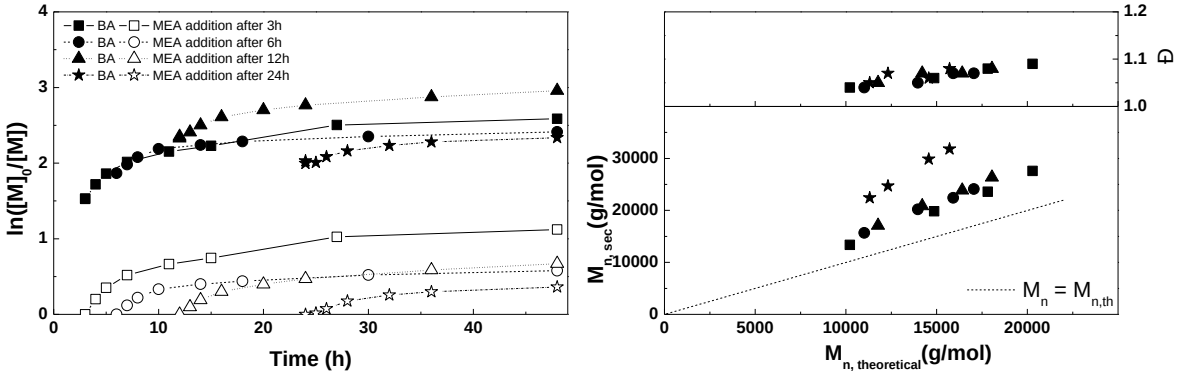

Figure 38. Left: first order kinetic plot for Cu(0)-mediated polymerization of BA with sequential addition of MEA using [BA]:[EBP]:[Me_6TREN]:[Cu(II)] = 100:1:0.15:0.1 and [MEA]:[EBP] = 100:1, 3M monomer concentration in DMF at 25°C and 12.5 mm^2/mL Cu(0) wire. Right: corresponding molecular weight and dispersity vs. theoretical molecular weight plot.

The results show that, in general, a higher MEA conversion is obtained when the second monomer is added at an earlier time, demonstrating that more PBA chains are still "living". However, too short BA polymerization times do not result in perfect block copolymers, because some of the BA is also incorporated into the polymer chain after addition of the MEA. When the MEA is added after 24 hours, in some cases not all chains are reinitiated, which can lead to higher $M_{n,SEC}$ values because of a higher monomer to growing chain ratio. This can be observed in Figure 38, right. From those results, the best moment for adding the second monomer is 12 hours after the start of the polymerization. The conversion of BA at that moment is around 97%, and almost no BA is converted after addition of the MEA. In this case the MEA reaches a monomer conversion of 64% 48 hours after the start of the polymerization for the 50:1 BA:EBP ratio and 49% for the 100:1 BA:EBP ratio.

Dispersities were below 1.1 in all cases. SEC traces of the block copolymers at different times during the reaction (Figure 39) show that almost all PBA homopolymer is converted into a block copolymer as only a very small shoulder is observed at low molecular weight in the final SEC trace. Even though the second block does not reach full conversion, quasi-perfect block copolymers can be obtained in this one-pot two-step approach.

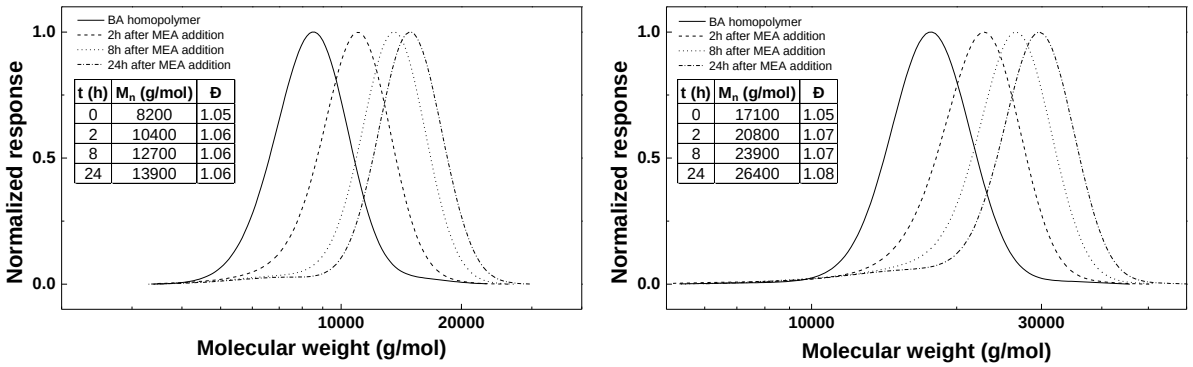

Figure 39. Left: SEC traces of PBA-*b*-PMEA block copolymers at different times during the polymerization after sequential addition of MEA at 12h BA polymerization time, using [MEA]:[EBP] = 50:1. Right: SEC traces of PBA-*b*-PMEA block copolymers at different times during the polymerization after sequential addition of MEA at 12h BA polymerization time, using [MEA]:[EBP] = 100:1.

2.4 Conclusions

Reproducible Cu(0)-mediated polymerization could be performed in an automated parallel synthesizer. Good near-linear first order kinetics up to almost full conversion were found in many cases, showing that Cu(0)-mediated polymerization leads to controlled polymerization under a variety of reaction conditions. The best results with good control over molecular weight (distribution) while maintaining a fast reaction speed were obtained with a [M]:[EBP]:[Me_6TREN]:[$CuBr_2$] ratio of [M]:1:0.15:0.1 with 12.5 mm^2/mL Cu(0) wire. Applying those conditions, it was possible to make polymers with narrow molecular weight distributions over a large range of molecular weights. One-pot block copolymerizations could also be performed, although these did not reach full conversion of the second monomer.

Altogether, this work shows the power of high-throughput optimization of Cu(0)-mediated polymerization reaction conditions. As such, it may serve to accelerate optimization of Cu(0)-mediated polymerization conditions and aid in gaining fundamental understanding of the effect of various parameters on the Cu(0)-mediated polymerization. Examples of effects that could be studied further using high-throughput Cu(0)-mediated polymerization are the cooperative and synergistic effects of mixtures of solvents on the disproportionation of copper and subsequent rate of polymerization,[48, 49] and the role of particle size and surface area of the copper.[50, 51] Furthermore, this high-throughput methodology allows fast preparation of libraries of defined (block co)polymers by Cu(0)-mediated polymerization. Synthesis of amphiphilic block copolymers using this technique is described in Chapter 3.

References

1. W. A. Braunecker, K. Matyjaszewski, *Prog. Polym. Sci.* **2007**, *32*, 93.
2. M. Ouchi, T. Terashima, M. Sawamoto, *Chem. Rev.* **2009**, *109*, 4963.
3. S. E. Averick, C. G. Bazewicz, B. F. Woodman, A. Simakova, R. A. Mehl, K. Matyjaszewski, *Eur. Polym. J.* **2013**, *49*, 2919.
4. G. Moad, E. Rizzardo, S. H. Thang, *Aust. J. Chem.* **2009**, *62*, 1402.
5. H. Liu, J. Zhang, X. Luo, N. Kong, L. Cui, J. Liu, *Eur. Polym. J.* **2013**, *49*, 2949.
6. C. J. Hawker, A. W. Bosman, E. Harth, *Chem. Rev.* **2001**, *101*, 3661.
7. V. Percec, T. Guliashvili, J. S. Ladislaw, A. Wistrand, A. Stjerndahl, M. J. Sienkowska, M. J. Monteiro, S. Sahoo, *J. Am. Chem. Soc.* **2006**, *128*, 14156.
8. B. M. Rosen, V. Percec, *Chem. Rev.* **2009**, *109*, 5069.
9. F. Nyström, A. H. Soeriyadi, C. Boyer, P. B. Zetterlund, M. R. Whittaker, *J. Polym. Sci., Part A: Polym. Chem.* **2011**, *49*, 5313.
10. N. H. Nguyen, M. E. Levere, V. Percec, *J. Polym. Sci., Part A: Polym. Chem.* **2012**, *50*, 860.
11. N. H. Nguyen, M. E. Levere, J. Kulis, M. J. Monteiro, V. Percec, *Macromolecules* **2012**, *45*, 4606.
12. D. Konkolewicz, Y. Wang, M. Zhong, P. Krys, A. A. Isse, A. Gennaro, K. Matyjaszewski, *Macromolecules* **2013**, *46*, 8749.
13. C.-H. Peng, M. Zhong, Y. Wang, Y. Kwak, Y. Zhang, W. Zhu, M. Tonge, J. Buback, S. Park, P. Krys, D. Konkolewicz, A. Gennaro, K. Matyjaszewski, *Macromolecules* **2013**, *46*, 3803.
14. Y. Wang, M. Zhong, W. Zhu, C.-H. Peng, Y. Zhang, D. Konkolewicz, N. Bortolamei, A. A. Isse, A. Gennaro, K. Matyjaszewski, *Macromolecules* **2013**, *46*, 3793.
15. Y. Gao, T. Zhao, W. Wang, *RSC Adv.* **2014**, *4*, 61687.
16. D. Konkolewicz, Y. Wang, P. Krys, M. Zhong, A. A. Isse, A. Gennaro, K. Matyjaszewski, *Polym. Chem.* **2014**, *5*, 4396.
17. F. Lorandi, M. Fantin, A. A. Isse, A. Gennaro, *Polymer* **2015**, *72*, 238.
18. G. Lligadas, V. Percec, *J. Polym. Sci., Part A: Polym. Chem.* **2008**, *46*, 2745.

19. X. Leng, N. H. Nguyen, B. van Beusekom, D. A. Wilson, V. Percec, *Polym. Chem.* **2013**, *4*, 2995.
20. S. R. Samanta, V. Percec, *Polym. Chem.* **2014**, *5*, 169.
21. S. Fleischmann, V. Percec, *J. Polym. Sci., Part A: Polym. Chem.* **2010**, *48*, 2243.
22. N. H. Nguyen, B. M. Rosen, V. Percec, *J. Polym. Sci., Part A: Polym. Chem.* **2010**, *48*, 1752.
23. N. H. Nguyen, C. Rodriguez-Emmenegger, E. Brynda, Z. Sedlakova, V. Percec, *Polym. Chem.* **2013**, *4*, 2424.
24. C. Waldron, Q. Zhang, Z. Li, V. Nikolaou, G. Nurumbetov, J. Godfrey, R. McHale, G. Yilmaz, R. K. Randev, M. Girault, K. McEwan, D. M. Haddleton, M. Droesbeke, A. J. Haddleton, P. Wilson, A. Simula, J. Collins, D. J. Lloyd, J. A. Burns, C. Summers, C. Houben, A. Anastasaki, M. Li, C. R. Becer, J. K. Kiviaho, N. Risangud, *Polym. Chem.* **2014**, *5*, 57.
25. C. Boyer, A. H. Soeriyadi, P. B. Zetterlund, M. R. Whittaker, *Macromolecules* **2011**, *44*, 8028.
26. A. H. Soeriyadi, C. Boyer, F. Nystrom, P. B. Zetterlund, M. R. Whittaker, *J. Am. Chem. Soc.* **2011**, *133*, 11128.
27. A. Anastasaki, C. Waldron, P. Wilson, C. Boyer, P. B. Zetterlund, M. R. Whittaker, D. Haddleton, *ACS Macro Lett.* **2013**, *2*, 896.
28. A. Anastasaki, V. Nikolaou, G. S. Pappas, Q. Zhang, C. Wan, P. Wilson, T. P. Davis, M. R. Whittaker, D. Haddleton, *Chem. Sci.* **2014**, *5*, 3536.
29. Y.-M. Chuang, A. Ethirajan, T. Junkers, *ACS Macro Lett.* **2014**, *3*, 732.
30. Q. Zhang, A. Anastasaki, G.-Z. Li, A. J. Haddleton, P. Wilson, D. M. Haddleton, *Polym. Chem.* **2014**, *5*, 3876.
31. F. Alsubaie, A. Anastasaki, P. Wilson, D. Haddleton, *Polym. Chem.* **2015**, *6*, 406.
32. D. Haddleton, A. Simula, V. Nikolaou, A. Anastasaki, F. Alsubaie, G. Nurumbetov, P. Wilson, K. Kempe, *Polym. Chem.* **2015**, *6*, 2226.
33. W. Ding, C. Lv, Y. Sun, H. Luan, T. Yu, G. Qu, *Polym. Bull.* **2011**, *67*, 1499.
34. C. Boyer, A. Derveaux, P. B. Zetterlund, M. R. Whittaker, *Polym. Chem.* **2012**, *3*, 117.
35. A. Ding, G. Lu, H. Guo, X. Zheng, X. Huang, *J. Polym. Sci., Part A: Polym. Chem.* **2013**, *51*, 1091.
36. M. W. M. Fijten, M. A. R. Meier, R. Hoogenboom, U. S. Schubert, *J. Polym. Sci., Part A: Polym. Chem.* **2004**, *42*, 5775.
37. C. R. Becer, A. M. Groth, R. Hoogenboom, R. M. Paulus, U. S. Schubert, *QSAR Comb. Sci.* **2008**, *27*, 977.
38. C. Guerrero-Sanchez, L. O'Brien, C. Brackley, D. J. Keddie, S. Saubern, J. Chiefari, *Polym. Chem.* **2013**, *4*, 1857.
39. J. J. Haven, C. Guerrero-Sanchez, D. J. Keddie, G. Moad, *Macromol. Rapid Commun.* **2014**, *35*, 492.
40. H. Zhang, M. W. M. Fijten, R. Hoogenboom, R. Reinierkens, U. S. Schubert, *Macromol. Rapid Commun.* **2003**, *24*, 81.
41. H. Zhang, H. Abeln Caroline, W. M. Fijten Martin, S. Schubert Ulrich, *e-Polym.* **2006**, *6*, 90.
42. P. Chapon, C. Mignaud, G. Lizarraga, M. Destarac, *Macromol. Rapid Commun.* **2003**, *24*, 87.
43. A. W. Bosman, A. Heumann, G. Klaerner, D. Benoit, J. M. J. Fréchet, C. J. Hawker, *J. Am. Chem. Soc.* **2001**, *123*, 6461.
44. T. M. Eggenhuisen, C. R. Becer, M. W. M. Fijten, R. Eckardt, R. Hoogenboom, U. S. Schubert, *Macromolecules* **2008**, *41*, 5132.
45. M. Ciampolini, N. Nardi, *Inorg. Chem.* **1966**, *5*, 41.
46. N. H. Nguyen, B. M. Rosen, V. Percec, *J. Polym. Sci., Part A: Polym. Chem.* **2011**, *49*, 1235.
47. A. Anastasaki, C. Waldron, P. Wilson, R. McHale, D. M. Haddleton, *Polym. Chem.* **2013**, *4*, 2672.
48. X. Jiang, S. Fleischmann, N. H. Nguyen, B. M. Rosen, V. Percec, *J. Polym. Sci., Part A: Polym. Chem.* **2009**, *47*, 5591.
49. N. H. Nguyen, B. M. Rosen, X. Jiang, S. Fleischmann, V. Percec, *J. Polym. Sci., Part A: Polym. Chem.* **2009**, *47*, 5577.
50. G. Lligadas, B. M. Rosen, C. A. Bell, M. J. Monteiro, V. Percec, *Macromolecules* **2008**, *41*, 8365.

51. N. H. Nguyen, B. M. Rosen, G. Lligadas, V. Percec, *Macromolecules* **2009**, *42*, 2379.

Chapter 3: One-pot synthesis of amphiphilic diblock and triblock copolymers via high-throughput Cu(0)-mediated polymerization

Abstract

In this chapter the synthesis of diblock copolymers and ABA-triblock copolymers containing poly(*n*-butyl acrylate) as a first or middle block and poly(2-(dimethylamino)ethyl acrylate), poly(1-ethoxyethyl acrylate) and poly(1-ethoxyethyl-2-carboxyethyl acrylate) as second or outer blocks is reported. The polymerizations were performed via one pot sequential monomer addition reactions via Cu(0)-mediated polymerization using an automated parallel synthesizer and manually on larger scale using schlenk techniques. The diblock and triblock copolymers could be synthesized with good control over molecular weight and dispersities around 1.1 were obtained. The synthesized ABA-triblock copolymers were used to prepare supramolecular thermoplastic elastomers, which is discussed further in Chapter 6.

3.1 Introduction

In the previous chapter the optimization of the Cu(0)-mediated polymerization of *n*-butyl acrylate and 2-methoxyethyl acrylate using an automated parallel synthesizer was reported. We also showed that, under optimized conditions, diblock copolymers could be synthesized by addition of a second monomer to the reaction mixture after most of the first monomer was polymerized. Here we expand this work by optimizing the one-pot automated synthesis of amphiphilic diblock and triblock copolymers using different, more challenging monomers.

Cu(0)-mediated polymerization is very well suited for one-pot block copolymerizations based on the excellent control over the polymerization.[1] An earlier pioneering paper showed the synthesis of multiblock copolymers containing very short blocks of monomers that were added sequentially to the reaction,[2] while other more recent publications also reported the synthesis of multiblock copolymers with longer blocks.[3-6] Synthesis of star-shaped block copolymers was also reported[7] and the synthesis of multiblock poly(acrylamides) was also shown recently.[8, 9]Generally almost full conversion of each block was obtained and dispersions are low even after the addition of several blocks, although some termination of chains can often be observed when the number of blocks increases. In each of these examples, relatively simple acrylates without functional groups were used. Moreover, each monomer had to be added manually, requiring labor-intensive work and careful planning of experiments. Here we aim to synthesize amphiphilic block copolymers containing functional acrylates using Cu(0)-mediated polymerization with sequential monomer addition in an automated system.

n-Butyl acrylate is used as a hydrophobic first or middle block in these polymerizations. The first hydrophilic block that will be attached is poly(2-(dimethylamino)ethyl acrylate) (PDMAEA), an amine-functionalized monomer that can carry a positive charge when protonated. The amine may create problems during Cu(0)-mediated polymerization because of its ability to act as a ligand for copper ions or by reaction with the halogen end group of the initiator or growing polymer chain.[10] A similar type of quarternization reaction was reported earlier for Cu(0)-mediated polymerization with Me_6TREN as ligand than was quarternized with EBP and bromine-containing chain ends.[11] However, Me_6TREN is usually present in much lower amounts than the monomer, so these reactions may be much more pronounced when using an amine-functionalized monomer.

A second hydrophilic block that will be incorporated constitutes of 1-ethoxyethyl acrylate (EEA), which is readily deprotected to form acrylic acid (AA) when it is heated or treated with water (Figure 40).[12-14] The thermal dissociation is reported to take place at 140 °C in a thin film,[12] but can also be observed slowly at lower temperatures.[13, 15] PAA is a water-soluble polymer that carries a negative charge when deprotonated. However, free AA cannot be present during ATRP or Cu(0)-mediated polymerization due to its disruptive interaction with the catalytic system by strong coordination of the copper ions and protonation of the nitrogen-containing ligands. A related newly developed monomer that will also be used to prepare the hydrophilic blocks is ethoxyethyl-protected 2-carboxyethyl acrylate (proCEA), which can be deprotected to 2-carboxyethyl acrylate (CEA). Both monofunctional and bifunctional initiators were used for the sequential Cu(0)-mediated polymerizations to be able to synthesize diblock and triblock copolymers (Figure 41). The amphiphilic ABA-triblock copolymers were also manually synthesized on a larger scale. Analysis of their mixtures as supramolecular materials, formed by electrostatic interaction between DMAEA and AA or CEA, is reported in Chapter 6.

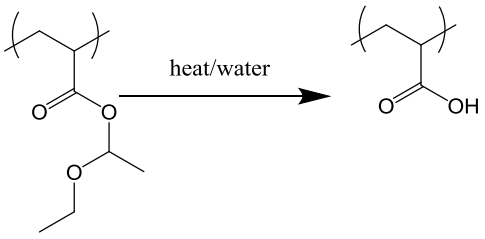

Figure 40. Deprotection of PEEA to PAA.

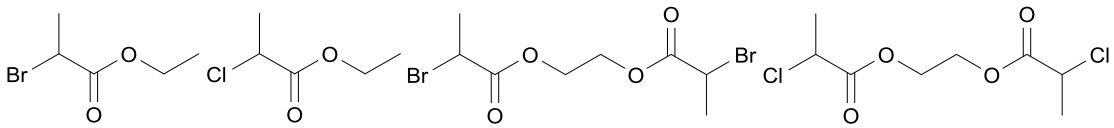

Figure 41. Initiators used in this chapter. From left to right: EBP, ECP, BPE and CPE.

3.2 Experimental section

Materials

N,N-Dimethylformamide (DMF, dry) and tetrahydrofuran (THF, dry, unstabilized and free of peroxides) were obtained from a solvent purification system (Meyer, custom made with a nitrogen, aluminum oxide drying system). Copper(II)bromide ($CuBr_2$, 99%) was purchased from Fluka. Dichloromethane (99.8%), ethyl 2-bromopropionate (EBP, 99%), ethyl 2-chloropropionate (ECP, 97%), copper(II)chloride ($CuCl_2$, 97%), acrylic acid (99%), ethyl vinyl ether (99%), phosphoric acid (99.99%), 4-(dimethylamino)pyridine (99%), ethylene glycol (99%), 2-chloropropionic acid (92%), 2-bromopropionyl bromide (97%), pyridine (99.8%), sodium bicarbonate ($NaHCO_3$, 99.7%), tris(2-aminoethyl)amine (96%), formic acid (95%), formaldehyde (37% solution) and inhibitor removers were purchased from Sigma-Aldrich. *N*-(3-Dimethylaminopropyl)-*N*'-ethylcarbodiimide hydrochloride was purchased from Iris Biotech. Hydrochloric acid (HCl, 37% solution) and sodium chloride (99%) were purchased from Acros. Magnesium sulfate ($MgSO_4$, dried) was purchased from Fisher Scientific. Aluminum oxide (90 standardized) was purchased from Merck. CupriSorb was purchased from Amazon. All were used as received. *N*-butyl acrylate (BA, 99%) was purchased from Sigma-Aldrich and purified by passing over a basic aluminum oxide column to remove the inhibitor. 2-(Dimethylamino)ethyl acrylate (DMAEA, 97%) was purchased from TCI and the inhibitor was removed

by stirring with inhibitor remover that was removed by filtration. Tris[2-(dimethylamino)ethyl]amine (Me_6TREN) was synthesized according to a previously published procedure.[16] Pre-cut copper wire (Sigma-Aldrich, 99.9%) was stirred in sulfuric acid, milliQ water and acetone before use.

Automated Cu(0)-mediated polymerization

Reactions were performed using a Chemspeed ASW2000 automated synthesizer equipped with 16 parallel reactors of 13 mL, a Huber Petite Fleur thermostat for heating/cooling, a Huber Ministat 125 for reflux and a Vacuubrand PC 3000 vacuum pump. Polymerization of BA was performed using the optimized reaction conditions from Chapter 2, which are a [BA]:[I]:[Me_6TREN]:[Cu(II)] ratio of 50:1:0.15:0.1 at 3.0 M in DMF at 25 °C and 12.5 mm^2/mL Cu(0) wire, with a reaction volume of 4 mL. A solution of the second monomer was added to the reactors after a certain time for the synthesis of block copolymers. Stock solutions of all components were prepared and bubbled with argon for at least 30 minutes before being introduced into the robot system and then kept under argon atmosphere. The hood of the automated synthesizer was continuously flushed with nitrogen and the reactors were flushed with argon to ensure an inert atmosphere. Before starting the polymerizations, the reactors were degassed through ten vacuum-argon cycles. Stock solutions were transferred to the reactors using the syringe of the automated synthesizer. During the reactions, 50 µL samples were taken at preset time intervals and directly injected into 1.5 mL sample vials, each containing a 0.1 mg/mL solution of phenothiazine in ~1.5 mL THF to quench the reaction. A detailed protocol for the homopolymerizations is described in the previous chapter.

Gas Chromatography

Samples were measured with GC to determine the monomer conversion from the ratio of the integrals from the monomer and the internal standard. GC was performed on an Agilent 7890A system equipped with a VWR Carrier-160 hydrogen generator and an Agilent HP-5 column of 30 m length and 0.320 mm diameter. An FID detector was used and the inlet was set to 250 °C with a split injection of ratio 25:1. Hydrogen was used as carrier gas at a flow rate of 2 mL/min. The oven temperature was increased with 20°C/min from 50°C to 120°C, followed by a ramp of 50°C/min to 300°C.

Size Exclusion Chromatography

The samples were run over a short aluminum oxide column to remove residual copper before the SEC measurements. SEC was performed on a Varian PL-GPC 50 Plus system using THF at 1 mL/min as eluent, and equipped with two PLgel 5 µm MIXED-D columns, a PL-AS RT autosampler and five detectors: RI, light scattering at 15° and 90°, a viscometer and a UV Knauer Wellchrom Spectro-Photometer K-2501. Molecular weights were determined with the RI detector and calculated against polystyrene standards.

Synthesis of ethylene glycol bis(2-bromopropionyl) ethane (BPE)

BPE was synthesized following a previously published method.[17] A solution of 2-bromopropionyl bromide (120 mmol, 25.9 g, 12.6 mL) in dry THF (40 mL) was added dropwise to a cooled solution of ethylene glycol (50 mmol, 3.1 g, 2.7 mL) and pyridine (120 mmol, 9.5 g, 9.7 mL) in dry THF (50 mL). The reaction was strirred overnight at room temperature and purified by filtration, washing and flash chromatography using silica as stationary phase and a gradient of hexane:ethyl acetace from 99:1 to 3:7 as eluent to yield 13.74 (81 %) of BPE.

Synthesis of ethylene glycol bis(2-chloropropionyl) ethane (CPE)

A solution of ethylene glycol (2.00 g, 32.2 mmol) and 2-chloropropionic acid (8.39 g, 77.3 mmol) in dichloromethane (30 mL) was cooled with an ice bath and a solution of *N*-(3-dimethylaminopropyl)-*N*'-ethylcarbodiimide hydrochloride (16.57 g, 80.6 mmol) and 4-(dimethylamino)pyridine (0.79 g, 6.4 mmol) in dichloromethane (60 mL) was added dropwise. The reaction was allowed to warm up to room temperature and stirred overnight. It was then washed with 1M HCl, distilled water, a $NaHCO_3$ solution and brine. The solution was dried with $MgSO_4$, filtered and the solvent was removed under reduced pressure to yield 7.35 g (94%) of CPE as a light yellow liquid.

^{1}H NMR ($CDCl_3$, 300 MHz) δ: 4.42 ppm (4H, s, 2 CH_2-CH_2), 4.41 ppm (2H, q, 2 CH-CH_3), 1.70 ppm (6H, d, 2 CH-CH_3)

Synthesis of 1-ethoxyethyl acrylate (EEA) and protected 2-carboxyethyl acrylate (proCEA)

EEA and proCEA were synthesized following a previously published procedure and distilled prior to use.[12] For the synthesis of proCEA, phosphoric acid (109 mg, 1.11 mmol) was weighed into a dry round bottom flask in a glovebox and then taken outside the glovebox, taking care that the phosphoric acid stayed dry. 2-Carboxyethyl acrylate (80 g, 555 mmol) and ethyl vinyl ether (48 g, 666 mmol) were added and the reaction was stirred for two days at room temperature. Hydrotalcite ($Mg_6Al_2(OH)_{16}CO_3 \cdot 4H2O$, ~1 g) was added, stirred for one hour and filtered off. Excess ethyl vinyl ether was removed under reduced pressure and the product was distilled under vacuum (80 °C, 1.3 mbar).

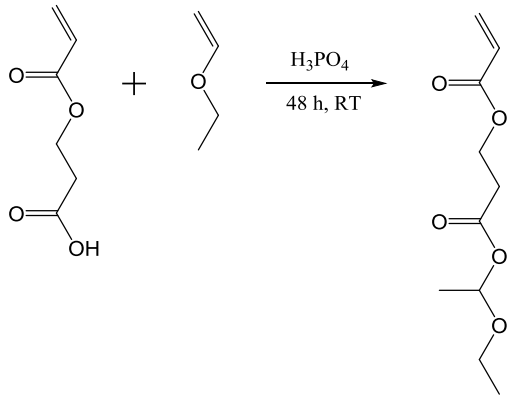

Figure 42. Synthesis of proCEA.

^{1}H NMR EEA ($CDCl_3$, 300 MHz) δ: 6.40 ppm (1H, dd, CH_2=CH-C(O)), 6.10 ppm (1H, dd, CH_2=CH-C(O)), 5.99 ppm (1H, q, CH_3-CH-$(O)_2$), 5.82 ppm (1H, dd, CH_2=CH-C(O)), 3.70 ppm (1H, m, CH_3-CH_2-O), 3.53 ppm (1H, m, CH_3-CH_2-O), 1.41 ppm (3H, d, CH_3-CH-$(O)_2$), 1.18 ppm (3H, t, CH_3-CH_2-O)

^{1}H NMR proCEA ($CDCl_3$, 300 MHz) δ: 6.32 ppm (1H, dd, CH_2=CH-C(O)), 6.06 ppm (1H, dd, CH_2=CH-C(O)), 5.93 ppm (1H, q, CH_3-CH-$(O)_2$), 5.80 ppm (1H, dd, CH_2=CH-C(O)), 4.39 ppm (2H, t, O-CH_2-CH_2-C(O)), 3.64 ppm (1H, m, CH_3-CH_2-O), 3.48 ppm (1H, m, CH_3-CH_2-O), 2.66 ppm (2H, t, O-CH_2-CH_2-C(O)), 1.35 ppm (3H, d, CH_3-CH-$(O)_2$), 1.14 ppm (3H, t, CH_3-CH_2-O)

^{13}C NMR proCEA ($CDCl_3$, 300 MHz) δ: 170 ppm (O-CH_2-CH_2-C(O)-O), 166 ppm (CH_2=CH-C(O)-O), 131 ppm ($C$$H_2$=CH-C(O)), 128 ppm ($CH_2$=$C$H-C(O)), 96 ppm ($CH_3$-$C$H-$(O)_2$), 64 ppm ($CH_3$-$C$$H_2$-O), 60 ppm (O-$C$$H_2$-$CH_2$-C(O)), 34 ppm (O-$CH_2$-$C$$H_2$-C(O)), 20 ppm ($C$$H_3$-CH-$(O)_2$), 14 ppm ($C$$H_3$-$CH_2$-O)

Manual polymerization of PDMAEA-*b*-PBA-*b*-PDMAEA

A solution of [BA]:[Me_6TREN]:[$CuCl_2$] = 50:0.3:0.2 at a monomer concentration of 3.0 M in DMF (total volume 21.00 mL) with 12.5 mm^2/mL Cu(0) wire was bubbled with argon for one hour, after which 1 eq. of CPE was added to the reaction mixture with a syringe to start the reaction. The polymerization was run at room temperature for 18.5 hours, after which a degassed solution of DMAEA (3.0 M in DMF, 50 eq.) was added using a cannula. The polymerization was continued to a total reaction time of 44 hours, after which the mixture was diluted with methanol (~10 mL) and stirred with CupriSorb overnight. The mixture was then filtered and a small amount of phenothiazine was added to prevent further polymerization. The solvent was removed under reduced pressure and the resulting mixture was transferred to a glass petri dish. The monomer and residual solvent were removed in a vacuum oven overnight.

Manual polymerization of PEEA-*b*-PBA-*b*-PEEA

A solution of [BA]:[Me_6TREN]:[$CuBr_2$] = 50:0.3:0.2 at a monomer concentration of 3.0 M in DMF (total volume 21.00 mL) with 12.5 mm^2/mL Cu(0) wire was bubbled with argon for one hour, after which 1 eq. of BPE was added to the reaction mixture with a syringe to start the reaction. The polymerization was run at room temperature for 6 hours, after which a degassed solution of EEA (3.0 M in DMF, 50, 20 and 12 eq. in separate experiments) was added using a cannula. The polymerization was continued to a total reaction time of 48 hours, after which the polymers were precipitated in water, dissolved in THF and dried in a petri dish in a vacuum oven.

Manual polymerization of PproCEA-*b*-PBA-*b*-PproCEA

A solution of [BA]:[Me_6TREN]:[$CuBr_2$] = 50:0.3:0.2 at a monomer concentration of 3.0 M in DMF (total volume 8.00 mL) with 12.5 mm^2/mL Cu(0) wire was bubbled with argon for one hour, after which 1 eq. of BPE was added to the reaction mixture with a syringe to start the reaction. The polymerization was run at room temperature for 4.5 hours, after which a degassed solution of proCEA (3.0 M in DMF, 25 eq.) was added using a cannula. The polymerization was continued to a total reaction time of 48 hours, after which the mixture was diluted with methanol (~10 mL) and stirred with CupriSorb overnight. The mixture was then filtered, diluted with water and dialyzed (MWCO = 1000) against water and freeze-dried.

3.3 Results and discussion

3.3.1 Homopolymerizations of DMAEA and EEA

To assess the feasibility of making amphiphilic block copolymers of PBA with PDMAEA and PEEA, homopolymerizations of DMAEA and EEA were first investigated. The homopolymerization of DMAEA was performed with [DMAEA]:[EBP]:[L]:[$CuBr_2$] = 50:1:0.18:0.05 and 50:1:0.09:0.025 at 3.0 M in DMSO at 25 °C, using both Me_6TREN and PMDETA as ligand. These conditions were chosen based on previous papers that used different monomers.[2] The first order kinetic plot and M_n vs. conversion plot (Figure 43) show that conversions up to 90 % could be obtained in several hours with good control over the M_n. However, the dispersities at high conversion are around 1.2-1.3, which is higher than previously observed for BA homopolymerizations (Chapter 2), possibly due to side reactions between the amine of DMAEA and the bromide end-group of the polymer chain, so further optimization is necessary for the polymerization of DMAEA. The polymerizations using Me_6TREN show a higher conversion and lower dispersity than those with PMDETA, which is expected from the higher activation of Me_6TREN complexes and was also found for the Cu(0)-mediated polymerization

of BA in Chapter 2. The reactions with a higher amount of ligand show a higher rate of polymerization, although both ratios give similar dispersities, which is also in line with earlier results.

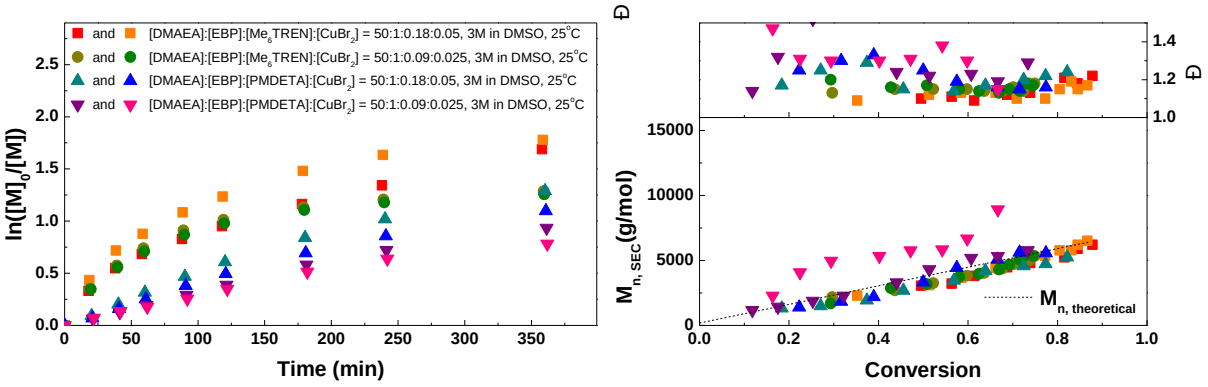

Figure 43. Left: first order kinetic plot for Cu(0)-mediated polymerization of DMAEA using different conditions and 14.3 mm^2/mL Cu(0) wire. Right: corresponding molecular weight and dispersity vs. conversion plot.

Homopolymerizations of EEA are shown in Figure 44. Again, reaction conditions from an earlier paper were used as a starting point, with [EEA]:[EBiB]:[Me_6TREN]:[$CuBr_2$] = 100:1:0.18:0.05 and lower amount of either ligand or EEA.[2] These reactions were relatively slow, and in some polymerizations an increase in dispersity up to 1.4 is seen, which is quite high for this type of polymerization. This may be from partial deprotection of the EEA to AA, which would interfere with the Me_6TREN/copper complex and disrupt the controlled polymerization. This would also explain why the increase in dispersity is seen in only some reactions and not in all duplicates, as the deprotection is difficult to control and is self-catalysing. Similar to the previous experiment, the reactions using a lower ligand ratio are slower. The reactions with a 50:1 ratio of monomer to initiator are faster than those with a 100:1 ratio, even though these were performed at a lower concentration, so it seems that the monomer concentration does not have a very large effect on the rate of polymerization. In summary, more optimization is needed but these preliminary reactions show that DMAEA and EEA can successfully be polymerized using Cu(0)-mediated polymerization. Further optimization will directly be performed for the block copolymerizations.

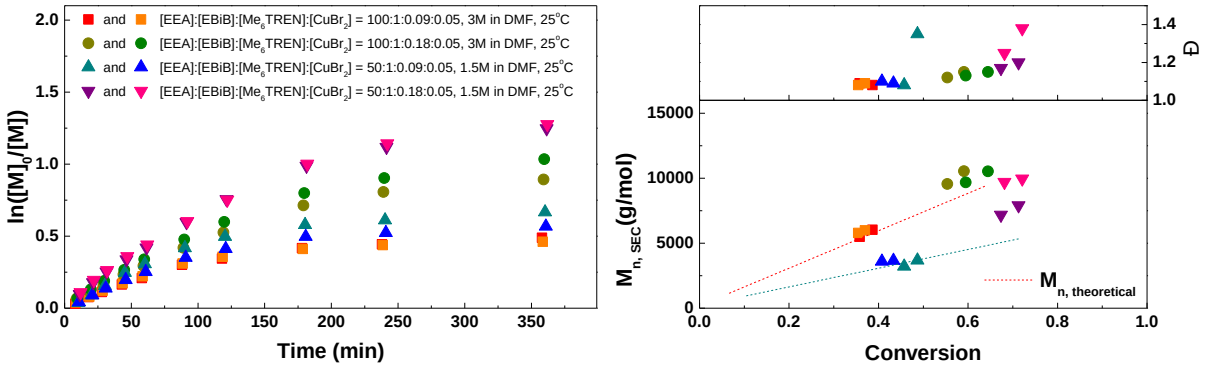

Figure 44. Left: first order kinetic plot for Cu(0)-mediated polymerization of EEA using different conditions and 12.8 mm^2/mL Cu(0) wire. Right: corresponding molecular weight and dispersity vs. conversion plot.

3.3.2 Synthesis of PBA-*b*-PDMAEA diblock copolymers

For the one-pot block copolymerization of BA with DMAEA, the first experiment was performed to determine which initiator was the most suitable for this reaction (Figure 45). The results of the block copolymerizations are shown as conversion vs. time plots instead of first order kinetic plots, because

the $\ln([M]_0/[M])$ of the second monomer is generally not linear and, in addition, the conversion of both monomers is clearer in the conversion versus time plots. Because it was expected that DMAEA may react with the halogen end group of the growing polymer chain, a bromide and a chloride–containing initiator were studied. The experiments in Chapter 2 showed EBP was a good initiator for the polymerization of BA, and ECP was used for its similar structure. In this experiment, $CuBr_2$ was used as Cu(II) source for both initiators, to be able to compare only the effect of the initiator itself. The polymerizations using EBP show higher conversion of both BA and DMAEA than the polymerizations using ECP, due to its higher activation rate.[18] At the last data point, after 48 hours of reaction time, almost no increase in conversion in seen anymore. This is likely from a loss of radicals, which may be due to increasing buildup of Cu(II) in the system. As Cu(II) acts as deactivator, an increased amount will slow down the polymerizations. Looking at the SEC data, the experimental molecular weights are in good agreement with $M_{n,th}$ for both initiators, with a linear increase of the M_n with increasing conversion of DMAEA. Importantly, the dispersity of the polymerizations with ECP is constant, while the dispersity of the EBP polymerizations increases with conversion.

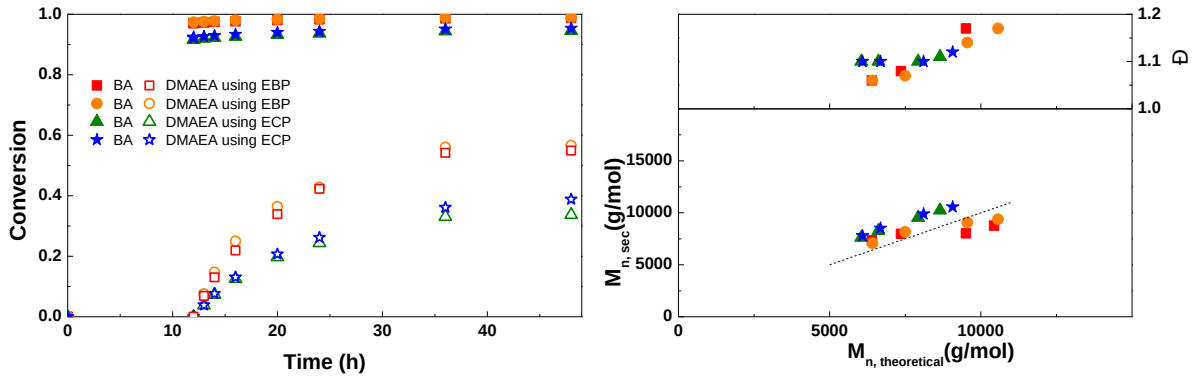

Figure 45. Left: conversion vs. time plot for Cu(0)-mediated one pot block copolymerization of BA and DMAEA using [BA]:[DMAEA]:[EBP]:[Me_6TREN]:[$CuBr_2$] = 50:50:1:0.15:0.1 and [BA]:[DMAEA]:[ECP]:[Me_6TREN]:[$CuBr_2$] = 50:50:1:0.15:0.1, 3.0 M in DMF at 25°C and 12.5 mm^2/mL Cu(0) wire. A 3.0 M solution of DMAEA in DMF was added after 12 hours reaction time. Right: corresponding molecular weight and dispersity vs. theoretical molecular weight plot.

When looking in detail at the SEC traces of the polymerizations (Figure 47), the difference between the reactions with the two different initiators becomes more obvious. While the homopolymerization of BA using EBP shows a well-controlled polymerization with a dispersity of 1.06, after addition of DMAEA the polymer peak broadens and the dispersity increases significantly. When ECP is used as an initiator, the dispersity for PBA is slightly higher at 1.10. When DMAEA is added a clean shift of the peak is observed, indicating growth of the polymer, and the dispersity and shape of the peak stay constant. So while ECP is a less effective initiator for BA compared to EBP, it works much better for DMAEA than EBP. This is probably due to the quarternization that can occur between the amine group of DMAEA and the ω-end of the polymer (Figure 46).[11] This is less pronounced when using a chloride-containing initiator compared to a bromide-containing initiator as alkyl bromides are stronger alkylating agents than alkyl chlorides. Therefore, further reactions were performed using ECP and $CuCl_2$.

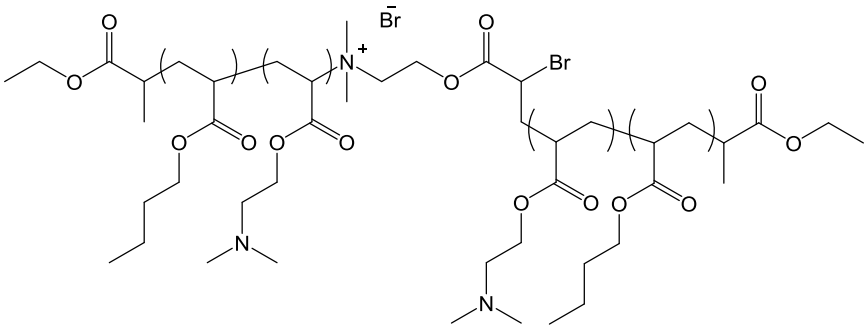

Figure 46. Proposed structure of branched PBA-*b*-PDMAEA resulting from quarternization of PDMAEA.

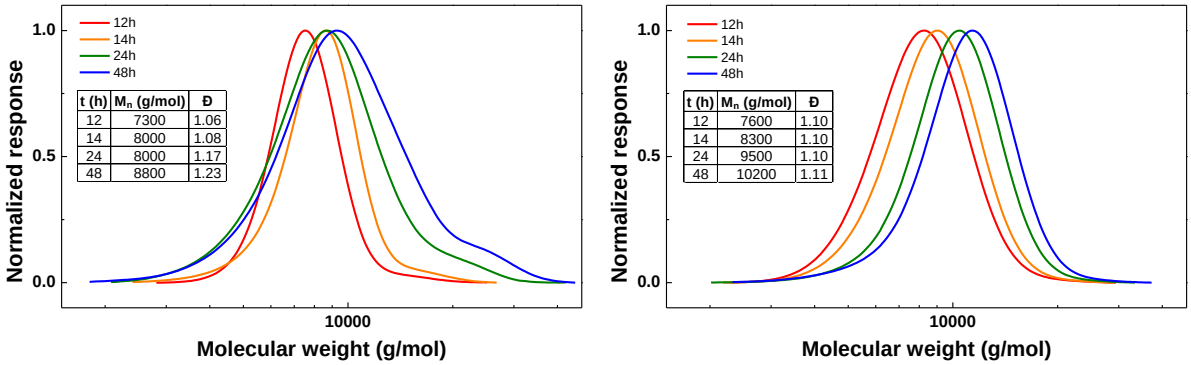

Figure 47. Left: SEC traces for PBA-*b*-PDMAEA using EBP as initiator. Right: SEC traces for PBA-*b*-PDMAEA using ECP as initiator.

For the next experiment, the solution of DMAEA was added to the reaction at different times to find out which would give the best diblock copolymer (Figure 48). When the DMAEA is added after 6 hours, BA conversion is still low, so this leads to the formation of a mixed second block. The same is true for 12 hours although to a lesser extent. When DMAEA is added after 18 or 24 hours, almost no further conversion of BA is seen after addition of DMAEA, so in these reactions almost pure diblock copolymers are formed. In further reactions DMAEA was added after 18 hours, because in that case the final conversion of DMAEA was a little higher. $M_{n,SEC}$ is in good agreement with $M_{n,th}$ for all polymerizations, with all dispersities around 1.1, showing good control.

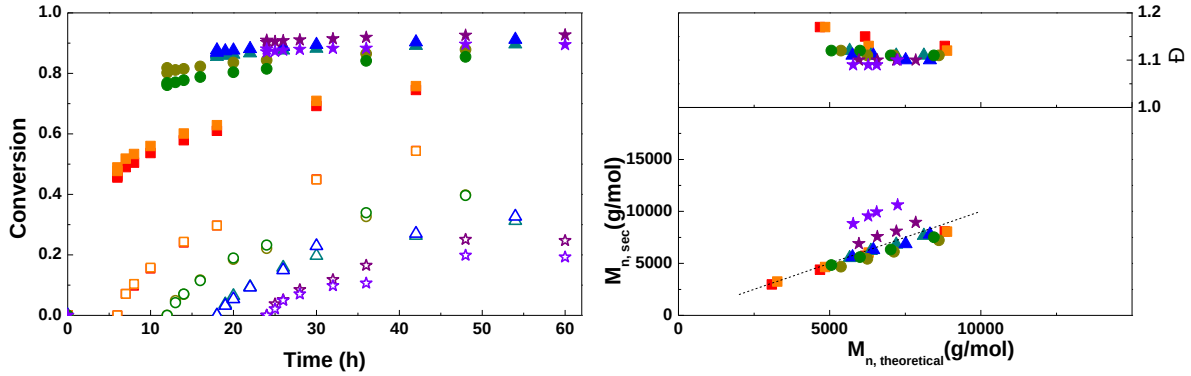

Figure 48. Left: conversion vs. time plot for Cu(0)-mediated one pot block copolymerization of BA and DMAEA using [BA]:[DMAEA]:[ECP]:[Me_6TREN]:[$CuCl_2$] = 50:50:1:0.15:0.1, 3.0 M in DMF at 25°C and 12.5 mm^2/mL Cu(0) wire. A 3.0 M solution of DMAEA in DMF was added after 6, 12, 18 or 24 hours reaction time. Right: corresponding molecular weight and dispersity vs. theoretical molecular weight plot.

The addition of DMAEA as pure monomer or as 3 M or 6 M solution in DMF was studied next. It was expected that a higher concentration would lead to a faster polymerization, due to higher availability of the monomer, though an increase in viscosity may also lead to slower polymerization due to diffusion limitations as well as higher dispersity due to inadequate mixing. As shown in Figure 49, no significant difference is observed between the reactions, so the increase in polymerization rate is negligible, which is similar to what was observed for reactions at different concentrations in Figure 44. Probably the small effects of increasing both concentration and viscosity cancel each other out, so the concentration of DMAEA was kept at 3.0 M for further reactions. As in the previous reactions, good control over molecular weight with a dispersity of 1.1 was obtained. This is lower than the dispersities reported by Whittaker *et al.* for diblock copolymers of different alkyl acrylates, although different reaction conditions were used and almost full conversion was obtained in multiple iterative steps.[3] More recent papers show dispersities of 1.09 for diblock poly(methyl acrylate) and 1.05 for poly(methyl acrylate-*block*-*tert*-butyl acrylate)[4], while a dispersity of 1.13 was obtained with photo-initiated Cu(0)-mediated synthesis of poly(methyl acrylate-*block*-*tert*-butyl acrylate).[6] So although a lower final conversion is obtained than in these examples using simple acrylates, the similar dispersity indicates that these polymerizations are similarly well-controlled.

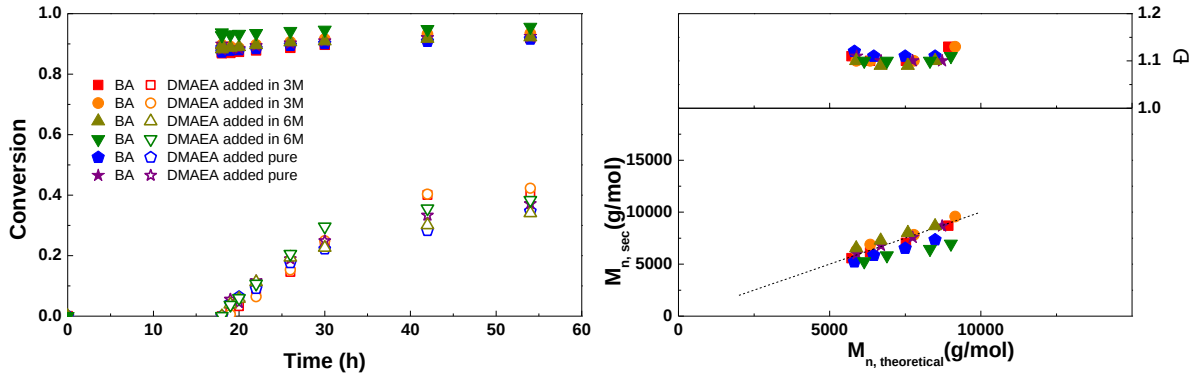

Figure 49. Left: conversion vs. time plot for Cu(0)-mediated one pot block copolymerization of BA and DMAEA using [BA]:[DMAEA]:[ECP]:[Me_6TREN]:[$CuCl_2$] = 50:50:1:0.15:0.1, 3.0 M in DMF at 25°C and 12.5 mm^2/mL Cu(0) wire. A 3.0 M or 6.0 M solution of DMAEA in DMF or pure DMAEA was added after 18 hours reaction time. Right: corresponding molecular weight and dispersity vs. theoretical molecular weight plot.

3.3.3 Synthesis of PDMAEA-*b*-PBA-*b*-PDMAEA triblock copolymers

After successful optimization of the PBA-b-PDMAEA diblock copolymer synthesis, a bifunctional chloride-containing initiator was used to synthesize PDMAEA-*b*-PBA-*b*-PDMAEA triblock copolymers. As this initiator is not commercially available, it was synthesized from 2-chloropropionic acid and ethylene glycol using EDC and DMAP. The product was washed with HCl, distilled water and $NaHCO_3$ to remove impurities, and as all impurities were water soluble column chromatography was not needed. The ^{1}H NMR spectrum of this initiator is shown in Figure 50.

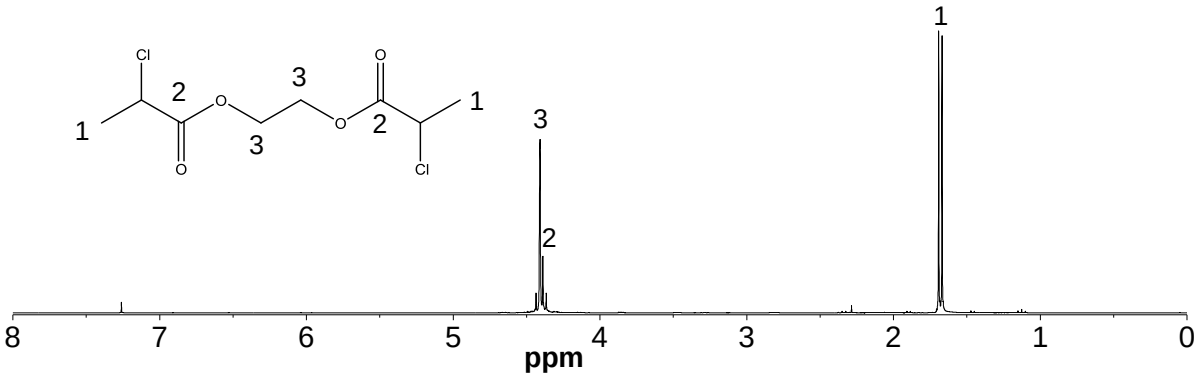

Figure 50. ^{1}H NMR spectrum of CPE.

In Figure 51 the polymerizations using the monofunctional ECP and bifunctional CPE are compared. Because CPE can be considered as two initiators, the amount of Me_6TREN and $CuCl_2$ was doubled compared to ECP. Conversions of BA and DMAEA are slightly higher using CPE than with ECP, which can be explained by the lower M/I ratio when CPE is considered as two initiators. Overall the reaction kinetics are very similar between the two initiators.

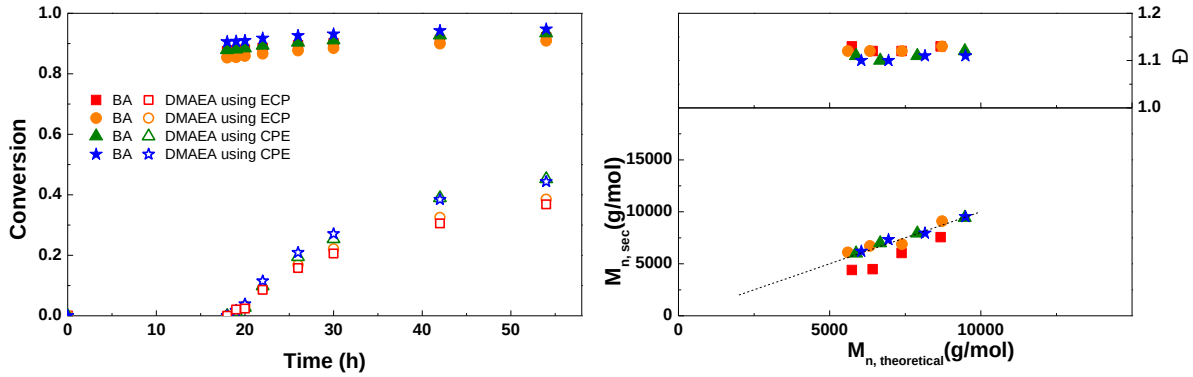

Figure 51. Left: conversion vs. time plot for Cu(0)-mediated one pot block copolymerization of BA and DMAEA using [BA]:[DMAEA]:[ECP]:[Me_6TREN]:[$CuCl_2$] = 50:50:1:0.15:0.1 and [BA]:[DMAEA]:[CPE]:[Me_6TREN]:[$CuCl_2$] = 50:50:1:0.3:0.2, 3.0 M in DMF at 25°C and 12.5 mm^2/mL Cu(0) wire. A 3.0 M solution of DMAEA in DMF was added after 18 hours reaction time. Right: corresponding molecular weight and dispersity vs. theoretical molecular weight plot.

Figure 52 shows the SEC traces for the triblock copolymerizations. A similar shift in molecular weight is observed as in earlier reactions with the monofunctional initiator (Figure 47), indicating that the triblock copolymer chains grow steadily with time and no significant side-reactions occur.

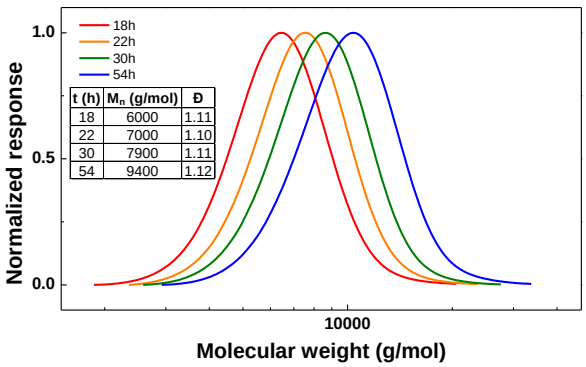

Figure 52. SEC traces for PDMAEA-*b*-PBA-*b*-PDMAEA prepared using CPE as initiator.

Inspired by the successful synthesis of defined PDMAEA-*b*-PBA-*b*-PDMAEA triblock copolymers, it was attempted to prepare triblock copolymers with different lengths (Figure 53). Here it is clear that the polymerization rate of both the BA and the DMAEA is lower when a higher monomer to initiator ratio is used, as may be expected from the lower initiator and ligand concentrations. In all samples a good agreement of $M_{n,SEC}$ with $M_{n,th}$ and a dispersity around 1.1 was found, indicating that the triblock copolymerizations are well-controlled.

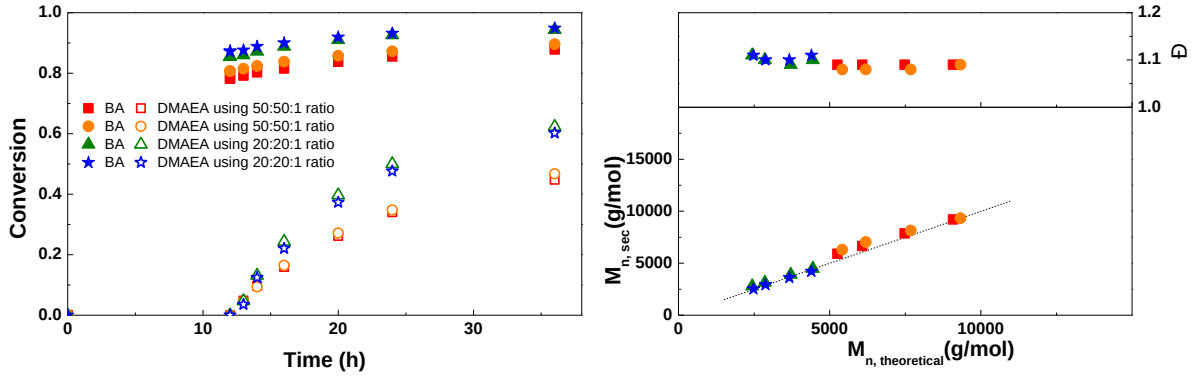

Figure 53. Left: conversion vs. time plot for Cu(0)-mediated one pot block copolymerization of BA and DMAEA using [BA]:[DMAEA]:[CPE]:[Me_6TREN]:[$CuCl_2$] = 50:50:1:0.3:0.2 and [BA]:[DMAEA]:[CPE]:[Me_6TREN]:[$CuCl_2$] = 20:20:1:0.3:0.2, 3.0 M in DMF at 25°C and 12.5 mm^2/mL Cu(0) wire. A 3.0 M solution of DMAEA in DMF was added after 12 hours reaction time. Right: corresponding molecular weight and dispersity vs. theoretical molecular weight plot.

3.3.4 Synthesis of PBA-*b*-PEEA diblock copolymers

For the block copolymerizations of BA and EEA, again a first experiment was performed to compare EBP and ECP as initiators. As shown in Figure 54, using EBP gives almost full conversion of BA after 12 hours, while the final conversion of EEA is relatively low, which is likely related to each other due to the amount of radicals in the system being lower at very high BA conversions. Using ECP as initiator, BA does not reach full conversion but the EEA reaches higher conversion compared to EBP, probably because here the amount of radicals is higher than in the reactions with EBP. For both initiators the M_n is close to $M_{n,th}$, but dispersities are slightly higher when ECP is used, as expected due to slower initiation.

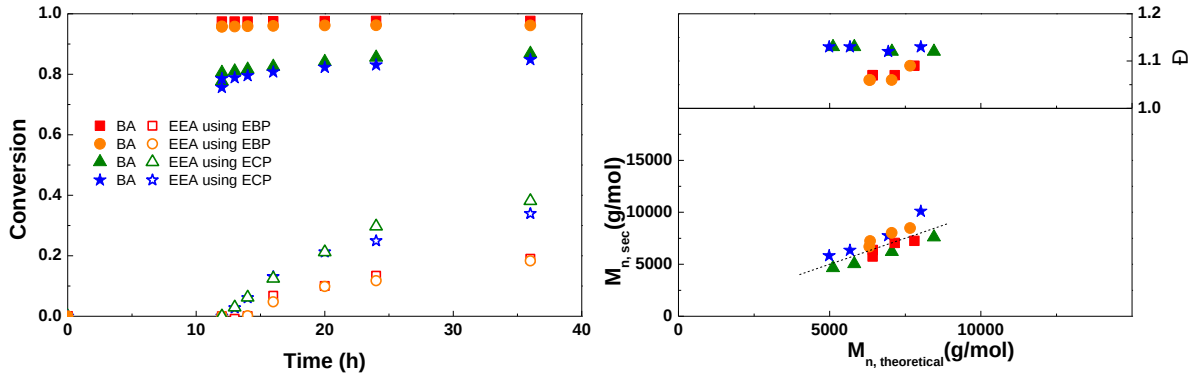

Figure 54. Left: conversion vs. time plot for Cu(0)-mediated one pot block copolymerization of BA and EEA using [BA]:[EEA]:[EBP]:[Me_6TREN]:[$CuBr_2$] = 50:50:1:0.15:0.1 and [BA]:[EEA]:[ECP]:[Me_6TREN]:[$CuCl_2$] = 50:50:1:0.15:0.1, 3.0 M in DMF at 25°C and 12.5 mm^2/mL Cu(0) wire. A 3.0 M solution of EEA in DMF was added after 12 hours reaction time. Right: corresponding molecular weight and dispersity vs. theoretical molecular weight plot.

When the SEC traces of these polymerizations are compared (Figure 55), it is clear that the polymerizations using ECP show significantly broader peaks, indicative for the slower initiation. With

EBP, some tailing at the low M_n side leads to a small increase in dispersity at higher conversion, possibly due to the presence of dead PBA chains resulting from too high conversion in the first step. Nonetheless, EBP was chosen as the most suitable initiator for the synthesis of block copolymers.

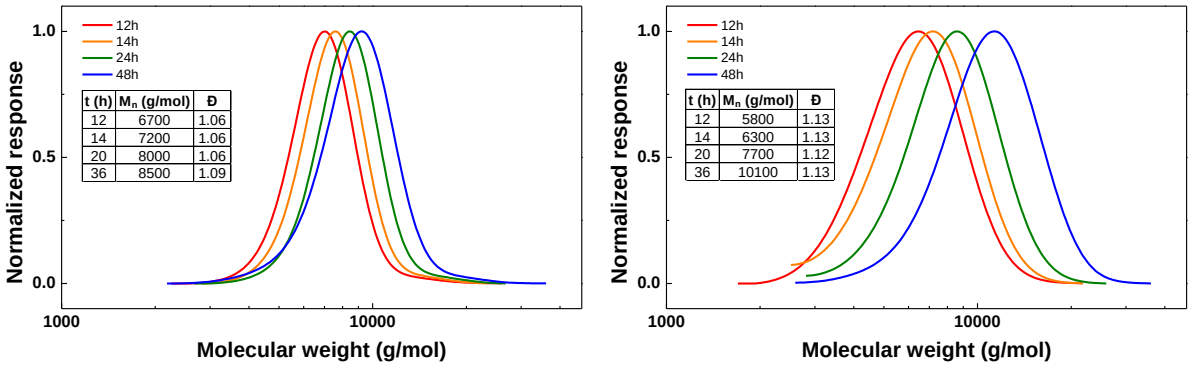

Figure 55. Left: SEC traces for PBA-*b*-PEEA using EBP as initiator. Right: SEC traces for PBA-*b*-PEEA using ECP as initiator.

To optimize the polymerizations with EBP, an experiment in which the solution of EEA was added at different times during the reaction was performed (Figure 56). After 3 hours the conversion of BA is not yet complete, but when EEA is added after 6 hours or later almost no further conversion of BA is seen. Final conversions of EEA in this experiment are slightly higher than in some of the other experiments, which may be due to freshness of the used chemicals, as both Me_6TREN and EEA were distilled immediately prior to this experiment. In all these reactions the conversion of EEA stops around 12 hours after the monomer is added. The SEC results generally show a good agreement of $M_{n,SEC}$ with $M_{n,th}$. Dispersities are around 1.05 at lower conversion, but above around 50 % conversion of EEA a large increase in dispersity is seen, together with the formation of a second peak at high M_n. This is believed to be caused by crosslinking through the formation of anhydrides, which was reported earlier for this monomer.[13, 19] Unfortunately we were not able to prevent this during the polymerization. However, the crosslinks can be broken through hydrolysis of the anhydrides, which could be achieved by simply stirring the polymers in water.

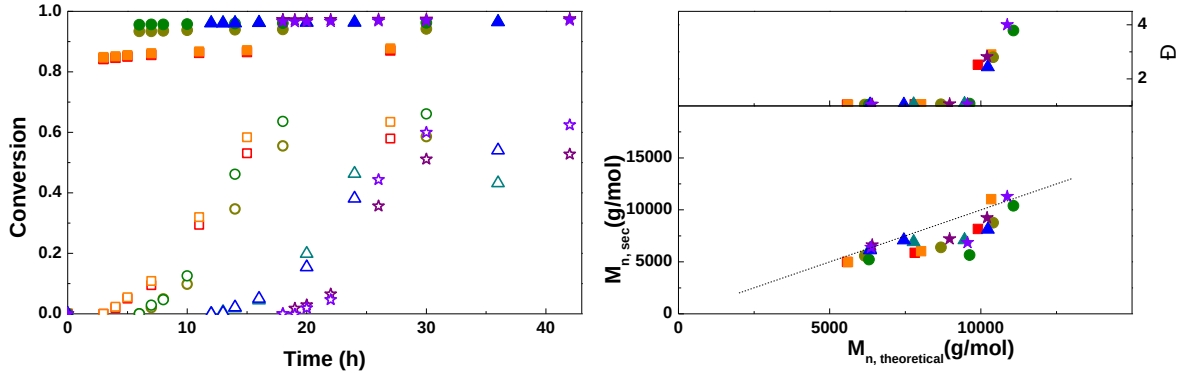

Figure 56. Left: conversion vs. time plot for Cu(0)-mediated one pot block copolymerization of BA and EEA using [BA]:[EEA]:[EBP]:[Me_6TREN]:[$CuBr_2$] = 50:50:1:0.15:0.1, 3.0 M in DMF at 25°C and 12.5 mm^2/mL Cu(0) wire. A 3.0 M solution of EEA in DMF was added after 3, 6, 12 or 18 hours reaction time (closed symbols: BA, open symbols: EEA). Right: corresponding molecular weight and dispersity vs. theoretical molecular weight plot.

To prove that the high M_n peaks observed in SEC were indeed caused by the formation of anhydrides between deprotected AA monomers, one of the polymers from this experiment, in which the EEA was added after 6 hours, was precipitated and stirred in a water/THF mixture at room temperature to hydrolyze the anhydrides. The resulting SEC traces are shown in Figure 57. After precipitation in

water, the high M_n peak is larger than before precipitation, probably because the larger aggregates of coupled polymer chains precipitate more easily than the individual polymer chains. The size of the high M_n peak decreases with time during stirring in water/THF and eventually it disappears, and only a high M_n shoulder remains, possibly resulting from termination through recombination. Additionally, a small shift of the main polymer peak towards higher molecular weight is observed, which is likely from increased solubility of the acrylic acid groups in the eluent, leading to a larger hydrodynamic radius. The reaction was relatively slow, which is probably due to the polymers being not completely water soluble because of the PBA block. The reaction conditions for this hydrolysis can probably be optimized to complete much faster. Nevertheless, the high M_n peak fully disappeared after several weeks, indirectly proving that the high molar mass polymer fraction is due to anhydride formation. Based on all these results, the optimal addition time of EEA was chosen at 6 hours.

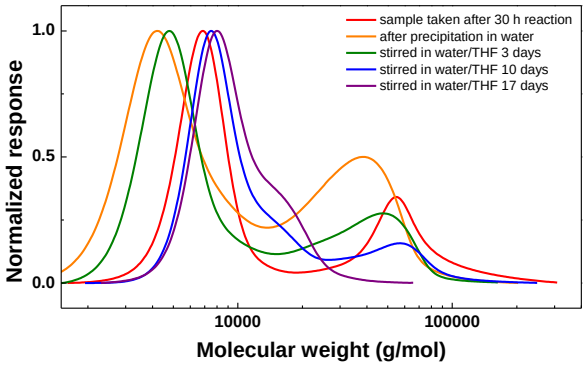

Figure 57. SEC traces of PBA-*b*-PEEA before and after precipitation and after stirring in water/THF for a longer time.

3.3.5 Synthesis of PEEA-*b*-PBA-*b*-PEEA triblock copolymers

A bifunctional bromine-containing initiator, BPE, was used for the synthesis of PEEA-*b*-PBA-*b*-PEEA triblock copolymers using the optimal conditions (Figure 58). Similar results were obtained for polymerizations with a monofunctional or bifunctional initiator, which was also seen for PDMAEA-*b*-PBA-*b*-PDMAEA triblock copolymers. Dispersities are below 1.1 in all reactions confirming well-controlled polymerizations leading to defined triblock copolymers.

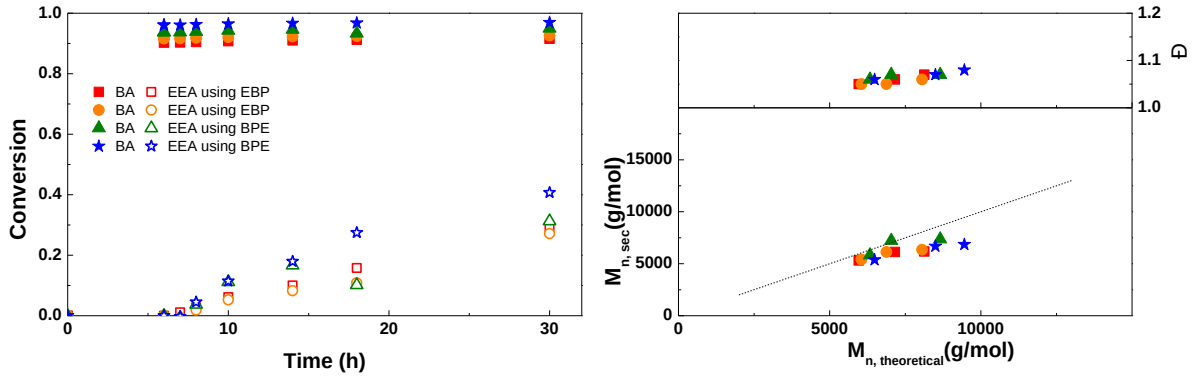

Figure 58. Left: conversion vs. time plot for Cu(0)-mediated one pot block copolymerization of BA and EEA using [BA]:[EEA]:[EBP]:[Me_6TREN]:[$CuBr_2$] = 50:50:1:0.15:0.1 and [BA]:[EEA]:[BPE]:[Me_6TREN]:[$CuBr_2$] = 50:50:1:0.3:0.2, 3.0 M in DMF at 25°C and 12.5 mm^2/mL Cu(0) wire. A 3.0 M solution of EEA in DMF was added after 6 hours reaction time. Right: corresponding molecular weight and dispersity vs. theoretical molecular weight plot.

3.3.6 Synthesis of PBA-*b*-PproCEA diblock and PproCEA-*b*-PBA-*b*-PproCEA triblock copolymers

Besides EEA, proCEA was used as an alternative acidic monomer containing a protective group that could be removed under mild conditions. The synthesis of this new monomer was performed similar to the previously reported synthesis of EEA and related monomers by acid catalyzed addition of ethyl vinyl ether to CEA.[12, 14] To prove the successful synthesis of proCEA, both 1D and 2D NMR spectra were measured. The ^{1}H NMR spectrum (Figure 59) is very similar to that of EEA, with two additional peaks around 4.39 and 2.66 ppm from the additional methylene groups. ^{1}H COSY NMR spectroscopy (Figure 60) shows the correlation between protons on neighboring carbon atoms, HSQC NMR spectroscopy (Figure 61) shows the correlation between protons and carbons that are directly attached to each other, and HMBC NMR spectroscopy (Figure 62) shows the correlation between protons and carbons separated by two or more chemical bonds. Because the HMBC NMR spectrum can also show correlation to quaternary carbons and across oxygen atoms, this provides the final confirmation that the correct structure was obtained.

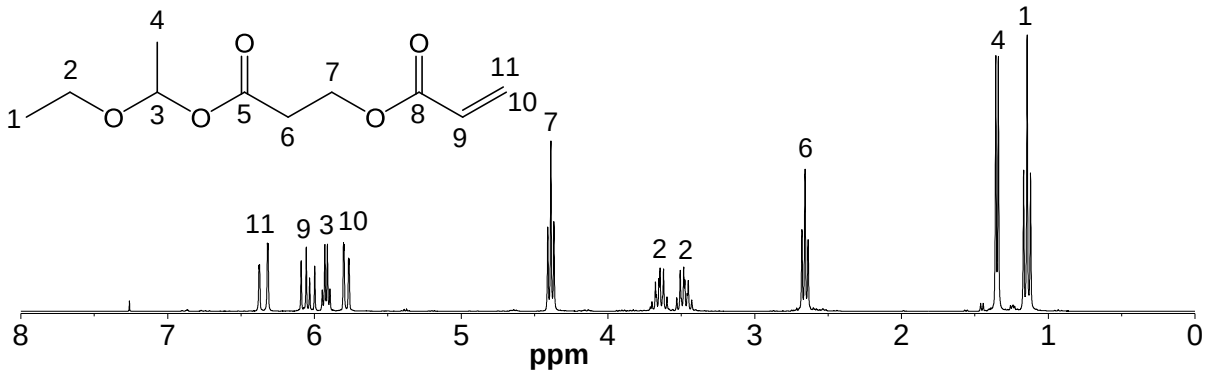

Figure 59. ^{1}H NMR spectrum of proCEA.

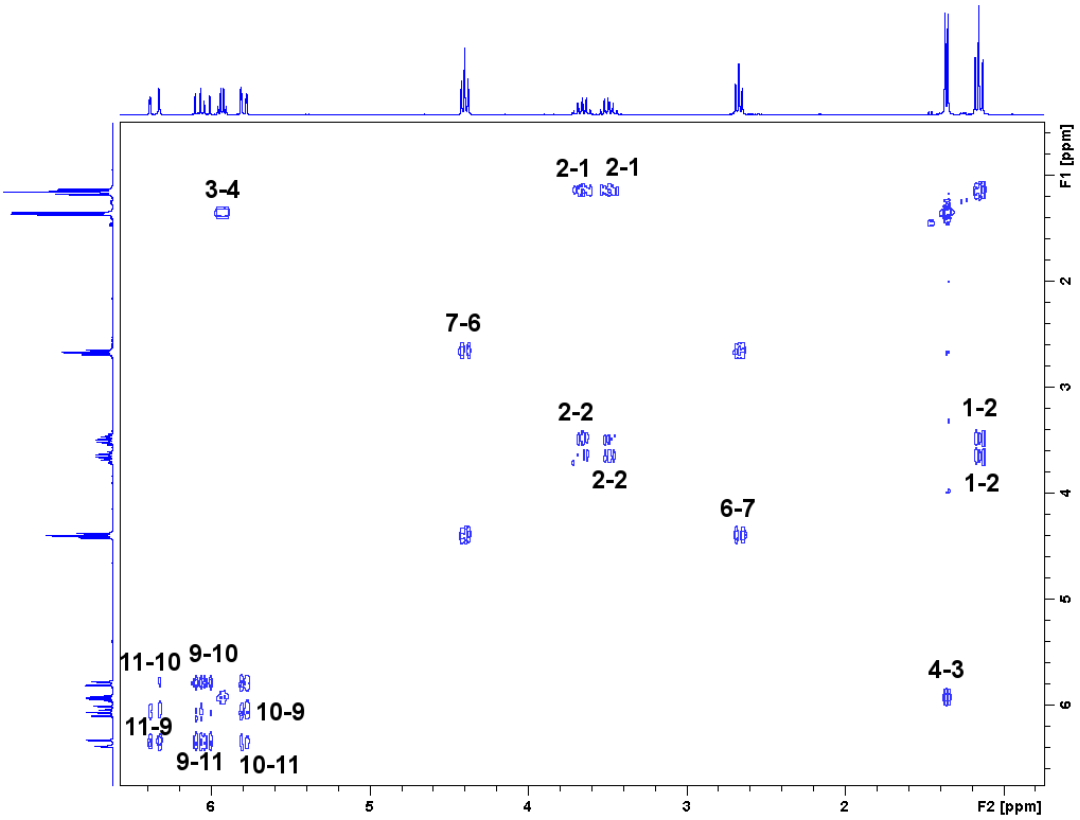

Figure 60. ^{1}H COSY NMR spectrum of proCEA.

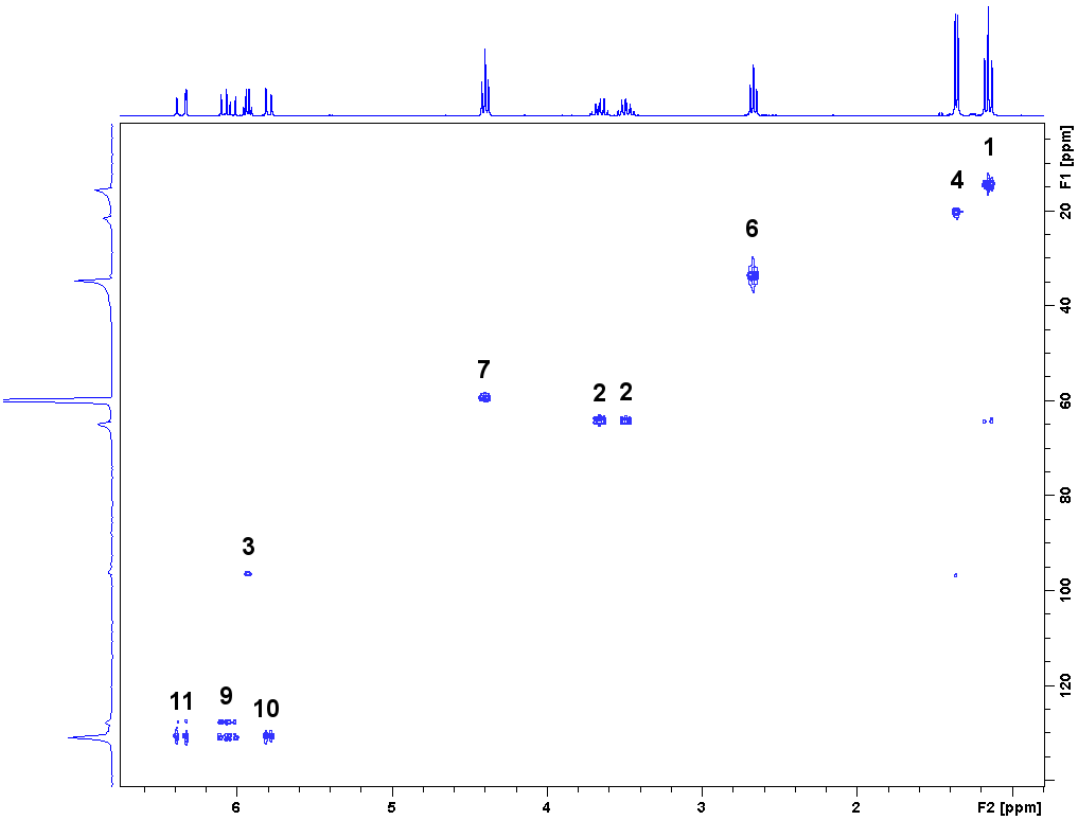

Figure 61. HSQC NMR spectrum of proCEA.

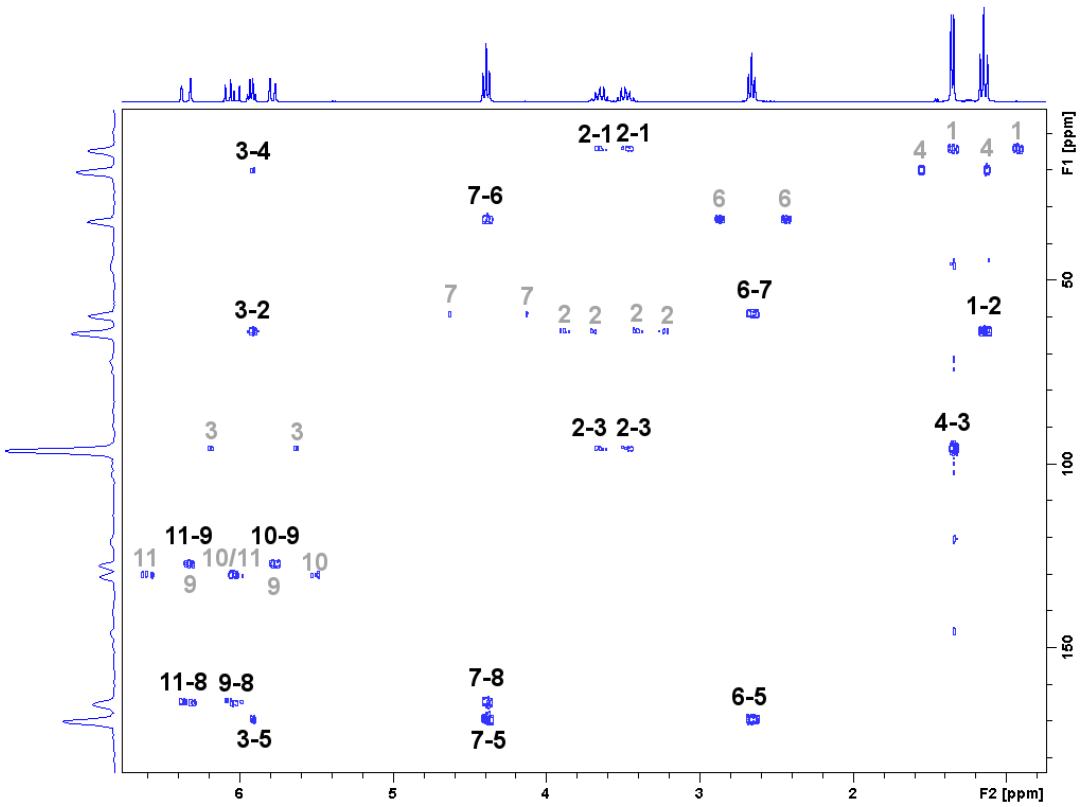

Figure 62. HMBC NMR spectrum of proCEA. Numbers in grey are split peaks of protons and carbons directly attached to each other.

For the diblock and triblock copolymerization of BA with proCEA, similar reaction conditions were used as those previously optimized for the block copolymerizations of BA with EEA. Figure 63 shows that the reaction kinetics observed are quite similar to the polymerizations of EEA. One reaction shows a significantly higher conversion at 30 hours, which seems to be a faulty data point because SEC shows a much lower M_n. It is possible that some of the monomer in this particular sample was deprotected due to moisture, leading to an inaccurate GC measurement. Other than that, the polymerizations seem to be well-controlled.

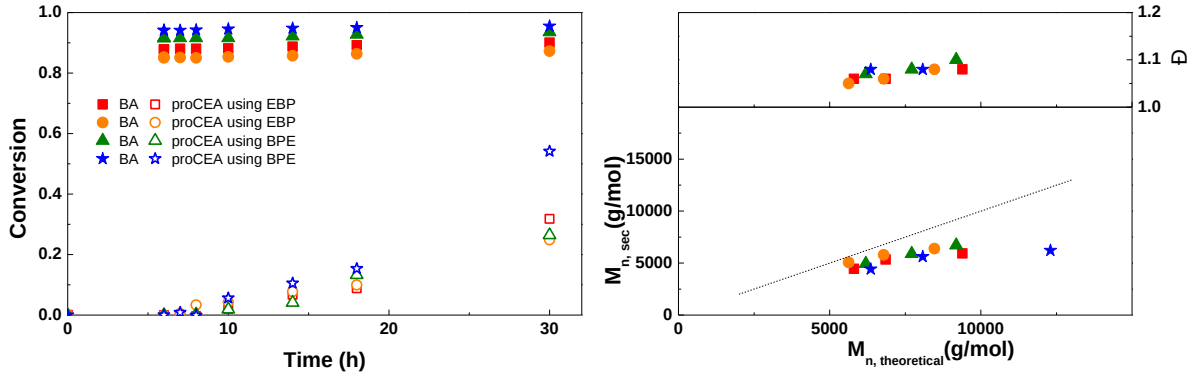

Figure 63. Left: conversion vs. time plot for Cu(0)-mediated one pot block copolymerization of BA and proCEA using [BA]:[proCEA]:[EBP]:[Me_6TREN]:[$CuBr_2$] = 50:50:1:0.15:0.1 and [BA]:[proCEA]:[BPE]:[Me_6TREN]:[$CuBr_2$] = 50:50:1:0.3:0.2, 3.0 M in DMF at 25°C and 12.5 mm^2/mL Cu(0) wire. A 3.0 M solution of proCEA in DMF was added after 6 hours reaction time. Right: corresponding molecular weight and dispersity vs. theoretical molecular weight plot.

3.3.7 Manual triblock copolymerizations

Triblock copolymerizations under the optimized conditions were performed manually on a larger scale to investigate whether these optimal conditions in the automated synthesizer (8 mL total volume) are also valid on larger scale (~40 mL total volume) (Table 4). SEC results of each of the polymers before addition of the second monomer and at the end of the polymerization show a clear shift in M_n towards higher molecular weight as the polymers grow longer. The dispersities observed are slightly higher than seen in the automated polymerizations, which may be due the larger reaction volumes resulting in less efficient stirring and lower temperature control in these exothermic reactions. To test this, it would be possible to perform a larger scale reaction using the automated synthesizer for comparison, but this was not done.

For PproCEA-*b*-PBA-*b*-PproCEA, which is spontaneously deprotected to PCEA-*b*-PBA-*b*-PCEA during the dialysis step of the purification in water, the percentage of BA in the polymer after purification is higher than calculated from monomer conversion, which was measured at 88 %. It seems that the conversion of proCEA is over-estimated by GC, due to monomer degradation during the longer reaction time, and is probably close to 40 %, which would be in line with the results from Figure 63. The exact percentage of AA in the PAA-*b*-PBA-*b*-PAA polymers could not be calculated from NMR, although a difference in viscosity between the polymers after purification could be observed from handling the materials. Full deprotection of EEA, which spontaneously happens during the precipitation step, was confirmed by ^{1}H NMR spectroscopy. Further characterization of thermal and mechanical properties of these polymers will be reported in Chapter 6.

Table 4. Details of manual triblock copolymerizations

polymer	DP of BA (GC)	DP second monomer (GC)	% BA (NMR)	M_n PBA (g/mol, SEC)	Đ PBA (SEC)	M_n triblock (g/mol, SEC)	Đ triblock (SEC)
PDMAEA-*b*-PBA-*b*-PDMAEA	47	19	68	5700	1.08	7000	1.08
PAA-*b*-PBA-*b*-PAA	49	21	-	5900	1.09	7500	1.18
PAA-*b*-PBA-*b*-PAA	49	18	-	5800	1.09	6500	1.12
PAA-*b*-PBA-*b*-PAA	49	9	-	5900	1.11	6900	1.12
PCEA-*b*-PBA-*b*-PCEA	48	21	84	4700	1.11	5300	1.26

3.4 Conclusions

The synthesis of amphiphilic diblock and triblock copolymers of BA with DMAEA, EEA and proCEA via high-throughput Cu(0)-mediated polymerization was optimized. Depending of the reaction conditions used, either a mixed monomer second block or a perfect block copolymer was produced. When DMAEA was used as the second monomer, reactions using EBP as initiator showed quarternization, while this was not observed when ECP was used as initiator and block copolymers with a dispersity of 1.1 could be prepared successfully. Although side reactions from the amine group of the DMAEA were expected, under the used conditions these were suppressed enough to yield well-controlled polymerizations.

When using EEA as the second monomer, unintended deprotection of the monomer can lead to disruption of the copper-ligand catalyst and cause uncontrolled polymerization. The formation of anhydrides can also cause problems by crosslinking polymers. However, under the chosen reaction conditions this was largely avoided and block copolymers of BA and EEA were synthesized successfully. The newly synthesized monomer proCEA could also be polymerized with good control. The optimal addition time of the second monomer was found to be 18 hours for DMAEA, due to the

slower polymerization rate when ECP is used as initiator, and 6 hours for EEA and proCEA. Using these times, almost full conversion of BA was obtained and pure (tri)block copolymers were produced.

However, it was still difficult to obtain high conversion of the second monomer. This may be due to buildup of Cu(II), which slows down the polymerizations over time. This may be improved by small changes in the equivalents of Cu(0), Cu(II) and Me_6TREN that are used in the polymerizations. The synthesis of shorter blocks, either by changing the monomer-initiator ratio or by using a bifunctional initiator, generally leads to a faster polymerization and a higher monomer conversion, in agreement with termination by oxygen as this would be less pronounced with higher radical concentration and shorter reaction times. In most reactions dispersities around 1.1 or lower were observed with good agreement between the M_n measured by SEC and the $M_{n,th}$, showing excellent control with very little termination. The optimized reaction conditions were used to successfully prepare amphiphilic triblock copolymers in a one-pot reaction on multigram scale.

References

1. C. Boyer, P. B. Zetterlund, M. R. Whittaker, *J. Polym. Sci., Part A: Polym. Chem.* **2014**, *52*, 2083.
2. A. H. Soeriyadi, C. Boyer, F. Nystrom, P. B. Zetterlund, M. R. Whittaker, *J. Am. Chem. Soc.* **2011**, *133*, 11128.
3. C. Boyer, A. H. Soeriyadi, P. B. Zetterlund, M. R. Whittaker, *Macromolecules* **2011**, *44*, 8028.
4. A. Anastasaki, C. Waldron, P. Wilson, C. Boyer, P. B. Zetterlund, M. R. Whittaker, D. Haddleton, *ACS Macro Lett.* **2013**, *2*, 896.
5. A. Anastasaki, V. Nikolaou, G. S. Pappas, Q. Zhang, C. Wan, P. Wilson, T. P. Davis, M. R. Whittaker, D. Haddleton, *Chem. Sci.* **2014**, *5*, 3536.
6. Y.-M. Chuang, A. Ethirajan, T. Junkers, *ACS Macro Lett.* **2014**, *3*, 732.
7. C. Boyer, A. Derveaux, P. B. Zetterlund, M. R. Whittaker, *Polym. Chem.* **2012**, *3*, 117.
8. F. Alsubaie, A. Anastasaki, P. Wilson, D. Haddleton, *Polym. Chem.* **2015**, *6*, 406.
9. D. Haddleton, A. Simula, V. Nikolaou, A. Anastasaki, F. Alsubaie, G. Nurumbetov, P. Wilson, K. Kempe, *Polym. Chem.* **2015**, *6*, 2226.
10. F. Zeng, Y. Shen, S. Zhu, *Macromol. Rapid Commun.* **2002**, *23*, 1113.
11. A. Anastasaki, C. Waldron, P. Wilson, R. McHale, D. M. Haddleton, *Polym. Chem.* **2013**, *4*, 2672.
12. Y. Nakane, M. Ishidoya, T. Endo, *J. Polym. Sci., Part A: Polym. Chem.* **1999**, *37*, 609.
13. R. Hoogenboom, U. S. Schubert, W. Van Camp, F. E. Du Prez, *Macromolecules* **2005**, *38*, 7653.
14. W. Van Camp, F. E. Du Prez, S. A. F. Bon, *Macromolecules* **2004**, *37*, 6673.
15. B. Dervaux, W. Van Camp, L. Van Renterghem, F. E. Du Prez, *J. Polym. Sci., Part A: Polym. Chem.* **2008**, *46*, 1649.
16. M. Ciampolini, N. Nardi, *Inorg. Chem.* **1966**, *5*, 41.
17. N. H. Nguyen, M. E. Levere, V. Percec, *J. Polym. Sci., Part A: Polym. Chem.* **2012**, *50*, 35.
18. W. A. Braunecker, K. Matyjaszewski, *Prog. Polym. Sci.* **2007**, *32*, 93.
19. S. Lu, Q.-L. Fan, S.-Y. Liu, S.-J. Chua, W. Huang, *Macromolecules* **2002**, *35*, 9875.

Chapter 4: High-throughput synthesis of thermoresponsive poly(oligoethylene glycol acrylate) copolymers by RAFT polymerization

Abstract

Thermoresponsive polymers are an interesting class of stimuli-responsive polymers because of their potential *in vivo* applications resulting from the easily controllable temperature trigger. In this chapter, the synthesis of two series of statistical copolymers of di(ethylene glycol) ethyl ether acrylate with di(ethylene glycol) methyl ether acrylate and tri(ethylene glycol) methyl ether acrylate, respectively, will be described using high-throughput automated parallel RAFT polymerization to accurately tune the polymer phase transition temperature. Cloud point temperature determination for each copolymer was performed by parallel turbidimetry and revealed a linear relationship with copolymer composition. The crystal structure of the used chain transfer agent 2-(((butylsulfanyl)carbonothioyl)sulfanyl)propanoic acid, which can easily be prepared and purified on large scale, is also reported.

4.1 Introduction

Thermoresponsive polymers are among the most studied stimuli-responsive polymers due to their large potential towards *in vivo* applications and easily controllable stimulus.[1, 2] Temperature responsiveness can be expressed in multiple ways including solid state transitions in shape memory materials,[3, 4] although solution phase transitions are by far the most commonly studied. The latter is characterized by a lower critical solution temperature (LCST) when the polymer becomes insoluble upon heating of the solution, or an upper critical solution temperature (UCST) when the polymer becomes soluble upon heating. In the case of an LCST polymer solution, heating above the cloud point temperature (T_{cp}) causes the phase separation of the solution with the formation of polymer rich droplets, which coalesce resulting in macroscopic phase separation, in a polymer-poor solution.[5, 6] The enthalpic gain originating from polymer – water interactions is upon heating no longer able to compensate for its entropic loss, leading to a negative Gibbs free energy and spontaneous phase separation. The T_{cp}, i.e. the temperature where the enthalpic gain exactly compensates the entropic loss, can be tuned by various parameters including polymer concentration and ionic strength of the aqueous solution, although predominantly by the identity of the polymer structure. Increasing the hydrophilicity of the monomer will increase the enthalpic gain and therefore increase the T_{cp}, while increasing the hydrophobicity will lower the T_{cp}, making it possible to adjust the T_{cp} by careful monomer design and copolymer composition.[7]

Poly(*N*-isopropylacrylamide) (PNIPAAm) is the most studied LCST polymer due to its stable T_{cp} close to body temperature (≈ 32 °C) showing little dependence on degree of polymerization, concentration and pH.[8] Recently, some other types of polymers such as poly(oligoethylene glycol (meth)acrylate)s (POEG(M)A)[9, 10] and poly(2-oxazolines)[11, 12] have been reported as alternatives of PNIPAM, showing similar thermoresponsive behavior. These polymers also show a highly tunable T_{cp} depending on the hydrophobicity and ratio of the comonomers. In the case of POEGA, polymers originating from various monomers have been reported with different T_{cp}, varying in both the length and end group of the side chains. Copolymerization of two of these monomers allows the accurate design of copolymers with T_{cp} ranging from 0 to 100 °C. In contrast to most other thermoresponsive polymers,

POEGAs have a very low T_g leading to a highly reversible LCST phase transition, which can be useful in their applications. While POEGAs are more sensitive to hydrolysis than POEGMAs, it was shown that they are not cytotoxic and can therefore be considered for biomedical applications.[13, 14] Examples of possible applications of POEGAs are hydrogels for drug delivery,[14] thermo- and light-responsive micelles[15] and thermoresponsive polymer films.[16, 17]

For the fast analysis of multiple series of statistical copolymers, high-throughput parallel synthesis is a very useful tool, since it allows for simultaneously performing many polymerizations under similar conditions.[18] This technique has previously been successfully used for high-throughput parallel synthesis of polymer libraries using reversible addition–fragmentation chain transfer (RAFT) polymerization,[19-21] macromolecular design via the interchange of xanthates (MADIX),[22] atom transfer radical polymerization (ATRP),[23] nitroxide mediated polymerization (NMP),[24] cationic ring-opening polymerization (CROP)[25] and Cu(0)-mediated polymerization.[26]

A recent review from our group provides an overview of different thermoresponsive poly(oligo ethylene glycol acrylate)s.[10] Most of the studies reported use a combination of the very hydrophilic hydroxyethyl acrylate or oligo(ethylene glycol) methyl ether acrylate with the very hydrophobic ethylene glycol methyl ether acrylate or di(ethylene glycol) ethyl ether acrylate (eDEGA) to tune the T_{cp}. This means that only about half of the available thermoresponsive oligo (ethylene glycol) acrylate monomers have currently been investigated in copolymers with tunable LCST behavior. In an effort to fill this gap, libraries of statistical copolymers of eDEGA with di(ethylene glycol) methyl ether acrylate (mDEGA) and tri(ethylene glycol) methyl ether acrylate (mTEGA) (Figure 64), respectively, were prepared in this study using high-throughput RAFT polymerization in a Chemspeed ASW2000 parallel synthesizer. After synthesis and purification of the polymers, T_{cp}s of the copolymers were measured by parallel turbidimetry. The utilized high-throughput synthesis and characterization can significantly reduce the time required to synthesize and analyze series of copolymers. The reported T_{cp}s of the homopolymers of eDEGA, mDEGA and mTEGA are around 13 °C, 40 °C and 70 °C,[10] respectively, so it is expected that the T_{cp}s of the copolymers can be tuned within these boundaries. The structures of eDEGA and mDEGA only differ in an ethoxy and methoxy group, constituting the smallest possible difference between two comonomers to tune the T_{cp}.

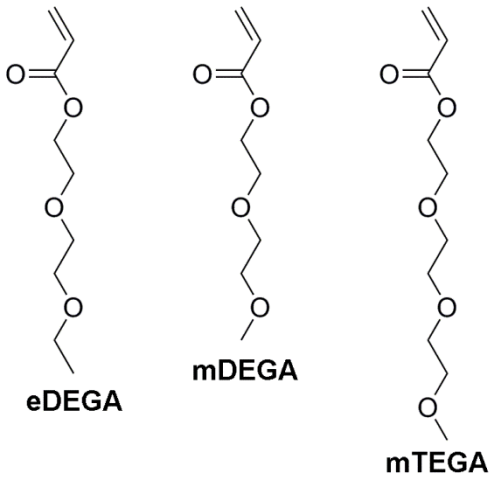

Figure 64. Chemical structures of di(ethylene glycol) ethyl ether acrylate (eDEGA), di(ethylene glycol) methyl ether acrylate (mDEGA) and tri(ethylene glycol) methyl ether acrylate (mTEGA).

4.2 Experimental section

Materials

Acetone (99.8%) and dichloromethane (DCM, 99.8%) were purchased from Sigma-Aldrich and used as received. *N,N*-dimethylformamide (DMF, peptide synthesis) was purchased from Biosolve and used as received. Di(ethylene glycol) ethyl ether acrylate (eDEGA) was purchased from TCI and run on a short aluminum oxide column before use. Di(ethylene glycol) methyl ether acrylate (mDEGA) and tri(ethylene glycol) methyl ether acrylate (mTEGA) were synthesized following a previously published procedure.[27, 28] 2-(((Butylsulfanyl)carbonothioyl)sulfanyl)propanoic acid (PABTC) was synthesized following a previously published method.[29] 2,2′-Azobis(2-methylpropionitrile) (AIBN) was purchased from Sigma and recrystallized from methanol before use.

Synthesis of copolymers

The copolymers were synthesized via RAFT polymerization using a Chemspeed ASW2000 automated synthesizer equipped with 16 parallel reactors of 13 mL, a Huber Petite Fleur thermostat for heating/cooling, a Huber Ministat 125 for reflux and a Vacuubrand PC 3000 vacuum pump. Stock solutions of PABTC, AIBN and monomers in DMF were prepared and bubbled with argon for at least 30 minutes before being introduced into the robot system and then kept under argon atmosphere. The hood of the automated synthesizer was continuously flushed with nitrogen and the reactors were flushed with argon to ensure an inert atmosphere. Before starting the polymerizations, the reactors were degassed through ten vacuum-argon cycles. Stock solutions were transferred to the reactors using the syringe of the automated synthesizer while the reactors were kept at 10 °C. Reactions were performed using [M]:[PABTC]:[AIBN] = 100:1:0.1 and a total monomer concentration of 2.0 M in DMF with a total volume of 4 mL. The [eDEGA]:[mDEGA] and [eDEGA]:[mTEGA] ratios were varied with 100:0, 80:20, 60:40, 50:50, 40:60, 20:80 and 0:100. Each reaction was performed in duplicate. A t = 0 minutes sample was taken from each reaction for later conversion calculation. The reactors were then heated to 70 °C, which takes about 11 minutes, to start the polymerizations. During the reactions, 50 µL samples were taken every 20 minutes and directly injected into 1.5 mL sample vials containing ~1.5 mL of acetone for GC and SEC measurements. After two hours the reactors were cooled to 10 °C to stop the reactions. The solutions were transferred to centrifuge tubes, diluted with distilled water, heated in a water bath at 80 °C and centrifuged for one minute at 7500 RPM. The water was poured off and the polymer was dissolved in cold distilled water, heated in a water bath at 80 °C and centrifuged again for one minute at 7500 RPM. The water was poured off and the polymer dissolved in dichloromethane and dried under vacuum. The mTEGA homopolymers were dialyzed (MWCO = 500-1000 Da) against distilled water to remove all traces of monomer.

Gas Chromatography (GC)

Samples were measured with GC to determine the monomer conversions. GC was performed on an Agilent 7890A system equipped with a VWR Carrier-160 hydrogen generator and an Agilent HP-5 column of 30 m length and 0.320 mm diameter. An FID detector was used and the inlet was set to 250 °C with a split injection of ratio 25:1. Hydrogen was used as carrier gas at a flow rate of 2 mL/min. The oven temperature was increased with 20 °C/min from 50 °C to 120 °C, followed by a ramp of 50 °C/min to 300 °C.

Size exclusion chromatography (SEC)

SEC was performed on a Agilent 1260-series HPLC system equipped with a 1260 online degasser, a 1260 ISO-pump, a 1260 automatic liquid sampler (ALS), a thermostatted column compartment (TCC) at 50 °C, a 1260 diode array detector (DAD) and a 1260 refractive index detector (RID). The poly(eDEGA-*stat*-mDEGA) copolymers were measured on a PSS GRAM30 column in series with a PSS GRAM1000 column using a flow rate of 1 mL/min, while two PLgel 5 µm mixed-D columns and a precolumn in series and a flow rate of 0.593 mL/min were used for the poly(eDEGA-*stat*-mTEGA) copolymers. The used eluent was DMA containing 50 mM of LiCl. The spectra were analyzed using the Agilent Chemstation software with the GPC add on. Molar mass and dispersity values were calculated against PMMA standards from Polymer Labs.

Nuclear magnetic resonance spectroscopy (NMR)

Proton NMR (^{1}H NMR) spectra were recorded on a Bruker Avance 300 MHz spectrometer at room temperature in deuterated solvents. The percentage of eDEGA in the purified copolymers was calculated by comparing the peaks of the CH_3-groups from both monomers at 1.20 and 3.36 ppm.

Crystal structure analysis

For the structure of PABTC, X-ray intensity data were collected on a Agilent Supernova Dual Source (Cu at zero) diffractometer equipped with an Atlas CCD detector using CuKα radiation (λ = 1.54184 Å) and ω scans. The images were interpreted and integrated with the program CrysAlisPro (Agilent Technologies).[30] Using Olex2,[31] the structure was solved by direct methods using the ShelXS structure solution program and refined by full-matrix least-squares on F^2 using the ShelXL program package.[32] Non-hydrogen atoms were anisotropically refined and the hydrogen atoms in the riding mode and isotropic temperature factors fixed at 1.2 times U(eq) of the parent atoms (1.5 times for methyl groups and the hydroxyl group).

CCDC 1031562 contains the supplementary crystallographic data for this paper and can be obtained free of charge via www.ccdc.cam.ac.uk/conts/retrieving.html (or from the Cambridge Crystallographic Data Centre, 12, Union Road, Cambridge CB2 1EZ, UK; fax: +44-1223-336033; or deposit@ccdc.cam.ac.uk) .

Crystal data for PABTC. $C_8H_{14}O_2S_3$, *M* = 238.40, triclinic, space group *P*-1 (No. 2), *a* = 6.4754(5) Å, *b* = 7.0940(4) Å, *c* = 13.7074(6) Å, *α* = 78.942(4)°, *β* = 84.035(5)°, *γ* = 68.379(6)°, *V* = 574.12(7) Å^3, *Z* = 2, *T* = 100 K, ρ_{calc} = 1.379 g cm^{-3}, μ(Cu-Kα) = 5.660 mm^{-1}, *F*(000) = 252, 5711 reflections measured, 2338 unique (R_{int} = 0.0225) which were used in all calculations. The final *R*1 was 0.0260 ($I > 2\sigma(I)$) and *wR*2 was 0.0718 (all data).

Cloud point temperature measurements

T_{cp} measurements were performed in 0.7 mL solutions containing 5 mg/mL of polymer in distilled water using an Avantium Crystal16 parallel crystallizer turbidimeter. The samples were heated/cooled at 1 °C/min while stirring at 700 RPM. Three heating and two cooling ramps were performed. The T_{cp}s and clearance point temperatures (T_{clear}) were determined as the temperature at 50% transmission during second and third heating and first and second cooling, respectively.

4.3 Results and discussion

4.3.1 Synthesis and crystal structure description of chain transfer agent

The chain transfer agent (CTA) 2-(((butylsulfanyl)carbonothioyl)sulfanyl)propanoic acid (PABTC) was selected for this study because it can mediate the RAFT polymerization of many different acrylates,[33-36] it can easily be synthesized on large scale (> 100 g) and purification is straightforward and efficient by recrystallization, yielding the relatively large amounts of CTA needed for high-throughput experimentation. The PABTC was synthesized by first dissolving butanethiol in water and adding a 50% NaOH solution to abstract the acidic proton of the thiol. Acetone is added to improve solubility, after which carbon disulfide is added to form the trithiocarbonate. This reacts with 2-bromopropionic acid via nucleophilic substitution to yield deprotonated PABTC, which is protonated by adding HCl (Figure 65). The crude product was purified by recrystallization from hexane to give pure PABTC in 85% yield (162 g in a single batch).[29] The ^{1}H NMR spectrum of PABTC is shown in Figure 66, which confirms the success of the synthesis and purification.

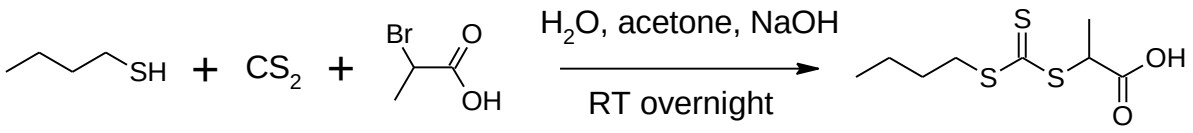

Figure 65. Synthesis of 2-(((butylsulfanyl)carbonothioyl)sulfanyl)propanoic acid (PABTC).

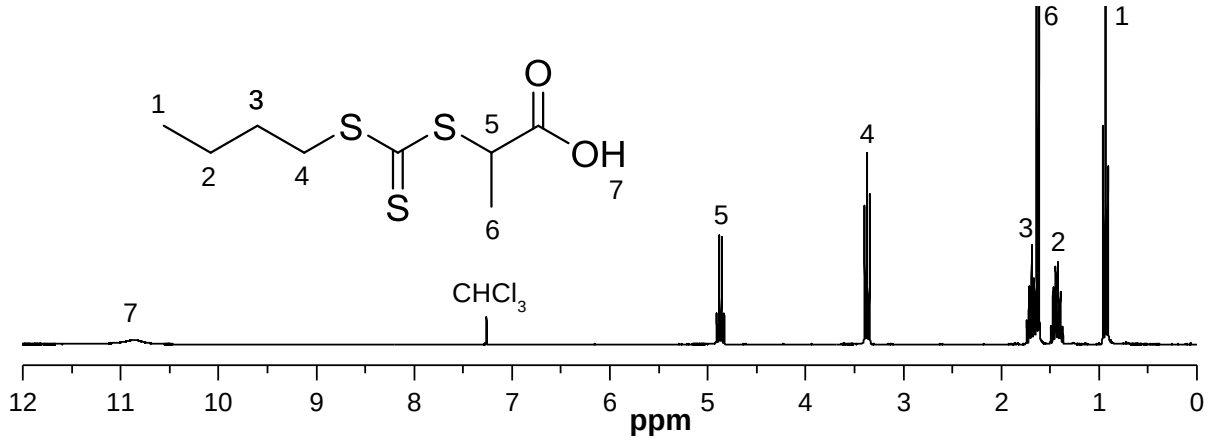

Figure 66. ^{1}H NMR spectrum of PABTC recorded in $CDCl_3$.

The recrystallization of PABTC directly provided single crystals that were suitable for single crystal structure determination. The crystal structure determination and interpretation were performed by Prof. Kristof Van Hecke. The PABTC crystallized in the centro-symmetric space group *P*-1, with one PABTC molecule in the asymmetric unit (Figure 67).

An almost perfectly planar, all-*trans*, zigzag conformation is adopted by the butyl chain and the trithiocarbonate segment, while the carboxyl group is observed in a +synclinal (+sc) position, relative to this chain direction, with a C4-S1-C2-C1 torsion angle of 64.10(11)°. In fact, for the S3-C8 chain fragment, the maximum deviation from the ideal 180° of the chain torsion angles is less than 0.6°. In addition, the S3-C3 chain fragment is also found almost perfectly *trans*-planar, with a maximum of 6.2° as the torsion angle deviation from ideal value. The +synclinal oriented carboxyl group, relative to this extended chain, can most probably be attributed to the formation of intermolecular hydrogen bonds.

The trithio central group is found almost symmetrical. The bond distances and angles in the trithio moiety are comparable to those reported for other trithio carbonate structures,[37-40] found in the Cambridge Structural Database (CSD version 5.35),[41] with the S1-C4 and C4-S3 single bonds of 1.7549(14) Å and 1.7408(14) Å, respectively and a C4-S2 double bond of 1.6338(14) Å.

In the crystal packing, hydrogen-bonded dimeric entities are formed around inversion centers, through intermolecular hydrogen bonding of the carboxylic acid functions of two symmetry equivalent molecules, i.e. between the carbonate O(1)-H(1) and carbonate $O(2)^{i}$ (symmetry code: (i) –x, -y, -z), with the O(1)-H(1)···$O(2)^{i}$ distance of 2.6216(14) Å. This is considered a typical feature of carboxylic acid structures. As such, these pairs of centro-symmetric dimers form cyclic structures, which can be described by the $R_2^2(8)$ motif, which means that a cycle is formed by eight atoms of two hydrogen-bonded molecules.[42] Furthermore, these dimers are connected to each other through weaker intermolecular C-H···O hydrogen bonds (C(5)-H(5B)···O(2) = 3.3017(17) Å), to form a chain of edge-fused rings, running along the [010] direction. This arrangement can be described as a molecular 1D ladder, in which the $R_2^2(8)$ rings alternate with and $R_4^4(20)$ rings, as previously observed for similar dodecyl trithio carbonates.[38, 40] In this case, such a ladder is hydrogen bonded through additional hydrogen bonds (C(2)-H(2)···O(1) = 3.5560(17) Å) to a parallel running ladder, building up 2D layers in (110) plane (Figure 68).

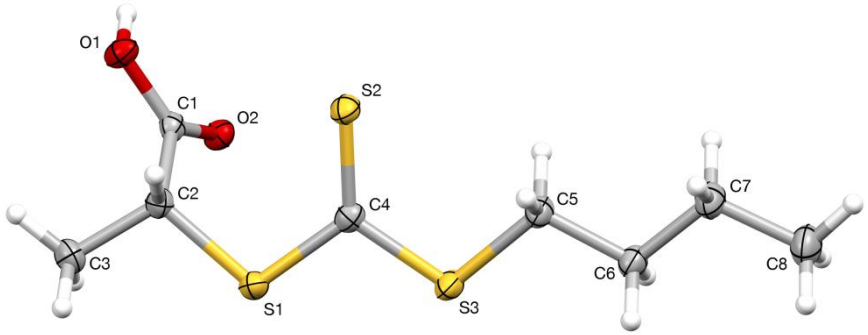

Figure 67. Asymmetric unit of the crystal structure of PABTC, showing thermal displacement ellipsoids at the 50% probability level and atom labeling scheme.

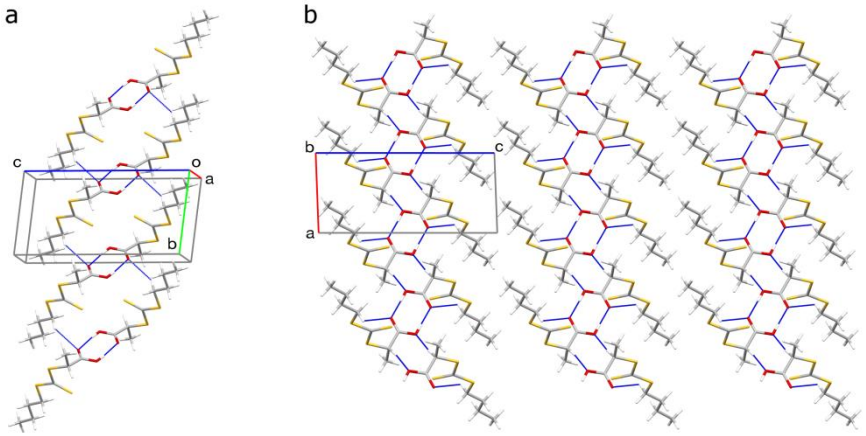

Figure 68. a: Part of the crystal structure of PABTC, showing the formation of a typical ladder, formed through hydrogen bonds, along the [010] direction, containing alternating $R_2^2(8)$ and $R_4^4(20)$ rings; b: Packing diagram of the crystal structure of PABTC, along the b-axis, showing 2D layers in the (110) plane.

4.3.2 High-throughput RAFT polymerizations

Two series of copolymers of eDEGA with mDEGA and mTEGA, respectively, were synthesized via RAFT copolymerization to be able to tune the T_{cp}. Each series of copolymers was synthesized in duplicate and in parallel using an automated synthesizer. Representative kinetic plots for two of the polymerizations are shown in Figure 69 and Figure 70. Each polymerization shows similar pseudo-first order linear kinetics, with both monomers showing the same rate of polymerization independent of the monomer ratios. This is to be expected since the structures of the utilized monomers only differ in the side chain end-groups, which does not influence the electronic nature of the acrylate group and will only have a minor steric effect. Some of the reactions showed a short inhibition time, which is likely caused by small amounts of oxygen present in the system. Because of this inhibition period, small variations in the degree of polymerization of the different copolymers were detected. All kinetic plots show a linear increase of $\ln([M]_0/[M])$ with time, demonstrating there is no significant termination.

Number average molar masses (M_n) determined by SEC were in good agreement with theoretical M_n and the polymers have narrow dispersities. This good agreement may not always be the case with different polymers, as the molar masses are determined relative to PMMA standards, which may have different hydrodynamic volumes due to differences in solubility. Small differences between the two series of copolymers were observed by SEC measurements, which can be attributed to differences in column conditions and calibration as the experiments were performed with some time in between, see also the experimental section. The linear increase in $M_{n,SEC}$ vs. $M_{n,theoretical}$ together with low dispersities are evident of a controlled polymerization.

Figure 71 shows the fraction of eDEGA incorporated into the polymers at around 30 % monomer conversion for all statistical copolymers. Non-linear least square fitting of this data shows the reactivity ratios ($r_{...}$) between the monomers are almost equal to 1 within the error margins, which confirms the synthesis of ideal random copolymers.

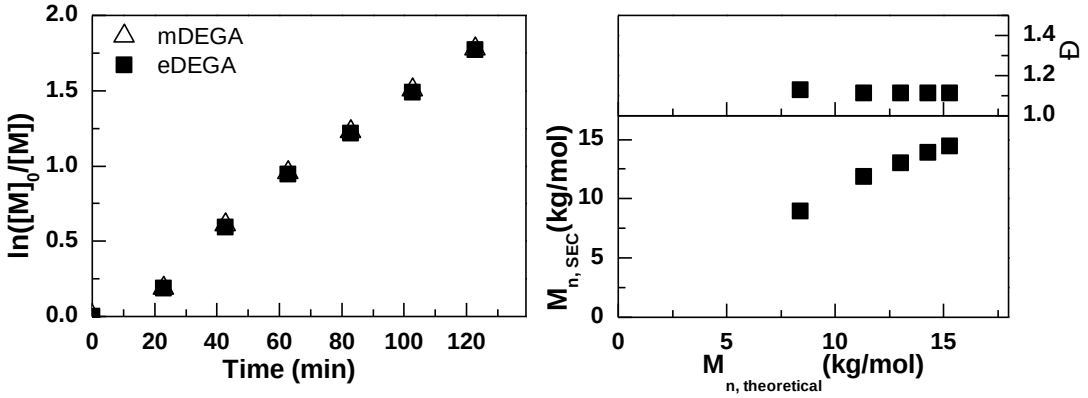

Figure 69. Left: a pseudo- first order kinetic plot for the RAFT copolymerization of mDEGA and eDEGA using [mDEGA]:[eDEGA]:[PABTC]:[AIBN] = 50:50:1:0.1, 2.0 M monomer concentration in DMF at 70 °C (polymer 4a from Table 5). Right: the corresponding molar mass and dispersity vs. theoretical molar mass plot.

The purification of the synthesized copolymers was simplified, exploiting their thermoresponsive properties by first dissolving the copolymers in cold water and subsequently centrifuging above their T_{cp}. The limitation of this procedure is that the polymers with high T_{cp} can be difficult to be precipitated upon heating, reducing the yield of the polymer samples. However, it is a very fast and easy method to isolate and purify large series of polymer samples, which is important for high-

throughput synthesis. For the mTEGA homopolymer, which has the highest T_{cp}, it was not possible to remove all traces of unreacted monomer using this method, so these samples were purified via dialysis against water. Table 5 and Table 6 summarize the properties of the obtained copolymers. Copolymers synthesized by different monomer feed ratios are coded with numbers while both polymerizations with the same feed ratio are labeled with a or b. The percentage of eDEGA in each copolymer, determined by ^{1}H NMR spectroscopy after purification, is in close agreement with the feed ratios of the comonomers for the copolymerizations. SEC characterization of the purified copolymers suggests the formation of well-defined copolymer structures as indicated by the low Đ (Đ < 1.2) values.

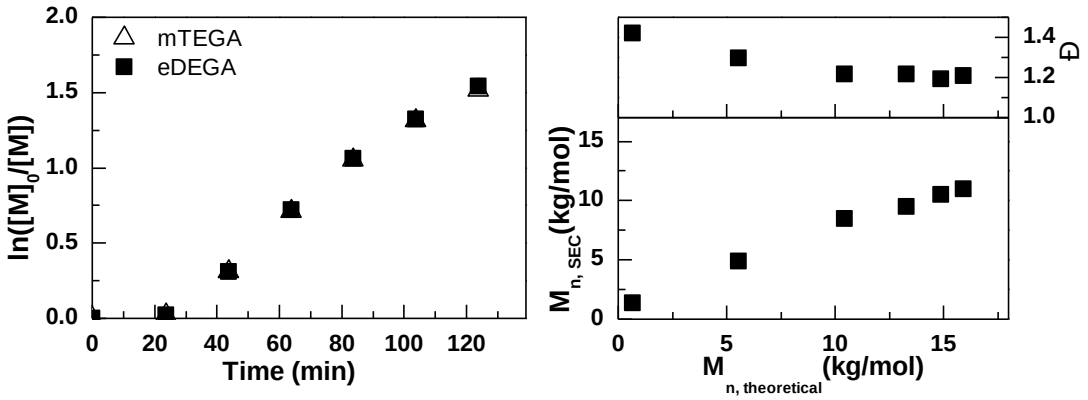

Figure 70. Left: a pseudo- first order kinetic plot for the RAFT copolymerization of mTEGA and eDEGA using [mTEGA]:[eDEGA]:[PABTC]:[AIBN] = 40:60:1:0.1, 2.0 M monomer concentration in DMF at 70 °C (polymer 15a from Table 6). Right: the corresponding molar mass and dispersity vs. theoretical molar mass plot.

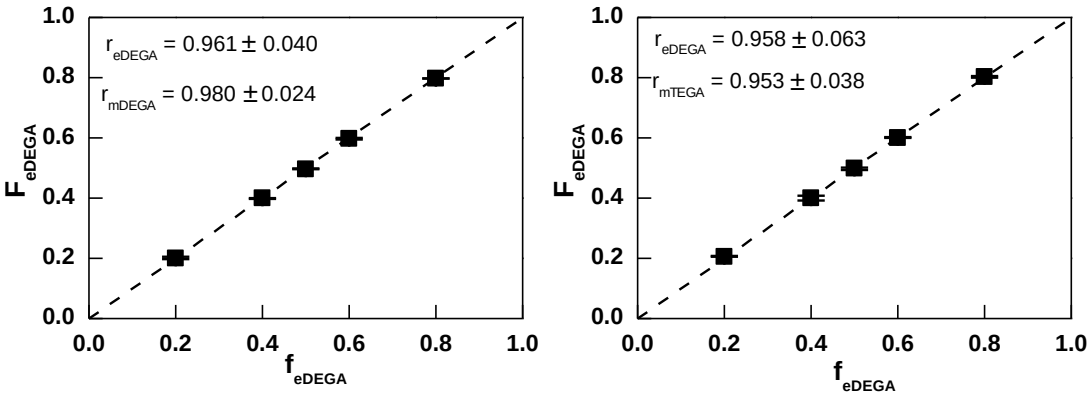

Figure 71. Plot of incorporated eDEGA fraction (F_{eDEGA}) vs. theoretical eDEGA fraction (f_{eDEGA}) at ~ 30 % monomer conversion. Left: poly(eDEGA-stat-mDEGA) copolymers, right: poly(eDEGA-stat-mTEGA) copolymers.

4.3.3 Cloud point temperature measurements

Turbidimetry was used to determine the T_{cp} and T_{clear} by increasing and decreasing the temperature of the polymer solution while measuring the transmittance. A transmittance of 100% indicates a clear solution, while 0% transmittance indicates a milky solution. Figure 72 and Figure 73 show the turbidity curves for all the copolymers. Three heating and two cooling ramps were performed, and the final heating ramps are shown here. In each solution a clear, fully reversible transition from 100% to 0% transmittance is observable as well as a shift in the transition temperature upon changing polymer compositions. Polymers containing a higher amount of the hydrophobic eDEGA show an expected lower T_{cp}.

Table 5. Properties of the poly(eDEGA-*stat*-mDEGA) copolymers.

#	*DP eDEGA (GC)*	*DP mDEGA (GC)*	*mol % eDEGA theoretical*	*mol % eDEGA (NMR)*	M_n *(g/mol, SEC)*	*Đ (SEC)*	T_{cp} *(°C)*	T_{clear} *(°C)*
1a	0	84	0	0	14100	1.12	48	46
1b	0	82	0	0	16100	1.09	48	46
2a	15	61	20	22	14300	1.11	39	37
2b	17	66	20	21	15900	1.08	39	38
3a	34	51	40	40	14600	1.13	34	32
3b	33	50	40	41	16000	1.08	32	29
4a	41	42	50	50	14400	1.11	27	25
4b	42	42	50	51	15400	1.08	25	24
5a	51	34	60	60	16900	1.11	23	21
5b	49	33	60	61	15200	1.09	21	22
6a	64	16	80	84	16900	1.09	18	16
6b	66	17	80	79	15200	1.09	19	18
7a	76	0	100	100	19400	1.11	15	13
7b	81	0	100	100	14800	1.09	14	12

Table 6. Properties of the poly(eDEGA-*stat*-mTEGA) copolymers.

#	*DP eDEGA (GC)*	*DP mTEGA (GC)*	*mol % eDEGA theoretical*	*mol % eDEGA (NMR)*	M_n *(g/mol, SEC)*	*Đ (SEC)*	T_{cp} *(°C)*	T_{clear} *(°C)*
11a	0	63	0	0	10800	1.20	69	68
11b	0	79	0	0	12000	1.19	67	68
12a	14	54	20	23	11600	1.19	60	58
12b	15	59	20	22	12100	1.20	62	60
13a	31	46	40	41	12200	1.21	47	45
13b	30	45	40	41	11900	1.20	47	45
14a	37	37	50	50	11400	1.21	40	38
14b	38	38	50	50	11700	1.20	39	37
15a	47	31	60	66	10900	1.21	30	28
15b	48	32	60	64	11400	1.20	32	30
16a	61	15	80	79	11000	1.20	26	24
16b	65	16	80	79	11600	1.21	25	23
17a	78	0	100	100	11900	1.21	15	13
17b	80	0	100	100	11200	1.21	15	13

The T_{cp} and T_{clear} values shown in Table 5 and Table 6 were calculated as the average temperature at 50% transmission from the last two heating and cooling ramps, respectively. While the different ramps usually lead to the same transition temperatures, in some cases a difference up to 0.4 °C was observed between the two ramps, which is within the measurement error of the experiments. Hence, all reported temperatures are rounded off to full degrees Celsius. The difference between T_{cp} and T_{clear} is around 2 °C indicating the presence of minor hysteresis, which will most likely disappear or be reduced when a slower heating and cooling ramp is applied.[43] This was also observed in unpublished experiments performed within our group.[44]

In some cases a small difference is observed between the two polymers with similar composition (a and b). These are generally in agreement with the corresponding variations in composition calculated from the ^{1}H NMR spectra, as the copolymers containing more eDEGA have slightly lower T_{cp}s. Other minor differences in T_{cp} may be explained by different degrees of polymerization, as already reported for P(mTEGA) and P(mDEGA).[45, 46]

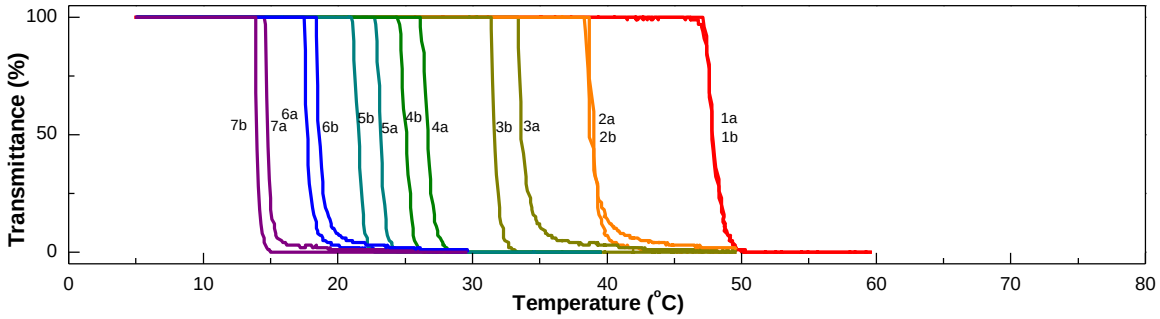

Figure 72. Transmittance versus temperature plots for poly(eDEGA-stat-mDEGA) copolymers in aqueous solutions at a concentration of 5 mg/ml.

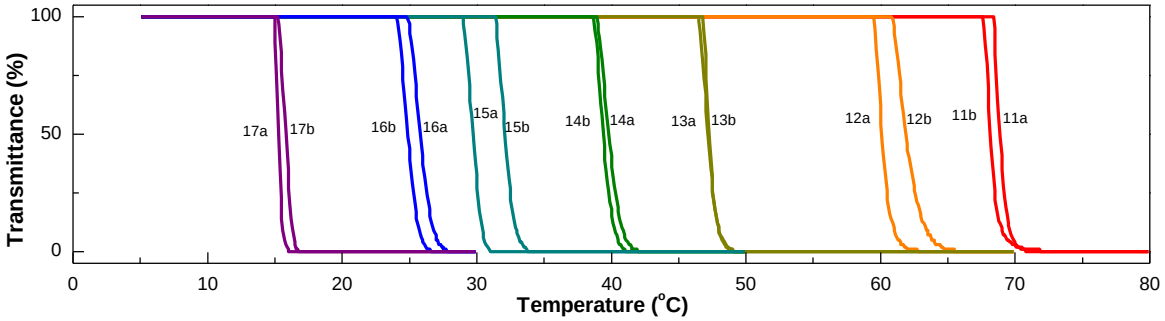

Figure 73. Transmittance versus temperature plots for poly(eDEGA-stat-mTEGA) copolymers in aqueous solutions at a concentration of 5 mg/ml.

In Figure 74 the T_{cp}s for both copolymer libraries are plotted against the weight percentage of eDEGA. Both plots show a linear decrease of the cloud point with increasing amount of eDEGA. From the linear fitting of these plots, the following general empirical formula can be determined to calculate the T_{cp} for a designed copolymer composition for these types of copolymers.

$T_{cp,P(A\text{-}stat\text{-}B)} = T_{cp,PB} + (T_{cp,PA} - T_{cp,PB})$ * weight fraction monomer A

A similar linear relationship between copolymer compositions and T_{cp}s was previously reported for gradient poly(2-oxazoline) copolymers, in which the gradient between the monomers was not steep so they behaved more like random copolymers.[12, 24] While this formula is valid for both of the copolymers reported in this chapter, it cannot be generalized for all OEGA combinations. For poly(2-hydroxyethyl acrylate-*stat*-2-hydroxypropyl acrylate)[47] and poly(2-hydroxyethyl acrylate-*stat*-ethylene glycol methyl ether acrylate)[48] copolymers, an exponential relationship was found between the fraction of 2-hydroxyethyl acrylate and T_{cp}. Although these examples have a larger possible range of accessible copolymer T_{cp}s, the exponential trend makes it more difficult to accurately pin-point specific T_{cp}s in the higher temperature regime. Since the effect of an additional HEA unit on the overal T_{cp} increases with every added unit, the consequences of minor variations in the polymerization on the T_{cp} can be severe. The here described linear dependencies of the used combinations allow for a far more robust and predictable thermoresponsive copolymer design across the entire accesible T_{cp} range.

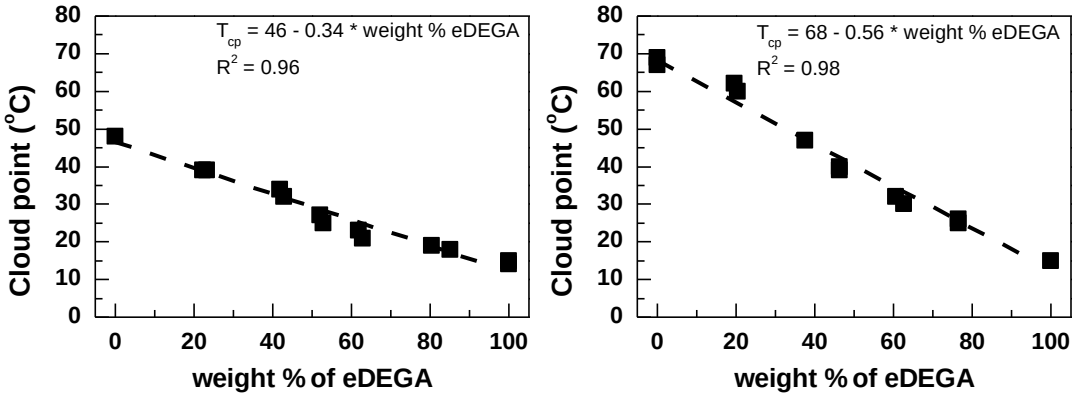

Figure 74. Cloud point temperatures for the copolymers plotted against the weight percentage of eDEGA. Left: poly(eDEGA-stat-mDEGA) copolymers, right: poly(eDEGA-stat-mTEGA) copolymers.

4.4 Conclusions

The chain transfer agent PABTC was successfully synthesized on large scale and the crystal structure was determined. Using high-throughput RAFT polymerization we were able to synthesize two series of defined thermoresponsive statistical copolymers in high efficiency and reproducibility. Excellent control over polymer composition and molecular weight was shown and near ideal random copolymers of eDEGA with mDEGA or mTEGA were obtained. Cloud point temperatures determined for these copolymers revealed a linear relationship with copolymer compositions. Using the general empirical relationship, the delicate design of a thermoresponsive copolymer with a desired cloud point temperature is possible, which represents a fast and easy method to synthesize low T_g polymers with any T_{cp} in between 15 and 70 °C.

References

1. C. de Las Heras Alarcon, S. Pennadam, C. Alexander, *Chem. Soc. Rev.* **2005**, *34*, 276.
2. D. Schmaljohann, *Adv. Drug Delivery Rev.* **2006**, *58*, 1655.
3. A. Lendlein, S. Kelch, *Angew. Chem. Int. Ed.* **2002**, *41*, 2034.
4. C. Liu, H. Qin, P. T. Mather, *J. Mater. Chem.* **2007**, *17*, 1543.
5. B. Jeong, A. Gutowska, *Trends Biotechnol.* **2002**, *20*, 305.
6. E. S. Gil, S. M. Hudson, *Prog. Polym. Sci.* **2004**, *29*, 1173.
7. C. Weber, R. Hoogenboom, U. S. Schubert, *Prog. Polym. Sci.* **2012**, *37*, 686.
8. H. G. Schild, *Prog. Polym. Sci.* **1992**, *17*, 163.
9. J.-F. Lutz, *J. Polym. Sci., Part A: Polym. Chem.* **2008**, *46*, 3459.
10. G. Vancoillie, D. Frank, R. Hoogenboom, *Prog. Polym. Sci.* **2014**, *39*, 1074.
11. R. Hoogenboom, H. M. L. Thijs, M. J. H. C. Jochems, B. M. van Lankvelt, M. W. M. Fijten, U. S. Schubert, *Chem. Commun.* **2008**, 5758.
12. M. Glassner, K. Lava, V. R. de la Rosa, R. Hoogenboom, *J. Polym. Sci., Part A: Polym. Chem.* **2014**, *52*, 3118.
13. C.-W. Chang, E. Bays, L. Tao, S. N. S. Alconcel, H. D. Maynard, *Chem. Commun.* **2009**, 3580.
14. B. Kostova, D. Momekova, P. Petrov, G. Momekov, N. Toncheva-Moncheva, C. B. Tsvetanov, N. Lambov, *Polymer* **2011**, *52*, 1217.
15. X. Jiang, C. A. Lavender, J. W. Woodcock, B. Zhao, *Macromolecules* **2008**, *41*, 2632.
16. Q. Zhong, J. Adelsberger, M. A. Niedermeier, A. Golosova, A. M. Bivigou-Koumba, A. Laschewsky, S. S. Funari, C. M. Papadakis, P. Müller-Buschbaum, *Colloid Polym. Sci.* **2013**, *291*, 1439.
17. Q. Zhong, E. Metwalli, M. Rawolle, G. Kaune, A. M. Bivigou-Koumba, A. Laschewsky, C. M. Papadakis, R. Cubitt, P. Müller-Buschbaum, *Macromolecules* **2013**, *46*, 4069.

18. R. Hoogenboom, M. A. R. Meier, U. S. Schubert, *Macromol. Rapid Commun.* **2003**, *24*, 15.
19. M. W. M. Fijten, M. A. R. Meier, R. Hoogenboom, U. S. Schubert, *J. Polym. Sci., Part A: Polym. Chem.* **2004**, *42*, 5775.
20. C. R. Becer, A. M. Groth, R. Hoogenboom, R. M. Paulus, U. S. Schubert, *QSAR Comb. Sci.* **2008**, *27*, 977.
21. C. Guerrero-Sanchez, L. O'Brien, C. Brackley, D. J. Keddie, S. Saubern, J. Chiefari, *Polym. Chem.* **2013**, *4*, 1857.
22. P. Chapon, C. Mignaud, G. Lizarraga, M. Destarac, *Macromol. Rapid Commun.* **2003**, *24*, 87.
23. H. Zhang, M. W. M. Fijten, R. Hoogenboom, R. Reinierkens, U. S. Schubert, *Macromol. Rapid Commun.* **2003**, *24*, 81.
24. T. M. Eggenhuisen, C. R. Becer, M. W. M. Fijten, R. Eckardt, R. Hoogenboom, U. S. Schubert, *Macromolecules* **2008**, *41*, 5132.
25. R. Hoogenboom, M. W. M. Fijten, M. A. R. Meier, U. S. Schubert, *Macromol. Rapid Commun.* **2003**, *24*, 92.
26. L. Voorhaar, S. Wallyn, F. E. Du Prez, R. Hoogenboom, *Polym. Chem.* **2014**, *5*, 4268.
27. J.-H. Ryu, R. Roy, J. Ventura, S. Thayumanavan, *Langmuir* **2010**, *26*, 7086.
28. Q. Zhang, N. Vanparijs, B. Louage, B. G. De Geest, R. Hoogenboom, *Polym. Chem.* **2014**, *5*, 1140.
29. C. J. Ferguson, R. J. Hughes, D. Nguyen, B. T. T. Pham, R. G. Gilbert, A. K. Serelis, C. H. Such, B. S. Hawkett, *Macromolecules* **2005**, *38*, 2191.
30. Agilent (2014). CrysAlis PRO (Version 1.171.37.31). Agilent Technologies UK Ltd, Yarnton, Oxfordshire, England.
31. O. V. Dolomanov, L. J. Bourhis, R. J. Gildea, J. A. K. Howard, H. Puschmann, *J. Appl. Crystallogr.* **2009**, *42*, 339.
32. G. M. Sheldrick, *Acta Crystallogr., Sect. A: Acta Crystallogr.* **2008**, *64*, 112.
33. C. J. Ferguson, R. J. Hughes, B. T. T. Pham, B. S. Hawkett, R. G. Gilbert, A. K. Serelis, C. H. Such, *Macromolecules* **2002**, *35*, 9243.
34. J. Rieger, W. Zhang, F. o. Stoffelbach, B. Charleux, *Macromolecules* **2010**, *43*, 6302.
35. A. Krieg, C. Weber, R. Hoogenboom, C. R. Becer, U. S. Schubert, *ACS Macro Lett.* **2012**, *1*, 776.
36. J. M. Heinen, A. C. M. Blom, B. S. Hawkett, G. G. Warr, *J. Phys. Chem. B* **2013**, *117*, 3005.
37. G.-S. Zeng, J.-P. Zou, Q. Peng, Z.-H. Wen, A.-Q. Zhang, *Acta Crystallogr., Sect. E: Struct. Rep. Online* **2008**, *64*, o2047.
38. S. Xiao, P. A. Charpentier, *Acta Crystallogr., Sect. E: Struct. Rep. Online* **2011**, *67*, o811.
39. R. Moreno-Fuquen, C. Grande, R. C. Advincula, J. C. Tenorio, J. Ellena, *Acta Crystallogr., Sect. E: Struct. Rep. Online* **2013**, *69*, o774.
40. F. Zuluaga, C. Grande, J. Cobo, C. Glidewell, *Acta Crystallogr., Sect. C: Cryst. Struct. Commun.* **2010**, *66*, o627.
41. F. Allen, *Acta Crystallogr., Sect. B: Struct. Sci.* **2002**, *58*, 380.
42. J. Bernstein, R. E. Davis, L. Shimoni, N.-L. Chang, *Angew. Chem. Int. Ed.* **1995**, *34*, 1555.
43. V. S. Joseph, S. Kim, Q. Zhang, R. Hoogenboom, J.-D. Hong, *Polymer* **2013**, *54*, 4894.
44. Q. Zhang, *Smart materials based on thermoresponsive polymers* (Ghent University, 2014).
45. F. Hua, X. Jiang, D. Li, B. Zhao, *J. Polym. Sci., Part A: Polym. Chem.* **2006**, *44*, 2454.
46. A. Miasnikova, A. Laschewsky, *J. Polym. Sci., Part A: Polym. Chem.* **2012**, *50*, 3313.
47. R. Hoogenboom, D. Popescu, W. Steinhauer, H. Keul, M. Möller, *Macromol. Rapid Commun.* **2009**, *30*, 2042.
48. W. Steinhauer, R. Hoogenboom, H. Keul, M. Moeller, *Macromolecules* **2010**, *43*, 7041.

Chapter 5: Synthesis of ABA-triblock copolymers with charged outer blocks via RAFT polymerization

Abstract

This chapter describes the synthesis of ABA-triblock copolymers, containing an uncharged middle block and charged outer blocks, via RAFT polymerization. These polymers will be used for the preparation of supramolecular materials based on electrostatic interaction (Chapter 6). First, kinetic studies of the homopolymerization of each monomer were performed, after which the kinetics of the block copolymerizations were studied. The triblock copolymers were then synthesized on a larger scale, purified and characterized. Polymers with different T_gs and solubility were used for the middle blocks, and several different monomers were used to form the charged outer blocks. The thermal and mechanical properties of some of these polymers and their mixtures will be described in Chapter 6.

5.1 Introduction

Supramolecular materials are held together by non-covalent interactions, such as hydrogen bonding, electrostatic interaction or host-guest complexation. An overview of these types of materials is given in Chapter 1 of this thesis. Here, we aim to synthesize a self-healing supramolecular material based on the electrostatic interaction between polymers containing opposite charges. To be able to form a supramolecular cross-linked network structure, triblock copolymers containing an uncharged middle block and charged outer blocks are used. When such triblock copolymers containing positive and negative charges are mixed together, the charged blocks are expected to associate and phase-separate from the uncharged blocks. This phase-separation will depend on the miscibility between the charged and uncharged blocks, while the mobility of the chain ends between different charged sections, and subsequently the self-healing ability, is also dependent on the glass transition temperature (T_g) of the material.

For this reason, several different monomers with different chemical properties were chosen to form the middle blocks of the polymers. Initially several low T_g monomers with different hydrophobicity were chosen for the middle blocks, specifically the hydrophobic *n*-butyl acrylate (BA)[1] (T_g = -54 °C)[2], less hydrophobic 2-methoxyethyl acrylate (MEA)[3-5] (T_g = -50 °C).[2] As hydrophobic higher T_g middle blocks, styrene (St)[6] (T_g = 100 °C)[2] and cyclohexyl acrylate (CHA)[7] (T_g = 19 °C)[2, 8] were used. The hydrophilic 2-hydroxyethyl acrylate (HEA)[3, 4, 9] (T_g = 22 °C)[10] was used to prepare water-soluble triblock copolymers. As cationic monomer the tertiary amine 2-(dimethylamino)ethyl acrylate (DMAEA)[11] (T_g = - 47 °C, see Chapter 6) was used, with the quaternary amine [2-(acryloyloxy)ethyl]trimethylammonium chloride (AETMAC)[12, 13] (T_m = 267 °C)[14] as a water-compatible alternative, as PDMAEA has been reported to be readily hydrolyzed in water.[15] For the anionic blocks the low T_g 2-carboxyethyl acrylate (CEA)[13, 16] (T_g = 22 °C, see Chapter 6) was chosen. The zwitterionic sulfobetaine monomer 2-(*N*-3-sulfopropyl-*N*,*N*-dimethyl ammonium)ethyl acrylate (SPDMAEA)[17-19] was used as an outer block containing both positive and negative charges, that can phase-separate and form a network structure without the need for mixing different polymers together. An overview of the structures of all used monomers is shown in Figure 75.

Reversible addition-fragmentation chain transfer (RAFT) polymerization was chosen as the most suitable method for the synthesis of these polymers, because of its ability to mediate the

polymerization of a wide variety of functional monomers, including direct polymerization of unprotected acid containing monomers.[20-24] This is in contrast with the Cu(0)-mediated polymerization of similar ABA-triblock copolymers that was discussed in Chapter 3, in which a protective group was necessary for controlled polymerization of acidic monomers while special precautions had to be taken for the amine containing monomer. A bifunctional chain transfer agent (CTA) was synthesized and used to make symmetrical ABA-triblock copolymers. To be able to synthesize well-defined triblock copolymers of a pre-determined molecular weight, first a kinetic study of each homopolymerization was performed to find the best reaction conditions and to determine the polymerization rate. The polymers used as middle blocks were then synthesized on larger scale and used for kinetic studies of the triblock copolymers. These reactions were followed by multigram-scale synthesis of the desired triblock copolymers to obtain enough material for further study of the thermal and mechanical properties in bulk as will be discussed in Chapter 6.

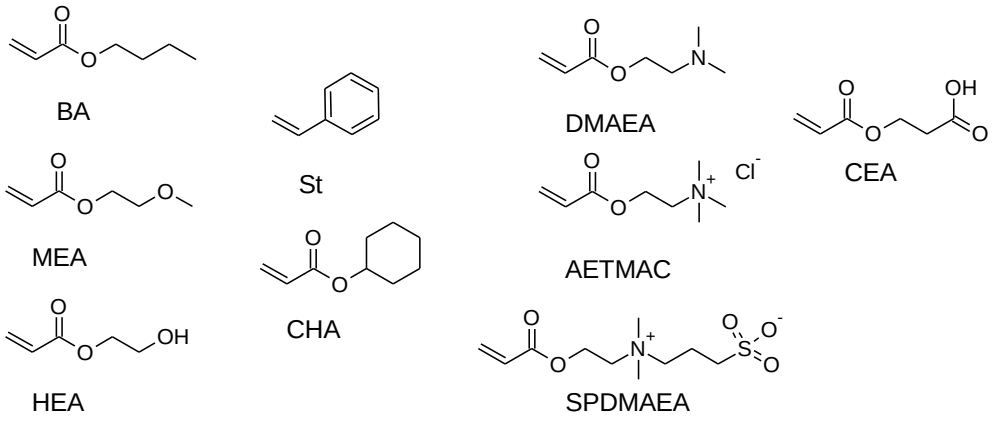

Figure 75. Overview of monomers used in this chapter: *n*-butyl acrylate (BA), 2-methoxyethyl acrylate (MEA), 2-hydroxyethyl acrylate (HEA), styrene (St), cyclohexyl acrylate (CHA), 2-(dimethylamino)ethyl acrylate (DMAEA), [2-(acryloyloxy)ethyl]trimethylammonium chloride (AETMAC), 2-(*N*-3-sulfopropyl-*N*,*N*-dimethyl ammonium)ethyl acrylate (SPDMAEA) and 2-carboxyethyl acrylate (CEA).

5.2 Experimental Section

Materials

Acetone (99.8%), dichloromethane (DCM, 99.8%), ethyl acetate (99.7%), diethyl ether (99.8%), tetrahydofuran (THF, 99.9%), ethylene glycol (99%), 1-butanethiol (99%), 2-bromopropionic acid (99%), 4-(dimethylamino)pyridine (99%), carbon disulfide (99.9%), pentaerythritol (98%), 1,3-propanesultone (98%), *n*-butyl acrylate (BA, 99%), ethylene glycol methyl ether acrylate (MEA, 98%), 2-hydroxyethyl acrylate (HEA, 96%), styrene (St, 99%), [2-(acryloyloxy)ethyl]trimethylammonium chloride (AETMAC, 80% in water), 2-carboxyethyl acrylate (CEA), and inhibitor removers (for removing hydroquinone and monomethyl ether hydroquinone) were purchased from Sigma-Aldrich. Hydrochloric acid (HCl, 37% solution), sodium chloride (99%), sodium hydroxide (pellets, 97%) and ammonium chloride (NH_4Cl, 99%) were purchased from Acros. 2-(Dimethylamino)ethyl acrylate (DMAEA, 97%) and cyclohexyl acrylate (CHA, 98%) were purchased from TCI. Hexane (95%) and magnesium sulfate ($MgSO_4$, dried) were purchased from Fisher Scientific. Methanol (99%) was purchased from Chem-Lab. Deuterated acetone (acetone-d6, 99.8%), deuterated chloroform ($CDCl_3$, 99.8%), deuterium oxide (D_2O, 99.9%) and deuterated dimethyl sulfoxide (DMSO-d6, 99.8%) were purchased from Euriso-top. Aluminum oxide (90 standardized) was purchased from Merck. *N,N*-dimethylformamide (DMF, peptide synthesis) was purchased from Biosolve. *N*-(3-

dimethylaminopropyl)-*N*'-ethylcarbodiimide hydrochloride was purchased from Iris Biotech. Dry THF (unstabilized and free of peroxides) was obtained from a solvent purification system (Meyer, custom made with a nitrogen, aluminum oxide drying system). Inhibitors were removed from the monomers by passing over an aluminum oxide column (for BA, MEA, St, CHA) or by stirring with inhibitor removers followed by filtration (for HEA, DMAEA, AETMAC, CEA). Other chemicals were used as received.

Gas Chromatography (GC)

Samples were measured with GC to determine the monomer conversion from the ratio of the integrals from the monomer and the reaction solvent. GC was performed on an Agilent 7890A system equipped with a VWR Carrier-160 hydrogen generator and an Agilent HP-5 column of 30 m length and 0.320 mm diameter. An FID detector was used and the inlet was set to 250 °C with a split injection of ratio 25:1. Hydrogen was used as carrier gas at a flow rate of 2 mL/min. The oven temperature was increased with 20°C/min from 50°C to 120°C, followed by a ramp of 50°C/min to 300°C.

Size Exclusion Chromatography (SEC)

SEC of most of the polymers was performed on a Agilent 1260-series HPLC system equipped with a 1260 online degasser, a 1260 ISO-pump, a 1260 automatic liquid sampler, a thermostatted column compartment at 50 °C equipped with two PLgel 5 µm mixed-D columns and a precolumn in series, a 1260 diode array detector and a 1260 refractive index detector. The used eluent was DMA containing 50 mM of LiCl at a flow rate of 0.593 mL/min. The spectra were analyzed using the Agilent Chemstation software with the GPC add on. Molar mass and dispersity values were calculated against PMMA standards from Polymer Labs. Some of the earlier polymers were measured on a PSS GRAM30 column in series with a PSS GRAM1000 column using a flow rate of 1 mL/min.

SEC of CHA-containing polymers and absolute M_n determination of star-shaped PBA polymers were performed on a Varian PL-GPC 50 Plus system using THF at 1 mL/min as eluent, and equipped with two PLgel 5 µm MIXED-D columns, a PL-AS RT autosampler and five detectors: RI, light scattering at 15° and 90°, a viscometer and a UV Knauer Wellchrom Spectro-Photometer K-2501. Molecular weights of PCHA polymers were determined with the RI detector using polystyrene standards.

Polymers containing AETMAC were measured on a Agilent HPLC with a 1260 refractive index detector (RID) with eluent of hexafluoro-2-propanol (HFIP) containing 20 mM sodium trifluoroacetate at a flow rate of 0.3 ml/min. The column set consisted of two PSS PFG 100 Å gel 5 µm mixed D columns and a similar guard column (Agilent) at 35 °C in series. The spectra were analyzed using the Agilent Chemstation software with the GPC add on. Molar mass and dispersity values were calculated against PMMA standards from Polymer Labs.

Nuclear magnetic resonance spectroscopy (NMR)

^{1}H NMR spectra were recorded on a Bruker Avance 300 MHz spectrometer at room temperature in deuterated solvents. ^{1}H NMR spectroscopy was used to measure the monomer conversion in some of the reactions, specifically the polymerizations of CEA and AETMAC, and to check the purity of the formed products.

Freezedryer

For the purification of some of the polymers a Martin Christ Freezedryer Alpha 2-4 LDPlus with an ice condenser capacity of 4 kg and temperature of -85 °C and 4 kg/24 h performance was used.

Synthesis of bifunctional trithiocarbonate chain transfer agent (BTCTA)

2-(((Butylsulfanyl)carbonothioyl)sulfanyl)propanoic acid (PABTC) was synthesized following a previously published method, see also Chapter 4.[25] A solution of PABTC (16.90 g, 71 mmol) and ethylene glycol (2.00 g, 32 mmol) in dichloromethane (300 mL) was cooled in an ice bath. A solution of *N*-(3-dimethylaminopropyl)-*N*'-ethylcarbodiimide hydrochloride (16.57 g, 81 mmol) and 4-(dimethylamino)pyridine (0.79 g, 0.64 mmol) in dichloromethane (100 mL) was added dropwise and the reaction was stirred overnight at room temperature. The mixture was subsequently washed with a saturated NH_4Cl solution, distilled water, 1M HCl and saturated brine, dried with $MgSO_4$, filtered and the solvent was removed under reduced pressure. The product was then purified over a short aluminum oxide column using hexane:ethyl acetate 3:1 as eluent. The solvent was removed under reduced pressure and a 12.27 g yield (76%) of orange liquid was obtained. A mass spectrum could not be measured due to degradation of the compound during the measurement.

^{1}H NMR ($CDCl_3$, 300 MHz) δ: 4.80 ppm (2H, q, -C*H*(CH_3)-S-), 4.32 ppm (4H, s, -C(O)-O-C*H*$_2$-CH_2), 3.33 ppm (4H, t, -CH_2-C*H*$_2$-S-), 1.65 ppm (4H, m, -CH_2-C*H*$_2$-CH_2-S-), 1.58 ppm (6H, d, C*H*$_3$-CH-), 1.40 ppm (4H, m, CH_3-C*H*$_2$-CH_2-), 0.90 ppm (6H, t, C*H*$_3$-CH_2-)

^{13}C NMR ($CDCl_3$, 300 MHz) δ: 171 ppm (-*C*(O)-O-), 63 ppm (-C(O)-O-*C*H_2-CH_2), 48 ppm (-*C*H(CH_3)-S-), 37 ppm (-CH_2-*C*H_2-S-), 30 ppm (-CH_2-*C*H_2-CH_2-S-), 22 ppm (CH_3-*C*H_2-CH_2-), 17 ppm (*C*H_3-CH-), 14 ppm (*C*H_3-CH_2-)

Synthesis of tetrafunctional trithiocarbonate chain transfer agent (4-CTA)

Synthesis of 4-CTA was reported before, using a different method than what is shown in this chapter.[26] A solution of PABTC (4.38 g, 18 mmol) and pentaerytritol (0.50 g, 3.7 mmol) in dichloromethane (50 mL) was cooled in an ice bath. A solution of *N*-(3-dimethylaminopropyl)-*N*'-ethylcarbodiimide hydrochloride (3.52 g, 18 mmol) and 4-(dimethylamino)pyridine (0.22 g, 1.8 mmol) in dichloromethane (50 mL) was added dropwise, during which the color changed to dark red, and the reaction was stirred overnight at room temperature, when the color turned back to yellow. The mixture was stirred with an excess of Na_2CO_3, filtered, washed with distilled water, dried with $MgSO_4$ and dried under vacuum. The product was purified on a short silica column using hexane:ethyl acetate 4:1 as eluent. The solvent was removed under reduced pressure and a 3.05 g yield (81%) of dark orange liquid was obtained. A mass spectrum could not be measured due to degradation of the compound during the measurement.

^{1}H NMR ($CDCl_3$, 300 MHz) δ: 4.81 ppm (4H, q, -C*H*(CH_3)-S-), 4.05 ppm (8H, m, -C(O)-O-C*H*$_2$-C), 3.37 ppm (8H, m, -CH_2-C*H*$_2$-S-), 1.68 ppm (8H, m, -CH_2-C*H*$_2$-CH_2-S-), 1.58 ppm (12H, d, C*H*$_3$-CH-), 1.42 ppm (8H, m, CH_3-C*H*$_2$-CH_2-), 0.94 ppm (12H, t, C*H*$_3$-CH_2-)

^{13}C NMR ($CDCl_3$, 300 MHz) δ: 171 ppm (-*C*(O)-O-), 63 ppm (-C(O)-O-*C*H_2-C), 47 ppm (-*C*H(CH_3)-S-), 42 ppm (*C*-(CH_2-)$_4$), 37 ppm (-CH_2-*C*H_2-S-), 30 ppm (-CH_2-*C*H_2-CH_2-S-), 22 ppm (CH_3-*C*H_2-CH_2-), 16 ppm (*C*H_3-CH-), 14 ppm (*C*H_3-CH_2-)

RAFT polymerizations

All polymerizations in this chapter were performed using schlenk techniques. Representative example for kinetic study of BA using BTCTA: A schlenk tube containing BA (1.00 g, 7.80 mmol), AIBN (1.28 mg, 0.078 mmol), BTCTA (39.2 mg, 0.78 mmol) and DMF (3.00 g, 3.18 mL) was degassed via five freeze-pump-thaw cycles. The flask was put under argon atmosphere and a t0 sample was taken using a degassed syringe. The polymerization was started by immersing the flask in an oil bath at 60 °C and during the reaction samples were taken every hour using a degassed syringe.

Representative example for kinetic study of DMAEA using PBA macroCTA: A schlenk tube containing DMAEA (1.00 g, 7.00 mmol), AIBN (1.14 mg, 0.070 mmol), PBA1 (50 wt% solution in DMF, 0.824 g, 0.70 mmol) and DMF (1.45 g, 1.54 mL) was degassed via five freeze-pump-thaw cycles. The flask was put under argon atmosphere and a t0 sample was taken using a degassed syringe. The polymerization was started by immersing the flask in an oil bath at 70 °C and during the reaction samples were taken every hour using a degassed syringe.

Representative example for large scale synthesis of PBA using BTCTA: A schlenk flask containing BA (60.0 g, 468 mmol), AIBN (76.8 mg, 0.468 mmol), BTCTA (2.35 g, 4.68 mmol) and DMF (182 g, 193 mL) was bubbled with argon and a t0 sample was taken using a degassed syringe. The polymerization was started by immersing the flask in an oil bath at 60 °C and after several hours a sample was taken using a degassed syringe to check the conversion via GC. The polymerization was stopped by cooling the flask in an ice bath when the desired conversion was reached.

Representative example for large scale synthesis of PDMAEA-*b*-PBA-*b*-PDMAEA using PBA as macroCTA: A schlenk flask containing DMAEA (10.0 g, 70 mmol), AIBN (11.5 mg, 0.070 mmol), PBA3 (50 wt% in DMF, 8.99 g, 0.70 mmol) and DMF (13.7 g, 14.5 mL) was bubbled with argon and a t0 sample was taken using a degassed syringe. The polymerization was started by immersing the flask in an oil bath at 70 °C and after several hours a sample was taken using a degassed syringe to check the conversion via GC. The polymerization was stopped by cooling the flask in an ice bath when the desired conversion was reached.

PBA: ^{1}H NMR ($CDCl_3$, 300 MHz) δ: 4.82 ppm (2H, q, -C*H*(CH_3)-S- of BTCTA), 4.03 ppm (2H, m, CH_3-CH_2-CH_2-C*H*$_2$-O-), 3.34 ppm (4H, t, -CH_2-C*H*$_2$-S- of BTCTA), 2.30 ppm (1H, m, backbone), 1.59 ppm (2H, m, CH_3-CH_2-C*H*$_2$-CH_2-O-), 1.37 ppm (2H, m, CH_3-C*H*$_2$-CH_2-CH_2-O-), 0.93 ppm (3H, t, C*H*$_3$-CH_2-CH_2-CH_2-O-), 2.20-0.60 ppm (additional peaks of polymer backbone and BTCTA)

PDMAEA: ^{1}H NMR ($CDCl_3$, 300 MHz) δ: 4.82 ppm (2H, q, -C*H*(CH_3)-S- of BTCTA), 4.13 ppm (2H, m, N-CH_2-C*H*$_2$-O-), 3.34 ppm (4H, t, -CH_2-C*H*$_2$-S- of BTCTA), 2.53 ppm (2H, m, N-C*H*$_2$-CH_2-O-), 2.24 ppm (6H, s, (*CH*$_3$)$_2$-N-CH_2) , 2.60-0.60 ppm (additional peaks of polymer backbone and BTCTA)

PDMAEA-*b*-PBA-*b*-PDMAEA: ^{1}H NMR ($CDCl_3$, 300 MHz) δ: 4.82 ppm (2H, q, -C*H*(CH_3)-S- of BTCTA), 4.15 ppm (2H, m, N-CH_2-C*H*$_2$-O-), 4.03 ppm (2H, m, CH_3-CH_2-CH_2-C*H*$_2$-O-), 3.34 ppm (4H, t, -CH_2-C*H*$_2$-S- of BTCTA), 2.54 ppm (2H, m, N-C*H*$_2$-CH_2-O-), 2.27 ppm (6H, s, (*CH*$_3$)$_2$-N-CH_2), 1.59 ppm (2H, m, CH_3-CH_2-C*H*$_2$-CH_2-O-), 1.36 ppm (2H, m, CH_3-C*H*$_2$-CH_2-CH_2-O-), 0.93 ppm (3H, t, C*H*$_3$-CH_2-CH_2-CH_2-O-), 2.50-0.60 ppm (additional peaks of polymer backbone and BTCTA)

PCEA: ^{1}H NMR (D_2O, 300 MHz) δ: 4.82 ppm (2H, q, -C*H*(CH_3)-S- of BTCTA), 4.38 ppm (2H, m, C(OOH)-CH_2-C*H*$_2$-O-), 3.45 ppm (4H, t, -CH_2-C*H*$_2$-S- of BTCTA), 2.74 ppm (2H, m, C(OOH)-C*H*$_2$-CH_2-O-), 2.60-0.60 ppm (additional peaks of polymer backbone and BTCTA)

PCEA-*b*-PBA-*b*-PCEA: ^{1}H NMR (acetone-d6, 300 MHz) δ: 4.87 ppm (2H, q, -C*H*(CH_3)-S- of BTCTA), 4.35 ppm (2H, m, C(OOH)-CH_2-C*H*$_2$-O-), 4.08 ppm (2H, m, CH_3-CH_2-CH_2-C*H*$_2$-O-), 3.44 ppm (4H, t, -CH_2-C*H*$_2$-S- of BTCTA), 2.72 ppm (2H, m, C(OOH)-C*H*$_2$-CH_2-O-), 1.64 ppm (2H, m, CH_3-CH_2-C*H*$_2$-CH_2-O-), 1.44 ppm (2H, m, CH_3-C*H*$_2$-CH_2-CH_2-O-), 0.97 ppm (3H, t, C*H*$_3$-CH_2-CH_2-CH_2-O-), 2.60-0.60 ppm (additional peaks of polymer backbone and BTCTA)

PMEA: ^{1}H NMR ($CDCl_3$, 300 MHz) δ: 4.82 ppm (2H, q, -C*H*(CH_3)-S- of BTCTA), 4.17 ppm (2H, m, CH_3-O-CH_2-C*H*$_2$-O-), 3.54 ppm (2H, m, CH_3-O-C*H*$_2$-CH_2-O-), 3.34 ppm (4H, t, -CH_2-C*H*$_2$-S- of BTCTA), 3.33 ppm (3H, t, C*H*$_3$-O-CH_2-CH_2-O-), 2.60-0.60 ppm (additional peaks of polymer backbone and BTCTA)

PDMAEA-*b*-PMEA-*b*-PDMAEA: ^{1}H NMR ($CDCl_3$, 300 MHz) δ: 4.82 ppm (2H, q, -C*H*(CH_3)-S- of BTCTA), 4.19 ppm (2H, m, CH_3-O-CH_2-C*H*$_2$-O-), 4.14 ppm (2H, m, N-CH_2-C*H*$_2$-O-), 3.56 ppm (2H, m, CH_3-O-C*H*$_2$-CH_2-O-), 3.47 ppm (4H, t, -CH_2-C*H*$_2$-S- of BTCTA), 3.35 ppm (3H, t, C*H*$_3$-O-CH_2-CH_2-O-), 2.53 ppm (2H, m, N-C*H*$_2$-CH_2-O-), 2.26 ppm (6H, s, (*CH*$_3$)$_2$-N-CH_2) , 2.60-0.60 ppm (additional peaks of polymer backbone and BTCTA)

PCEA-*b*-PMEA-*b*-PCEA: ^{1}H NMR (acetone-d6, 300 MHz) δ: 4.87 ppm (2H, q, -C*H*(CH_3)-S- of BTCTA), 4.35 ppm (2H, m, C(OOH)-CH_2-C*H*$_2$-O-), 4.17 ppm (2H, m, CH_3-O-CH_2-C*H*$_2$-O-), 3.54 ppm (2H, m, CH_3-O-C*H*$_2$-CH_2-O-), 3.43 ppm (4H, t, -CH_2-C*H*$_2$-S- of BTCTA), 3.33 ppm (3H, t, C*H*$_3$-O-CH_2-CH_2-O-), 2.71 ppm (2H, m, C(OOH)-C*H*$_2$-CH_2-O-), 2.60-0.60 ppm (additional peaks of polymer backbone and BTCTA)

PHEA: ^{1}H NMR (DMSO-d6, 300 MHz) δ: 4.82 ppm (2H, q, -C*H*(CH_3)-S- of BTCTA), 4.74 ppm (1H, s, *H*O-CH_2-CH_2-O-), 4.01 ppm (2H, m, HO-CH_2-C*H*$_2$-O-), 3.56 ppm (2H, m, HO-C*H*$_2$-CH_2-O-), 3.39 ppm (4H, t, -CH_2-C*H*$_2$-S- of BTCTA), 2.60-0.60 ppm (additional peaks of polymer backbone and BTCTA)

PCEA-*b*-PHEA-*b*-PCEA: ^{1}H NMR (D_2O, 300 MHz) δ: 4.82 ppm (2H, q, -C*H*(CH_3)-S- of BTCTA), 4.39 ppm (2H, m, C(OOH)-CH_2-C*H*$_2$-O-), 4.20 ppm (2H, m, HO-CH_2-C*H*$_2$-O-), 3.81 ppm (2H, m, HO-C*H*$_2$-CH_2-O-), 3.46 ppm (4H, t, -CH_2-C*H*$_2$-S- of BTCTA), 2.77 ppm (2H, m, C(OOH)-C*H*$_2$-CH_2-O-), 2.60-0.60 ppm (additional peaks of polymer backbone and BTCTA)

PAETMAC-*b*-PHEA-*b*-PAETMAC: ^{1}H NMR (D_2O, 300 MHz) δ: 4.82 ppm (2H, q, -C*H*(CH_3)-S- of BTCTA), 4.59 ppm (2H, m, N-CH_2-C*H*$_2$-O-), 4.23 ppm (2H, m, HO-CH_2-C*H*$_2$-O-), 3.82 ppm (4H, m, HO-C*H*$_2$-CH_2-O- and N-C*H*$_2$-CH_2-O-), 3.52 ppm (4H, t, -CH_2-C*H*$_2$-S- of BTCTA), 3.28 ppm (9H, s, (*CH*$_3$)$_3$-N-), 2.60-0.60 ppm (additional peaks of polymer backbone and BTCTA)

PSt: ^{1}H NMR ($CDCl_3$, 300 MHz) δ: 7.24-6.85 ppm (3H, m, C*H*=CH-C*H*=CH-C*H*), 6.85-6.25 ppm (2H, m, CH=C*H*-CH=C*H*-CH), 4.85 ppm (2H, q, -C*H*(CH_3)-S- of BTCTA), 3.90 ppm (4H, s, -C(O)-O-C*H*$_2$-CH_2 of BTCTA), 3.26 ppm (4H, t, -CH_2-C*H*$_2$-S- of BTCTA), 2.60-0.60 ppm (additional peaks of polymer backbone and BTCTA)

PDMAEA-*b*-PSt-*b*-PDMAEA: ^{1}H NMR ($CDCl_3$, 300 MHz) δ: 7.24-6.85 ppm (3H, m, C*H*=CH-C*H*=CH-C*H*), 6.85-6.25 ppm (2H, m, CH=C*H*-CH=C*H*-CH), 4.85 ppm (2H, q, -C*H*(CH_3)-S- of BTCTA), 4.15 ppm (2H, m, N-CH_2-C*H*$_2$-O-), 3.35 ppm (4H, t, -CH_2-C*H*$_2$-S- of BTCTA), 2.54 ppm (2H, m, N_2-C*H*$_2$-CH_2-O-), 2.27 ppm (6H, s, (C*H*$_3$)$_2$-N-), 2.60-0.60 ppm (additional peaks of polymer backbone and BTCTA)

PBA-*b*-PSt-*b*-PBA: ^{1}H NMR ($CDCl_3$, 300 MHz) δ: 7.24-6.85 ppm (3H, m, C*H*=CH-C*H*=CH-C*H*), 6.85-6.25 ppm (2H, m, CH=C*H*-CH=C*H*-CH), 4.82 ppm (2H, q, -C*H*(CH_3)-S- of BTCTA), 4.02 ppm (2H, m, CH_3-CH_2-CH_2-C*H*$_2$-O-), 3.34 ppm (4H, t, -CH_2-C*H*$_2$-S- of BTCTA), 1.58 ppm (2H, m, CH_3-CH_2-C*H*$_2$-CH_2-O-), 1.37 ppm (2H, m, CH_3-C*H*$_2$-CH_2-CH_2-O-), 0.93 ppm (3H, t, C*H*$_3$-CH_2-CH_2-CH_2-O-), 2.60-0.60 ppm (additional peaks of polymer backbone and BTCTA)

PDMAEA-*b*-PBA-*b*-PSt-*b*-PBA-*b*-PDMAEA: ^{1}H NMR ($CDCl_3$, 300 MHz) δ: 7.24-6.85 ppm (3H, m, C*H*=CH-C*H*=CH-C*H*), 6.85-6.25 ppm (2H, m, CH=C*H*-CH=C*H*-CH), 4.82 ppm (2H, q, -C*H*(CH_3)-S- of BTCTA), 4.15 ppm (2H, m, N-CH_2-C*H*$_2$-O-), 4.02 ppm (2H, m, CH_3-CH_2-CH_2-C*H*$_2$-O-), 3.34 ppm (4H, t, -CH_2-C*H*$_2$-S- of BTCTA), 2.54 ppm (2H, m, N-C*H*$_2$-CH_2-O-), 2.27 ppm (6H, s, (C*H*$_3$)$_2$-N-CH_2), 1.58 ppm (2H, m, CH_3-CH_2-C*H*$_2$-CH_2-O-), 1.37 ppm (2H, m, CH_3-C*H*$_2$-CH_2-CH_2-O-), 0.93 ppm (3H, t, C*H*$_3$-CH_2-CH_2-CH_2-O-), 2.60-0.60 ppm (additional peaks of polymer backbone and BTCTA)

PCHA: ^{1}H NMR ($CDCl_3$, 300 MHz) δ: 4.82 ppm (2H, q, -C*H*(CH_3)-S- of BTCTA), 4.70 ppm (1H, s, (CH_2)$_2$-C*H*-O), 3.34 ppm (4H, t, -CH_2-C*H*$_2$-S- of BTCTA), 2.24 ppm (1H, m, backbone), 2.00-0.80 ppm (additional peaks of methylene groups cyclohexane, polymer backbone and BTCTA)

PDMAEA-*b*-PCHA-*b*-PDMAEA: ^{1}H NMR ($CDCl_3$, 300 MHz) δ: 4.82 ppm (2H, q, -C*H*(CH_3)-S- of BTCTA), 4.70 ppm (1H, s, (CH_2)$_2$-C*H*-O), 4.15 ppm (2H, m, N-CH_2-C*H*$_2$-O-), 3.34 ppm (4H, t, -CH_2-C*H*$_2$-S- of BTCTA), 2.54 ppm (2H, m, N-C*H*$_2$-CH_2-O-), 2.26 ppm (6H, s, (*CH*$_3$)$_2$-N-CH_2) and (1H, m, backbone), 2.50-0.80 ppm (additional peaks of methylene groups cyclohexane, polymer backbone and BTCTA)

PCEA-*b*-PCHA-*b*-PCEA: ^{1}H NMR (acetone-d6, 300 MHz) δ: 4.82 ppm (2H, q, -C*H*(CH_3)-S- of BTCTA), 4.74 ppm (1H, s, (CH_2)$_2$-C*H*-O), 4.35 ppm (2H, m, C(OOH)-CH_2-C*H*$_2$-O-), 3.34 ppm (4H, t, -CH_2-C*H*$_2$-S- of BTCTA), 2.72 ppm (2H, m, C(OOH)-C*H*$_2$-CH_2-O-), 2.34 ppm (1H, m, backbone), 2.50-0.80 ppm (additional peaks of methylene groups cyclohexane, polymer backbone and BTCTA)

PBA star: ^{1}H NMR ($CDCl_3$, 300 MHz) δ: 4.82 ppm (4H, q, -C*H*(CH_3)-S- of 4-CTA), 4.03 ppm (2H, m, CH_3-CH_2-CH_2-C*H*$_2$-O-), 3.34 ppm (8H, t, -CH_2-C*H*$_2$-S- of 4-CTA), 2.27 ppm (1H, m, backbone), 1.58 ppm (2H, m, CH_3-CH_2-C*H*$_2$-CH_2-O-), 1.38 ppm (2H, m, CH_3-C*H*$_2$-CH_2-CH_2-O-), 0.93 ppm (3H, t, C*H*$_3$-CH_2-CH_2-CH_2-O-), 2.00-0.60 ppm (additional peaks of polymer backbone and 4-CTA)

PCEA star: ^{1}H NMR (DMSO-d6, 300 MHz) δ: 4.82 ppm (4H, q, -C*H*(CH_3)-S- of 4-CTA), 4.21 ppm (2H, m, C(OOH)-CH_2-C*H*$_2$-O-), 3.34 ppm (8H, t, -CH_2-C*H*$_2$-S- of 4-CTA), 2.64 ppm (2H, m, C(OOH)-C*H*$_2$-CH_2-O-), 2.60-0.80 ppm (additional peaks of polymer backbone and 4-CTA)

Synthesis of zwitterionic triblock copolymer

An ABA-triblock copolymer containing P(2-(*N*-3-sulfopropyl-*N*,*N*-dimethyl ammonium)ethyl acrylate) (SPDMAEA) as charged betaine end blocks and PMEA as middle block was synthesized via post-polymerization modification of a PDMAEA-*b*-PMEA-*b*-PDMAEA triblock copolymer.[18, 27] The polymer (1.00 g, containing 2.8 mmol DMAEA groups) was dissolved in dry THF (20 mL), stirred in an ice bath and 1,3-propanesultone (0.36, 2.9 mmol) in dry THF (10 mL) was added. The reaction was slowly warmed up and stirred overnight at 40 °C, after which the solvent was removed under reduced pressure. The polymer was purified on a PD-10 Sephadex G-25 column, using distilled water as eluent, and freeze-dried.

^{1}H NMR (D_2O, 300 MHz) δ: 4.58 ppm (2H, m, N-CH_2-C*H*$_2$-O-), 4.27 ppm (2H, m, CH_3-O-CH_2-C*H*$_2$-O-), 3.83 ppm (2H, m, N-C*H*$_2$-CH_2-O-), 3.70 ppm (2H, m, CH_3-O-C*H*$_2$-CH_2-O-), 3.64 ppm (2H, m, S-CH_2-CH_2-

C*H*$_2$-N-), 3.41 ppm (3H, s, C*H*$_3$-O-CH$_2$-CH$_2$-O-), 3.26 ppm (6H, s, (*CH*$_3$)$_2$-N-CH$_2$), 3.00 ppm (2H, m, S-C*H*$_2$-CH$_2$-CH$_2$-N-), 2.48 ppm (2H, m, S-CH$_2$-C*H*$_2$-CH$_2$-N-)

5.3 Results and discussion

5.3.1 Synthesis of bifunctional trithiocarbonate chain transfer agent (BTCTA)

For the synthesis of ABA-triblock copolymers, the bifunctional BTCTA was synthesized from PABTC using the reaction shown in Figure 76. Purification was done by washing and column chromatography. ^{1}H and ^{13}C APT NMR spectra of the purified BTCTA are shown in Figure 77 and Figure 78, demonstrating its successful synthesis and high purity. All homopolymers in this chapter, except for the star polymers, were synthesized using BTCTA.

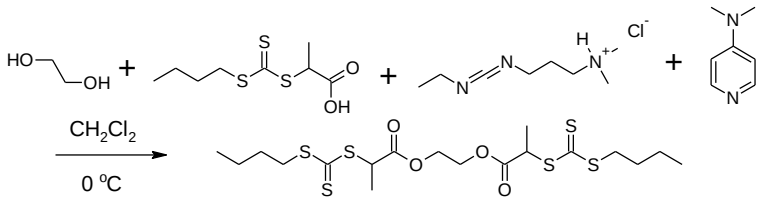

Figure 76. Synthesis of bifunctional trithiocarbonate chain transfer agent (BTCTA).

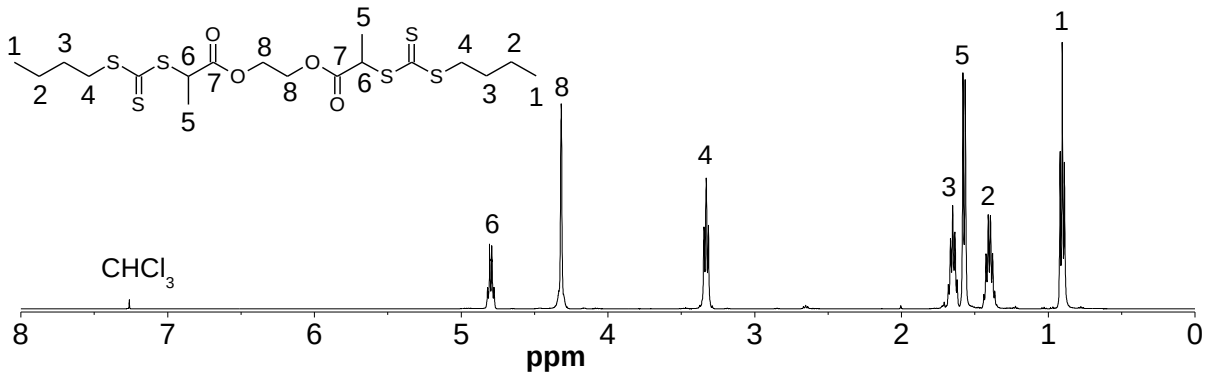

Figure 77. ^{1}H NMR spectrum ($CDCl_3$) of BTCTA.

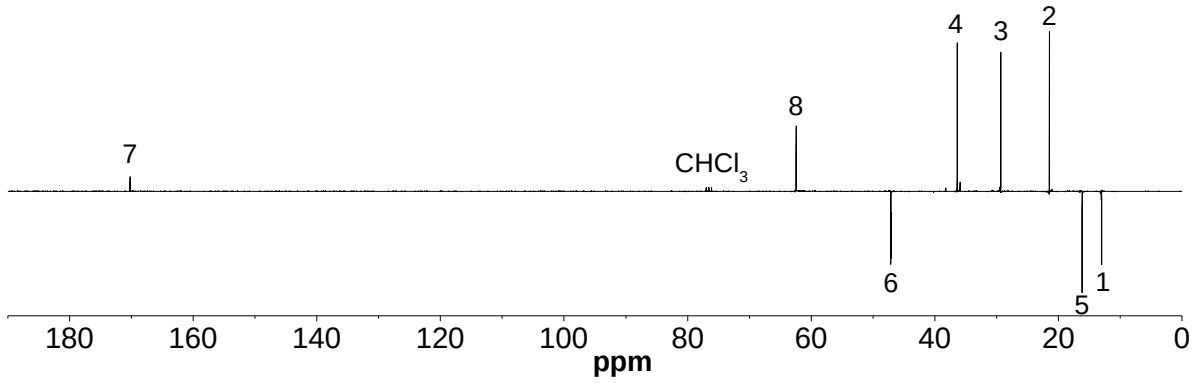

Figure 78. Attached proton test (APT) ^{13}C NMR spectrum ($CDCl_3$) of BTCTA.

5.3.2 Homopolymerization of *n*-butyl acrylate (BA)

As a hydrophobic monomer that forms polymers with a low T_g of -54 °C, BA was chosen as a first option for the uncharged middle block of the triblock copolymers. To determine the best reaction conditions, the homopolymerization of BA was performed with BTCTA at different temperatures, using different monomer concentrations and different ratios of AIBN to BTCTA (Figure 80). The reactions at 70 °C proceeded relatively fast, but showed a decrease in slope of the first-order kinetic plot and higher dispersities (Đ > 1.5) at higher conversions, which are indicative of termination. Reactions at 65 °C were slower but still showed a similar increase in dispersity. Of the reactions at 60 °C, the reaction using 0.17 eq. of AIBN also shows a dispersity around 1.5, while the reaction using 0.05 eq. of AIBN was too slow to yield a high enough conversion within a reasonable time frame. However, at [BA]:[BTCTA]:[AIBN] = 100:1:0.1 and a concentration of 1.8 M at 60 °C, a well-controlled polymerization was obtained with a linear first-order kinetic plot, showing no termination, and a dispersity around 1.2 up to 70 % conversion within 7 hours. These conditions were chosen for further synthesis of PBA homopolymers with different molar masses (Table 7). The polymers were purified by precipitation in methanol:distilled water 2:1 and dried under reduced pressure. The larger differences in $M_{n,theoretical}$ and $M_{n,SEC}$ in the later reactions can be explained by the switch to a new column set. While earlier measurements were performed on polyester-based columns, the later measurements used polystyrene-based columns, and a different column interaction is expected with reference to the PMMA standards.

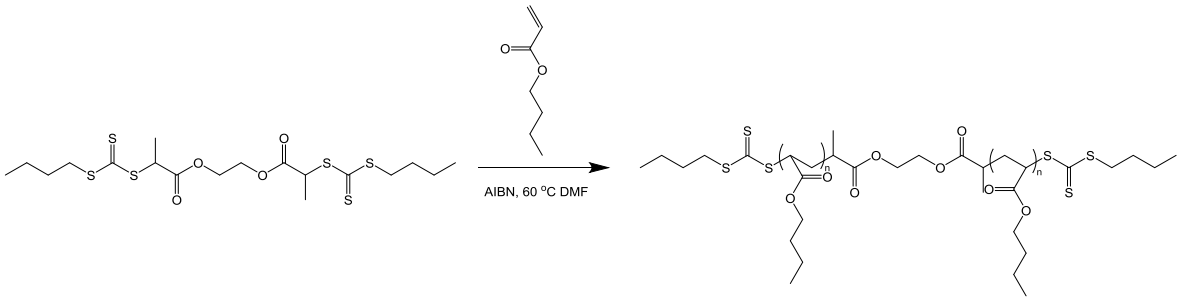

Figure 79. Homopolymerization of BA using BTCTA.

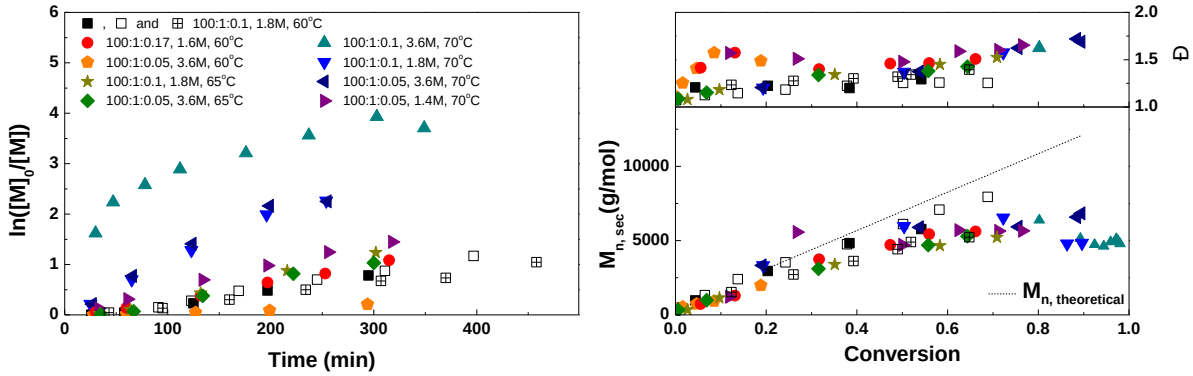

Figure 80. Left: first order kinetic plot for RAFT polymerization of BA using different [BA]:[BTCTA]:[AIBN] ratios, concentrations and temperatures. Right: corresponding molecular weight and dispersity vs. conversion plot.

Table 7. Overview of PBA homopolymers synthesized on large scale, using [BA]:[BTCTA]:[AIBN] = 100:1:0.1, 60 °C in DMF at 1.8 M. * [BA]:[BTCTA]:[AIBN] = 50:1:0.1.

Polymer #	Conversion (GC)	$M_{n,theoretical}$ (g/mol)	M_n (g/mol, SEC)	Đ (SEC)	Yield
PBA1	41 %	6400	5900	1.24	2.80 g (63 %)
PBA2	56 %	7700	8100	1.18	17.91 g (75 %)
PBA3	54 %	7400	6400	1.21	14.22 g (61 %)
PBA4	53 %	7300	6800	1.22	21.66 (76 %)
PBA5	56 %	7600	7700	1.13	31.85 g (88 %)
PBA6	56 %	7500	7600	1.17	32.69 g (91 %)
PBA7	20 %	3100	1700	1.07	5.23 g (100 %)
PBA8	16 %	2600	1400	1.15	2.70 g (68 %)
PBA9	38 %	5700	3000	1.13	16.80 g (80 %)
PBA10	55 %	7600	5100	1.16	34.89 g (99 %)
PBA11	42 %*	3200	1600	1.14	24.34 g (97 %)
PBA12	54 %	7500	6500	1.12	15.25 g (88 %)
PBA13	53 %	7100	5100	1.18	26.03 g (89 %)
PBA14	23 %	3300	1500	1.44	9.71 g (90 %)

5.3.3 Homopolymerization of 2-(dimethylamino)ethyl acrylate (DMAEA)

DMAEA was chosen as the positively charged monomer, because it has a similar structure and low T_g (-47 °C) as BA. A reaction using [DMAEA]:[BTCTA]:[AIBN] = 100:1:0.1, 1.8 M in DMF at 60 °C showed no polymerization, indicating that DMAEA is a less reactive monomer than BA. To counteract this observation, a higher radical concentration is needed for the polymerization and therefore the temperature was increased to 70 °C leading to faster dissociation of AIBN. Two homopolymerizations of DMAEA using similar conditions were performed, both showing similar results (Figure 81). While the reactions are relatively slow, the first-order kinetic plots were linear. Dispersities are low around 1.2 and the theoretical M_ns are in good agreement with those measured by SEC. One homopolymerization was performed on larger scale using these conditions and the polymer was purified by precipitation in cold hexane and dried under reduced pressure (Table 8).

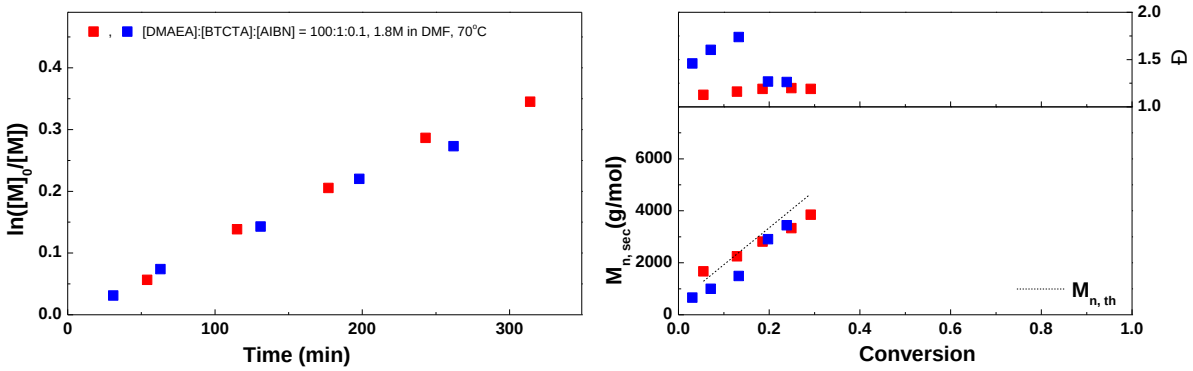

Figure 81. Left: first order kinetic plot for RAFT polymerization of DMAEA. Right: corresponding molecular weight and dispersity vs. conversion plot.

Table 8. Overview of PDMAEA homopolymer synthesized on large scale, using [DMAEA]:[BTCTA]:[AIBN] = 100:1:0.1, 70 °C in DMF at 1.8 M.

Polymer #	Conversion (GC)	$M_{n,theoretical}$ (g/mol)	M_n (g/mol, SEC)	Đ (SEC)	Yield
PDMAEA1	27 %	4400	5000	1.35	6 g (98 %)

5.3.4 Block copolymerization of DMAEA with PBA as macro CTA

For these triblock copolymerizations of DMAEA, the purified PBA homopolymers were used as a macro chain transfer agent (Figure 83). Similar conditions were used as for the homopolymerization, generally leading to good results. Linear kinetic plots were observed for all reactions up to 40 % conversion. A small increase in monomer concentration to 2.0 M instead of 1.5 M showed lower dispersities around 1.2 and therefore this concentration was used for large scale reactions aiming for different polymer chain length and composition (Table 9). Polymers were purified either by precipitation in hexane/diethyl ether mixtures or by first removing the DMF under reduced pressure followed by precipitation in hexane, followed by drying under reduced pressure. Because the precipitation in hexane/diethyl ether did not work very well, attempts were made to precipitate the polymer (PDMAEA-*b*-PBA-*b*-PDMAEA4) in milliQ water, which unfortunately led to partial hydrolysis of the DMAEA groups. Several reactions were also performed under different conditions using anisole or THF as solvent to attempt to get a higher monomer conversion. While in some of these reactions a higher conversion was observed with GC, in SEC either no change in molecular weight was observed or the formation of multiple or multimodal peaks (Đ > 2) due to chain coupling, indicating that these solvents were not suitable for this triblock copolymerization.

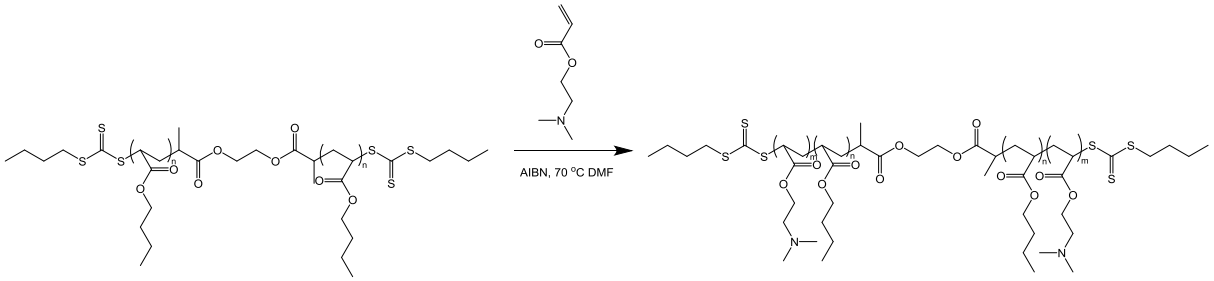

Figure 82. Triblock copolymerization of DMAEA using PBA as macroCTA.

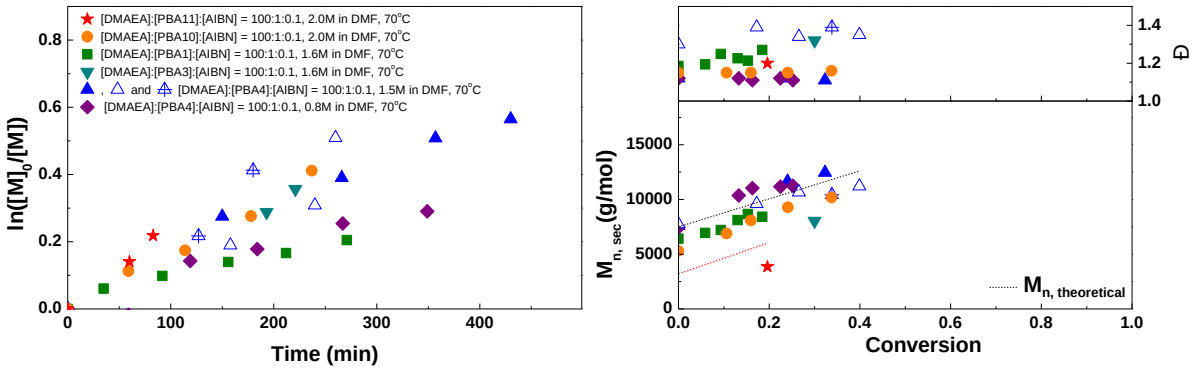

Figure 83. Left: first order kinetic plot for RAFT block copolymerization of DMAEA using PBA as macro CTA. Right: corresponding molecular weight and dispersity vs. conversion plot. Reactions in the same color were performed using the same macro CTA.

Table 9. Overview of PDMAEA-*b*-PBA-*b*-PDMAEA triblock copolymers synthesized on large scale, using [DMAEA]:[PBA]:[AIBN] = 100:1:0.1, 70 °C in DMF at 2.0 M.

Polymer #	macroCTA	Conversion (GC)	$M_{n,theoretical}$ (g/mol)	M_n (g/mol, SEC)	Đ (SEC)	% DMAEA (NMR)	Yield
PDMAEA-*b*-PBA-*b*-PDMAEA1	PBA2	10 %	9600	8300	1.30	12	3.00 g (57 %)
PDMAEA-*b*-PBA-*b*-PDMAEA2	PBA3	30 %	8300	8000	1.32	40	6.18 g (69 %)
PDMAEA-*b*-PBA-*b*-PDMAEA3	PBA5	41 %	13600	9500	1.14	42	4.92 g (35 %)
PDMAEA-*b*-PBA-*b*-PDMAEA4	PBA6	40 %	12600	11200	1.35	-	purification failed
PDMAEA-*b*-PBA-*b*-PDMAEA5	PBA6	34 %	11800	10400	1.39	33	7.74 g (57 %)
PDMAEA-*b*-PBA-*b*-PDMAEA6	PBA10	34 %	12400	10200	1.16	45	11.79 g (68 %)
PDMAEA-*b*-PBA-*b*-PDMAEA7	PBA11	20 %	6000	3900	1.20	58	7.72 g (46 %)
PDMAEA-*b*-PBA-*b*-PDMAEA8	PBA10	10 %	9000	9600	1.11	18	4.82 g (82 %)
PDMAEA-*b*-PBA-*b*-PDMAEA9	PBA13	26 %	10800	9200	1.22	40	3.5 g (31 %)
PDMAEA-*b*-PBA-*b*-PDMAEA10	PBA13	26 %	10800	7100	1.30	34	7.5 g (66 %)
PDMAEA-*b*-PBA-*b*-PDMAEA11	PBA9	20 %	8500	3100	1.11	29	3.47 g (100 %)

5.3.5 Homopolymerization of 2-carboxyethyl acrylate (CEA)

CEA was chosen as the negatively charged monomer, also for its similar structure to BA and its low T_g of 22 °C, which is higher than that of BA or DMAEA, but still much lower than the T_g of 105 °C of the more commonly used anionic AA. Based on the homopolymerization of DMAEA, the temperature was chosen at 70 °C using [CEA]:[BTCTA]:[AIBN] = 100:1:0.1 and 1.7 M in DMF. While linear kinetics and no termination were observed under these conditions, very high dispersities up to 1.7 were found at higher conversion (Figure 84). The high $M_{n,SEC}$ found at low conversion under these conditions, with $M_{n,SEC}$ dropping with increasing conversion, indicates that a combination of free and controlled radical polymerization is taking place, which explains the high dispersities. When the monomer and radical concentrations were lowered dispersities improved and $M_{n,SEC}$ was closer to $M_{n,theoretical}$, with the reaction at 0.56 M showing the best results. Two homopolymers were synthesized under these conditions and purified by precipitation in hexane:diethyl ether 1:1 and dried under reduced pressure (Table 10).

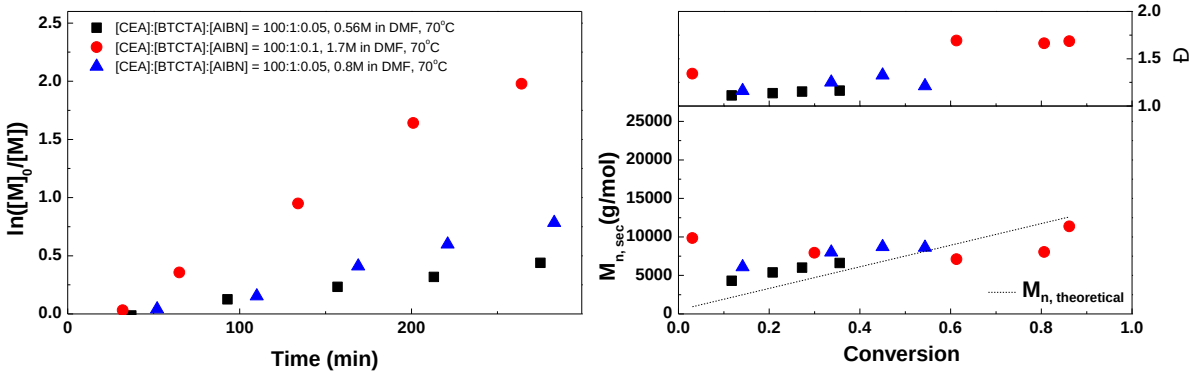

Figure 84. Left: first order kinetic plot for RAFT polymerization of CEA. Right: corresponding molecular weight and dispersity vs. conversion plot.

Table 10. Overview of PCEA homopolymers synthesized on large scale, using [CEA]:[BTCTA]:[AIBN] = 100:1:0.05, 70 °C in DMF at 0.56 M.

Polymer #	Conversion (NMR)	$M_{n,theoretical}$ (g/mol)	M_n (g/mol, SEC)	Đ (SEC)	Yield
PCEA1	36 %	5800	10700	1.32	3.2 g (23 %)
PCEA2	34 %	5400	12000	1.32	1.5 g (80 %)

5.3.6 Block copolymerization of CEA with PBA as macro CTA

In the next step, which is the triblock copolymerization of CEA using PBA as macro CTA, similar reaction conditions were used as for the homopolymerizations of CEA. Even though most of the reactions in Figure 85 were performed under similar conditions, with only a change in the PBA used, there is some variation in polymerization rate, with some reactions showing termination while others do not. This may be related to small amounts of oxygen present in those specific reactions or differences in monomer purity. Polymerizations using a shorter PBA as macroCTA, shown in blue, also show more termination than reactions with longer PBAs. $M_{n,SEC}$ is generally in good agreement with $M_{n,theoretical}$ and dispersities are around 1.1-1.2. In some cases, at higher conversion a bimodal SEC peak was observed, so the larger scale reactions were usually stopped below 35 % conversion. This bimodal peak is probably caused by coupling of polymer chains, which is more likely to happen with these triblock copolymers because of the ability of CEA to form hydrogen bonds with other CEA units, increasing the chance that two polymer chain ends, and subsequently two radicals, are close together and react. Triblock copolymers containing different sizes of CEA blocks were synthesized and purified by precipitation in distilled water, followed by drying under reduced pressure (Table 11).

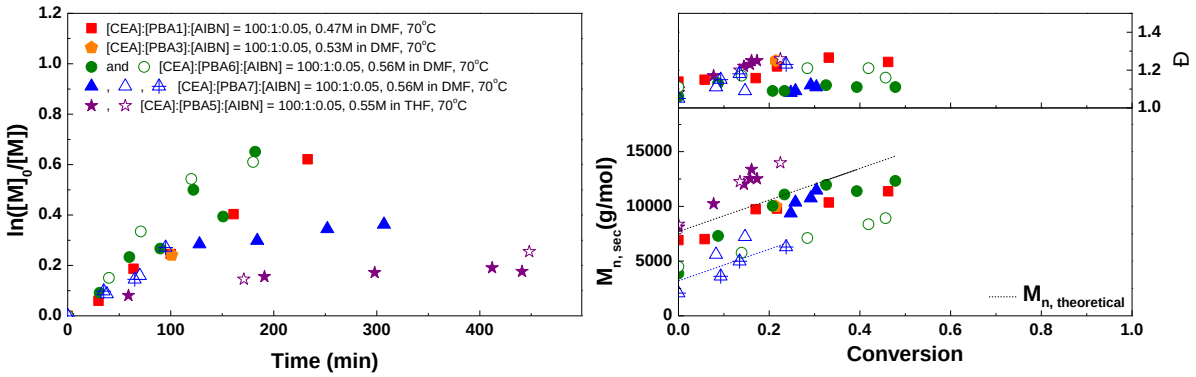

Figure 85. Left: first order kinetic plot for RAFT block copolymerization of CEA using PBA as macro CTA. Right: corresponding molecular weight and dispersity vs. conversion plot. Reactions in the same color were performed using the same macro CTA.

Table 11. Overview of PCEA-*b*-PBA-*b*-PCEA triblock copolymers synthesized on large scale, using [CEA]:[PBA]:[AIBN] = 100:1:0.05, 70 °C in DMF at 0.56 M.

Polymer #	macroCTA	Conversion (NMR)	$M_{n,theoretical}$ (g/mol)	M_n (g/mol, SEC)	Đ (SEC)	% CEA (NMR)	Yield
PCEA-*b*-PBA-*b*-PCEA1	PBA3	21 %	10500	10000	1.25	24	2.56 g (32 %)
PCEA-*b*-PBA-*b*-PCEA2	PBA5	22 %	10900	14000	1.26	18	5.50 g (48 %)
PCEA-*b*-PBA-*b*-PCEA3	PBA6	20 %	10400	15300	1.17	26	10 g (69 %)
PCEA-*b*-PBA-*b*-PCEA4	PBA7	25 %	6800	9400	1.08	55	1.09 g (82 %)
PCEA-*b*-PBA-*b*-PCEA5	PBA7	26 %	6900	10400	1.09	56	1.46 g (100 %
PCEA-*b*-PBA-*b*-PCEA6	PBA7	29 %	7400	10700	1.12	59	1.14 g (79 %)
PCEA-*b*-PBA-*b*-PCEA7	PBA7	30 %	7600	11500	1.11	60	1.13 g (76 %)
PCEA-*b*-PBA-*b*-PCEA8	PBA5	9 %	9000	7300	1.13	14	0.77 g (100 %)
PCEA-*b*-PBA-*b*-PCEA9	PBA7	8 %	4300	5600	1.11	29	0.47 g (78 %)
PCEA-*b*-PBA-*b*-PCEA10	PBA7	15 %	5200	7200	1.09	42	0.85 g (100 %)
PCEA-*b*-PBA-*b*-PCEA11	PBA8	11 %	4200	6500	1.21	40	1.87 g (45 %)
PCEA-*b*-PBA-*b*-PCEA12	PBA10	14 %	9600	4600	1.33	18	2.94 g (59 %)
PCEA-*b*-PBA-*b*-PCEA13	PBA11	9 %	4500	2400	1.27	31	2.93 g (94 %)
PCEA-*b*-PBA-*b*-PCEA14	PBA11	13 %	5100	2700	1.31	47	4.76 g (100 %)
PCEA-*b*-PBA-*b*-PCEA15	PBA13	20 %	9900	5000	1.71	35	14.0 g (100 %)
PCEA-*b*-PBA-*b*-PCEA16	PBA13	16 %	9500	4400	1.42	23	10.0 g (98 %)
PCEA-*b*-PBA-*b*-PCEA17	PBA14	22 %	6400	6900	1.14	42	9.0 g (67 %)

5.3.7 Homopolymerization of 2-methoxyethyl acrylate (MEA)

MEA was chosen as a second type of middle block for the triblock copolymers, being less hydrophobic than BA, thus expected to lead to better miscibility with the charged outer blocks. Furthermore its molecular structure is very similar to BA and the T_g of MEA homopolymers is around -50 °C. For the homopolymerization of MEA, similar conditions were used as for the BA polymerization. Because this yielded very nice results (Figure 86), with linear first order kinetics and linear increase of M_n with low dispersities, no further kinetic studies were performed. Several polymers were synthesized on larger scale, purified by precipitation in distilled water and dried under reduced pressure (Table 12).

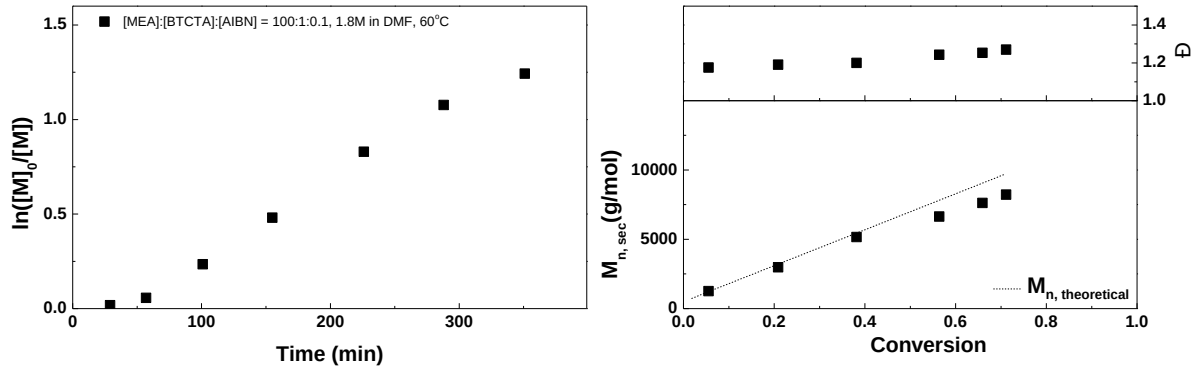

Figure 86. Left: first order kinetic plot for RAFT polymerization of MEA. Right: corresponding molecular weight and dispersity vs. conversion plot.

Table 12. Overview of PMEA homopolymers synthesized on large scale, using [MEA]:[BTCTA]:[AIBN] = 100:1:0.1, 60 °C in DMF at 1.8 M.

Polymer #	Conversion (GC)	$M_{n,theoretical}$ (g/mol)	M_n (g/mol, SEC)	Đ (SEC)	Yield
PMEA1	50 %	7000	8000	1.24	8.73 g (100 %)
PMEA2	36 %	5100	5100	1.19	8.71 g (81 %)
PMEA3	57 %	7900	7400	1.23	17.80 g (73 %)
PMEA4	35 %	5000	3400	1.16	8.70 g (83 %)
PMEA5	57 %	8000	7600	1.13	12.09 g (100 %)

5.3.8 Block copolymerization of DMAEA with PMEA as macro CTA

The triblock copolymerization of DMAEA using PMEA as macro CTA was performed several times under similar reaction conditions as the PDMAEA-*b*-PBA-*b*-PDMAEA triblock copolymerization, with only small differences in concentration (Figure 87). The polymerization rate was similar to what was observed in other reactions with DMAEA, with linear first order kinetics. Measured M_ns were in agreement with $M_{n,theoretical}$ and increased linearly with conversion. Dispersities were around 1.1 for most reactions, with one reaction showing an increase in dispersity to 1.3 which may be due to the macroCTA not being reinitiated completely. The larger scale synthesized polymers were purified by precipitation in hexane/diethyl ether mixtures and dried under reduced pressure (Table 13).

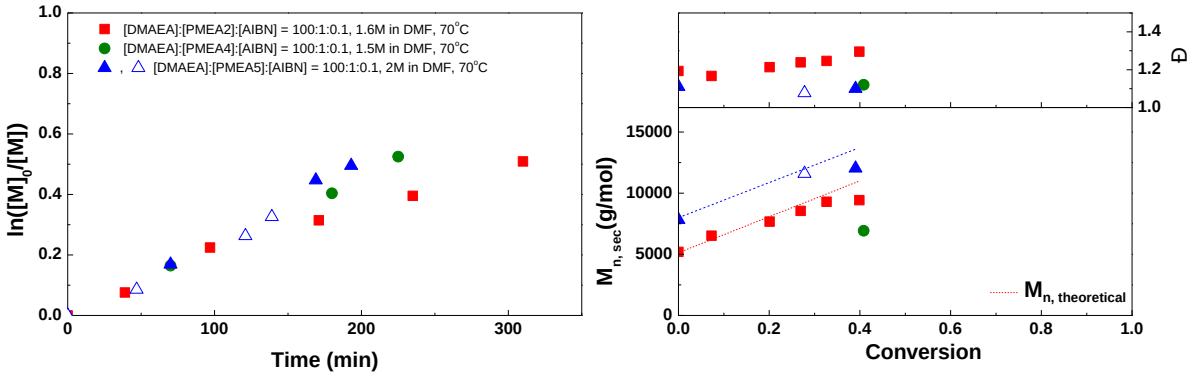

Figure 87. Left: first order kinetic plot for RAFT block copolymerization of DMAEA using PMEA as macro CTA. Right: corresponding molecular weight and dispersity vs. conversion plot. Reactions in the same color were performed using the same macro CTA.

Table 13. Overview of PDMAEA-*b*-PMEA-*b*-PDMAEA triblock copolymers synthesized on large scale, using [DMAEA]:[PMEA]:[AIBN] = 100:1:0.1, 70 °C in DMF at 2.0 M.

Polymer #	macroCTA	Conversion (GC)	$M_{n,theoretical}$ (g/mol)	M_n (g/mol, SEC)	Đ (SEC)	% DMAEA (NMR)	Yield
PDMAEA-*b*-PMEA-*b*-PDMAEA1	PMEA4	41 %	10800	7800	1.13	42	7.42 g (100 %)
PDMAEA-*b*-PMEA-*b*-PDMAEA2	PMEA5	39 %	13600	12000	1.10	40	3 g (63 %)
PDMAEA-*b*-PMEA-*b*-PDMAEA3	PMEA5	28 %	12000	11700	1.11	34	2.5 g (83 %)

5.3.9 Block copolymerization of CEA with pMEA as macro CTA

The triblock copolymerization of CEA using pMEA as macro CTA was somewhat problematic, as in most cases multiple or multimodal peaks were observed soon after the start of the polymerization, especially when monomer concentrations of 1 M or higher were used. Although mostly the absence of termination was observed from linear first order kinetics (Figure 88), the formation of multimodal SEC peaks indicates that some kind of side reaction was going on that led to coupling of chains, which may be from transesterification or anhydride formation. However, in some reactions well-defined polymers were obtained at lower conversion. Two larger scale reactions were performed (Table 14), with one leading to a well-defined triblock copolymer. These polymers were purified by precipitation in distilled water and dried under reduced pressure.

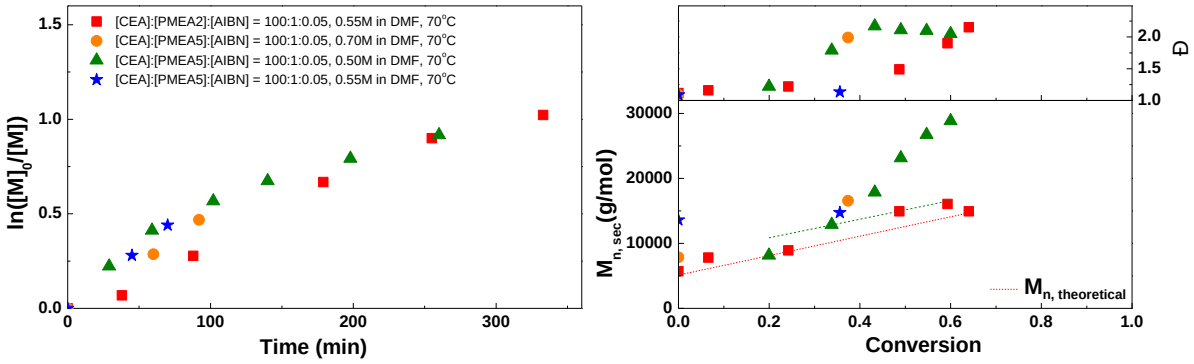

Figure 88. Left: first order kinetic plot for RAFT block copolymerization of CEA using PMEA as macro CTA. Right: corresponding molecular weight and dispersity vs. conversion plot.

Table 14. Overview of PCEA-*b*-PMEA-*b*-PCEA triblock copolymers synthesized on large scale, using [CEA]:[PMEA]:[AIBN] = 100:1:0.1, 70 °C in DMF at 0.55 M.

Polymer #	Conversion (NMR)	macroCTA	$M_{n,theoretical}$ (g/mol)	M_n (g/mol, SEC)	Đ (SEC)	% DMAEA (NMR)	Yield
PCEA-*b*-PMEA-*b*-PCEA1	38 %	PMEA4	10400	10200 58700	1.34 1.12	56	5.97 g (88 %)
PCEA-*b*-PMEA-*b*-PCEA2	36 %	PMEA5	13100	16100	1.14	39	2.3 g (70 %)

5.3.10 Homopolymerization of 2-hydroxyethyl acrylate (HEA)

HEA was chosen as a hydrophilic, water soluble middle block with low T_g (10 °C). Homopolymerizations of HEA were performed using different eq. of AIBN and at different concentrations (Figure 89). All reactions show linear first order kinetics at low conversions, with termination starting around 80 % conversion. The large diversion from the theoretical M_n is observed in all reactions and is due to the good solubility of PHEA in DMA leading to a large hydrodynamic radius. An increase in dispersity is observed at higher conversion, which could be caused by the presence of bisacrylates that are easily formed in HEA or by transesterification. This can also been seen in the SEC traces at higher conversion (Figure 90), in which a high molar mass shoulder appears that is formed by coupling between chains. While this does not cause observable problems when very short polymers are formed, in longer polymers the chance of cross-linking between polymers becomes higher, leading to more high M_n species and a higher dispersity at higher conversion. One large scale reaction was performed using 0.025 eq. of AIBN and 1.0 M concentration, as these conditions showed the lowest dispersities (Table 15). The polymer was purified by precipitation in hexane:diethyl ether 1:1 and dried under reduced pressure.

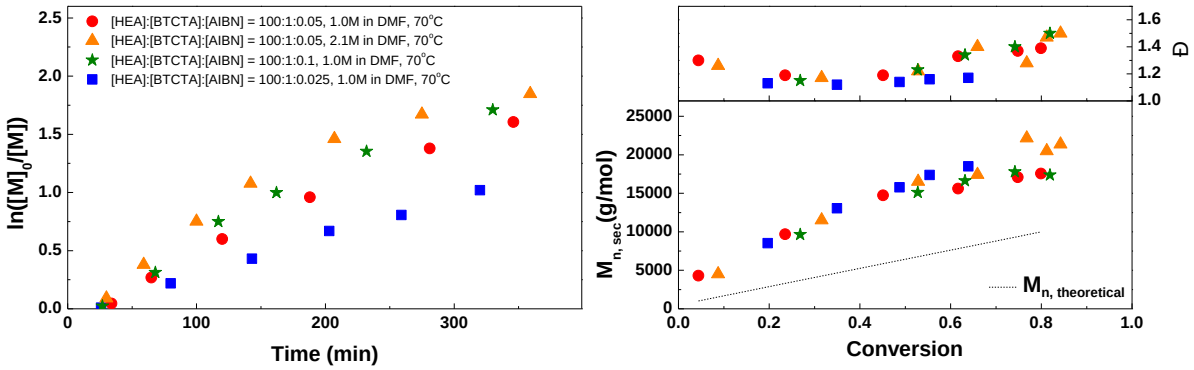

Figure 89. Left: first order kinetic plot for RAFT polymerization of HEA. Right: corresponding molecular weight and dispersity vs. conversion plot.

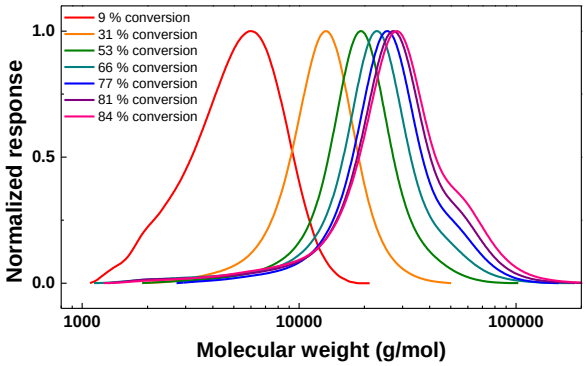

Figure 90. SEC traces of homopolymerization of HEA using [HEA]:[BTCTA]:[AIBN] = 100:1:0.05, 2.1 M in DMF at 70 °C.

Table 15. Overview of PHEA homopolymer synthesized on large scale, using [HEA]:[BTCTA]:[AIBN] = 100:1:0.025, 70 °C in DMF at 1.0 M.

Polymer #	Conversion (GC)	$M_{n,theoretical}$ (g/mol)	M_n (g/mol, SEC)	Đ (SEC)	Yield
PHEA1	47 %	5900	13700	1.35	13.68 g (83 %)

5.3.11 Block copolymerization of CEA with PHEA as macro CTA

One triblock copolymerization of CEA using PHEA as macro CTA was performed (Figure 91). A long inhibition time was observed and the reaction was slower than other CEA polymerizations. An increase in dispersity is seen above 20 % conversion. Similarly to other block copolymerizations with CEA, this may be due to transesterification or anhydride formation.

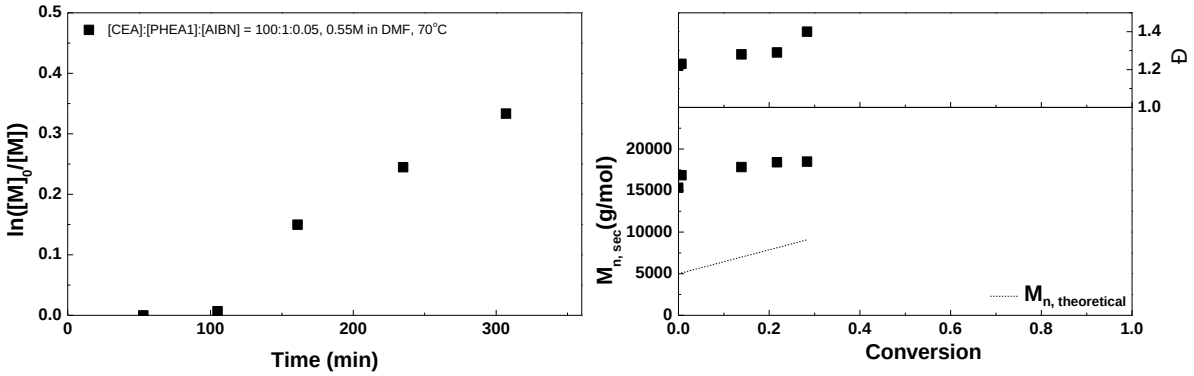

Figure 91. Left: first order kinetic plot for RAFT block copolymerization of CEA using pHEA as macro CTA. Right: corresponding molecular weight and dispersity vs. conversion plot.

Besides this reaction, also a one-pot quasi-block copolymerization was performed (Figure 92, Table 16). First, the homopolymerization of HEA was performed in DMF up to around 80 % conversion, after which a degassed 2.0 M solution of CEA in water was added to the reaction using a cannula and the reaction was continued for several hours. In this case, the conversion of CEA was significantly faster compared to the two-pot reaction and the molecular weight measured by SEC showed an increase while the dispersity remained below 1.2. From these results we can conclude that the one-pot reaction seems to work better than the two-pot reaction. The polymer was purified by dialysis and freeze-drying. The percentage of CEA in the polymer after purification calculated from ^{1}H NMR is a little higher than expected from the conversion, so there may be some inaccuracy in the NMR integration.

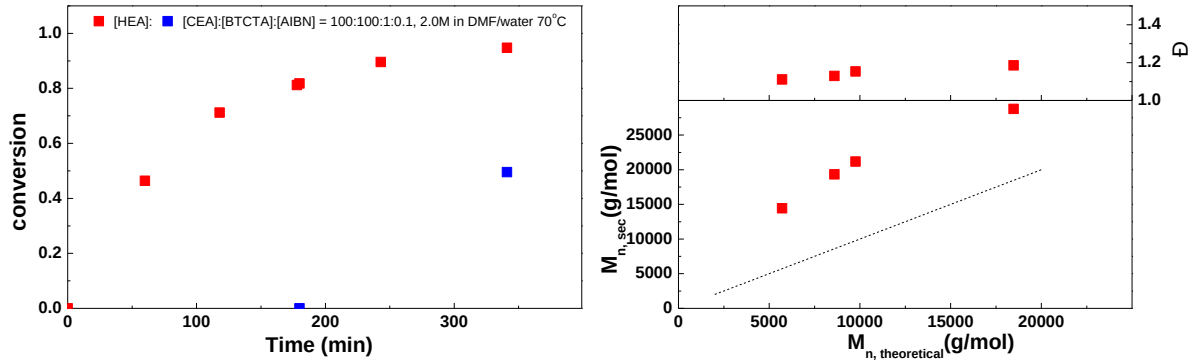

Figure 92. Left: monomer conversion vs. time plot for RAFT one-pot quasi-block copolymerization of HEA and CEA. Right: corresponding molecular weight and dispersity vs. theoretical molecular weight plot.

Table 16. Overview of PCEA-*b*-PHEA-*b*-PCEA triblock copolymer synthesized in one-pot reaction, using [HEA]:[CEA]:[BTCTA]:[AIBN] = 100:100:1:0.1, 70 °C in DMF/water at 2.0 M.

Polymer #	Conversion (GC/NMR)	$M_{n,theoretical}$ (g/mol)	M_n (g/mol, SEC)	Đ (SEC)	% CEA (NMR)	Yield
PCEA-*b*-PHEA-*b*-PCEA1	95 % HEA 50 % CEA	18500	28800	1.19	42	0.64 g (42 %)

5.3.12 Block copolymerization of [2-(acryloyloxy)ethyl]trimethylammonium chloride (AETMAC) with PHEA as macro CTA

Instead of DMAEA, AETMAC was also used as a positively charged monomer in combination with the water-soluble PHEA, because DMAEA readily hydrolyzes in water while this does not happen with AETMAC.[15, 28] One kinetic study of the triblock copolymerization of AETMAC using PHEA as macroCTA was performed (Figure 93). Because the polymers formed by this ionic monomer are only soluble in water or water-containing mixtures, a DMF/water mixture was used for the polymerization. Using a water-only reaction mixture would make the AIBN insoluble and thus unusable. The reaction shows linear first order kinetics and a relatively fast reaction, in contrast to all performed polymerizations of the very similar DMAEA. It seems that the change from tertiary to quarternary amine has a very large influence on the reactivity of the monomer. Only one SEC sample of the end product was measured because the HFIP SEC was not available in our group when the reaction was performed. Nonetheless, this end sample revealed a M_n of 29300 g/mol, which is close to $M_{n,theoretical}$ of 23200 g/mol, and a relatively low dispersity of 1.35 at almost full conversion of the monomer, so this polymerization was well controlled.

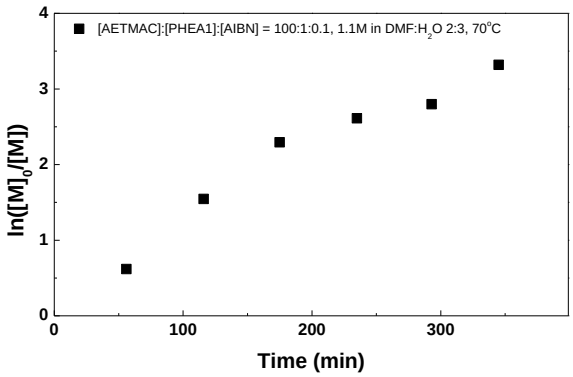

Figure 93. First order kinetic plot for RAFT block copolymerization of AETMAC using PHEA as macro CTA.

A one-pot quasi-block copolymerization was also performed similar to the reaction with CEA, by first performing a homopolymerization of HEA in DMF and adding a 2.0 M solution of AETMAC in water after the conversion had reached 80 % (Figure 94, Table 17). Around 60 % conversion of AETMAC is reached within several hours. SEC samples measured before the addition of AETMAC and after the polymerization was stopped show the expected increase in molecular weight and a small increase in dispersity. The polymer was purified by precipitation in acetone, dissolving in water and freeze-drying. The percentage of AETMAC in the purified polymer was higher than expected from the conversion, which may be explained by the conversion being inaccurate or polymers with more AETMAC precipitating preferentially compared to polymers with shorter AETMAC blocks.

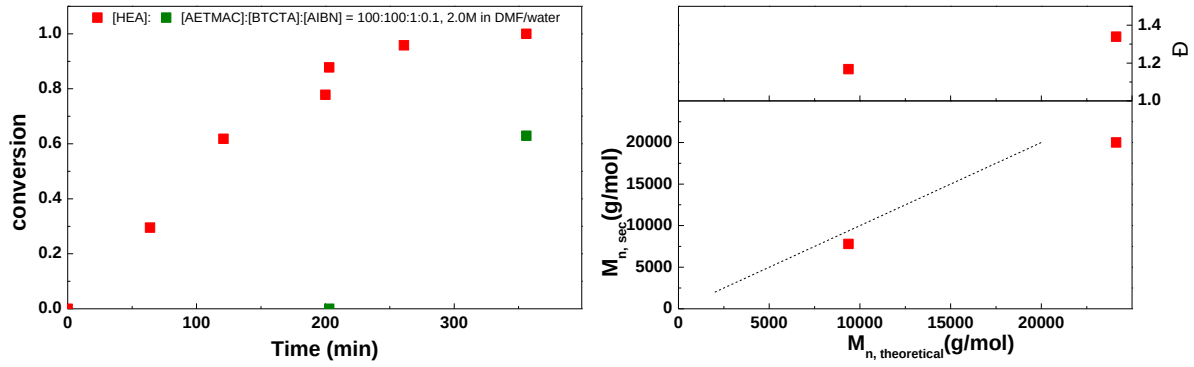

Figure 94. Left: monomer conversion vs. time plot for RAFT one-pot quasi-block copolymerization of HEA and AETMAC. Right: corresponding molecular weight and dispersity vs. theoretical molecular weight plot.

Table 17. Overview of PAETMAC-*b*-PHEA-*b*-PAETMAC triblock copolymer synthesized in one-pot reaction, using [HEA]:[AETMAC]:[BTCTA]:[AIBN] = 100:100:1:0.1, 70 °C in DMF/water at 2.0 M.

Polymer #	Conversion (GC/NMR)	$M_{n,theoretical}$ (g/mol)	M_n (g/mol, SEC)	Đ (SEC)	% AETMAC (NMR)	Yield
PAETMAC-*b*-PHEA-*b*-PAETMAC1	100 % HEA 63 % CEA	24100	20000	1.34	49	1.59 g (82 %)

5.3.13 Homopolymerization of styrene (St)

St was used as a hydrophobic polymer with a T_g of 100 °C to be able to compare the low T_g polymers with triblock copolymers containing a high T_g middle block. The polymerizations (Figure 95) were performed at very high concentrations, in which the DMF mostly served as an internal standard, because at lower concentrations almost no conversion was observed after several hours. Even though the polymerizations were very slow due to the low reactivity of St, linear first order kinetics were observed with no termination even at reaction times of more than 24 hours. An increase of the AIBN to 0.4 eq. led to a faster reaction, but also a large increase in dispersity, which is why longer reaction times with lower amounts of AIBN were used. Values for $M_{n,SEC}$, in these specific reactions determined relative to PSt standards, were in agreement with $M_{n,theoretical}$. Though suggested by the very slow reactions and increasing dispersity, it seems that BTCTA is probably not the best CTA for St. One large scale polymerization was performed and the polymer was purified by precipitation in MeOH and dried under reduced pressure (Table 18).

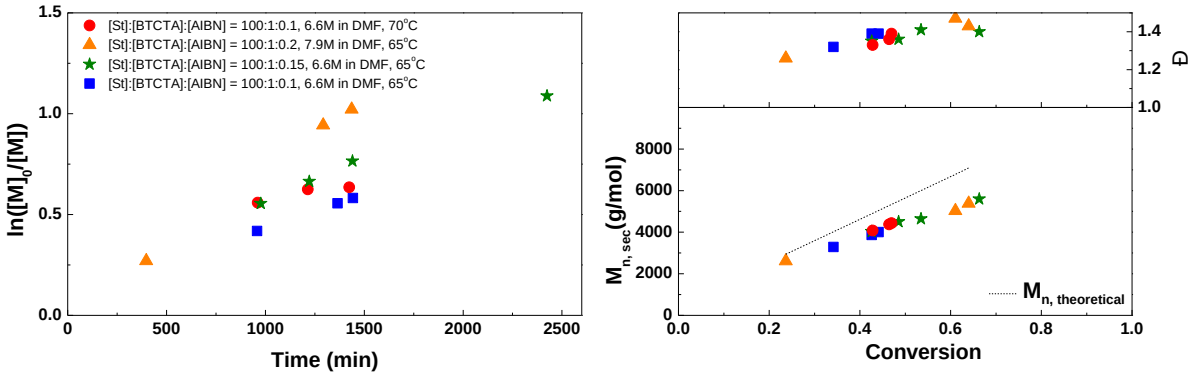

Figure 95. Left: first order kinetic plot for RAFT polymerization of St. Right: corresponding molecular weight and dispersity vs. conversion plot.

Table 18. Overview of PSt homopolymer synthesized on large scale, using [St]:[BTCTA]:[AIBN] = 100:1:0.1, 65 °C in DMF at 6.6 M.

Polymer #	Conversion (NMR)	$M_{n,theoretical}$ (g/mol)	M_n (g/mol, SEC)	Đ (SEC)	Yield
PSt1	44 %	5100	4000	1.39	13.60 g (100 %)

5.3.14 Block copolymerization of DMAEA with PSt as macro CTA

The triblock copolymerization of DMAEA using PSt as macro CTA is shown in Figure 96. A slow initiation is observed in both reactions, which may indicate that re-initiation of the macroCTA is difficult due to its low solubility in DMF. Additionally, DMAEA is a more reactive monomer than St, which also contributes to the slow re-initiation. Generally when preparing block copolymers of monomers with such different reactivity, the faster monomer is reacted first, so in this case the polymerizations were performed in the wrong order. While the reaction containing 0.2 eq. of AIBN proceeded faster than the one containing 0.1 eq., an increase in dispersity and formation of a bimodal peak was observed in SEC at conversions above 20 % (Figure 97), making these conditions not suitable. One triblock copolymer was successfully synthesized on larger scale using 0.1 eq. AIBN, purified by precipitation in hexane/diethyl ether mixtures and dried under reduced pressure (Table 19).

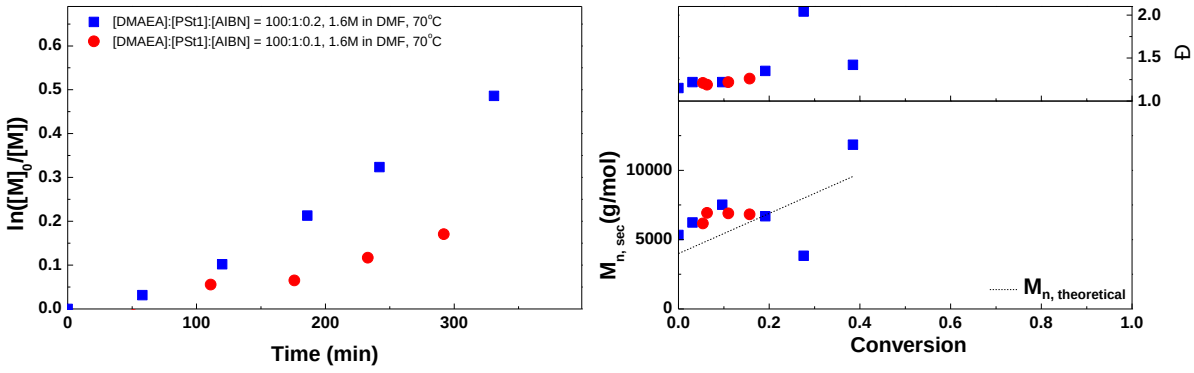

Figure 96. Left: first order kinetic plot for RAFT block copolymerization of DMAEA using PSt as macro CTA. Right: corresponding molecular weight and dispersity vs. conversion plot.

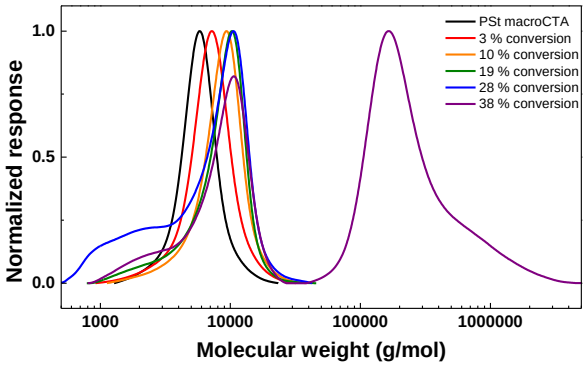

Figure 97. SEC traces of triblock copolymerization of DMAEA using [DMAEA]:[PSt1]:[AIBN] = 100:1:0.2, 1.6 M in DMF at 70 °C.

Table 19. Overview of PDMAEA-*b*-PSt-*b*-PDMAEA triblock copolymer synthesized on large scale, using [DMAEA]:[PMEA]:[AIBN] = 100:1:0.1, 70 °C in DMF at 2.0 M.

Polymer #	macroCTA	Conversion (GC)	$M_{n,theoretical}$ (g/mol)	M_n (g/mol, SEC)	Đ (SEC)	% DMAEA (NMR)	Yield
PDMAEA-*b*-PSt-*b*-PDMAEA1	PSt1	18 %	7700	9600	1.08	29	1.06 g (58 %)

5.3.15 Block copolymerization of CEA with PSt as macro CTA

The block copolymerization of CEA using PSt as macro CTA was performed several times using a concentration of 0.56 M in DMF and different AIBN ratios, however in all cases very low conversion of CEA was observed. After precipitation of the polymer in MeOH, a white powder was obtained, suggesting the trithiocarbonate groups were no longer present. NMR spectra of the purified polymers showed that almost no CEA was present. These problems may be due to the large difference in solubility between the CEA and PSt, as well as the general slow re-initiation of PSt with more reactive monomers that was also observed in the block copolymerization of DMAEA with the PSt macroCTA.

5.3.16 Block copolymerization of BA with PSt as macro CTA

Triblock copolymerization of BA using PSt as macro CTA was done with the purpose of preparing charged ABCBA-pentablock copolymers in which the low T_g of PBA may facilitate self-healing ability while the high T_g PSt domains could reinforce the material to get higher mechanical strength (Figure 98). All reactions showed a long inhibition time, again suggesting difficult re-initiation of the polymer chains. While the reaction at 60 °C was very slow, the reactions at 70 °C led to a faster well-controlled reaction after the inhibition time. SEC results showed an M_n close to $M_{n,theoretical}$ that increased linearly with conversion and low dispersities. One large scale triblock copolymerization was performed and the polymer was precipitated in MeOH and dried under reduced pressure (Table 20).

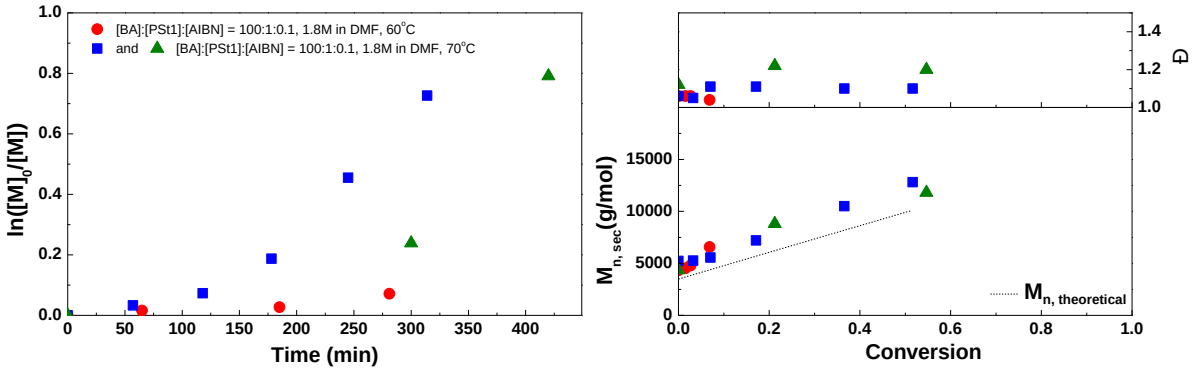

Figure 98. Left: first order kinetic plot for RAFT block copolymerization of BA using PSt as macro CTA. Right: corresponding molecular weight and dispersity vs. conversion plot.

Table 20. Overview of PBA-*b*-PSt-*b*-PBA triblock copolymer synthesized on large scale, using [BA]:[PSt]:[AIBN] = 100:1:0.1, 70 °C in DMF at 1.8 M.

Polymer #	mactoCTA	Conversion (GC)	$M_{n,theoretical}$ (g/mol)	M_n (g/mol, SEC)	Đ (SEC)	Yield
PBA-*b*-PSt-*b*-PBA1	PSt1	55 %	12100	8600	1.19	7.63 g (89 %)

5.3.17 Block copolymerization of DMAEA with PBA-*b*-PSt-*b*-PBA as macro CTA

The pentablock copolymerization of DMAEA using PBA-*b*-PSt-*b*-PBA as macro CTA is shown in Figure 99. While the reaction is relatively slow and first-order kinetics are not linear, an increase in molecular weight is observed by SEC and dispersities are below 1.2. The polymer was purified by precipitation in hexane/diethyl ether mixtures and dried under reduced pressure yielding a defined pentablock copolymer (Table 21).

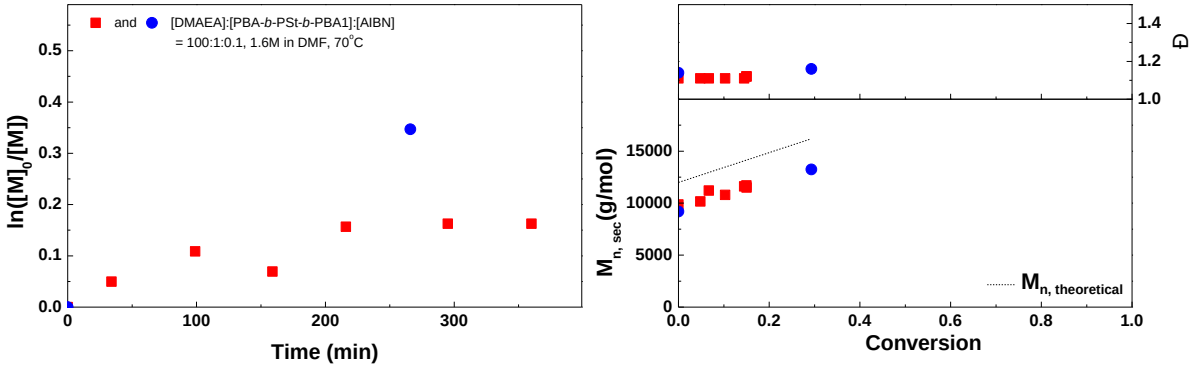

Figure 99. Left: first order kinetic plot for RAFT block copolymerization of DMAEA using PBA-*b*-PSt-*b*-PBA as macro CTA. Right: corresponding molecular weight and dispersity vs. conversion plot.

Table 21. Overview of PDMAEA-*b*-PBA-*b*-PSt-*b*-PBA-*b*-PDMAEA triblock copolymers synthesized on large scale, using [DMAEA]:[PMEA]:[AIBN] = 100:1:0.1, 70 °C in DMF at 2.0 M.

Polymer #	macroCTA	Conversion (GC)	$M_{n,theoretical}$ (g/mol)	M_n (g/mol, SEC)	Đ (SEC)	composition (NMR)	Yield
PDMAEA-*b*-PBA-*b*-PSt-*b*-PBA-*b*-PDMAEA1	PBA-*b*-PSt-*b*-PBA1	29 %	16300	13200	1.16	24 % DMAEA 45 % BA 31 % St	2.39 g (82 %)

5.3.18 Block copolymerization of CEA with PBA-*b*-PSt-*b*-PBA as macro CTA

Several pentablock copolymerizations of CEA using PBA-*b*-PSt-*b*-PBA as macro CTA were performed using a monomer concentration of 0.56 M in DMF, however the formation of a second peak was

observed in SEC already at low conversion. This indicated that the polymer is cross-linked, which could unfortunately not be prevented.

5.3.19 Homopolymerization of cyclohexyl acrylate (CHA)

As a last attempt to make triblock copolymers with a higher T_g hydrophobic middle block compared to PBA, CHA was used. This hydrophobic monomer forms polymers with a T_g of 19 °C. It was chosen because its structure is more similar to BA than St or IBA, which may be beneficial for the triblock copolymerizations. The CHA polymerizations in DMF (Figure 100) were relatively fast with almost linear first order kinetics. Even though only the end samples of the polymerizations were measured in SEC, these showed low dispersity around 1.1 and M_n in agreement with $M_{n,theoretical}$ (see Table 22), which indicates the polymerizations are well controlled. The two polymers were purified by precipitation in MeOH and dried under reduced pressure yielding defined PCHA.

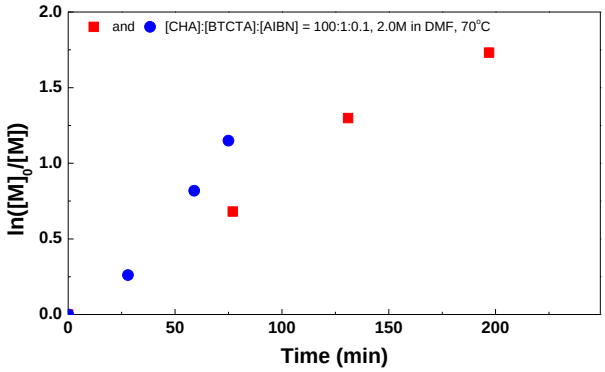

Figure 100. First order kinetic plot for RAFT polymerization of CHA.

Table 22. Overview of PCHA homopolymers synthesized on large scale, using [CHA]:[BTCTA]:[AIBN] = 100:1:0.1, 70 °C in DMF at 1.8 M.

Polymer #	Conversion (GC)	$M_{n,theoretical}$ (g/mol)	M_n (g/mol, SEC)	Đ (SEC)	Yield
PCHA1	82 %	13200	11200	1.11	1.5 g (69 %)
PCHA2	68 %	11000	7800	1.09	8.45 g (83 %)

5.3.20 Block copolymerization of DMAEA with PCHA as macro CTA

The results of the triblock copolymerization of DMAEA using PCHA as macro CTA are shown in Figure 101. The conversion data obtained from GC measurements seem to be inaccurate, but a clear cause for this could not be found. The M_n observed in SEC did not change much and dispersities are around 1.1. However, inclusion of DMAEA in the polymer was confirmed by ^{1}H NMR spectroscopy after precipitation in MeOH and drying under reduced pressure (Table 23), so it seems that the addition of DMAEA end groups changes the solubility of the polymer in THF leading to lower $M_{n,SEC}$.

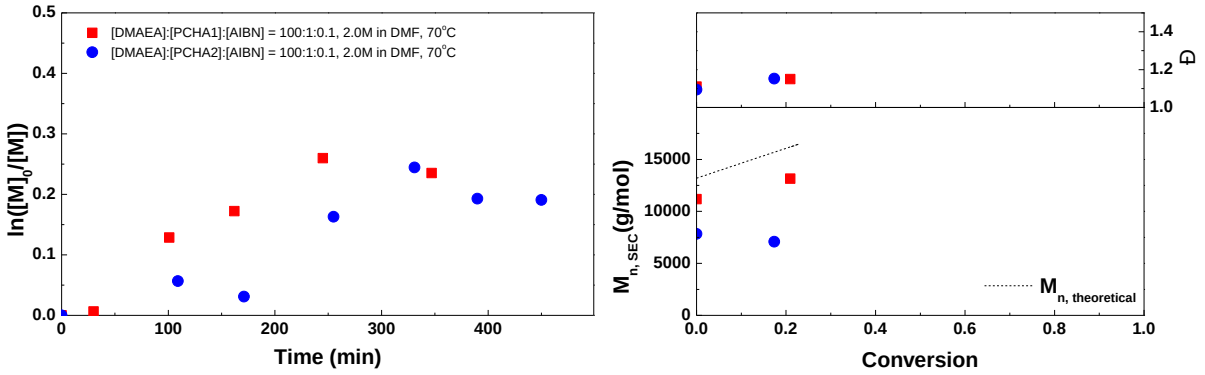

Figure 101. Left: first order kinetic plot for RAFT block copolymerization of DMAEA using PCHA as macro CTA. Right: corresponding molecular weight and dispersity vs. conversion plot.

Table 23. Overview of PDMAEA-b-PCHA-b-PDMAEA triblock copolymer synthesized on large scale, using [DMAEA]:[PCHA:[AIBN] = 100:1:0.1, 70 °C in DMF at 2.0 M.

Polymer #	macroCTA	Conversion (GC)	$M_{n,theoretical}$ (g/mol)	M_n (g/mol, SEC)	Đ (SEC)	% DMAEA (NMR)	Yield
PDMAEA-*b*-PCHA-*b*-PDMAEA1	PCHA2	18 %	13500	7100	1.15	37	3.29 g (69 %)

5.3.21 Block copolymerization of CEA with PCHA as macro CTA

Several attempts were made to polymerize CEA using a PCHA macroCTA in DMF; however in all cases the SEC data showed no growth of the polymer. Instead the peak of the PCHA homopolymer slowly disappeared, while a new species appeared around double molecular weight, indicating cross-linking or coupling of the polymer. This is most likely caused by the low solubility of PCHA in DMF when CEA is also present, making re-initiation of the homopolymer very difficult and leading to small emulsion droplets of PCHA in DMF, greatly increasing the chance of radical coupling. Several reactions in other solvents showed similar results, so instead a one-pot quasi-block copolymerization was performed (Figure 102). The homopolymerization of CHA was performed in DMF and when this had reached almost full conversion, a 2.0 M solution of CEA in DMF was added using a cannula. From the SEC results it is clear that there is an increase in dispersity after the CEA is added, but only one peak is observed that increases in M_n as the reaction continues. Clearly the one-pot method is working much better for this polymerization than the two-pot method. The polymer was purified by precipitation in water followed by centrifugation and dried under reduced pressure (Table 24).

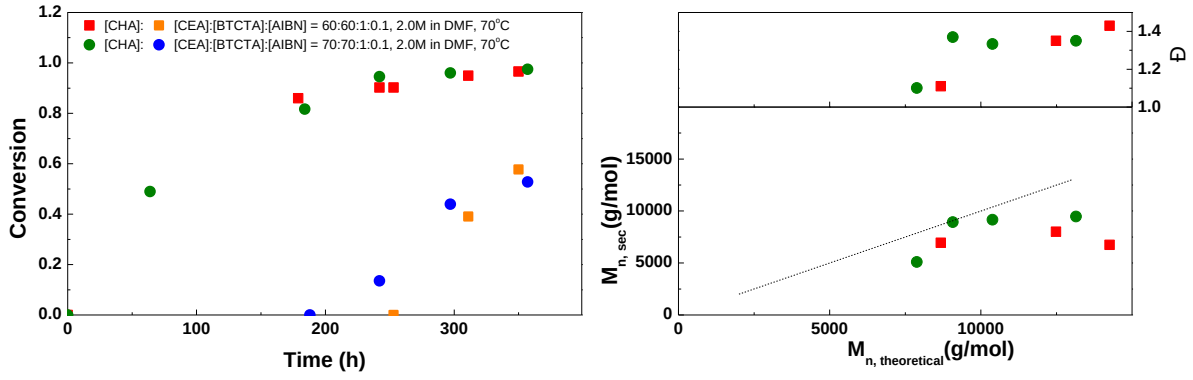

Figure 102. Left: monomer conversion vs. time plot for RAFT one-pot quasi-block copolymerization of CHA and CEA Right: corresponding molecular weight and dispersity vs. theoretical molecular weight plot.

Table 24. Overview of PCEA-b-PCHA-b-PCEA triblock copolymer synthesized on large scale, using [CHA]:[CEA]:[BTCTA]:[AIBN] = 70:70:1:0.1, 70 °C in DMF at 2.0 M.

Polymer #	Conversion (GC/NMR)	$M_{n,theoretical}$ (g/mol)	M_n (g/mol, SEC)	Đ (SEC)	% CEA (NMR)	Yield
PCEA-*b*-PCHA-*b*-PCEA1	97 % CHA 68 % CEA	14300	6700	1.43	37	3.84 g (41 %)

5.3.22 Synthesis of PSPDMAEA-*b*-PMEA-*b*-PSPDMAEA

In addition to mixtures of cationic and anionic ABA-triblock copolymers, we were also interested in testing a triblock copolymer with zwitterionic end groups. Attempts to polymerize the zwitterionic betaine SPDMAEA using a PBA or PMEA macroCTA were unsuccessful due to solubility problems. SPDMAEA could only be dissolved in pure water or mixtures containing large amounts of water, while the macroCTAs would not dissolve in these mixtures. Therefore, the post-polymerization modification reaction of PDMAEA-*b*-PMEA-*b*-PDMAEA2 containing 40 % DMAEA (Figure 103, top) with 1,3-propanesultone was successfully performed as ^{1}H NMR spectroscopy showed full conversion of DMAEA into SPDMAEA groups (Figure 103, bottom). SEC could not be measured due to incompatibility of the polymer with common solvents.

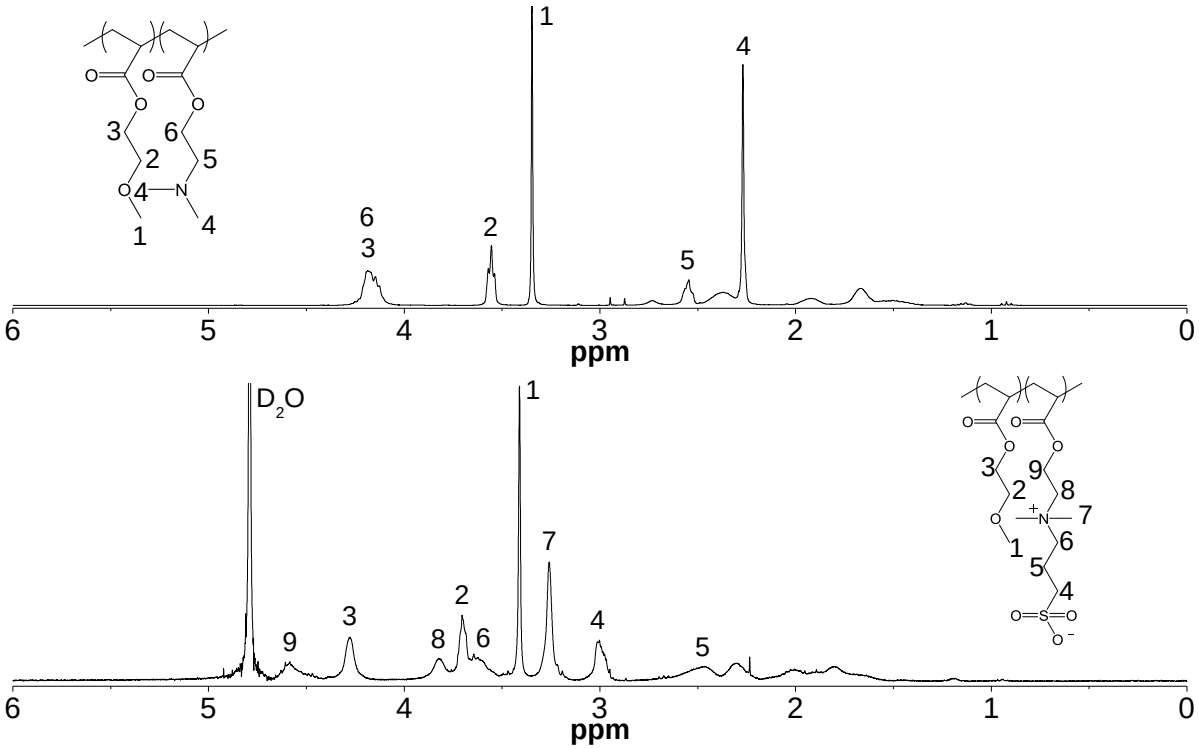

Figure 103. Top: ^{1}H NMR spectrum ($CDCl_3$) of PDMAEA-*b*-PMEA-*b*-PDMAEA2 triblock copolymer containing 40 % DMAEA. Bottom: ^{1}H NMR spectrum (D_2O) of PSPDMAEA-b-PMEA-b-PSPDMAEA with 40 % SPDMAEA.

5.3.23 Synthesis of tetrafunctional trithiocarbonate chain transfer agent (4-CTA)

Besides the linear triblock copolymers, charged star shaped polymers were also synthesized. Because a much denser distribution of the charges is expected compared to a linear polymer of the same molar mass, we expect this to have an influence on the morphology of the mixed polymer material. A tetrafunctional trithiocarbonate chain transfer agent (4-CTA) was synthesized following a procedure similar to the synthesis of BTCTA (Figure 104).[26] The ^{1}H NMR spectrum of 4-CTA is shown in Figure 105 and the APT ^{13}C NMR spectrum in Figure 106, demonstrating its successful synthesis and high purity. This CTA was used for the synthesis of four-armed star polymers.

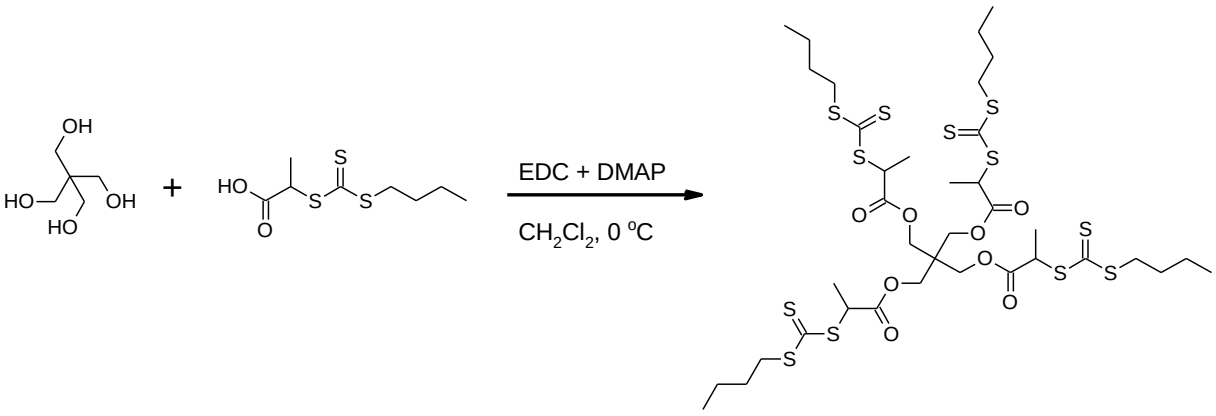

Figure 104. Synthesis tetrafunctional trithiocarbonate chain transfer agent (4-CTA).

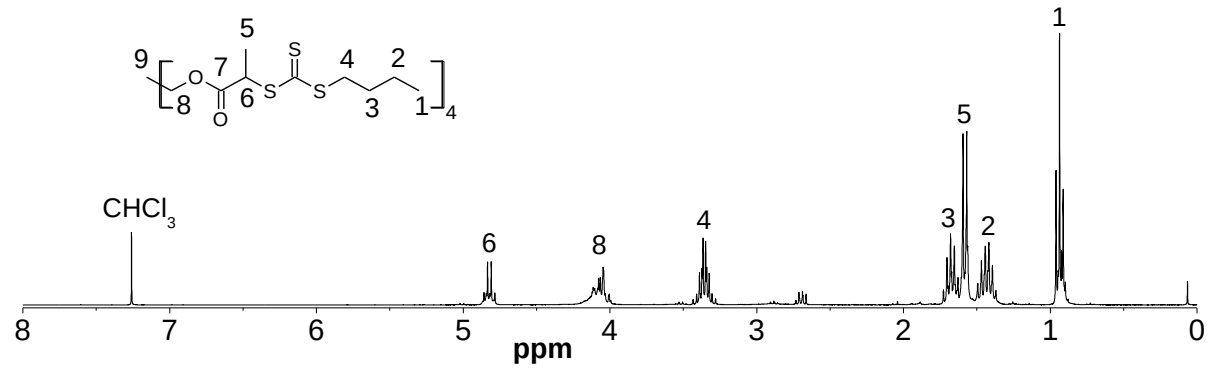

Figure 105. ^{1}H NMR spectrum ($CDCl_3$) of tetrafunctional trithiocarbonate chain transfer agent (4-CTA).

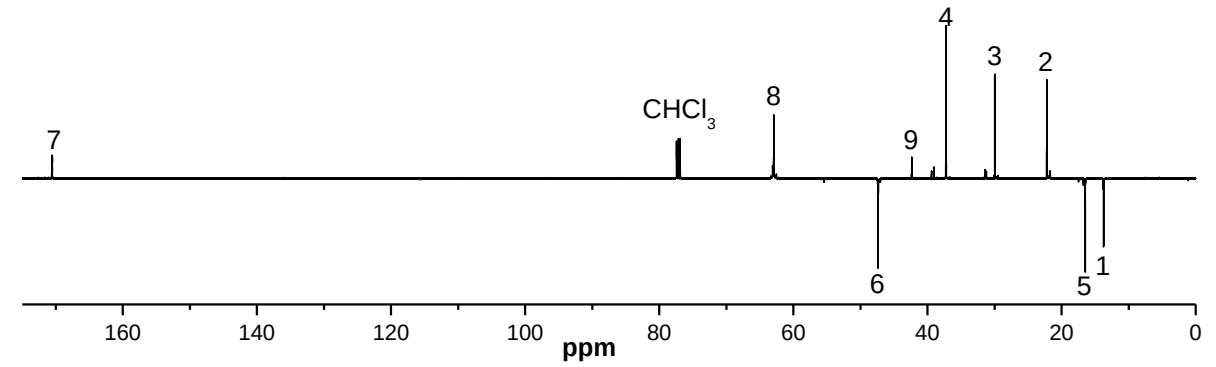

Figure 106. Attached proton test (APT) ^{13}C NMR spectrum ($CDCl_3$) of 4-CTA.

5.3.24 Star-shaped polymers

In addition to the previously discussed linear polymers, several star-shaped homopolymers were synthesized using 4-CTA. Figure 107 shows the homopolymerization of BA using this CTA. A long inhibition time of almost two hours is observed, after which the polymerizations are relatively slow compared to those with BTCTA, which is partly due to the lower AIBN concentration. The very long inhibition time may indicate difficult initiation of 4-CTA, possibly because the trithiocarbonate groups are close together causing steric hindrance and interference with each other. However, after the slow initiation linear first order kinetics are observed. M_ns measured by SEC showed a linear increase with conversion, but were much lower than $M_{n,theoretical}$. This can be explained by the star architecture of the polymers, which will lead to a lower hydrodynamic radius compared to linear polymers with

similar chemical properties and molecular weight. To confirm this, the absolute M_n of one of the polymers was determined using a SEC with light scattering, viscometer and RI detector. An absolute M_n of 16200 g/mol was determined, in agreement with the theoretical M_n of 16400 g/mol, which confirms the successful synthesis of a star-shaped PBA homopolymer. The polymers from these kinetic studies were purified by precipitation in methanol:distilled water 2:1 and dried under reduced pressure, but the polymerizations were not performed on larger scale.

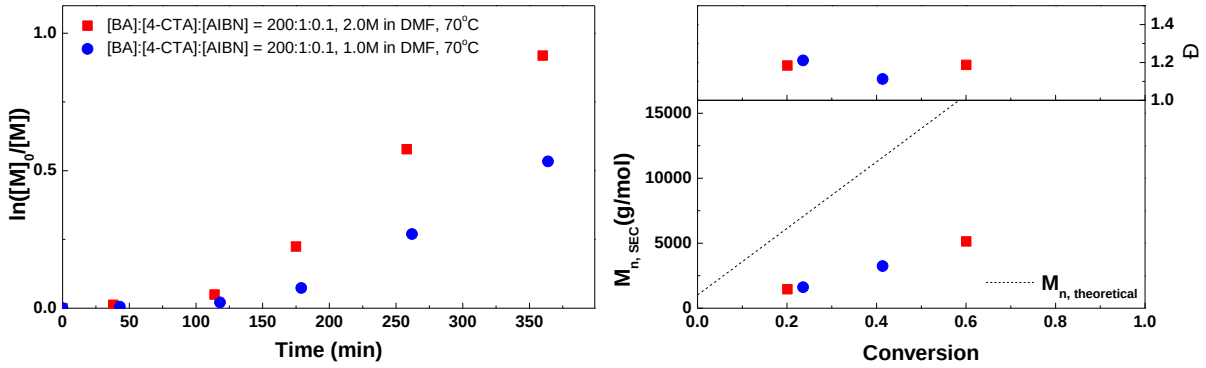

Figure 107. Left: first order kinetic plot for RAFT polymerization of BA using 4-CTA. Right: corresponding molecular weight and dispersity vs. conversion plot.

Star-shaped PCEA was also prepared (Figure 108). Reactions with 0.05 eq. AIBN at different concentrations showed almost no conversion. At 0.1 eq. AIBN, again a long inhibition time and slow polymerization is observed, after which the first order kinetic plot is linear, similar to the BA with 4-CTA polymerizations. No significant difference in the rate of polymerization is observed between the different concentrations of 1.0 M and 2.0 M. For these reactions, the M_ns measured by SEC were much higher than $M_{n,theoretical}$ but increased linearly with conversion, so the large difference with $M_{n,theoretical}$ is likely caused by a large hydrodynamic radius resulting from good solubility in DMA. The absolute M_n of this polymer could not be determined due to low solubility in THF. While the polymerizations showed low dispersities at low conversion, after 6 hours reaction time dispersities of 10.83 (for 1.0 M) and 29.88 (for 2.0 M) with multiple peaks were observed, likely from crosslinking of the polymers. Because of this, the larger-scale reaction was stopped after four hours (Table 25). The polymer was purified by precipitation in diethyl ether and dried under reduced pressure.

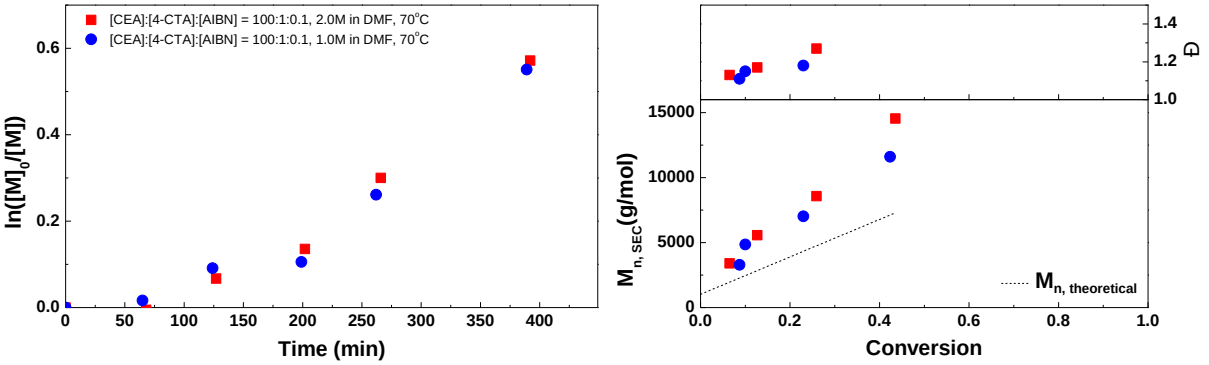

Figure 108. Left: first order kinetic plot for RAFT polymerization of CEA using a tetrafunctional CTA. Right: corresponding molecular weight and dispersity vs. conversion plot.

Table 25. Overview of PCEA star homopolymer synthesized on large scale.

Polymer #	Conversion (NMR)	$M_{n,theoretical}$ (g/mol)	M_n (g/mol, SEC)	Đ (SEC)	Yield
S-PCEA1	25 %	4600	7400	1.22	1.52 g (68 %)

5.4 Conclusions

A variety of different types and chain lengths of ABA-triblock copolymers containing an uncharged middle block and charged end blocks were successfully synthesized. Middle blocks with different chemical properties and a range of T_gs were used, which could be synthesized in a controlled way on multigram scale. While triblock copolymers containing DMAEA as a positively charged end group could often be easily synthesized, it was much more difficult to copolymerize the negatively charged CEA with the different types of middle blocks. This was partly due to differences in solubility with the more hydrophobic polymers, and partly because CEA can form hydrogen bonds that are not easily broken in aprotic solvents. This often led to crosslinking between polymers either by radical coupling or anhydride formation, or no polymerization at all. However, several combinations of positively and negatively charged triblock copolymers containing PBA, PMEA, and PCHA as middle blocks were synthesized successfully. In addition, a PDMAEA-*b*-PBA-*b*-PSt-*b*-PBA-*b*-PDMAEA pentablock copolymer, a triblock copolymer containing zwitterionic end groups and a star-shaped PCEA homopolymer were successfully synthesized. The further characterization of thermal and mechanical properties of these polymers and their mixtures is discussed in Chapter 6.

References

1. R. Wang, C. L. McCormick, A. B. Lowe, *Macromolecules* **2005**, *38*, 9518.
2. J. Brandrup, E. H. Immergut, E. A. Grulke, A. Abe, D. R. Bloch, *Polymer handbook*. (Wiley New York, 1999), vol. 89.
3. W. Steinhauer, R. Hoogenboom, H. Keul, M. Moeller, *Macromolecules* **2010**, *43*, 7041.
4. W. Steinhauer, R. Hoogenboom, H. Keul, M. Moeller, *Macromolecules* **2013**, *46*, 1447.
5. I. Javakhishvili, K. Jankova, S. Hvilsted, *Polym. Chem.* **2013**, *4*, 662.
6. A. Goto, K. Sato, Y. Tsujii, T. Fukuda, G. Moad, E. Rizzardo, S. H. Thang, *Macromolecules* **2001**, *34*, 402.
7. B. Yamada, M. Azukizawa, H. Yamazoe, D. J. T. Hill, P. J. Pomery, *Polymer* **2000**, *41*, 5611.
8. J. A. Shetter, *J. Polym. Sci., Part B: Polym. Lett.* **1963**, *1*, 209.
9. S. Coca, C. B. Jasieczek, K. L. Beers, K. Matyjaszewski, *J. Polym. Sci., Part A: Polym. Chem.* **1998**, *36*, 1417.
10. A. Kyritsis, P. Pissis, J. L. Gómez Ribelles, M. Monleón Pradas, *J. Non-Cryst. Solids* **1994**, *172–174, Part 2*, 1041.
11. N. Suchao-in, S. Chirachanchai, S. Perrier, *Polymer* **2009**, *50*, 4151.
12. A. Chakrabarty, N. K. Singha, *Macromol. Chem. Phys.* **2015**, *216*, 650.
13. L. Mi, M. T. Bernards, G. Cheng, Q. Yu, S. Jiang, *Biomaterials* **2010**, *31*, 2919.
14. B. L. Rivas, M. d. Carmen Aguirre, E. Pereira, J.-C. Moutet, E. S. Aman, *Polym. Eng. Sci.* **2007**, *47*, 1256.
15. N. P. Truong, Z. Jia, M. Burges, N. A. J. McMillan, M. J. Monteiro, *Biomacromolecules* **2011**, *12*, 1876.
16. J. M. Ting, T. S. Navale, F. S. Bates, T. M. Reineke, *ACS Macro Lett.* **2013**, *2*, 770.
17. K. E. Doncom, *Expanding the scope of responsive polymeric nanostructures* (University of Warwick, 2014).
18. T. Wu, D. Wang, M. Zhang, J. R. Heflin, R. B. Moore, T. E. Long, *ACS Appl. Mater. Interfaces* **2012**, *4*, 6552.

19. G. Yuan, Y. Peng, Z. Liu, J. Hong, Y. Xiao, J. Guo, N. W. Smith, J. Crommen, Z. Jiang, *J. Chromatogr. A* **2013**, *1301*, 88.
20. J. Chiefari, Y. K. Chong, F. Ercole, J. Krstina, J. Jeffery, T. P. T. Le, R. T. A. Mayadunne, G. F. Meijs, C. L. Moad, G. Moad, E. Rizzardo, S. H. Thang, *Macromolecules* **1998**, *31*, 5559.
21. G. Moad, E. Rizzardo, S. H. Thang, *Aust. J. Chem.* **2005**, *58*, 379.
22. G. Moad, E. Rizzardo, S. H. Thang, *Aust. J. Chem.* **2009**, *62*, 1402.
23. G. Moad, E. Rizzardo, S. H. Thang, *Aust. J. Chem.* **2012**, *65*, 985.
24. L. Martin, G. Gody, S. Perrier, *Polym. Chem.* **2015**, *6*, 4875.
25. C. J. Ferguson, R. J. Hughes, D. Nguyen, B. T. T. Pham, R. G. Gilbert, A. K. Serelis, C. H. Such, B. S. Hawkett, *Macromolecules* **2005**, *38*, 2191.
26. K. O. Sebakhy, M. Gavrilov, D. Valade, Z. Jia, M. J. Monteiro, *Macromol. Rapid Commun.* **2014**, *35*, 193.
27. A. B. Lowe, N. C. Billingham, S. P. Armes, *Chem. Commun.* **1996**, 1555.
28. W. Zhao, P. Fonsny, P. FitzGerald, G. G. Warr, S. Perrier, *Polym. Chem.* **2013**, *4*, 2140.

Chapter 6: Electrostatic supramolecular thermoplastic materials

Abstract

Supramolecular polymeric materials constitute a unique class of materials held together by non-covalent interactions. These dynamic supramolecular interactions can provide unique properties, such as a strong decrease in viscosity upon relatively mild heating as well as self-healing ability. In this chapter we demonstrate the unique mechanical properties of phase separated electrostatic supramolecular materials based on mixing of low molar mass, oligomeric, ABA-triblock copolyacrylates with oppositely charged outer blocks. The synthesis of these polymers was described in Chapters 3 and 5. The resulting mixtures revealed phase separation of the charged domains into hexagonally packed cylindrical domains, leading to thermoplastic elastomers with a rubbery plateau that is retained, significantly, beyond the glass transition temperature of the phase separated domains. This unique behavior is ascribed to the electrostatic attraction between the block copolymers in the charged domains. Moreover, we are able to explain the mechanical properties by the phase separated structures that are formed and provide a direct correlation of the nanomorphology and properties of the material based on a broader set of materials having systematical variations in triblock copolymer structures.

6.1 Introduction

Thermoplastic elastomers generally consist of phase-separated block copolymers in which higher glass transition temperature (T_g) segments form physical crosslinks that control the entropy-elastic modulus, while lower T_g segments provide the material with flexibility and elasticity. The prime examples of such materials are SBS rubbers based on high molar mass polystyrene-polybutadiene-polystyrene triblock copolymers. Different block lengths will lead to different morphologies, ranging from a spherical and/or cylindrical dispersed morphology (thermoplastic elastomer) to a co-continuous morphology and eventually to phase inversal (high-impact thermoplastic). The main advantage of thermoplastic elastomers is that they behave like a rubber at the application temperature, similar to chemically crosslinked elastomers, but they can also be processed as viscous melts at temperatures above the highest T_g, due to the reversible nature of the physical crosslinks. However, processing requires significant energy input to shape and transport the highly viscous melts that are formed at highly elevated temperatures.

Supramolecular polymer networks provide new possibilities for materials with special properties, such as self-healing and stimuli-responsiveness, including a strong decrease in viscosity upon heating enabled by dissociation of the supramolecular interactions.[1-3] Several examples of supramolecularly crosslinked thermoplastic elastomers have been reported previously. Such crosslinks can for example be formed by multiple hydrogen bonds,[4-15] π-π stacking interactions,[16] ionic interaction,[17-20] or metal-ligand interaction.[21-24] Supramolecular materials based on self-assembly of oligopeptides,[25] and nucleobases,[26] have also been reported. Even relatively weak hydrogen bonds in combination with phase segregation can form a relatively strong network from low molecular weight components.[27] Ionically crosslinked networks are often based on mixtures of ionomers[28, 29] or neutral polymers with telechelic ionic functionalization.[30, 31] Supramolecular networks based on electrostatic interactions in the form of hydrogels have also been reported.[32-34] A more extensive review of supramolecular network materials can be found in Chapter 1.

Here we report a new type of supramolecular thermoplastic elastomer material, consisting of mixtures (blends) of oppositely charged oligomeric ABA-type triblock copolymers with an uncharged hydrophobic middle block B and oppositely charged outer segments. Separately these polymers behave as easy to handle viscous liquids, while a phase-separated supramolecular network is formed through electrostatic interaction between the oppositely charged outer segments when the polymers are mixed. The formation of dispersed phase separated structures is found to lead to unique thermoplastic elastomers that retain the elastic rubber plateau even beyond the T_g of the phase separated domains, with high potential for use as semi-conductive and self-healing coatings. The design and hierarchical self-assembly of such a triblock copolymer blend is illustrated in Figure 109.

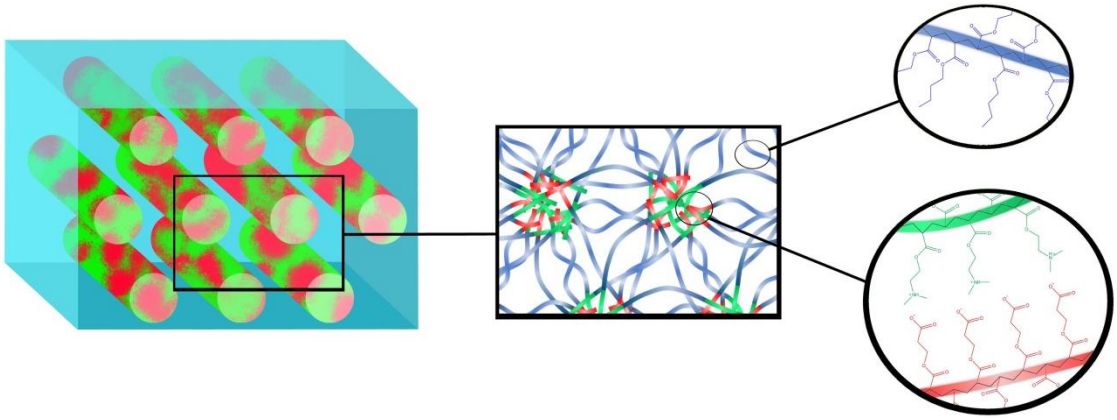

Figure 109. Schematic view of the structure of an electrostatic supramolecular thermoplastic elastomer with cylindrical dispersed phase separated charged domains.

6.2 Experimental section

Polymer synthesis

The synthesis of the polymers is described in detail in Chapter 3 and Chapter 5 (Figure 110). Mixtures were prepared by dissolving both polymers separately in THF, mixing them together and drying under reduced pressure.

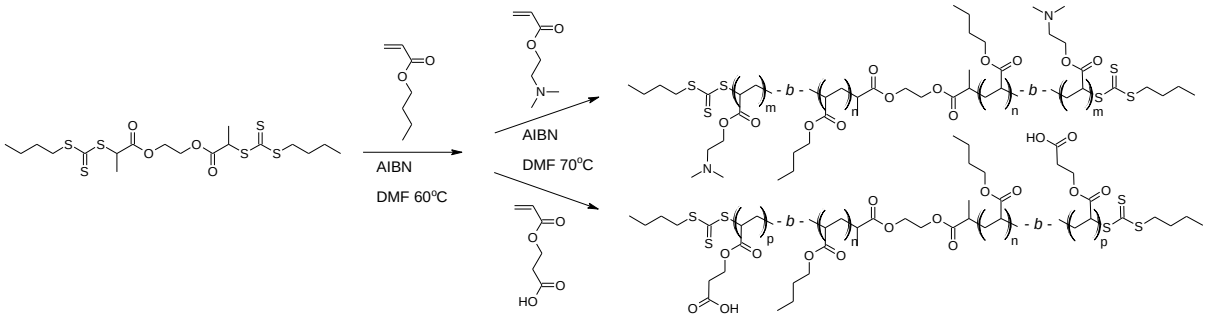

Figure 110. Synthesis via of the BA-containing triblock copolymers via RAFT polymerization.

Thermogravimetric Analysis (TGA)

Thermogravimetric measurements were performed to determine the degradation temperature of the synthesized polymers. Additionally, it was used as a tool to assess the molar fraction of CEA in the PCEA-*b*-PBA-*b*-CEA block copolymers in addition to ^{1}H NMR spectroscopy. Since the degradation of PCEA takes place at earlier temperatures than the pure PBA it was possible to determine the CEA

composition in the triblocks by this method. Measurements of RAFT BA-containing polymers were carried out in a TA Instruments TGA Q5000IR, a ramping procedure was followed at 20 °C/min from 50 °C to 650 °C in air. These measurements were performed by Maria Diaz (VUB).

TGA of the other polymers was performed on a Mettler-Toledo TGA/SDTA851e with Large Furnace and autosampler, using 70 µL alumina cubicles. Measurements were performed at 10 °C/min from 25 °C to 800 °C under nitrogen atmosphere. Evaluation was done via the STARe software, using blank corrections.

Differential Scanning Calorimetry (DSC) and Modulated Temperature DSC (MTDSC)

DSC and MTDSC were used to evaluate the thermal transitions of the triblock copolymers and their mixtures. Measurements of the RAFT BA-containing polymers were performed in a DSC Q2000 from TA Instruments equipped with a cooling system RCS 90. Ramp experiments were done at a heating rate of 2 °C/min using amplitude of ±0.4 °C and a period of 80 seconds. For these measurements, only the reversible heat flow is shown. T_gs were determined by the peaks in the first derivative of the reversible heat flow. These measurements were performed by Maria Diaz (VUB).

DSC and MTDSC of the other polymers were performed on a Mettler-Toledo DSC1/700 equipped with a FRS5 sensor containing 56 thermocouples, an Automatic Sample Robot and cooling with liquid nitrogen. DSC measurements were performed in standard 40 µL aluminium pans using a heating and cooling rate of 10 °C/min. MTDSC was performed at a heating rate of 0.5 °C/min with a pulse height of 1 °C. Evaluation was done via the STARe software.

Dynamic Mechanical Analysis (DMA)

DMA measurements of RAFT BA-containing samples were conducted in DMA Q800 from TA Instruments. Film pressed specimens were measured in tension mode with a frequency of 1 Hz using a strain of 0.05 % and scanning at 2.5 °C/min. These measurements were performed by Maria Diaz (VUB).

DMA of the other polymers was performed on a Mettler-Toledo DMA/SDTA861e using shear mode on hot pressed samples of ~ 5 mm diameter, using 2 µm displacement amplitude, 5 N force amplitude, 1 Hz frequency and a heating rate of 3 °C/min. Evaluation was done via the STARe software.

Rheology

Rheology measurements were performed in TA Instruments AR-G2 rheometer equipped with electrical heating plates and parallel plate geometry with a diameter of 5 mm. A temperature scan was performed starting from 30°C at 2 °C/min. During the thermal scan frequencies were recorded continuously during the scan in the range from 0.2 Hz to 4.6 Hz. These measurements were performed by Maria Diaz (VUB).

Small-angle Neutron Scattering (SANS)

SANS was carried out on the Sans2d small-angle diffractometer at the ISIS Pulsed Neutron Source (STFC Rutherford Appleton Laboratory, Didcot, U.K.).[35] A simultaneous Q-range of 0.0045 – 0.75 $Å^{-1}$ was achieved utilizing an incident wavelength range of 1.75 – 16.5 Å and employing an instrument set up of L1 = L2 = 4 m, with the 1 m^2 detector offset vertically 150 mm and sideways 50 mm. Q is defined as:

$$Q = \frac{4\pi \sin\frac{\theta}{2}}{\lambda}$$

where θ is the scattered angle and λ is the incident neutron wavelength. Samples were prepared in deuterated solvents, providing the necessary contrast and were contained in 1 mm path length quartz cells. Each raw scattering data set was corrected for the detector efficiencies, sample transmission and background scattering and converted to scattering cross-section data (∂Σ/∂Ω vs. Q) using the instrument-specific software. These data were placed on an absolute scale (cm^{-1}) using the scattering from a standard sample (a solid blend of hydrogenous and perdeuterated polystyrene) in accordance with established procedures.[36] These measurements were performed by Sarah Rogers (ISIS-STFC Neutron Scattering Facility).

HAADF-STEM

Ultrathin sections of 60 nm from Mixtures 1-4 were obtained by cryosectioning at -80 °C using a LEICA EM UC7 microtome equipped with a FC7 cryochamber. Sections were collected on a Quantifoil grid and vapor stained with osmium tetroxide (2 %) for 30 minutes. Alternatively sections were stained with a 2 % solution of uranyl acetate and a final rinse in ultrapure water. A 3 nm layer of amorphous carbon was deposited using a LEICA ACE600 carbon evaporator in order to increase the stability of the sections. The samples were analyzed in a HAADF-STEM mode using an FEI Titan transmission electron microscope operated at 200 kV. A Fischione (model 3000) annular detector was used to acquire dark field images. These measurements were performed by Frederic Leroux (EMAT, University of Antwerp).

Electrical conductivity measurements

The samples for the conductivity measurements were film pressed to a thickness of around 0.2 mm. Cuts of 1 cm length were made in the samples which were filled with graphite conductive paste to improve the contact between the sample and the electrodes and to measure in a well-defined area of 1 cm^2. A Fluke 1587 multimeter was used to record the electrical resistance of the sample at a potential of 100 V and 250 V from which the bulk resistivity and conductivity is calculated. These measurements were performed by Maria Diaz (VUB).

6.3 Results and discussion

6.3.1 Mixtures of PDMAEA-*b*-PBA-*b*-PDMAEA and PCEA-*b*-PBA-*b*-PCEA synthesized via RAFT polymerization

This part of the chapter reports work that was done in collaboration with Maria Diaz from the Vrije Universiteit Brussel, Frederic Leroux from the University of Antwerp and Sarah Rogers from the ISIS-STFC Neutron Scattering Facility. The defined oligomeric ABA-type triblock copolymers were reproducibly synthesized by RAFT free radical polymerization using a bifunctional chain transfer agent (see Chapter 5). Poly(*n*-butyl acrylate) (PBA) was chosen as middle block to form a soft continuous matrix. As oppositely charged outer blocks, poly(2-(dimethylamino)ethyl acrylate) (PDMAEA) and poly(2-carboxyethyl acrylate) (PCEA) were chosen as soft low T_g positively and negatively charged blocks, respectively. The characteristics of the synthesized triblock copolymers that are used to prepare the supramolecular materials are summarized in Table 26. The triblock copolymer chains had to be relatively short to allow for low viscosities, high mobility and migration through the matrix. Two different lengths for the core PBA blocks were chosen, around 7000 Da (P0-

2) and 2500 Da (P3 and P4). The length of the positively charged PDMAEA blocks was kept constant at 2000 Da (P0a-c) while the negatively charged PCEA blocks were varied between 1000 Da (P1 and P3), 1500 Da (P2) and 2000 Da (P4). The block lengths were varied in this way to monitor the effect of a mismatch between the core blocks of the mixed polymers as well as the length of the charged blocks. All these individual oligomeric triblock copolymers are obtained as viscous liquids.

Table 26. Details of the polymers used in this section.

	Polymer type	Composition (NMR after purification)	DP (from conversion in GC/NMR)	M_n (g/mol, SEC)	Đ (SEC)	% charged in mixture[a]
PBA	PBA2 	100% BA	56 BA	8100	1.18	-
PDMAEA	PDMAEA1 	100% DMAEA	27 DMAEA	5000	1.35	-
PCEA	PCEA1 	100% CEA	37 CEA	10700	1.32	-
P0a	PDMAEA-*b*-PBA-*b*-PDMAEA6 	45% DMAEA 55% BA	34 DMAEA 55 BA	10200	1.16	-
P0b	PDMAEA-*b*-PBA-*b*-PDMAEA9 	40% DMAEA 60% BA	26 DMAEA 53 BA	9200	1.22	-
P0c	PDMAEA-*b*-PBA-*b*-PDMAEA5 	37% DMAEA 63% BA	34 DMAEA 56 BA	10400	1.39	-
P1	PCEA-*b*-PBA-*b*-PCEA12 	18% CEA 82% BA	14 CEA 55 BA	4600	1.33	28 (P0a)
P2	PCEA-*b*-PBA-*b*-PCEA16 	23% CEA 77% BA	16 CEA 53 BA	4400	1.42	32 (P0b)
P3	PCEA-*b*-PBA-*b*-PCEA17 	42% CEA 58% BA	19 CEA 23 BA	6900	1.14	40 (P0b)
P4	PCEA-*b*-PBA-*b*-PCEA7 	60% CEA 40% BA	30 CEA 20 BA	11500	1.11	47 (P0c)

[a] Volume percentage of charged monomers in the mixture with the polymer in between brackets, containing equimolar amounts of cationic and anionic groups.

The supramolecular triblock copolymer blends were prepared by dissolving the oppositely charged viscous polymers separately in tetrahydrofuran (THF; 10 wt%), mixing them with equimolar amounts of charged monomers followed by solvent evaporation. Mixing the two polymer solutions led to increased viscosity and gel-like behavior, already indicating the formation of physical crossinks between the polymers. After evaporation of the solvent, a solid supramolecular polymer material was formed, as shown in Figure 111. This clear, rubbery material could be bended or torn manually and be pressed into different shapes at elevated temperatures. The material properties of the individual triblock copolymers and their mixtures were characterized by thermogravimetric analysis (TGA) (Figure 112), modulated temperature differential scanning calorimetry (MTDSC) (Figure 113-Figure 115), dynamic mechanical analysis (DMA) (Figure 115) and dynamic rheometry (Figure 118) in collaboration with Maria Diaz (VUB). The PDMAEA containing triblock copolymers (P0a-c) show a single T_g around -50 °C to -40 °C (Figure 114), consistent with the similar low values for pure PBA (T_g= -50 °C) and PDMAEA (T_g= -46 °C) (Figure 113), indicative of the absence of phase separation. The situation is different for the PCEA containing triblock copolymers of different composition (P1-4). The pure PCEA has a much higher T_g around 22 °C than pure PBA. These block copolymers show a double T_g with an important interphasial region, indicative for a phase separated morphology with partially mixed phases. In P1 and P2, a major PBA-rich phase is observed (Figure 114A and B) and a minor PCEA rich phase with a T_g around 0 °C. P4 has a major strongly phase segregated PCEA-rich phase (Figure 114D), while P3 shows a co-continuous morphology with a broad intermediate T_g spanning

the entire range from -40 to 0 °C (Figure 114C). In stark contrast to the individual triblock copolymers, each of the block copolymer mixtures Mix 1 (P0+P1), Mix 2 (P0+P2), Mix 3 (P0+P3) and Mix 4 (P0+P4) has a strongly phase separated morphology with two clear T_gs, one around -50 °C to -40 °C, resulting from the PBA-rich phase, and one at a higher temperature, ranging from 30 °C to 50 °C ascribed to the electrostatically supramolecular associated domains consisting of the PDMAEA and PCEA outer blocks.

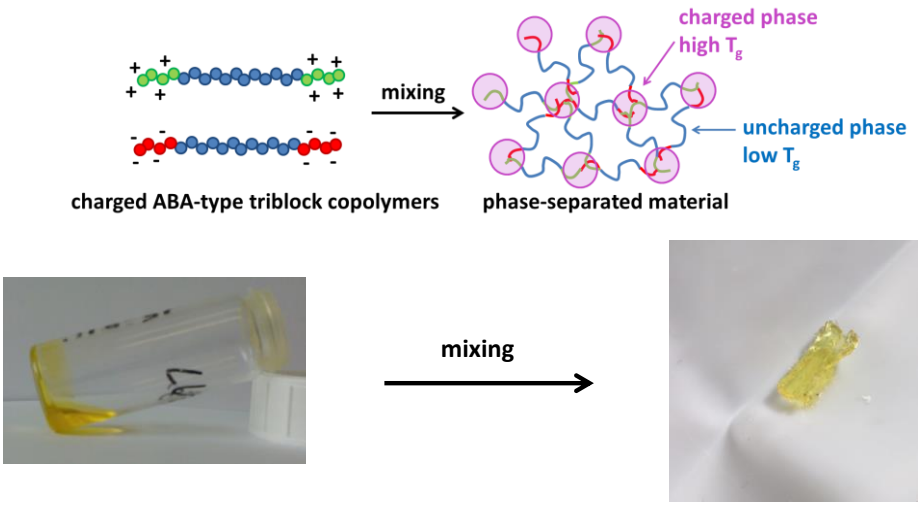

Figure 111. Mixing of the viscous triblock copolymers resulting in supramolecular solid materials.

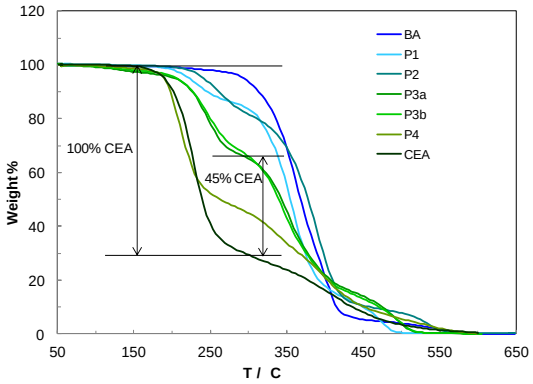

Figure 112. TGA measurements of the different CEA-BA-CEA triblock copolymers, showing how the percentage of CEA in the polymers can be calculated from TGA.

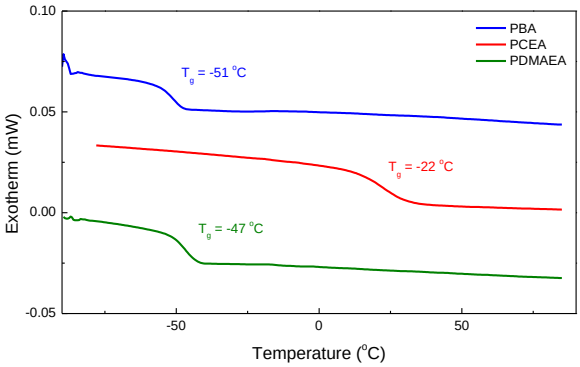

Figure 113. MTDSC of PBA, PCEA and PDMAEA homopolymers.

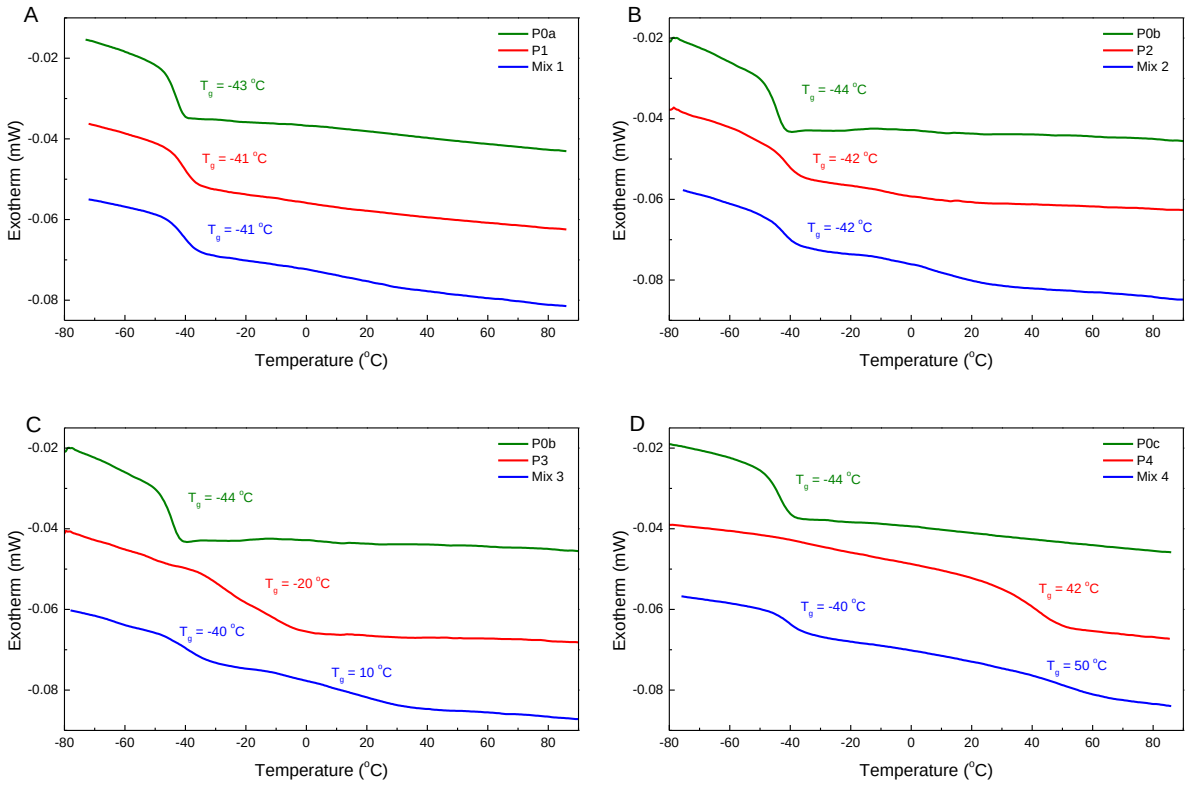

Figure 114. MTDSC measurements of individual triblock copolymers and the resulting mixtures (A) triblocks P0a, P1 and Mix 1, (B) triblocks P0b, P2 and Mix 2, (C) triblocks P0c, P3a and Mix 3 (D) triblocks P0c, P4 and Mix 4.

The volume fractions of the uncharged PBA-phase and of the charged phase (Table 26) suggests that the higher T_g charged fraction is dispersed into the uncharged low T_g matrix for Mix 1 and Mix 2. For Mix 3 and Mix 4, the almost 50/50 ratio of the volume fractions is expected to lead to a co-continuous morphology. Indeed, variation of the volume fractions of both phases leads to distinctly different thermomechanical properties as illustrated in Figure 115. The storage (elastic) modulus and the loss angle from DMA are compared to the heat capacity and their derivatives against temperature from MTDSC for each of the mixtures. All mixtures revealed an elastic modulus in the GPa range at temperatures below the lower T_g of -40 °C, indicating glassy behavior. Crossing this T_g is accompanied by a drop in the elastic modulus and a peak in the loss angle. When the temperature is further increased, a clear difference between the mixtures becomes apparent.

Mixtures 1 and 2 revealed a rubbery plateau with an elastic modulus around 1 MPa (Mix 1) and 10 MPa (Mix 2) with a loss angle below 15°, which is indicative of elastomeric behavior. This elastomeric behavior of Mix 1 and Mix 2 may be ascribed to the formation of a low T_g continuous PBA phase with dispersed phase separated charged domains acting as physical crosslinks by the electrostatic supramolecular interactions of the oppositely charged outer blocks. The volume fraction of crosslinks is lower for Mix 1 than for Mix 2; this lower crosslink density leads to a lower entropy-elastic modulus, as observed in DMA. The soft elastomer formed by Mix 1 has a rubbery plateau in the temperature regime from -20 to 40 °C while Mix 2 has a rubbery plateau that extends from -20 to 120°C as revealed by low loss angles (< 30°) in rheology (Figure 118 left). This broad rubber plateau regime of Mix 2 strikingly exceeds the T_g of the high T_g dispersed phase with is ~40 °C. Such unprecedented thermal behavior can be ascribed to the strong electrostatic supramolecular attraction in the phase separated domains that are able to hold together the material even when the

phase separated domains become mobile. The differences between Mix 1 and Mix 2 may indicate that Mix 1 consists of spherical phase separated domains while Mix 2 comprises cylindrical phase separated domains, as dictated by the volume fractions of the charged blocks.

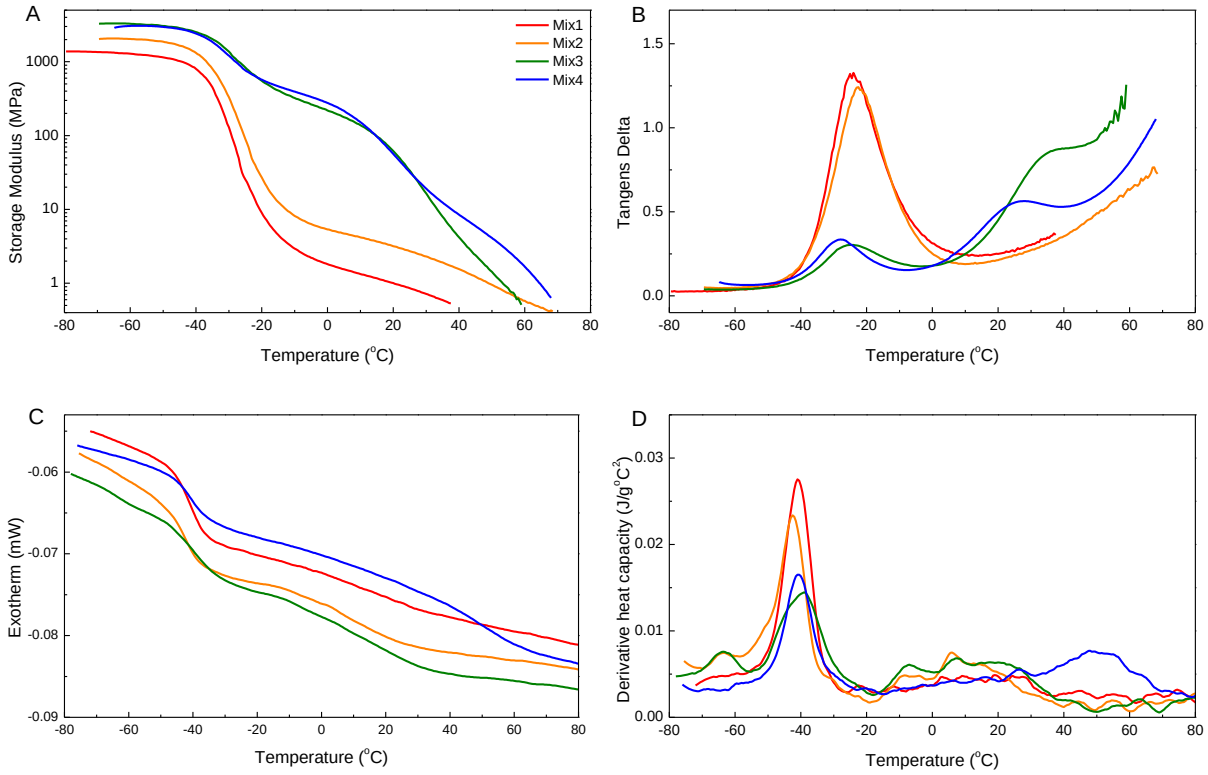

Figure 115. DMA and MTDSC measurements for the different mixtures (A) Storage modulus E', (B) Tangens delta, (C) Heat flow, and (D) Derivative of the heat capacity.

In both mixtures 3 and 4, the modulus drops in two distinct stages from a few GPa to ca. 0.5 GPa and further to values below 1 MPa. The loss angle increases quickly above 0 °C with an intermediate peak around 20-30 °C indicative for crossing the higher T_g of the PDMAEA-PCEA phase-separated phase. Further heating leads to a continuous increase in loss angle indicative for a decrease in viscosity. This behavior of Mix 3 and Mix 4 is typical for viscoelastic low molar mass thermoplastics. The higher volume fraction of the charged phase in Mix 3 and Mix 4 is expected to lead to co-continuous or lamellar morphology, thereby destroying the dispersed crosslinks and the associated elastomeric behavior as present in Mix 1 and Mix 2. Note that the observations of DMA are in agreement with the results of MTDSC (comparison of Figure 115A and B with C and D). The heat capacity derivative is sensitive for the low T_g phase, and also demonstrates the interphasial region, especially for the thermoplastic Mix 3.

To confirm this speculative interpretation of MTDSC and DMA results based on the volume fractions and expected phase separation, the actual phase separation and morphology in these mixtures was studied using small angle neutron scattering (SANS, collaboration with Sarah Rogers, ISIS-STFC Neutron Scattering Facility) and high angle annular dark field scanning transmission electron microscopy (HAADF-STEM, collaboration with Frederic Leroux, University of Antwerp). SANS measurements on each of the materials showed a single peak (Figure 116), indicating a characteristic length of the major spatial correlations in the samples. This correlation length is estimated to be 8.4 ± 2.0 nm for Mix 2, 9.4 ± 3.0 nm for Mix 3 and 14.0 ± 4.0 nm for Mix 4.

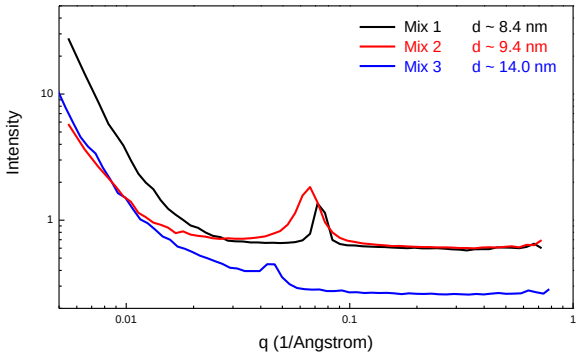

Figure 116. SANS measurement for the different mixtures Mix 2, Mix 3 and Mix 4.

Although repeating distances can be accurately determined by SANS, the exact molecular organization of the multiphase polymers cannot be univocally determined by scattering data only. Real-space HAADF-STEM analysis of ultrathin polymer sections provides a detailed assessment of the nano-morphology of the mixtures. The well-known advantage of the HAADF-STEM imaging technique is its sensitivity towards the variation of the scattering density in the sample. The intensity on HAADF-STEM images scales approximately proportional to Z^2, where Z is an average atomic number at the place of the electron probe.[37, 38] However, poor contrast between the phase-separated blocks impedes imaging of the microstructure without staining. Therefore, osmium tetroxide OsO_4 was used as a selective staining agent for the charged PDMAEA-PCEA phase to enhance contrast prior to HAADF-STEM imaging. Uranylacetate staining was also applied and provided the same morphological information with the charged PDMAEA-PCEA phase seen as bright domains.

HAADF-STEM images of Mixtures 1-4 are shown in Figure 117A-D. They all exhibit a nano-phase separated morphology which can be described as (i) a dispersed phase/continuous matrix morphology for Mix 1 and Mix 2, and (ii) a co-continuous morphology for Mix 3 and Mix 4. These HAADF-STEM results are consistent with the foregoing discussion and confirm the MTDSC and DMA results and their interpretation. Mix 1 shows dispersed charged PDMAEA-PCEA domains of spherical or (short) cylindrical shape randomly distributed in space, as confirmed with images in perpendicular planes and by the Fourier transform (FT) of the HAADF-STEM image (see inset of Figure 117A). The characteristic size of the dispersed domains is 6.7 ± 1.1 nm. Mix 2 shows curled bundles of hexagonally packed cylinders of the charged PDMAEA-PCEA phase. Figure 117B provides a view across the bundles demonstrating characteristic repeat period between the packed cylinders. The insert at the bottom of Figure 117B is demonstrating the nearly close-packed hexagonal arrangement of the cylinders of PDMAEA-PCEA. The upper inset of Figure 117B shows a fourier transform of the HAADF-STEM image and provides a direct comparison with the SANS diffractogram. Two reflection rings can be observed: a more diffuse ring corresponding to the average interplanar spacing of ~14.7 nm and a sharp ring with the interplanar spacing of ~8.3 nm in agreement with SANS. These rings can be considered as the 100 and 110 reflections of the hexagonal unit cell of the packed array of the cylinders resulting in the in-plane unit cell parameter a ~ 16.6 nm.

For Mix 3 (Figure 117C) and Mix 4 (Figure 117D) repeat distances of 8-10 nm and 14-18 nm respectively, were obtained from the HAADF-STEM images, fully consistent with the data obtained from the SANS measurements. These results show that while Mix 2 has a well ordered structure with a regular stacking, the lamellar (co-continuous) Mix 3 and Mix 4 demonstrate strong disorder. The

size differences of the core blocks of the triblock copolymers that are blended in Mix 3 and Mix 4 will make it more difficult to form a phase-separated material with uniform spacing between the phases. As the charged PCEA segments in P3 are very short, these are likely to partially mix with the PBA phase (see partial miscibility of P3 and interphase of Mix 3 in Figure 114C). In P4 this is not possible because of the length of the charged blocks. It is expected that these polymers with a shorter PBA block will not all be able to fully extend across the BA phase, and instead also partially form loops that fold both charged outer ends into the same charged phase leading to disturbance of the spacing of the phase separated structures.

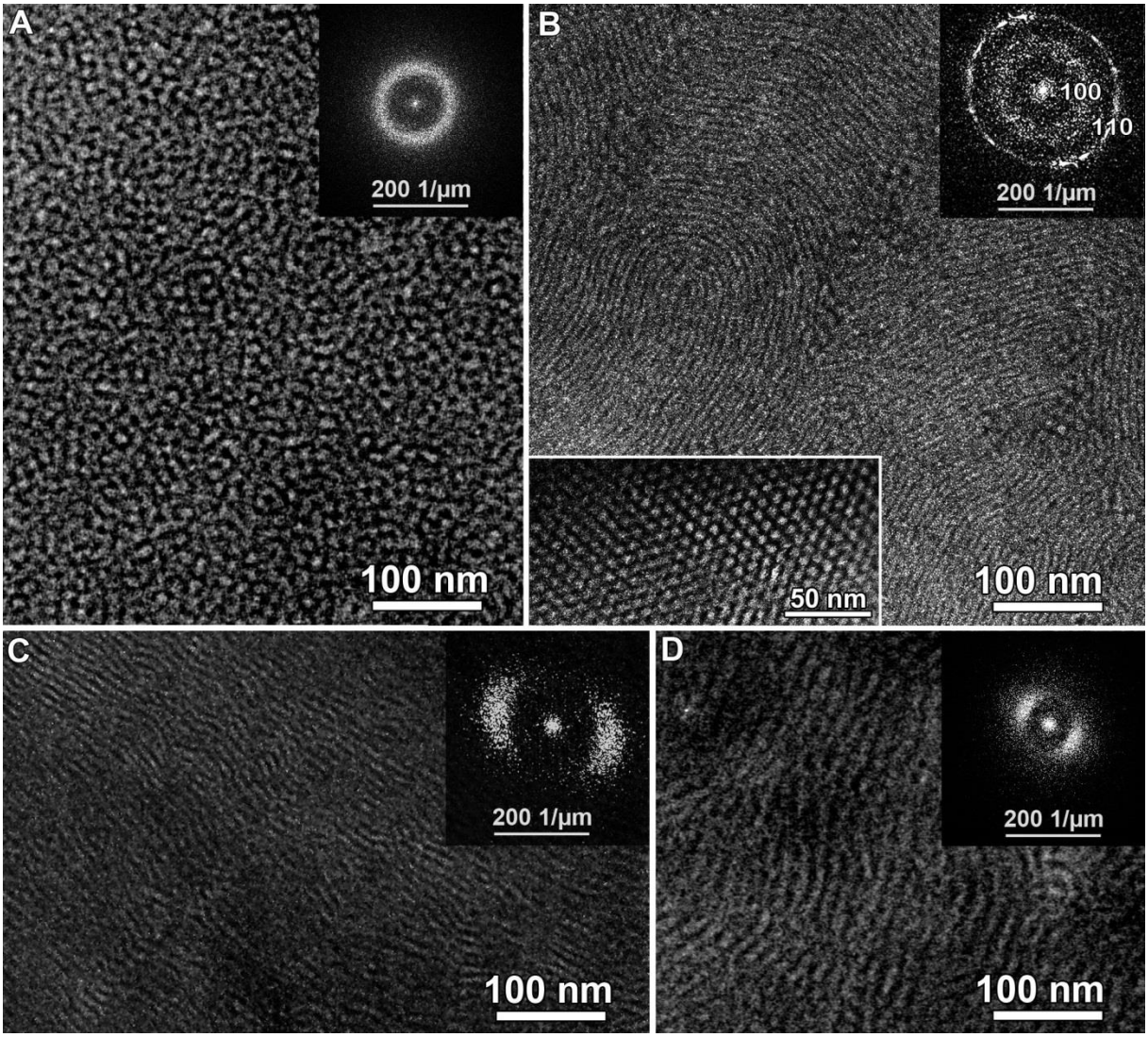

Figure 117. HAADF-STEM images of the different mixtures (A) Mix 1, (B) Mix 2, (C) Mix 3, and (D) Mix 4. The brighter areas of the images represent the stained parts of the mixtures. The inserts in the upper right corners show Fourier transforms of the HAADF-STEM images, which can be used as indication of the prevailing correlation length and spatial anisotropy of the systems. The insert at the left bottom corner of Fig. B shows the HAADF-STEM image of the closed-packed cylinders of the DMAEA-CEA phase.

Electrical conductivity measurements were performed on Mix 1 and Mix 3 at room temperature, 30°C and 40°C. Electrically insulating properties were observed for Mix 1 at all investigated temperatures. For Mix 3 a conductivity value of 2.87×10^{-5} S/m (250 V) was found at room temperature, 5.22×10^{-5} S/m (100 V) at 30 °C and 1.02×10^{-4} S/m[1] (100 V) at 40 °C. All these conductivity values of Mix3 lie in the range of semi-conductive materials and may be useful for

flexible electronics.[39, 40] These conductivity results can be further related to the morphology of the mixtures. For Mix 1, in which charged parts are dispersed and have no communication among each other, no conductivity is observed. However, Mix 3 does show semi-conductivity given that its charged phase is co-continuous throughout the material; therefore it is able to transport charges although it is not entirely sure how the charge transport takes place across these phase separated charged domains. The increased conductivity observed for Mix 3 at higher temperatures can be explained by the fact that above the second T_g there is significantly higher mobility in the charged phase facilitating charge transfer, while the consistency of the material is still retained up to 40 °C.

Finally, it should be pointed out that the electrostatic supramolecular thermoplastic elastomers show interesting properties as potential self-healing coatings. This ability is illustrated for Mix 1 by means of dynamic rheometry. Figure 118 (right) shows the loss angle for Mix 1 and for the individual triblocks (P0a and P1) as a function of temperature. P0a and P1 show a pure viscous behavior with a slight visco-elastic response up to 50 °C for P1 due to the PCEA-fraction. The mixture, however, maintains a pronounced visco-elastic response clearly beyond the higher T_g of the charged phase. This result is striking in view of the low molar masses involved, and could be explained by persisting electrostatic interactions between the charges of the PDMAEA and PCEA blocks. This effect might be beneficial for self-healing of coatings, providing sufficient mechanical integrity and form stability of the coating in mobile sealing conditions. A proof-of-concept experiment was performed with a thin layer of Mix 3 on a glass substrate. A 50 µm wide scratch could be healed by heating up the material up to 43 °C, easily attainable when placing a substrate in direct sunlight, which is above the T_g of the dispersed phase albeit the materials consistency is retained with a modulus around 1 MPa (Figure 119).

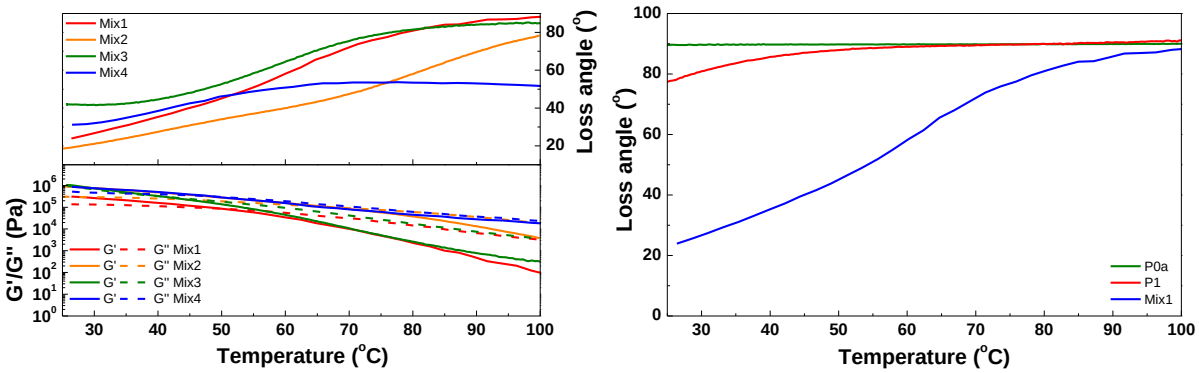

Figure 118. Left: rheology measurements of all four mixtures.Right: loss angle from rheometry of individual components P0a, P1 and Mix 1.

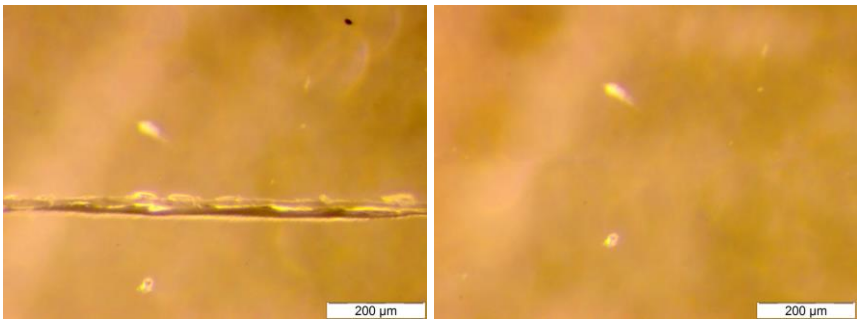

Figure 119. A 50 µm scratch was healed by heating the material to 43 °C.

In summary, we have demonstrated the first thermoplastic elastomer material that retains the rubbery plateau above the T_g of the dispersed phase separated phase. These unique properties are enabled by the strong electrostatic attraction within the charged phase separated domains of this novel class of electrostatic supramolecular materials based on mixtures of oligomeric triblock copolymers with oppositely charged outer blocks. The volume fraction of the charged domains dictates the resulting supramolecular material properties, being thermoplastic elastomers with dispersed spherical (Mix 1) or cylindrical (Mix 2) domains or viscous low molar mass thermoplastics when co-continuous phase separation takes place (Mix 3 and Mix 4). These novel materials are highly promising for future applications in conducting and self-healing coatings as demonstrated by proof-of-concept experiments.

6.3.2 Mixtures of PDMAEA-*b*-PBA-*b*-PDMAEA and PCEA-*b*-PBA-*b*-PCEA or PAA-*b*-PBA-*b*-PAA synthesized via Cu(0)-mediated polymerization

All the experiments that are discussed in the remainder of this chapter were performed by myself at UGent. Charged triblock copolymers with PBA middle blocks were also synthesized via Cu(0)-mediated polymerization, as described in Chapter 3. Polymers containing AA as negatively charged outer blocks were also used because of easier synthesis compared to CEA blocks using 1-ethoxyethyl acrylate. Details of these polymers are shown in Table 27. Polymer 0 was mixed with polymers 1, 2, 3 and 4 at stoichiometric ratios of the charged monomers to form supramolecular materials with rubbery properties.

TGA of the individual polymers (Figure 120) shows that both the PBA and PAA block decompose at the same temperature, making it impossible to observe a difference for the different AA block lengths. The PDMAEA and PCEA do show degradation at a lower temperature than PBA, with the ratio between the monomers in agreement with those determined by ^{1}H NMR spectroscopy. In the case of PCEA-*b*-PBA-*b*-PCEA, this means that the determined monomer conversion from GC was an overestimation as expected based on the difficulties of CEA analysis.

Table 27. Details of BA-containing triblock copolymers synthesized via Cu(0)-mediated polymerization.

#	Polymer type	Composition (NMR after purification)	DP (from conversion in GC)	M_n (g/mol, SEC)	Đ (SEC)	% charged in mixture[a]
0	PDMAEA-*b*-PBA-*b*-PDMAEA 	32% DMAEA 68% BA	19 DMAEA 47 BA	7000	1.08	-
1	PAA-*b*-PBA-*b*-PAA 	-	21 AA 49 BA	7500	1.18	32
2	PAA-*b*-PBA-*b*-PAA 	-	18 AA 49 BA	6500	1.12	30
3	PAA-*b*-PBA-*b*-PAA 	-	9 AA 49 BA	6900	1.12	23
4	PCEA-*b*-PBA-*b*-PCEA 	16% CEA 84% BA	21 CEA 48 BA	5300	1.26	22

[a] Molar percentage of charged monomers in the mixture with stoichiometric amounts of cationic and anionic groups of each polymer with polymer 0.

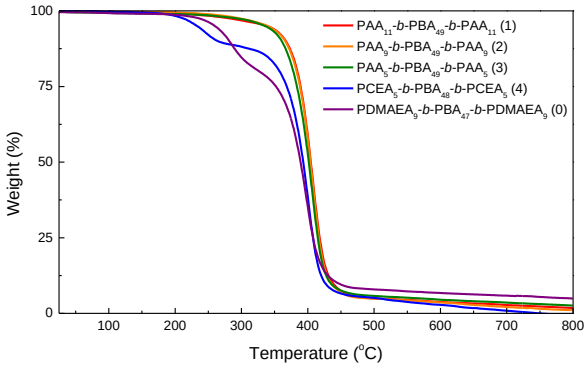

Figure 120. TGA of PBA-containing triblock copolymers synthesized via Cu(0)-mediated polymerization.

DSC of the individual polymers (Figure 121, left) reveals that all polymers show a T_g around -42 °C of the PBA, with a second T_g only observed for the PCEA at 23 °C. Almost all the polymers show a kind of transition around 130 °C, however as this was not seen in the cooling curves this is not a T_g and may be loss of residual water or melting of incorporated water.

In the DSC traces of the mixtures of the AA and CEA-containing polymers with the PDMAEA-*b*-PBA-*b*-PDMAEA (Figure 121, right), only a single T_g is found for each of the mixtures around -43 °C, which is from the PBA blocks. However, differences in mechanical properties were already quite apparent, as Mix 3 was a highly viscous liquid at room temperature, Mix 2 a very soft rubbery material and Mix 1 and 4 more solid rubbers.

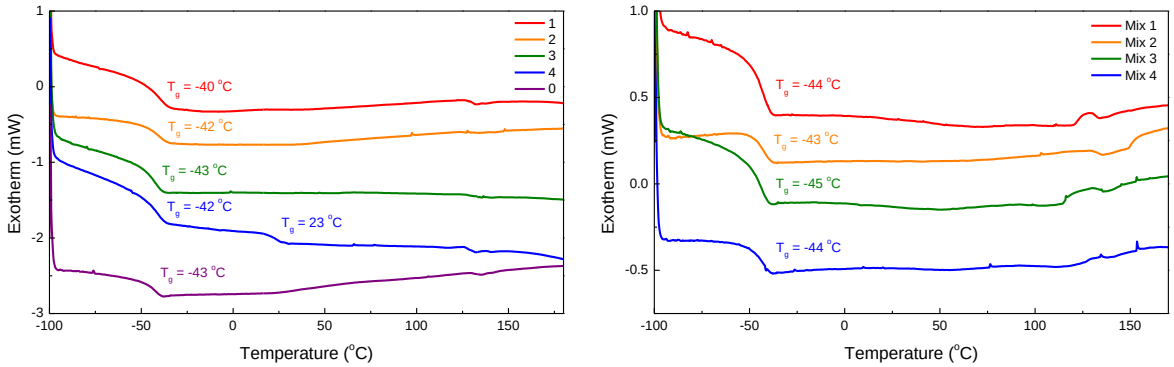

Figure 121. Left: DSC of PBA-containing triblock copolymers synthesized via Cu(0)-mediated polymerization, right: DSC of mixtures of polymer 0 with polymer 1-4.

DMA measurements of the mixtures (Figure 122) show that that all four materials are glassy below -40 °C with a storage modulus (M') around 200 MPa. The absolute values of M' are difficult to compare to the E' of the polymers from section 6.3.1 because of the different procedure used for the measurements, which explains why the values are quite different for similar polymers. The polymer mixtures from section 6.3.1 show a E' above 1000 MPa in the glassy state as determined in tension mode, while M' for the polymers in this section is around 200 MPa at similarly low temperatures measured in shear mode. Even though theoretically E' should be around 3M' for viscoelastic materials based on the Poisson ratio, this can only be used as a rough estimation. The T_g of BA is clearly visible in each mixture as a drop in M' and a peak in tangens delta around -30 °C. The M' is then around 1 MPa for the mixtures with PAA-*b*-PBA-*b*-PAA (1-3), with Mix 3 showing the lowest

value followed by Mix 2 and Mix 1, and a little bit higher for the mixture with PCEA-*b*-PBA-*b*-PCEA (4), each showing rubbery properties.

When the temperature is increased further, both mixtures 1 and 4 show a second peak in tangens delta indicating the T_g of the charged sections, while this is much less clear for mixtures 2 and 3. This second T_g could not be observed with DSC, because DMA as a technique is more sensitive to T_gs than DSC, allowing weaker transitions to be observed. It is unclear why the M' for Mix 1 and 2 show two crossovers, even though they are very close in composition. At temperatures above the second T_g, a rubber plateau is observed for all polymers with the temperature range dependent on the length of the PAA or PCEA blocks. When the temperatures are increased further the materials start to flow, shown by a drop of M' below 0.1 MPa and a sharp increase in tangens delta. It is interesting to note that the temperature of flow increases with the percentage of charged monomers for mixtures 1-3, showing that a higher amount of charges will keep the material together up to higher temperatures. Mixture 4, containing CEA instead of AA, only starts to flow around 120 °C, which is similar to the materials observed in the previous section with similar design (Figure 115). This temperature is also much higher than for mixtures 1-3, even though the amount of charges in material 4 is close to that in material 3, showing that CEA forms much stronger electrostatic interactions with DMAEA. This may be due to more steric constraints resulting from the shorter distance between the acidic group and the polymer backbone in the case of PAA.

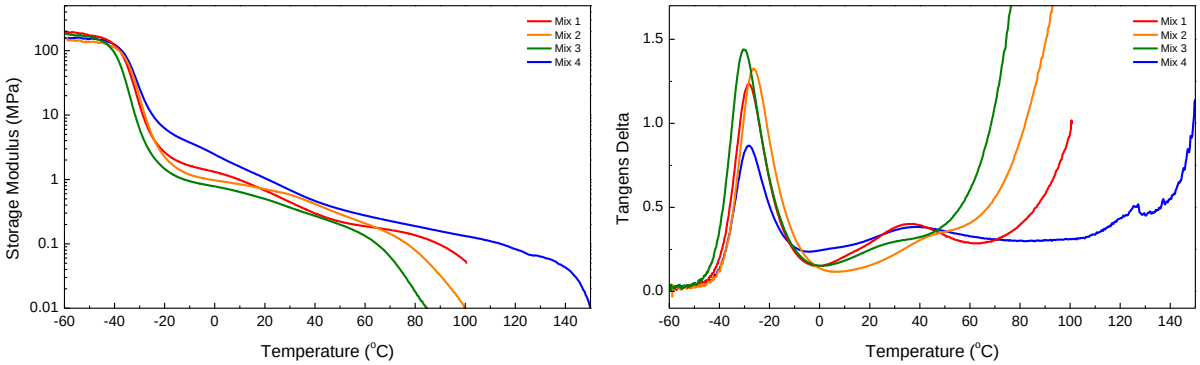

Figure 122. Left: storage modulus and right: tangens delta from DMA measurements of mixtures of polymer 0 with polymer 1-4.

6.3.3 Mixtures of PDMAEA-*b*-PBA-*b*-PDMAEA and star PCEA synthesized via RAFT polymerization

In addition to the linear triblock copolymers, a star PCEA was prepared via RAFT polymerization and mixed with linear PDMAEA-*b*-PBA-*b*-PDMAEA (Table 28). TGA (Figure 123, left) shows that degradation of the star PCEA homopolymer starts around 200 °C, similar to the CEA-containing block copolymers, with the second degradation likely being from the backbone of the polymer. The TGA of PDMAEA-*b*-PBA-*b*-PDMAEA looks similar to that of previously measured PDMAEA-*b*-PBA-*b*-PDMAEA polymers, with two separate degradation steps. DSC (Figure 123, right) reveals a T_g of 59 °C for star PCEA, which is significantly higher than the T_g observed for a linear PCEA homopolymer, and an expected low T_g of -51 °C for PDMAEA-*b*-PBA-*b*-PDMAEA. In the mixture of the two polymers, only one T_g of -47 °C was found for the PBA blocks, which is surprising since this material contains around 50 % of charged blocks that are expected to be immiscible with PBA.

Table 28. Details of PDMAEA-*b*-PBA-*b*-PDMAEA and star PCEA synthesized via RAFT polymerization.

Polymer type	Composition (NMR after purification)	DP (from conversion in GC)	M_n (g/mol, SEC)	Đ (SEC)	% charged in mixture[a]
PDMAEA-*b*-PBA-*b*-PDMAEA11 	29 % DMAEA 71 % BA	20 DMAEA 38 BA	3100	1.11	-
star PCEA1 	100 % CEA	25 CEA	7400	1.22	48

[a] Molar percentage of charged monomers in the mixture of the two polymers with stoichiometric amounts of cationic and anionic groups.

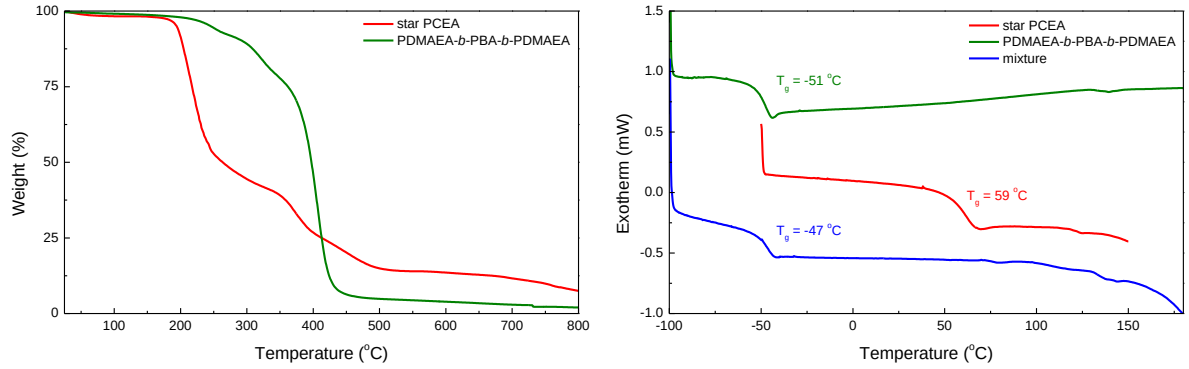

Figure 123. Left: TGA, right: DSC of star PCEA and linear PDMAEA-*b*-PBA-*b*-PDMAEA and their mixture.

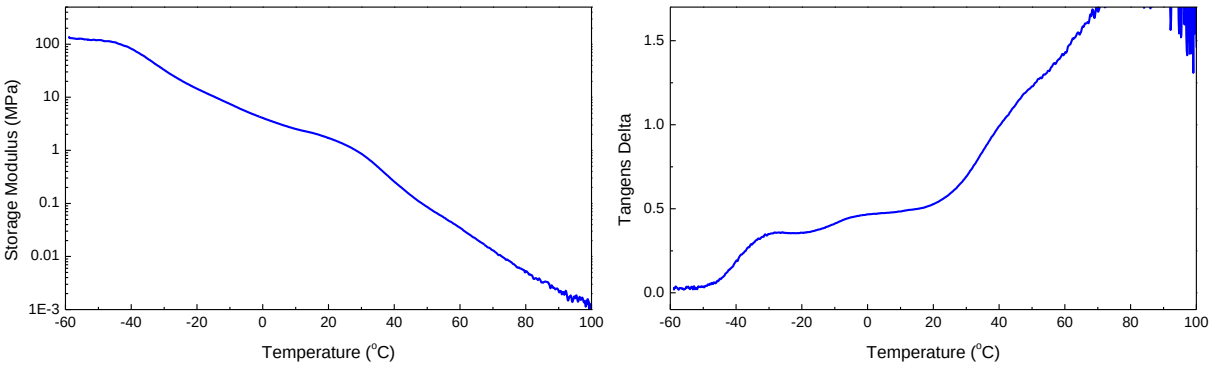

Figure 124. Left: storage modulus and right: tangens delta for mixture of star PCEA and linear PDMAEA-*b*-PBA-*b*-PDMAEA.

The mixed material was sticky, highly viscous and difficult to handle compared to the other prepared materials, which is very different compared to the mixtures of linear triblock copolymers with close to 50 % charged blocks. DMA measurements of the material (Figure 124) confirmed this different mechanical behavior. While two T_gs can be observed around -30 °C and 0 °C from small peaks in tangens delta, these T_gs are much less clear than in the materials made from mixtures of triblock copolymers and tangens delta keeps increasing to failure from 20 °C onwards, while the M' shows an almost continuous drop. It seems that this material does not have a phase-separated morphology like the previous samples, and behaves as a thermoplastic rather than a thermoplastic elastomer. This different behavior seems to stem from a different morphology of the material due to the different design using a star homopolymer as one of the components; however the exact morphology was not confirmed. It may be that the star shape of the PCEA leads to macroscale phase separation between clusters of star PCEA and the PBA blocks, with only very weak electrostatic

interactions between the DMAEA groups and most outer CEA groups. This weak crosslinking is not enough to transform the viscous liquid polymer into a solid material.

6.3.4 Mixtures of PDMAEA-*b*-PMEA-*b*-PDMAEA and PCEA-*b*-PMEA-*b*-PCEA synthesized via RAFT polymerization

PMEA was used as an alternative, less hydrophobic, middle block to PBA (Table 29). It was expected that this would increase miscibility between the charged and uncharged blocks of the polymer, anticipated to improve the chain mobility and thereby also the self-healing ability. In Figure 125 (left) the TGA of the homopolymer and block copolymers is shown. As in previous results, the PCEA and PDMAEA show slightly lower degradation temperatures than the PMEA. DSC (Figure 125, right) shows that each of the polymers has a single T_g, with the T_g of the triblock copolymers in between that of the homopolymers, showing that they are miscible. The mixture of the triblock copolymers has a T_g of -34 °C, which is similar to the T_g of the PMEA homopolymer, indicating miscibility of all blocks and absence of phase separation. This mixture with PMEA as middle blocks was much more liquid-like compared to the PBA-containing polymers with similar design.

Table 29. Details of MEA-containing triblock copolymers.

Polymer type	Composition (NMR after purification)	DP (from conversion in GC/NMR)	M_n (g/mol, SEC)	Đ (SEC)	% charged in mixture[a]
PDMAEA-*b*-PMEA-*b*-PDMAEA3 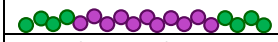	34% DMAEA 66% MEA	28 DMAEA 57 MEA	11600	1.08	-
PCEA-*b*-PMEA-*b*-PCEA2 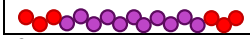	39% CEA 61% MEA	36 CEA 57 MEA	14700	1.13	36

[a] Molar percentage of charged monomers in the mixture of the two polymers with stoichiometric amounts of cationic and anionic groups.

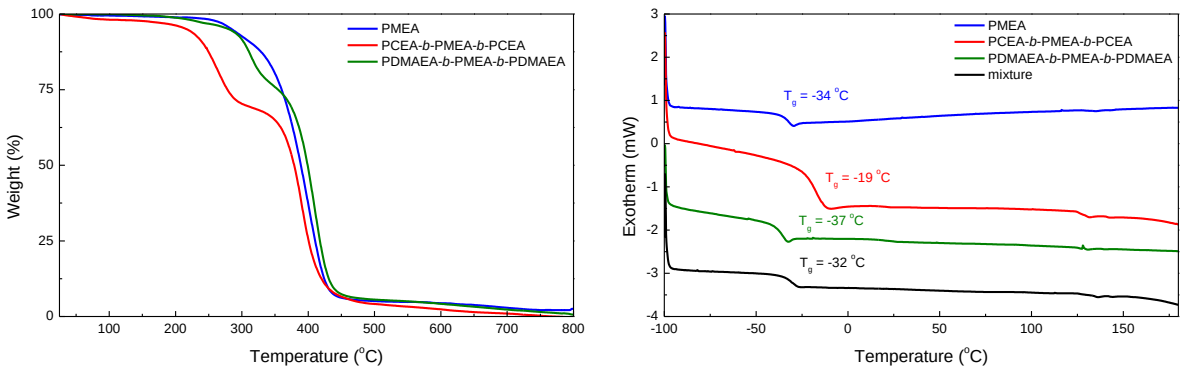

Figure 125. Left: TGA, right: DSC of MEA-containing triblock copolymers and their mixture.

DMA of the mixture of the two polymers (Figure 126) shows a M' around 100 MPa for the glassy material. A weak T_g is seen around -20 °C in agreement with the T_g observed in DSC. When the temperature is increased further, the M' drops continuously until the material flows while the tangens delta shows an almost continuous increase without clear transitions. In contrast to the materials containing PBA as middle blocks that showed two separate glass transitions from phase-separation between the charged and uncharged blocks, it seems that there is no phase-separation in this material, leading to very broad and weak transitions. Failure also occurs at a lower temperature than in the PBA-containing materials, showing that a combination of electrostatic interaction and phase separation is needed to form thermoplastic elastomeric materials with good mechanical properties.

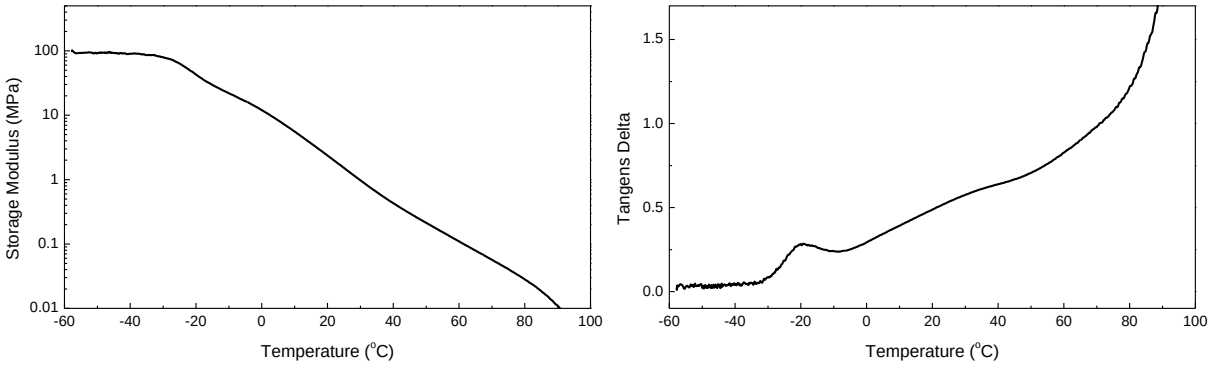

Figure 126. Left: storage modulus and right: tangens delta from DMA measurements of mixture of MEA-containing triblock copolymers.

6.3.5 Mixtures of PDMAEA-*b*-PCHA-*b*-PDMAEA and PCEA-*b*-PCHA-*b*-PCEA synthesized via RAFT polymerization

PCHA was chosen as a higher-T_g hydrophobic middle block for the charged triblock copolymers. Both the DMAEA and CEA containing triblock copolymers contained 37 mol % charged groups as shown by ^{1}H NMR spectroscopy, and had a molecular weight around 14000 g/mol (Table 30).

Figure 127, left shows the TGA measurements of the PCHA homopolymer and the two charged triblock copolymers. The first degradation step of PCEA-*b*-PCHA-*b*-PCEA is ascribed to CEA, as was shown earlier for PCEA-*b*-PBA-*b*-PCEA polymers in Figure 112. Both the DMAEA and CHA show the same degradation temperature, while the last 30 % weight loss is probably from the backbone of the polymers.

DSC (Figure 127, right) of the individual polymers shows that each polymer has a single T_g, which in the case of the triblock copolymers is in between the T_g of PCHA (23 °C) and PDMAEA (-46 °C) or PCEA (~40 °C). This suggests that the polymer blocks are miscible and not phase-separated. The 1:1 mixture of the polymers shows two apparent T_gs, one of the PCHA phase at 26 °C and one at 125 °C possibly resulting from the charged sections.

Table 30. Details of CHA-containing triblock copolymers.

Polymer type	Composition (NMR after purification)	DP (from conversion in GC/NMR)	M_n (g/mol, SEC)	Đ (SEC)	% charged in mixture[a]
PDMAEA-*b*-PCHA-*b*-PDMAEA1 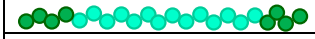	37% DMAEA 63% CHA	40 DMAEA 68 CHA	7100	1.15	-
PCEA-*b*-PCHA-*b*-PCEA1 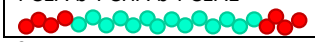	37% CEA 63% CHA	40 CEA 68 CHA	6700	1.43	37

[a] Molar percentage of charged monomers in the mixture of the two polymers with stoichiometric amounts of cationic and anionic groups.

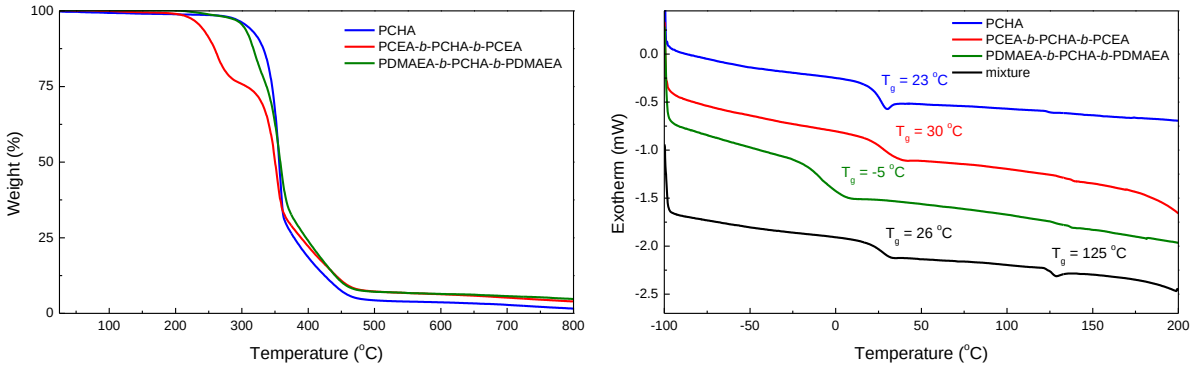

Figure 127. Left: TGA, right: DSC of CHA-containing triblock copolymers.

MTDSC was used to further investigate these T_gs of the mixed polymers (Figure 128). The T_g at 26 °C is also found in the reversing heat flow around 20 °C, indicating that this is a true T_g, which is a reversible phase transition. Several transitions can be found in the non-reversing heat flow, around 30 °C, 50 °C and 145 °C. Since a T_g should also be visible in the reversing heat flow, these other transitions are probably enthalpy relaxations rather than a true glass transition.

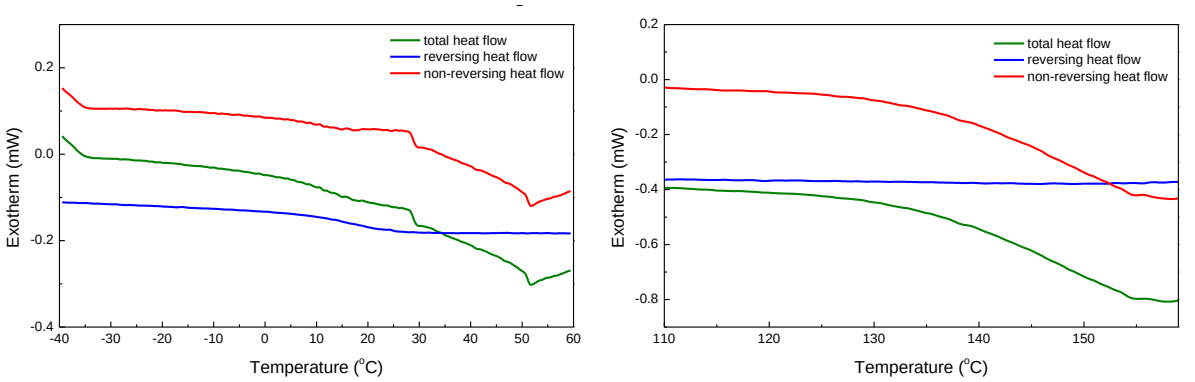

Figure 128. MTDSC of mixture of PCEA-*b*-PCHA-*b*-PCEA and PMAEA-*b*-PCHA-*b*-PDMAEA.

DMA of the mixture (Figure 129) also shows multiple transitions. The T_g of the PCHA segments is found around 30 °C, while a second T_g is observed around 80 °C, which was not seen in DSC, which could probably be the T_g of the associated charged sections. This confirms that this material may be phase separated. In between the two T_gs the M' is around 0.5 MPa, which is lower than what was observed for materials with PBA as middle blocks. However, since the T_gs in this material are at higher temperatures, this also shifts the extended rubber plateau regime for the material to a higher temperature. Above the second T_g the M' stays around 0.1 MPa with tangens delta around 0.3, so it seems that the material does not turn liquid yet at this temperature, although the measurement shows more noise at higher temperatures. Importantly, the rubber plateau is retained up to at least 180 °C, which can be ascribed to the electrostatic interactions. The sample was not heated further to prevent degradation.

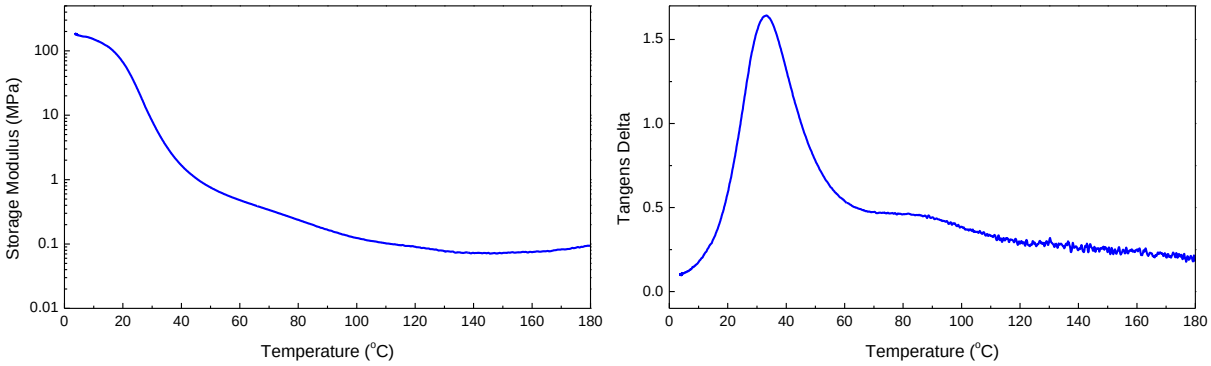

Figure 129. DMA of mixture of PCEA-*b*-PCHA-*b*-PCEA and PMAEA-*b*-PCHA-*b*-PDMAEA.

While it seems that the use of higher T_g blocks in the triblock copolymers will lead to stronger materials, this may also increase brittleness at lower temperatures as was observed in this sample. To obtain a harder supramolecular thermoplastic elastomer, the inclusion of a higher T_g block in combination with a low T_g matrix, for example in a pentablock copolymer with the middle block being high T_g and surrounded by softer blocks, may be a better design. Unfortunately this could not be tested within this research due to time constraints.

6.3.6 PSPDMAEA-*b*-PMEA-*b*-PSPDMAEA synthesized via RAFT polymerization and post-polymerization modification

Besides the mixtures of triblock copolymers containing DMAEA as positively charged group and CEA as negatively charged group, a single triblock copolymer containing the zwitterionic SPDMAEA was also tested. First a PDMAEA-*b*-PMEA-*b*-PDMAEA triblock copolymer containing 40 mol % DMAEA was synthesized, which was then treated with 1,3-propanesultone to yield the zwitterionic PSPDMAEA-*b*-PMEA-*b*-PSPDMAEA (details in Chapter 5, Table 31). For this polymer, it was expected that the zwitterionic blocks of the polymers will self-associate and phase-separate from the uncharged PMEA middle blocks.

Table 31. Details of zwitterionic triblock copolymer.

Polymer type	Composition (NMR after purification)	DP (from conversion in GC/NMR)	M_n (g/mol, SEC) before modification	Đ (SEC) before modification	% charged in polymer
PSPDMAEA-*b*-PMEA-*b*-PSPDMAEA 	40% SPDMAEA 60% MEA	39 SPDMAEA 57 MEA	12000	1.10	40

Figure 130, left shows the TGA of the polymer. The weight loss between 25 °C and 100 °C is attributed to the evaporation of water. This was difficult to remove completely by freeze-drying due to its strong ionic-dipole interaction with the polymer. At 300 °C to 400 °C, the degradation of the polymer can be observed in two steps, which are probably the two different types of monomer.

Water evaporation was also observed by DSC during the first heating ramp. Shown in Figure 130, right is the second heating ramp of two separate measurements. A T_g of -34 °C was found for the PMEA middle block, in agreement with previous results. At 147 °C a transition which looks like a melting point is observed, but the shape of this peak was different in each measurement. This peak probably results from enthalpic dissociation of the electrostatic associated state, which can be expected to have a slightly different structure during each cooling and heating cycle. When the DSC

measurement was started at room temperature and not cooled any lower, no melting point was observed, so cooling to very low temperature is needed to form these associated domains.

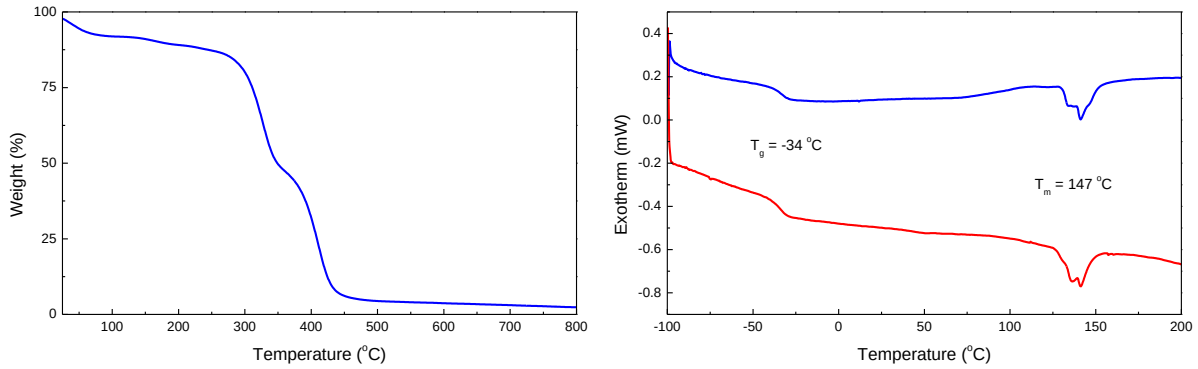

Figure 130. Left: TGA, right: DSC of PSPDMAEA-*b*-PMEA-*b*-PSPDMAEA.

DMA samples of PSPDMAEA-*b*-PMEA-*b*-PSPDMAEA were prepared differently from the other polymers. Because hot pressing in a mold did not provide a useful sample, which may be due to the formation of strongly associated charged sections, the material was solvent casted from water and dried in a vacuum oven. Immediately after taking the sample out of the vacuum oven, the material was very brittle, while after around 20 minutes it was more rubbery, probably from the uptake of moisture from the atmosphere. Since this is difficult to control, we can assume that all samples of this polymer contain variable amounts of water.

Figure 131 shows the DMA measurements of PSPDMAEA-*b*-PMEA-*b*-PSPDMAEA. Multiple measurements were performed that each showed somewhat different results. Based on the visual observations, these differences are likely caused by different amounts of moisture in the sample. While all measurements show multiple T_gs, the temperature and intensity of the T_gs vary significantly. Based on the DMA measurements of the other materials in this chapter, we would expect the T_g of the PMEA blocks to be around -20 °C, with a second T_g of the PSPDMAEA blocks at a higher temperature. It seems that moisture increases the T_g of PMEA, possibly by forming bound ice crystals which have been reported before,[41] and decreases the T_g of PSPDMAEA by partially dissolving the charged section and thereby weakening the electrostatic interaction. Based on these results, it is difficult to draw any conclusions about the properties of this polymer. Nonetheless, it appears that this polymer won't be useful for applications due to its highly variable properties.

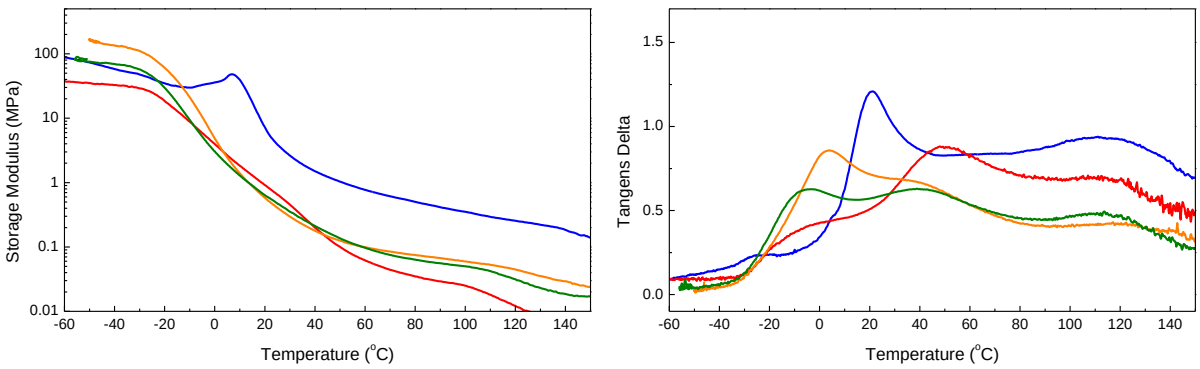

Figure 131. DMA of PSPDMAEA-*b*-PMEA-*b*-PSPDMAEA, with each color representing a different measurement on the same material.

6.4 Conclusions

Several different types of supramolecular materials based on electrostatic interaction were prepared from triblock copolymers containing an uncharged middle block and charged end blocks. Some of the materials behaved like supramolecular thermoplastic elastomers, while others show only thermoplastic behavior. These properties could be tuned by varying the length and polymer type of the different blocks. Mixtures of triblock copolymers containing the hydrophobic PBA or PCHA as middle blocks showed a phase-separated system with two T_gs, while this phase separation was not observed for mixtures of triblock copolymers containing the less hydrophobic PMEA as middle blocks or mixtures of PDMAEA-*b*-PBA-b-PDMAEA with a star PCEA homopolymer. The non-phase separated materials also showed inferior mechanical properties compared to the phase-separated materials, with behavior close to a viscous melt at room temperature, indicating that a phase-separated structure is essential to obtain electrostatic supramolecular materials with elastomeric properties.

Mixtures of PCEA-*b*-PBA-*b*-PCEA and PDMAEA-*b*-PBA-b-PDMAEA with 20 % to 30 % of charged blocks behaved as thermoplastic elastomers with good mechanical properties up to temperatures well above the highest T_g. While mixtures of PAA-*b*-PBA-*b*-PAA and PDMAEA-*b*-PBA-b-PDMAEA also showed two T_gs, these materials showed a lower storage modulus and flow at lower temperatures, indicating that CEA is a better anionic monomer for this purpose than AA, most likely due to lower steric constraints. Mixtures of PCHA-containing triblock copolymers may be useful as thermoplastic elastomers at temperatures above around 30 °C, however below the T_g of 26 °C the material is brittle and breaks easily. The zwitterionic PSPDMAEA-*b*-PMEA-*b*-PSPDMAEA also showed two transitions and thermoplastic elastomeric behavior, however for this material the amount of moisture was difficult to control and had a large effect on the thermal and mechanical properties. Overall, the mixtures of PCEA-*b*-PBA-*b*-PCEA and PDMAEA-*b*-PBA-b-PDMAEA with around 20 % to 30 % charged blocks and middle blocks of the same length showed the best mechanical properties and usefulness as a thermoplastic elastomer that retained the rubber plateau even beyond the second T_g ascribed to electrostatic association. Further improvement of the properties, for example by including small high T_g blocks inside the PBA matrix, is still possible and required as well as more in depth studies of self-healing ability.

References

1. T. Aida, E. W. Meijer, S. I. Stupp, *Science* **2012**, *335*, 813.
2. S. Seiffert, J. Sprakel, *Chem. Soc. Rev.* **2012**, *41*, 909.
3. R. Hoogenboom, *Angew. Chem. Int. Ed.* **2012**, *51*, 11942.
4. P. Cordier, F. Tournilhac, C. Soulie-Ziakovic, L. Leibler, *Nature* **2008**, *451*, 977.
5. Y. Chen, A. M. Kushner, G. A. Williams, Z. Guan, *Nat. Chem.* **2012**, *4*, 467.
6. J. Hentschel, A. M. Kushner, J. Ziller, Z. Guan, *Angew. Chem. Int. Ed.* **2012**, *51*, 10561.
7. G. M. L. van Gemert, J. W. Peeters, S. H. M. Söntjens, H. M. Janssen, A. W. Bosman, *Macromol. Chem. Phys.* **2012**, *213*, 234.
8. R. F. M. Lange, M. Van Gurp, E. W. Meijer, *J. Polym. Sci., Part A: Polym. Chem.* **1999**, *37*, 3657.
9. L. R. Rieth, R. F. Eaton, G. W. Coates, *Angew. Chem. Int. Ed.* **2001**, *40*, 2153.
10. K. P. Nair, V. Breedveld, M. Weck, *Macromolecules* **2008**, *41*, 3429.
11. O. Colombani, C. Barioz, L. Bouteiller, C. Chanéac, L. Fompérie, F. Lortie, H. Montès, *Macromolecules* **2005**, *38*, 1752.
12. M. Kashif, Y.-W. Chang, *Polym. Int.* **2014**, *63*, 1936.
13. H. Kautz, D. J. M. van Beek, R. P. Sijbesma, E. W. Meijer, *Macromolecules* **2006**, *39*, 4265.

14. D. Montarnal, P. Cordier, C. Soulie-Ziakovic, F. Tournilhac, L. Leibler, *J. Polym. Sci., Part A: Polym. Chem.* **2008**, *46*, 7925.
15. J. Cui, A. d. Campo, *Chem. Commun.* **2012**, *48*, 9302.
16. S. Burattini, B. W. Greenland, D. H. Merino, W. G. Weng, J. Seppala, H. M. Colquhoun, W. Hayes, M. E. Mackay, I. W. Hamley, S. J. Rowan, *J. Am. Chem. Soc.* **2010**, *132*, 12051.
17. M. A. Aboudzadeh, M. E. Muñoz, A. Santamaría, R. Marcilla, D. Mecerreyes, *Macromol. Rapid Commun.* **2012**, *33*, 314.
18. A. Aboudzadeh, M. Fernandez, M. E. Muñoz, A. Santamaría, D. Mecerreyes, *Macromol. Rapid Commun.* **2014**, *35*, 460.
19. M. A. Malmierca, A. González-Jiménez, I. Mora-Barrantes, P. Posadas, A. Rodríguez, L. Ibarra, A. Nogales, K. Saalwächter, J. L. Valentín, *Macromolecules* **2014**, *47*, 5655.
20. X. Wang, J. Vapaavuori, Y. Zhao, C. G. Bazuin, *Macromolecules* **2014**, *47*, 7099.
21. D. Mozhdehi, S. Ayala, O. R. Cromwell, Z. Guan, *J. Am. Chem. Soc.* **2014**, *136*, 16128.
22. B. Yang, H. Zhang, H. Peng, Y. Xu, B. Wu, W. Weng, L. Li, *Polym. Chem.* **2014**, *5*, 1945.
23. S. Bode, L. Zedler, F. H. Schacher, B. Dietzek, M. Schmitt, J. Popp, M. D. Hager, U. S. Schubert, *Adv. Mater.* **2013**, *25*, 1634.
24. M. Burnworth, L. Tang, J. R. Kumpfer, A. J. Duncan, F. L. Beyer, G. L. Fiore, S. J. Rowan, C. Weder, *Nature* **2011**, *472*, 334.
25. E. Croisier, S. Liang, T. Schweizer, S. Balog, M. Mionić, R. Snellings, J. Cugnoni, V. Michaud, H. Frauenrath, *Nat. Commun.* **2014**, *5*.
26. B. D. Mather, M. B. Baker, F. L. Beyer, M. A. G. Berg, M. D. Green, T. E. Long, *Macromolecules* **2007**, *40*, 6834.
27. S. Sivakova, D. A. Bohnsack, M. E. Mackay, P. Suwanmala, S. J. Rowan, *J. Am. Chem. Soc.* **2005**, *127*, 18202.
28. R. J. Varley, S. van der Zwaag, *Acta Mater.* **2008**, *56*, 5737.
29. D. Wang, J. Guo, H. Zhang, B. Cheng, H. Shen, N. Zhao, J. Xu, *J. Mater. Chem. A* **2015**, *3*, 12864.
30. Y. Furusho, T. Endo, *J. Polym. Sci., Part A: Polym. Chem.* **2014**, *52*, 1815.
31. A. Noro, K. Ishihara, Y. Matsushita, *Macromolecules* **2011**, *44*, 6241.
32. H. Wei, S. Du, Y. Liu, H. Zhao, C. Chen, Z. Li, J. Lin, Y. Zhang, J. Zhang, X. Wan, *Chem. Commun.* **2014**, *50*, 1447.
33. J. N. Hunt, K. E. Feldman, N. A. Lynd, J. Deek, L. M. Campos, J. M. Spruell, B. M. Hernandez, E. J. Kramer, C. J. Hawker, *Adv. Mater.* **2011**, *23*, 2327.
34. Q. Wang, J. L. Mynar, M. Yoshida, E. Lee, M. Lee, K. Okuro, K. Kinbara, T. Aida, *Nature* **2010**, *463*, 339.
35. R. K. Heenan, S. E. Rogers, D. Turner, A. E. Terry, J. Treadgold, S. M. King, *Neutron News* **2011**, *22*, 19.
36. G. D. Wignall, F. S. Bates, *J. Appl. Crystallogr.* **1987**, *20*, 28.
37. P. D. Nellist, S. J. Pennycook, *Adv. Imaging Electron Phys.* **2000**, *113*, 147.
38. J. Loos, E. Sourty, K. B. Lu, G. de With, S. van Bavel, *Macromolecules* **2009**, *42*, 2581.
39. S. R. Forrest, *Nature* **2004**, *428*, 911.
40. R. E. Hummel, *Electronic properties of materials*. (Springer, New York, ed. 4, 2011), pp. 80-82.
41. I. Javakhishvili, M. Tanaka, K. Ogura, K. Jankova, S. Hvilsted, *Macromol. Rapid Commun.* **2012**, *33*, 319.

Chapter 7: One-pot automated synthesis of triblock copolymers for self-healing supramolecular hydrogels

Abstract

In this chapter, the preparation of supramolecular hydrogels from ABA-triblock copolymers with a water-soluble middle block and hydrophobic end groups is reported. The hydrophilic monomer *N*-acryloylmorpholine (NAM) was copolymerized with the hydrophobic isobornyl acrylate (IBA) via one-pot sequential monomer addition RAFT polymerization in an automated parallel synthesizer, using an approach similar to the block copolymer synthesis reported in Chapter 3. Hydrophobic interactions between the outer blocks cause them to phase-separate into larger hydrophobic aggregates in water, forming physical crosslinks between the polymers. The resulting hydrogels were studied using rheology and their self-healing ability after large strain damage was shown.

7.1 Introduction

Hydrogels are soft solid materials that contain a large amount of water in addition to a polymeric network. They are commonly used in contact lenses,[1] tissue engineering and many other applications.[2] While many hydrogels consist of covalently crosslinked polymers, in supramolecular hydrogels the polymers are crosslinked solely by physical forces, such as hydrophobic, electrostatic or host-guest interaction.[3] Generally supramolecular crosslinks are reversible, leading to injectable and self-healing hydrogels that often show stimuli-responsiveness enabling advanced applications as drug delivery systems and other uses.[4, 5]

Supramolecular hydrogels based on hydrophobic interactions have been previously reported, using different materials and experimental approaches. Hydrogels formed by ABA-triblock copolymers with a hydrophilic poly(sodium acrylate) middle block and hydrophobic polystyrene end groups were reported by Tsilitanis *et al*.[6, 7] Vlassopoulos studied the effect of polymer and surfactant concentration on the gel formation of polybutadiene-*b*-poly(sodium methacrylate)-*b*-polybutadiene.[8] Other hydrogels with the hydrophobic-hydrophilic-hydrophobic polymer structure were reported by multiple other research groups.[9-11] The hydrophobic sections can also be formed by a thermoresponsive polymer such as poly(*N*-isopropylacrylamide), yielding a thermoresponsive supramolecular hydrogel.[12]

The hydrophobic domains do not necessarily need to be located at the ends of a hydrophilic polymer to be able to form hydrogels. An example of a supramolecular hydrogel formed by hydrophobic interactions, synthesized from statistically copolymerized acrylamide and hydrophobic acrylates in the presence of SDS, was shown by Okay.[13-15] Percec showed that supramolecular hydrogels can also be formed by miscible blends of water soluble and insoluble polymers that associate via hydrogen bonds.[16] Hydrophobic domains in covalently crosslinked hydrogels can be used to increase toughness[17] or add self-healing ability[18, 19] by acting as secondary physical crosslinks in addition to the covalent crosslinks. A more extensive overview of supramolecular hydrogels is given in Chapter 1.

Here we will try to efficiently synthesize ABA-triblock copolymers containing hydrophobic-hydrophilic-hydrophobic blocks with different sizes of the blocks for the preparation of supramolecular hydrogels. For the hydrophilic blocks, *N*-acryloylmorpholine (NAM, Figure 132) is chosen as this can be polymerized up to high monomer conversion with good control over molar

mass via RAFT polymerization to form water-soluble polymers. One-pot synthesis of multiblock copolymers via RAFT using NAM and other monomers has been reported by the group of Perrier.[20-23] Additionally hydrogels prepared from NAM have shown biocompatibility,[24] which is needed for most possible applications. Isobornyl acrylate (IBA) will be used to form the hydrophobic blocks, because this is a highly hydrophobic acrylate that can be polymerized under similar conditions as NAM. The high T_g of PIBA (T_g = 94 °C)[25] may lead to stronger hydrogels compared to using a low T_g polymer due to the formation of glassy hydrophobic aggregates. RAFT polymerization in an automated parallel synthesizer, including the synthesis of block copolymers, was shown by Schubert, Moad, Hoogenboom and colleagues.[26-30] Using this technique will allow us to systematically vary the block lengths of the polymers, enabling the investigation of the relationship between polymer structure and hydrogel properties.

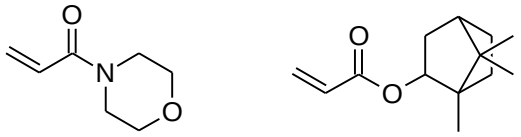

NAM IBA

Figure 132. Structures of *N*-acryloylmorpholine (NAM) and isobornyl acrylate (IBA).

7.2 Experimental section

Materials

1,4-Dioxane (99.5%, extra dry over molecular sieves, stabilized with 2-5 ppm BHT) was purchased from Acros and used as received. *N*-acryloylmorpholine (NAM) (98%) was purchased from TCI and passed over an aluminium oxide column to remove the inhibitor before use. Isobornyl acrylate (IBA) (tech. grade) was purchased from Sigma-Aldrich and distilled before use. 2,2'-Azobis(2-methylpropionitrile) (AIBN) (98%) was purchased from Sigma-Aldrich and recrystallized from methanol before use. Tetrahydrofuran (THF) (dry, unstabilized and free of peroxides) was obtained from a solvent purification system (Meyer, custom made with a nitrogen, aluminium oxide drying system).

Synthesis of bifunctional trithiocarbonate chain transfer agent (BTCTA)

Synthesis and ^{1}H and ^{13}C NMR spectra of BTCTA were already reported in Chapter 5.

Automated RAFT polymerizations

The triblock copolymers were synthesized via RAFT polymerization using a Chemspeed ASW2000 automated synthesizer equipped with 16 parallel reactors of 13 mL, a Huber Petite Fleur thermostat for heating/cooling, a Huber Ministat 125 for reflux and a Vacuubrand PC 3000 vacuum pump. Stock solutions of BTCTA, AIBN, NAM and IBA in dioxane were prepared and bubbled with argon for one hour before being introduced into the robot system and then kept under argon atmosphere. The hood of the automated synthesizer was continuously flushed with nitrogen (flow rate 20 L/min) and the reactors were flushed with argon (flow rate 2 L/min) to ensure an inert atmosphere. Before starting the polymerizations, the reactors were degassed through twenty vacuum-argon cycles. Stock solutions of NAM, BTCTA and AIBN were transferred to the reactors, to a total volume of 4.0 mL, using the syringe of the automated synthesizer while the reactors were kept at 10 °C. The syringes were rinsed with DMF in between liquid transfers. A t = 0 minutes sample was taken from each

reaction for later conversion calculation. The reactors were then heated to 70 °C to start the polymerizations. During the reactions, 50 µL samples were taken at timely intervals and directly injected into 1.5 mL sample vials, containing ~1.5 mL of THF with 0.1 mg/mL of phenothiazine to stop the polymerization, for GC and SEC measurements. The reactions were stopped by cooling the reactors down to 10 °C. For the triblock copolymerizations of NAM with IBA, first the homopolymerization of NAM was performed with 0.05 eq. of AIBN and different NAM:BTCTA ratios. After three hours, a 2.0 M solution of IBA in dioxane was added to all reactors in different amounts (1.0, 0.7, 0.4 or 0.2 mL) and the polymerization was continued for four hours, after which the reactors were cooled to 10 °C to stop the polymerizations. The PIBA-*b*-PNAM-*b*-PIBA triblock copolymers were precipitated two times in MeOH, dissolved in THF and dried in a vacuum oven.

Gas Chromatography (GC)

Samples were measured with GC to determine the monomer conversion from the ratio of the integrals from the monomer and the reaction solvent. GC was performed on an Agilent 7890A system equipped with a VWR Carrier-160 hydrogen generator and an Agilent HP-5 column of 30 m length and 0.320 mm diameter. An FID detector was used and the inlet was set to 250 °C with a split injection of ratio 25:1. Hydrogen was used as carrier gas at a flow rate of 2 mL/min. The oven temperature was increased with 20°C/min from 50°C to 120°C, followed by a ramp of 50°C/min to 300°C.

Size Exclusion Chromatography (SEC)

SEC was performed on a Agilent 1260-series HPLC system equipped with a 1260 online degasser, a 1260 ISO-pump, a 1260 automatic liquid sampler (ALS), a thermostatted column compartment (TCC) at 50 °C equipped with two PLgel 5 µm mixed-D columns and a precolumn in series, a 1260 diode array detector (DAD) and a 1260 refractive index detector (RID). The used eluent was DMA containing 50 mM of LiCl at a flow rate of 0.5 mL/min. The spectra were analyzed using the Agilent Chemstation software with the GPC add on. Molar mass and dispersity values were calculated against PMMA standards from Polymer Labs.

Nuclear magnetic resonance spectroscopy (NMR)

Proton NMR (^{1}H NMR) spectra were used to calculate the ratio of NAM and IBA in each polymer and recorded on a Bruker Avance 300 MHz spectrometer at room temperature in deuterated chloroform.

Hydrogel preparation

Hydrogels of PIBA-*b*-PNAM-*b*-PIBA were prepared by first fully dissolving the purified polymers in THF (~75 wt% with regard to the polymer), adding distilled water (90 or 85 wt%) and letting the THF slowly evaporate. By checking the weight of the hydrogels, more water was added as needed to ensure the amount of polymer was 10 or 15 wt% in each hydrogel.

Rheology

Rheology was measured on an Anton Paar Physica MCR 301 rheometer equipped with a Lauda Eco RE 420 S thermostat. Frequency and amplitude sweeps were used to determine the linear viscoelastic range and all measurements were performed in oscillatory mode at 21 °C. Frequency sweeps of the 10 wt% hydrogels were carried out with a gap of 0.6 mm, strain of γ = 0.3 % and an angular frequency ranging from ω = 0.5-500 rad/s (0.1-100 Hz). For the 15 wt% hydrogels, step strain test were performed using a gap of 0.35 mm with alternating measurements in the linear viscoelastic range (ω = 6.28 rad/s (1 Hz) and 0.3 % < γ < 5 %) and measurements with high amplitude strain (100

% < γ < 1000 %) beyond the sol transition point of the gel, with multiple cycles of several minutes at high and low strain.

7.3 Results and discussion

7.3.1 Polymer synthesis

To estimate the polymerization rate of NAM and to select appropriate reaction conditions, a kinetic study using different [NAM]:[BTCTA]:[AIBN] ratios was performed, which is shown in Figure 133. All reactions showed a fast polymerization with mostly linear first order kinetics up to 98 % conversion, after which the polymerizations start showing termination by negative deviation from linear first order kinetics. As expected, the polymerizations using higher amounts of AIBN are faster. While $M_{n,SEC}$ is in agreement with $M_{n,theoretical}$ for polymers with DP 200, a significant difference between the two values was observed for the higher molar mass polymers. This discrepancy resulted from a relatively large amount of tailing on the low M_n side observed in SEC in these polymers, and is also seen in increased dispersities. This tailing was also observed for RAFT polymerization of NAM by other research groups.[22] The dispersities were slightly lower when the lowest amount of AIBN (0.05 eq.) was used, so these conditions were chosen for further experiments.

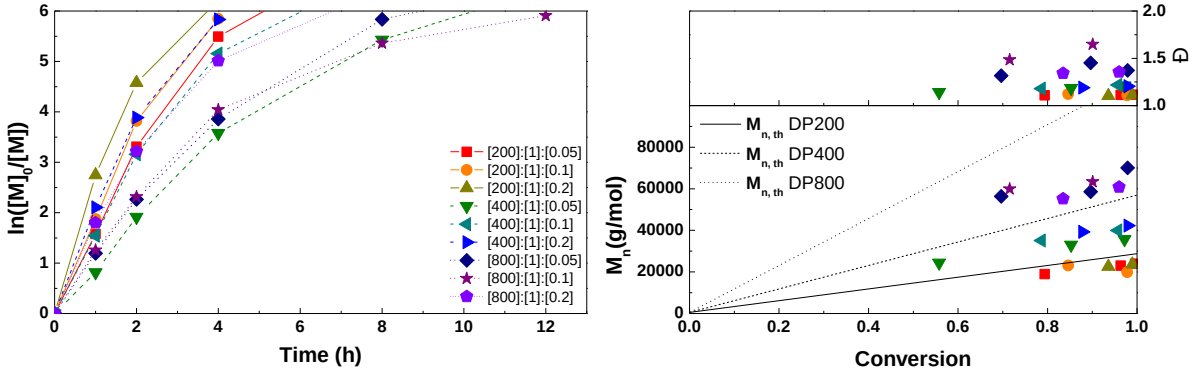

Figure 133. Left: first order kinetic plot for RAFT polymerization of NAM using different [NAM]:[BTCTA]:[AIBN] ratios at a monomer concentration of 2.0 M in dioxane at 70°C. Right: the corresponding molecular weight and dispersity vs. conversion plot.

For the PIBA-*b*-PNAM-*b*-PIBA triblock copolymer synthesis, first a homopolymerization of NAM was performed using a bifunctional CTA, 0.05 eq. of AIBN and a NAM/BTCTA ratio of 200, 400 and 800. After three hours, the conversion of NAM was between 96 and 100% for all reactions as determined by GC. A 2.0 M solution of IBA in dioxane was then added to the reactions in different amounts to allow for the synthesis of ABA-triblock copolymers with different outer block lengths. In the polymerizations with a NAM DP of 200, the conversion of IBA was around 50% after four hours as determined by GC. The conversion of IBA could not be determined accurately for the higher DPs due to inadequate mixing due to the very high viscosity of the reaction mixtures, leading to inaccurate samples. The molar percentage of IBA was determined by ^{1}H NMR spectroscopy after purification of the polymers (Table 32). However, it should be noted that these values may have some inaccuracy, as the polymers show very broad peaks in the ^{1}H NMR spectra which are difficult to accurately integrate, especially since very large and small peaks had to be compared.

SEC samples were taken immediately before the addition of IBA and at the end of the reaction. M_ns determined by SEC were lower after addition of the IBA in many cases, likely resulting from a smaller hydrodynamic radius of the formed triblock copolymers in DMA due to the hydrophobic end groups

leading to collapse of PIBA in DMA. SEC traces of all polymers are shown in Figure 134. While a clear shift in the polymer peak is observed for some of the shorter triblock copolymers compared to the homopolymers, the majority of polymers show almost no difference. This is because the PIBA blocks are generally very short compared to the PNAM blocks, especially for the longer PNAM blocks, which also means that the differences between the polymers with the same size PNAM block are very small. The polymers with higher M_n show a shoulder at low molecular weight, which is not observed in the low M_n polymers. This is likely from termination of some of the polymer chains. In some polymers, most notably #1, 2 and 5, the addition of IBA leads to a broader peak and thus a higher dispersity indicating less efficient chain extension. Even though SEC results are inconclusive, ^{1}H NMR spectroscopy clearly showed that both polymers were present in the polymer samples.

Table 32. Results of the ABA-triblock copolymerization of NAM and IBA.

#	[NAM]:[IBA]:[BTCTA] :[AIBN] reaction ratio	M_n (g/mol, SEC) homopolymer	Đ (SEC) homopolymer	mol% IBA (NMR)	M_n (g/mol, SEC) triblock copolymer	Đ (SEC) triblock copolymer
1	200:50:1:0.05	24200	1.12	13.2	14100	1.39
2	200:35:1:0.05	24200	1.10	8.9	17100	1.20
3	200:20:1:0.05	21400	1.12	7.9	19300	1.14
4	200:10:1:0.05	23400	1.13	3.6	23100	1.13
5	400:100:1:0.05	39800	1.21	9.9	24000	1.57
6	400:70:1:0.05	38400	1.19	7.7	32300	1.25
7	400:40:1:0.05	42300	1.22	3.5	40200	1.25
8	400:20:1:0.05	48700	1.32	2.7	49800	1.34
9	800:200:1:0.05	58800	1.42	8.9	58200	1.43
10	800:140:1:0.05	58700	1.38	6.3	57500	1.42
11	800:80:1:0.05	54700	1.40	4.6	55700	1.40
12	800:40:1:0.05	56200	1.41	2.6	56800	1.44

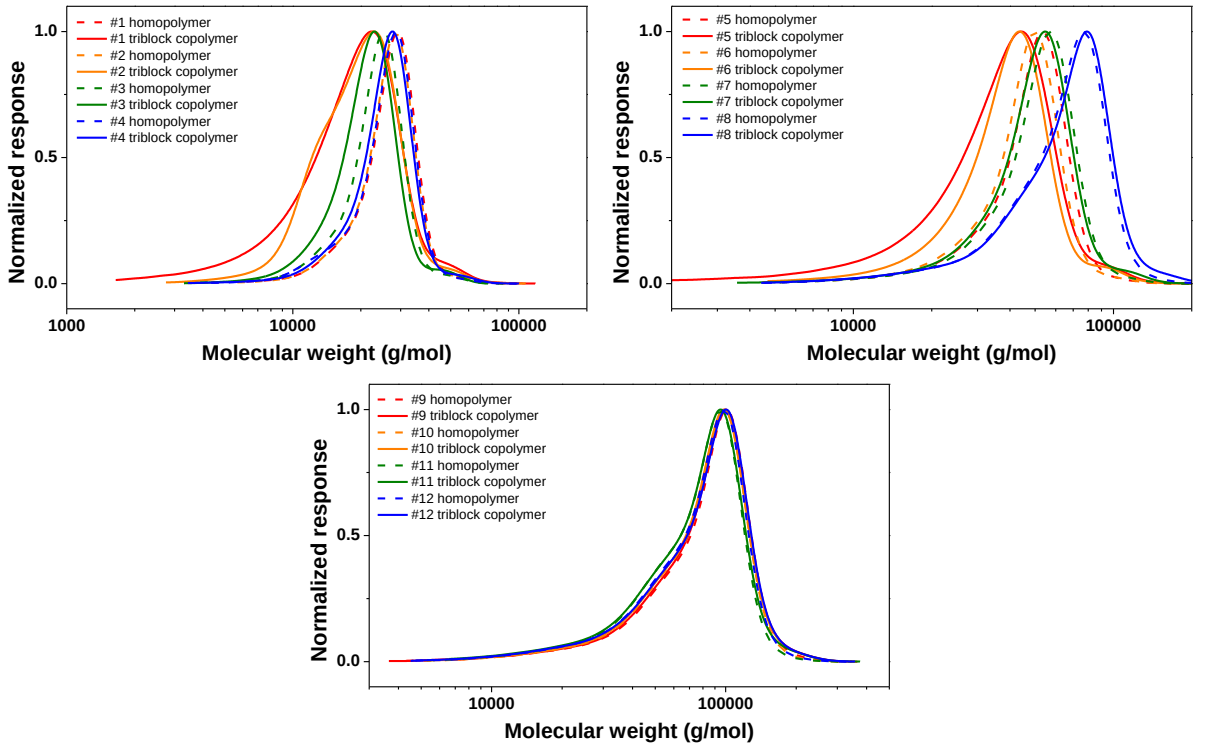

Figure 134. SEC traces of all PIBA-*b*-PNAM-*b*-PIBA triblock copolymers and the PNAM homopolymer middle blocks.

7.3.2 Hydrogel formation and rheology

Hydrogels of the triblock copolymers were prepared by first dissolving the polymers in a small amount of THF, after which water was added and the THF slowly evaporated. Hydrogels were first prepared with 10 wt% of polymer. From visual observation by inverting the vials, it was concluded that polymers 4, 8 and 12 did not form hydrogels at this concentration, but viscous solutions, so in these polymers the hydrophobic blocks were probably too short to form strongly associated domains at the chosen concentration. Polymers #1, 2, 5, 6, 9 and 10 did form hydrogels; however these contained broken pieces of gel, opaque parts and free-flowing water. In these polymers the amount of polymer was likely too little to form a homogeneous hydrogel of the entire solution at the chosen wt%. Polymers #3, 7 and 11 formed homogeneous looking hydrogels.

The hydrogels were characterized using rheology. We expected an influence of both the length of the middle blocks and the outer blocks of the polymers on the storage modulus (G') and loss modulus (G'') of the hydrogels. A hydrogel is most commonly defined by G' > G'', which means the material has more elastic character than viscous character. As polymers with shorter end blocks will likely have weaker hydrophobic crosslinks, these are expected to have a lower G'.

Frequency sweep measurements of the 10 wt% hydrogels of polymers #3, 7 and 11 are shown in Figure 135. All three hydrogels show a similar value for the storage modulus around 500 Pa representative for soft gels, while the loss modulus is higher for the shorter polymers. This indicates a higher liquid character and thus a weaker gel for the shorter polymers. Frequency sweeps of the other materials at 10 wt% did not result in reliable data due to the inhomogeneity of the material and free flowing water being pushed out from under the spindle. Longer time measurements of any of the materials did not show reproducible data because of the fast water evaporation, so self-healing tests could not be performed accurately.

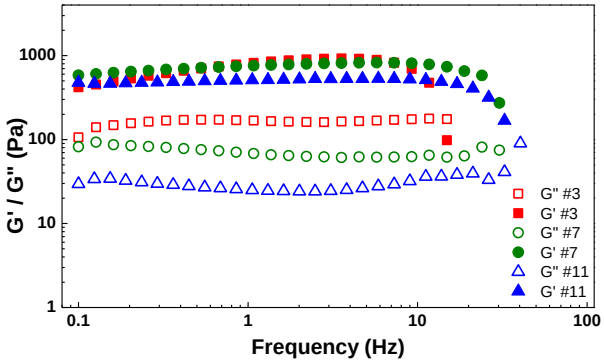

Figure 135. Frequency sweeps of 10 wt% hydrogels prepared from polymers 3, 7 and 11.

By increasing the wt% of polymer in the hydrogels, it was found that almost all 12 polymers formed stable hydrogels at 15 wt%, which was used for further investigation. Frequency sweeps and amplitude sweeps were used to determine the linear viscoelastic range of the materials, i.e. the range in which the storage and loss modulus are constant even when small changes in measuring frequency or amplitude occur. In the linear viscoelastic region the deformations in the material are reversible. Only polymers #8 and 12 had visible flow when the vials were inverted, indicating that these did not form hydrogels. While G'' was larger than G' over the entire amplitude strain range for polymer #8, polymer #12 showed a G' slightly larger than G'' over a large strain and frequency range. However, in contrast to the other polymers, there was no clear linear viscoelastic range as G' and G''

were strongly dependent on frequency for both polymers 8 and 12. These polymers have the shortest hydrophobic domains demonstrating that a minimal hydrophobic driving force is required for hydrogel formation. To be able to compare the obtained data, the frequency was kept at 1 Hz for all materials. As polymers #4 and 7 did form a hydrogel at 15 wt% concentration with G' > G'' and no visible flow was observed when the vials were inverted, we can conclude that around 3 mol% of IBA is the minimum needed in the triblock copolymers for hydrogel formation at these conditions. A performed temperature ramp on one of the hydrogels did not show significant dependence of G' and G'' on the temperature between 10 and 80 °C, evident of no change in enthalpic and entropic driving forces.

When looking at the G' and G'' values for each of the hydrogels (Figure 136D), measured in the viscoelastic range, the relationship between these values and the block lengths of the polymers becomes more clear. The G'', which denotes the viscous or liquid character of the material, is mostly dependent on the size of the hydrophilic middle block of the polymers. This value is higher for shorter polymers, indicating that these are more liquid than the longer polymers. G' is more dependent on the length and percentage of the hydrophobic blocks, as polymers with longer hydrophobic blocks show a more elastic response due to the physical crosslinks being broken less easily and longer hydrophobic blocks being less water soluble. However, it seems that the G' reaches an optimum value after which increasing the hydrophobic block length does not increase the G' any further but leads to a small decrease. Similar observations were reported by Vermonden, who showed that weaker hydrogels were formed when longer thermoresponsive end blocks were used.[31] This was explained by the longer blocks leading to a lower crosslink density in the hydrogels due to the formation of a smaller number of larger hydrophobic clusters.

Some differences in G' may be also attributed to small differences in concentration and residual THF in the hydrogels. Additionally, the structure of the triblock polymers synthesized may not always resemble perfect triblock copolymers, as there is always a small amount of NAM monomer left in the mixture when IBA is added that can be added into the hydrophobic blocks. The high viscosity of the polymerization mixtures and resulting inhomogeneity will likely also lead to some differences between individual polymer chains. When comparing Figure 135 to Figure 136D, it is clear that the increase in polymer concentration from 10 to 15 wt% has a significant effect on G' and G''. While relatively high concentrations of 10 to 15 wt% of polymer were needed to form stable hydrogels, this is in line with previously reported hydrogels of similar design.[9] Addition of surfactants, as shown by Vlassopoulos,[8] may decrease the needed polymer concentration and improve the material properties of the hydrogels.

To test the self-healing ability, or reversibility of the crosslink formation, the hydrogels were first measured in the linear viscoelastic range for several minutes, after which the amplitude strain was increased to high enough values to break the hydrophobic crosslinks, resulting in a gel-sol crossover at which the G'' was larger than G' (Figure 136A-C). The strain required for this crossover differed for each sample, and generally a larger strain was needed for higher molecular weight polymers, which can be explained by the longer polymers needing more strain to go from a coiled to a fully stretched state and the higher penalty to break hydrophobic domains with larger hydrophobic blocks. When switching again to a smaller strain, the G'' and G' returned to their initial values, showing very fast full recovery of the crosslinks. While recovery of hydrogels #1-4 was instantaneous, the longer polymer hydrogels took around 10 to 20 seconds to return to their initial G' and G'' values. Similar

results have been reported previously for self-healing supramolecular hydrogels.[32-35] This shear-thinning and recovery was repeated for several cycles, and full healing of the sample was observed for all polymers except 8, which was already in the sol state at lower strain, and polymers 10 and 11, which did not fully recover to the initial G' after the first deformation but did recover to a slightly lower G'. This may be due to the length of these polymers resulting in a longer time needed for full recovery and reequilibration.

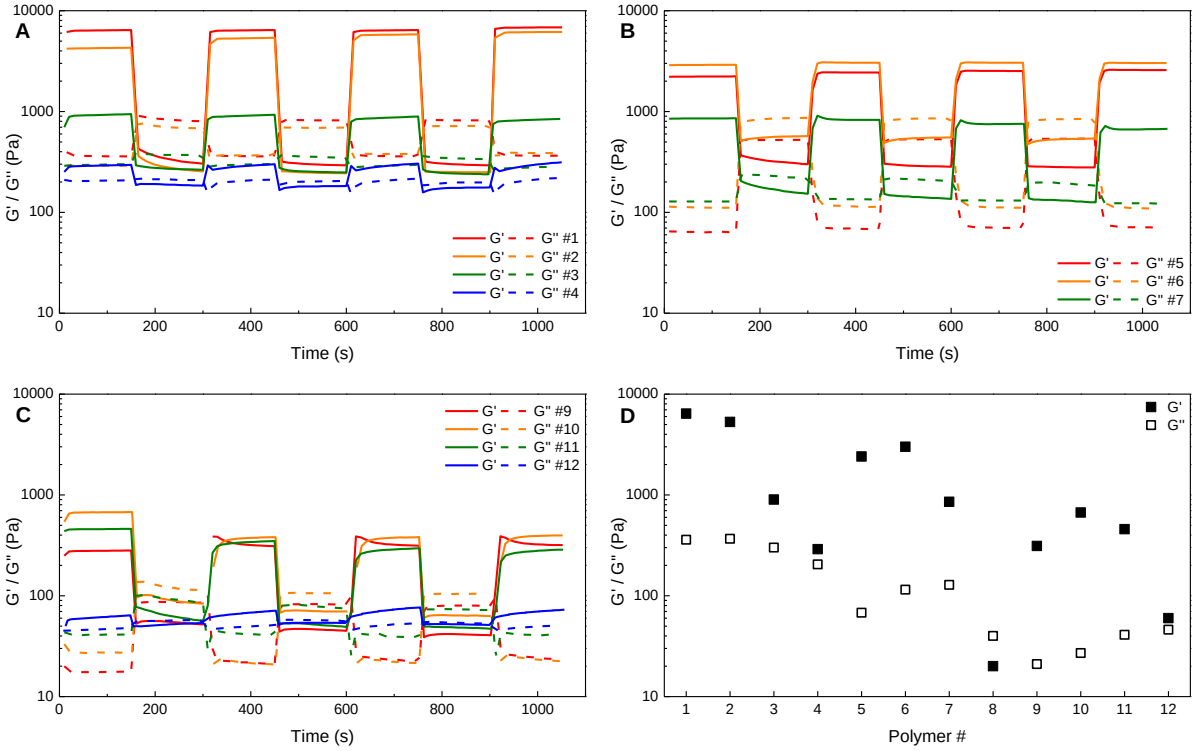

Figure 136. A-C: Step strain measurements for each of the 15 wt% hydrogels, performed at 1 Hz and different strains. D: Overview of G' and G'' measured for all 15 wt% hydrogels at 1 HZ in the linear viscoelastic range.

To test the self-healing behavior on macroscopic scale, a small piece of hydrogel #3 was cut with a scalpel, the pieces were carefully pressed together again and left resting for one minute (Figure 137). The healed piece of hydrogel could be placed on top of two vials, showing that a free-standing hydrogels is formed that can quickly self-heal under ambient conditions. Similar observations were made for the other prepared hydrogels. This successful macroscopic self-healing ability is in agreement with the rapid recovery of the crosslinks that was found with the step-strain measurements (Figure 136). Although many supramolecular hydrogels show self-healing, this is not always the case. Other papers of similar hydrophobic interaction-based triblock copolymer systems do not mention any macroscopic self-healing behavior.[6, 8, 11] While hydrogels composed of polyacrylamide with random blocks of poly(stearyl methacrylate) showed self-healing when they were prepared in the presence of surfactants, this self-healing behavior disappeared when the surfactants were removed, indicating that hydrophobic interactions are not always reversible.[15]

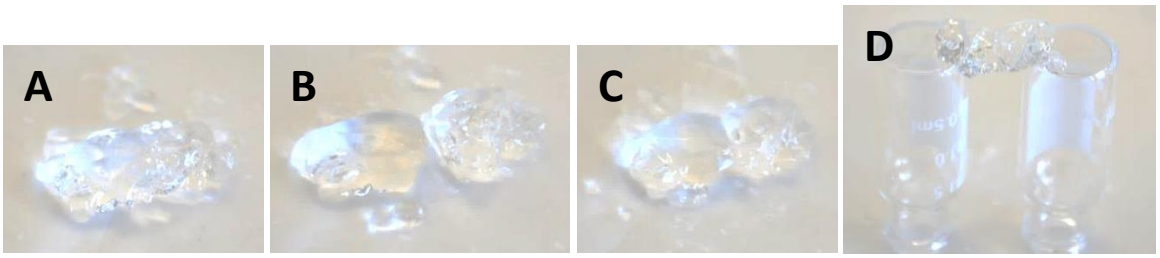

Figure 137. Self-healing of hydrogel #3. A: a fresh piece of hydrogel, B: the hydrogel is cut with a scalpel, C: the cut pieces are carefully pressed back together, and D: the healed hydrogel free-standing on top of two vials.

7.4 Conclusions

ABA-type triblock copolymers containing a hydrophilic PNAM middle block and hydrophobic PIBA end blocks were successfully synthesized using one-pot automated RAFT polymerization. These polymers were used to prepare supramolecular hydrogels based on hydrophobic interactions. Using rheology, fast recovery of the supramolecular crosslinks in the 15 wt% polymer hydrogels after damage was shown. Self-healing ability of the hydrogels on macroscopic scale was also demonstrated. Both the G' and G'' were shown to be dependent of the sizes of the hydrophilic and hydrophobic blocks, with G' mostly increasing with hydrophobic block length up to an optimum value and G'' decreasing with increasing hydrophilic block length. Using this information, it is possible to prepare self-healing supramolecular hydrogels with tunable properties.

References

1. P. C. Nicolson, J. Vogt, *Biomaterials* **2001**, *22*, 3273.
2. B. V. Slaughter, S. S. Khurshid, O. Z. Fisher, A. Khademhosseini, N. A. Peppas, *Adv. Mater.* **2009**, *21*, 3307.
3. W. E. Hennink, C. F. van Nostrum, *Adv. Drug Delivery Rev.* **2002**, *54*, 13.
4. N. M. Sangeetha, U. Maitra, *Chem. Soc. Rev.* **2005**, *34*, 821.
5. T. R. Hoare, D. S. Kohane, *Polymer* **2008**, *49*, 1993.
6. C. Tsitsilianis, I. Iliopoulos, G. Ducouret, *Macromolecules* **2000**, *33*, 2936.
7. C. Tsitsilianis, I. Iliopoulos, *Macromolecules* **2002**, *35*, 3662.
8. S. Pispas, D. Vlassopoulos, G. Fytas, B. Loppinet, N. Hadjichristidis, *Polymer* **2006**, *47*, 7302.
9. A. Miasnikova, A. Laschewsky, G. De Paoli, C. M. Papadakis, P. Müller-Buschbaum, S. S. Funari, *Langmuir* **2012**, *28*, 4479.
10. A. Klymenko, T. Nicolai, L. Benyahia, C. Chassenieux, O. Colombani, E. Nicol, *Macromolecules* **2014**, *47*, 8386.
11. H. Niu, F. Wang, R. A. Weiss, *Macromolecules* **2015**, *48*, 645.
12. C. Li, Y. Tang, S. P. Armes, C. J. Morris, S. F. Rose, A. W. Lloyd, A. L. Lewis, *Biomacromolecules* **2005**, *6*, 994.
13. D. C. Tuncaboylu, M. Sari, W. Oppermann, O. Okay, *Macromolecules* **2011**, *44*, 4997.
14. D. C. Tuncaboylu, A. Argun, M. Sahin, M. Sari, O. Okay, *Polymer* **2012**, *53*, 5513.
15. D. C. Tuncaboylu, M. Sahin, A. Argun, W. Oppermann, O. Okay, *Macromolecules* **2012**, *45*, 1991.
16. V. Percec, T. K. Bera, R. J. Butera, *Biomacromolecules* **2002**, *3*, 272.
17. S. Abdurrahmanoglu, V. Can, O. Okay, *Polymer* **2009**, *50*, 5449.
18. D. C. Tuncaboylu, A. Argun, M. P. Algi, O. Okay, *Polymer* **2013**, *54*, 6381.
19. R. Long, K. Mayumi, C. Creton, T. Narita, C.-Y. Hui, *Macromolecules* **2014**, *47*, 7243.
20. G. Gody, T. Maschmeyer, P. B. Zetterlund, S. Perrier, *Nat. Commun.* **2013**, *4*.
21. G. Gody, T. Maschmeyer, P. B. Zetterlund, S. Perrier, *Macromolecules* **2014**, *47*, 3451.
22. G. Gody, T. Maschmeyer, P. B. Zetterlund, S. Perrier, *Macromolecules* **2014**, *47*, 639.
23. G. Gody, M. Danial, R. Barbey, S. Perrier, *Polym. Chem.* **2015**, *6*, 1502.

24. M. Gorman, Y. H. Chim, A. Hart, M. O. Riehle, A. J. Urquhart, *J. Biomed. Mater. Res., Part A* **2014**, *102*, 1809.
25. J. A. Shetter, *J. Polym. Sci., Part B: Polym. Lett.* **1963**, *1*, 209.
26. C. Guerrero-Sanchez, L. O'Brien, C. Brackley, D. J. Keddie, S. Saubern, J. Chiefari, *Polym. Chem.* **2013**, *4*, 1857.
27. J. J. Haven, C. Guerrero-Sanchez, D. J. Keddie, G. Moad, *Macromol. Rapid Commun.* **2014**, *35*, 492.
28. J. Haven, C. Guerrero-Sanchez, D. Keddie, G. Moad, S. Thang, U. S. Schubert, *Polym. Chem.* **2014**, *5*, 5236.
29. S. Maji, Z. Zhang, L. Voorhaar, S. Pieters, B. Stubbe, S. Van Vlierberghe, P. Dubruel, B. G. De Geest, R. Hoogenboom, *RSC Adv.* **2015**, *5*, 42388.
30. B. Louage, Q. Zhang, N. Vanparijs, L. Voorhaar, S. Vande Casteele, Y. Shi, W. E. Hennink, J. Van Bocxlaer, R. Hoogenboom, B. G. De Geest, *Biomacromolecules* **2014**, *16*, 336.
31. T. Vermonden, N. A. M. Besseling, M. J. van Steenbergen, W. E. Hennink, *Langmuir* **2006**, *22*, 10180.
32. J. R. McKee, E. A. Appel, J. Seitsonen, E. Kontturi, O. A. Scherman, O. Ikkala, *Adv. Funct. Mater.* **2014**, *24*, 2706.
33. Z. Wei, J. H. Yang, J. Zhou, F. Xu, M. Zrinyi, P. H. Dussault, Y. Osada, Y. M. Chen, *Chem. Soc. Rev.* **2014**, *43*, 8114.
34. H. Meng, P. Xiao, J. Gu, X. Wen, J. Xu, C. Zhao, J. Zhang, T. Chen, *Chem. Commun.* **2014**, *50*, 12277.
35. C. B. Rodell, A. L. Kaminski, J. A. Burdick, *Biomacromolecules* **2013**, *14*, 4125.

Chapter 8: Conclusions and outlook

Supramolecular materials are an emerging class of new materials with intriguing properties, such as multi stimuli responsiveness, adaptability and self-healing. Controlled radical polymerization provides an efficient methodology to synthesize some of these materials in a very controlled way, allowing for careful variation and fine-tuning of polymer structures. Chapter 1 showed an overview of several different types of controlled radical polymerization and recent developments in the field of supramolecular materials, in which both supramolecular hydrogels and bulk materials were discussed. This overview served as basic introduction for the remainder of the work.

In Chapter 2 an automated parallel synthesizer was used to optimize the Cu(0)-mediated polymerization of *n*-butyl acrylate and 2-methoxyethyl acrylate. Cu(0)-mediated polymerization is a relatively new technique, allowing for very good control of molecular weight at almost full monomer conversion with high end-group fidelity, making it ideal for one-pot synthesis of block copolymers. This chapter serves as the basis for the other chapters in which the automated parallel synthesizer was used. Both the general settings of the synthesizer as well as the reaction conditions for the homopolymerizations were optimized, leading to very well-controlled polymerizations. Although only two different monomers were used in this chapter, their reactivity was very similar, indicating that many other acrylates can be polymerized in a controlled way using similar conditions.

Chapter 3 is the follow-up of this work in which amphiphilic diblock and triblock copolymers were synthesized by Cu(0)-mediated polymerization with sequential monomer addition, using poly(*n*-butyl acrylate) as the first or middle block and poly(2-(dimethylamino)ethyl acrylate), poly(1-ethoxyethyl acrylate) and poly(1-ethoxyethyl-2-carboxyethyl acrylate) as the second block or outer blocks. After optimization, all diblock and triblock copolymers were obtained with low dispersity and good control over molecular weight. Although several recent publications show the synthesis of multiblock copolymers to almost full conversion using Cu(0)-mediated polymerization,[1, 2] we have not been able to achieve this using our system. Although full conversion of multiblock copolymers using the automated parallel synthesizer may be possible, this likely requires more optimization using somewhat different success selection criteria than we used. Our optimization was focused on finding the reaction conditions at which the most narrow molecular weight distribution was obtained within a reasonable time, which may differ somewhat from the reaction conditions with the highest end-group fidelity that is needed for chain extension. Additionally, the polymerizations are likely slowed down by a build-up of Cu(II), which acts as a deactivator. Adding a reducing agent to generate new Cu(0) may help prevent this problem. Altogether, while the polymers we aimed for could be synthesized in a controlled and reproducible way, both in the automated synthesizer and using schlenk techniques, there is still some room for improvement in this synthesis protocol.

In Chapter 4 RAFT copolymerization of different combinations of thermoresponsive oligoethylene glycol acrylates was performed using the automated parallel synthesizer. Random copolymers with low dispersity were formed in two hours reaction time with each monomer showing similar reactivity, and a cloud point temperature that showed a linear dependence on the polymer composition. This same method can also be applied to other combinations of monomers,[3] making it possible to synthesize systematical libraries of different copolymers in a very short time. Careful tuning of the cloud point temperature can be very useful for biomedical and other applications in which thermoresponsive polymers are used.

Chapter 5 reports the RAFT synthesis of ABA-triblock copolymers with charged outer blocks, using different combinations of monomers for the preparation of materials with different thermal and mechanical properties. Not all polymerizations led to good results and especially the block copolymerizations of 2-carboxyethyl acrylate with high T_g macroCTAs showed difficulties. However, combinations of positively and negatively charged triblock copolymers with poly(*n*-butyl acrylate), poly(2-methoxyethyl acrylate) and poly(cyclohexyl acrylate) as uncharged middle blocks and 2-(dimethylamino)ethyl acrylate and 2-carboxyethyl acrylate as charged outer blocks were synthesized with good control.

In Chapter 6 the thermal and mechanical properties of mixtures of triblock copolymers with oppositely charged outer blocks were studied using TGA, DSC and DMA. Most of the materials with hydrophobic middle blocks showed a phase-separated morphology, with a charged and an uncharged phase. Comparison to a non-phase separated material with a less hydrophobic PMEA middle block showed that phase-separation was a prerequisite to obtain good material properties, as the phase-separated materials behaved as rubbers while the non-phase separated material behavior was a viscous liquid, even though the T_gs of the individual polymers were very similar. The lengths and ratios of the different blocks were found to have a large influence on the morphology of the material, going from a spherical structure with a low amount of charged monomers to a lamellar morphology when close to 50 % of charged monomers are present. For future applications, the mixture of PDMAEA-*b*-PBA-*b*-PDMAEA and PCEA-*b*-PBA-*b*-PCEA seems to be the most useful of the studied polymer mixtures. A unique property that was found in these materials was a rubber plateau that was retained at temperatures above the highest T_g, ascribed to the electrostatic supramolecular interactions.

As for possible applications, this material was found to be not very suitable for the initial goal of a self-healing coating for metal substrates. Although self-healing at elevated temperature in a thick coating could be obtained, this seems to be related to flow of the polymer above the T_g and was only observed for the material with lamellar phase separation. Additionally, the current coating could be washed of the substrate with water, which would of course limit its applicability. Several other possible designs of the material could not be studied because of time limitations. To improve the hardness, mixing of short high T_g blocks within a low T_g matrix may work well. This could for example be done using ABCBA-pentablock copolymers, in which the C-block has a high T_g and the B-block a low T_g. Another option would be a mixture of a charged low T_g ABA-triblock with an oppositely charged high T_g ABA-triblock, which would also result in a three-phase system depending on the monomer choice. Although in this case, a macroscale phase separation may lead to an unusable material.

Another possible future option will be the utilization of linear homopolymers with telechelic end-functionalization of defined multiple charged groups. For example, charged dendrons similar to those shown by Aida[4] could be synthesized and used to put two, four or eight charges on each end of the polymer. This will likely lead to a material with different morphology, as this structure would favor a more one-to-one association between oppositely charged chain ends, instead of the different typical block copolymer phase separated morphologies we obtained with the linear polymers. Whether this would improve adhesion and self-healing ability remains to be seen. Additionally, the synthesis of star-shaped block copolymers was not possible anymore due to time constraints. This would likely lead to a stronger material, as each polymer would be connected to multiple crosslinks, depending

on the number of arms, instead of just two. In this case the use of shorter end blocks may work better, as a high density of weak crosslinks compared to a lower density of stronger crosslinks may improve self-healing. Though less force would be needed to break the individual crosslinks, more crosslinks generally result in a higher storage modulus and the smaller charged blocks would show more mobility through the uncharged phase, which would allow for better self-healing.

The currently synthesized material may be more useful for other applications than the originally targeted anti-corrosion coatings. Conductivity measurements revealed that the material acts as a semiconductor, which opens the door to many possible uses in electronics. Because this is a flexible and stretchable rubber, it may be useful for development of flexible electronics[5] or artificial skin.[6] More extensive purification and RAFT end-group cleavage will lead to a completely colorless transparent material. To increase the conductivity, a conducting polymer such as polythiophene or polypyrrole can be mixed in with the charged phase of the material with cylindrical morphology, potentially leading to nanoscale electrical wires within an insulating matrix, with possible applications in solar cells, batteries or supercapacitators.[7, 8] Another possible application is in the field of artificial muscles.[9]

Chapter 7 reported the automated one-pot sequential monomer addition RAFT synthesis of ABA-triblock copolymers with a water soluble middle block and hydrophobic end blocks, which were used for the preparation of self-healing hydrogels based on hydrophobic interactions. This was mainly a proof of principle, as the same method can also be used with other monomers to screen a large variety of building blocks. For example, the oligoethylene glycol acrylates used in Chapter 4 can be combined with this concept to make thermoresponsive supramolecular hydrogels in which the gelling temperature as well as the precipitation temperature, storage modulus and loss modulus can be controlled. Hydrogels of *N*-acryloylmorpholine may be useful in drug delivery and tissue engineering applications,[10, 11] but further improvements of biocompatibility or hydrogel strength may be necessary to make the hydrogels synthesized here useful for possible applications. Incorporation of cyclodextrin into the polymers chain can be used to form host-guest complexes with hydrophobic drug molecules that can be released slowly over time. Although it is unclear if the use of poly(isobornyl acrylate) hydrophobic blocks would lead to toxic effects because polymers are often not toxic, according to the MSDS the isobornyl acrylate monomer is toxic to aquatic life and can cause irritation, indicating that another hydrophobic monomer may be more suited for use in biomedical applications.

In summary, we have shown the optimized automated synthesis of defined homopolymers, statistical copolymers and block copolymers via both RAFT polymerization and Cu(0)-mediated polymerization. This technique could be used for the synthesis of supramolecular hydrogels and bulk materials with various properties that can be useful in many different applications.

References

1. C. Boyer, A. Derveaux, P. B. Zetterlund, M. R. Whittaker, *Polym. Chem.* **2012**, *3*, 117.
2. F. Alsubaie, A. Anastasaki, P. Wilson, D. Haddleton, *Polym. Chem.* **2015**, *6*, 406.
3. S. Maji, Z. Zhang, L. Voorhaar, S. Pieters, B. Stubbe, S. Van Vlierberghe, P. Dubruel, B. G. De Geest, R. Hoogenboom, *RSC Adv.* **2015**, *5*, 42388.
4. Q. Wang, J. L. Mynar, M. Yoshida, E. Lee, M. Lee, K. Okuro, K. Kinbara, T. Aida, *Nature* **2010**, *463*, 339.
5. S. R. Forrest, *Nature* **2004**, *428*, 911.

6. T. Someya, T. Sekitani, S. Iba, Y. Kato, H. Kawaguchi, T. Sakurai, *Proc. Natl. Acad. Sci. U. S. A.* **2004**, *101*, 9966.
7. Z. Yin, Q. Zheng, *Adv. Energy Mater.* **2012**, *2*, 179.
8. X. Lu, W. Zhang, C. Wang, T.-C. Wen, Y. Wei, *Prog. Polym. Sci.* **2011**, *36*, 671.
9. E. Smela, *Adv. Mater.* **2003**, *15*, 481.
10. M. M. Fares, A. M. Al-Shboul, *J. Biomed. Mater. Res., Part A* **2012**, *100A*, 863.
11. L. Martin, G. Gody, S. Perrier, *Polym. Chem.* **2015**, *6*, 4875.

Summary

Supramolecular materials are materials consisting of molecules that are not held together by chemical bonds, but by non-covalent interactions such as hydrogen bonds or electrostatic interactions. These materials can consist of polymers or smaller molecules, and can be either a bulk material or a gel. The supramolecular interactions can for example be used to make a material more easily processable, give it self-healing properties or make it responsive. Chapter 1 gives a summary of examples from literature of these types of materials. The subject of this thesis is the high-throughput synthesis of charged triblock copolymers via different controlled radical polymerization techniques. These polymers were designed to prepare supramolecular bulk materials based on electrostatic interactions, with the aim of making a self-healing coating that could be used on different metallic substrates to protect them against degradation. Additionally supramolecular hydrogels based on hydrophobic interactions were prepared.

In Chapter 2 the optimization of the Cu(0)-mediated polymerization of *n*-butyl acrylate and 2-methoxyethyl acrylate using an automated parallel synthesizer is reported. Using this robot, up to 16 kinetic reactions could be performed in parallel, resulting in a fast screening of different reaction conditions. Several parameters, such as the amount of Cu(0), Cu(II) and ligand and the type of ligand and initiator, were optimized to determine the optimal reaction conditions with regard to control over the polymerizations and a fast reaction rate. A larger amount of Cu(0) or ligand resulted in a faster polymerization with higher dispersity due to a higher radical concentration, while a larger amount of Cu(II) resulted in a lower polymerization rate and dispersity. The optimal reaction conditions, being a [M]:[EBP]:[Me6TREN]:[Cu(II)] ratio of [M]:1:0.15:0.1, were then used for the one-pot two-step synthesis of diblock copolymers of the two monomers by sequential monomer addition.

Chapter 3 describes the synthesis of diblock copolymers and ABA-triblock copolymers containing poly(*n*-butyl acrylate) as a first or middle block and poly(2-(dimethylamino)ethyl acrylate), poly(1-ethoxyethyl acrylate) and poly(1-ethoxyethyl-2-carboxyethyl acrylate) as second or outer blocks. 2-(Dimethylamino)ethyl acrylate was used to form positively charged blocks, while 1-ethoxyethyl acrylate and 1-ethoxyethyl-2-carboxyethyl acrylate can be deprotected to form the negatively charged acrylic acid and 2-carboxyethyl acrylate, respectively, using heat or water. The polymerizations were performed via one pot sequential monomer addition reactions via Cu(0)-mediated polymerization using an automated parallel synthesizer and manually on larger scale using schlenk techniques. When poly(2-(dimethylamino)ethyl acrylate) was synthesized as the second block, a quarternization reaction with the bromine end group of the polymer took place leading to crosslinking of the polymers, which could be suppressed by using a chloride initiator. The block copolymerizations of 1-ethoxyethyl acrylate and 1-ethoxyethyl-2-carboxyethyl acrylate were successful using the bromide initiator. The different diblock and triblock copolymers could be synthesized with good control over molecular weight and dispersities around 1.1 were obtained. The synthesized ABA-triblock copolymers were used to prepare supramolecular thermoplastic elastomers, which is discussed further in Chapter 6.

In Chapter 4, the automated RAFT polymerization of thermoresponsive poly(oligo ethylene glycol acrylate) copolymers is discussed. Two series of statistical copolymers of di(ethylene glycol) ethyl ether acrylate with di(ethylene glycol) methyl ether acrylate and tri(ethylene glycol) methyl ether acrylate, respectively, were successfully prepared, in which the fraction of each monomer was varied

from 0 to 100 % in seven steps. Because all three monomers react at the same rate, perfectly random copolymers could be synthesized. Cloud point temperature determination for each copolymer was performed by parallel turbidimetry and revealed a linear relationship with copolymer composition. This relationship can be used to tune the phase transition of a copolymer, which can be useful for *in vivo* applications.

Chapter 5 describes the synthesis of ABA-triblock copolymers, containing an uncharged middle block and charged outer blocks, via RAFT polymerization. First, kinetic studies of the homopolymerization of each monomer were performed, after which the kinetics of the block copolymerizations were studied. The triblock copolymers were then synthesized on a larger scale, purified and characterized. Polymers with different T_gs and solubility were used for the middle blocks, specifically poly(*n*-butyl acrylate) as low T_g hydrophobic polymer, poly(2-methoxyethyl acrylate) as low T_g less hydrophobic polymer, polystyrene and poly(cyclohexyl acrylate) as high T_g hydrophobic polymers and poly(2-hydroxyethyl acrylate) as water-soluble polymer. Poly(2-carboxyethyl acrylate) was used for the negatively charged end groups and poly(2-(dimethylamino)ethyl acrylate) for the positively charged end groups. Additionally a triblock copolymer with zwitterionic end groups was prepared. Almost all these triblock copolymers could be synthesized successfully and with good control on larger scale.

The thermal and mechanical properties of some of these triblock copolymers and their mixtures are described in Chapter 6. Triblock copolymers containing oppositely charged end groups were mixed together, which in many cases resulted in a phase separation between the mixed ionic blocks and the uncharged blocks. The morphology of the phases was dependent on the length of the different blocks. The electrostatic interactions, together with the phase separation, resulted in the formation of supramolecular thermoplastic elastomers from a mixture of two liquid polymers through physical crosslinking. The triblock copolymers containing poly(*n*-butyl acrylate) as middle block and around 30 % charged groups resulted in a thermoplastic elastomer with a cylindrical morphology and good mechanical properties. A higher concentration of charged groups or unequal sizes of the middle blocks resulted in a less defined morphology with inferior properties. When poly(2-methoxyethyl acrylate) was used as middle block a viscous liquid material was obtained by mixing the oppositely charged triblock copolymers in which no clear phase separation could be observed, which is because of the better miscibility with the charged groups compared to poly(*n*-butyl acrylate). A similar result was obtained when a star-shaped charged homopolymer was mixed with an ABA-triblock copolymer containing poly(*n*-butyl acrylate) as middle block, which likely resulted in a macroscopic phase separation instead of a microscopic phase separation. The higher T_g middle block poly(cyclohexyl acrylate) resulted in the formation of a supramolecular elastomer that has a broad rubber plateau at higher temperatures, but is very brittle at room temperature. Zwitterionic end groups resulted in a rubbery material of which the properties were very dependent on the moisture content of the material.

In Chapter 7, the preparation of supramolecular hydrogels from ABA-triblock copolymers with a water-soluble middle block and hydrophobic end groups is reported. The hydrophilic monomer *N*-acryloylmorpholine (NAM) was copolymerized with the hydrophobic isobornyl acrylate (IBA) via one-pot sequential monomer addition RAFT polymerization in an automated parallel synthesizer. Hydrophobic interactions between the outer blocks cause them to phase-separate into larger hydrophobic aggregates in water, forming physical crosslinks between the polymers. The resulting hydrogels were studied using rheology and their self-healing ability was shown.

Nederlandse samenvatting

Supramoleculaire materialen zijn materialen die opgebouwd zijn uit moleculen die niet via een chemische binding met elkaar verbonden zijn, maar met niet-covalente interacties zoals waterstofbruggen of elektrostatische interacties. Deze materialen kunnen bestaan uit polymeren of kleinere moleculen, en kunnen zowel als bulk materiaal of als gel voorkomen. De supramoleculaire interacties kunnen er bijvoorbeeld voor zorgen dat een materiaal gemakkelijker te verwerken is, zelfhelende eigenschappen heeft of responsief gedrag vertoont. Hoofdstuk 1 geeft een overzicht van voorbeelden uit de literatuur van deze soorten materialen. Het onderwerp van dit proefschrift is de high-throughput synthese van geladen triblok copolymeren via verschillende controlled radical polymerization technieken. Deze polymeren werden ontworpen voor het maken van supramoleculaire bulk materialen op basis van elektrostatisch interacties. Het doel hiervan was om een zelfhelende coating te maken die gebruikt kan worden voor verschillende metalen om degradatie hiervan tegen te gaan. Daarnaast werden ook supramoleculaire hydrogelen op basis van hydrofobe interacties gemaakt.

In Hoofdstuk 2 wordt de optimalisatie van de Cu(0)-mediated polymerization van *n*-butyl acrylaat en 2-methoxyethyl acrylaat besproken, wat werd gedaan met een synthese robot. Met deze robot kunnen 16 kinetische studies tegelijkertijd parallel worden uitgevoerd, wat zorgt voor een snelle screening van verschillende reactiecondities. Verschillende parameters, zoals de hoeveelheid Cu(0), Cu(II) en ligand en het soort ligand en initiator, werden gevarieerd om de optimale reactiecondities te vinden waarbij goede controle over het molecuulgewicht werd verkregen bij een hoge reactiesnelheid. Een grotere hoeveelheid Cu(0) of ligand zorgde voor een snellere reactie en een hogere dispersiteit door de hogere radicaalconcentratie, terwijl een grotere hoeveelheid Cu(II) juist zorgde voor een lagere reactiesnelheid en dispersiteit. De geoptimaliseerde condities, namelijk een [M]:[EBP]:[Me6TREN]:[Cu(II)] ratio van [M]:1:0.15:0.1, werden vervolgens gebruikt om diblok copolymeren te maken van de twee monomeren in een één-pot reactie door de opeenvolgende toevoeging van monomeren.

Hoofdstuk 3 beschrijft de synthese van diblok en ABA-triblok copolymeren met poly(*n*-butyl acrylaat) als het eerste of middelste blok en poly(2-(dimethylamino)ethyl acrylaat), poly(1-ethoxyethyl acrylaat) en poly(1-ethoxyethyl-2-carboxyethyl acrylaat) als het tweede blok of buitenste blokken. 2-(Dimethylamino)ethyl acrylaat vormt positief geladen blokken, terwijl 1-ethoxyethyl acrylaat en 1-ethoxyethyl-2-carboxyethyl acrylaat ontschermd kunnen worden door middel van warmte of water om het negatief geladen acrylzuur en 2-carboxyethyl acrylaat te vormen. Deze polymerizaties werden in één-pot reacties gedaan via Cu(0)-mediated polymerization, zowel met een synthese robot als handmatig via schlenk technieken. Wanneer poly(2-(dimethylamino)ethyl acrylaat) als tweede blok werd gesynthetiseerd, trad er een quarternisatie op met de bromide eindgroep van het polymeer die zorgde voor gecrosslinkte polymeren, wat onderdrukt kon worden door gebruik te maken van een chloride initiator. De blok copolymerisaties van 1-ethoxyethyl acrylaat en 1-ethoxyethyl-2-carboxyethyl acrylaat verliepen goed met de bromide initiator. De verschillende diblok en triblok copolymeren konden worden gesynthetiseerd met goede controle over het molecuulgewicht en met een dispersiteit van ongeveer 1.1. Deze polymeren werden in Hoofdstuk 6 gebruikt om supramoleculaire thermoplastische elastomeren te vormen.

In Hoofdstuk 4 wordt de geautomatiseerde RAFT polymerisatie van thermoresponsieve poly(oligo ethyleen glycol acrylaat) copolymeren in een synthese robot besproken. Twee series statistische

copolymeren van di(ethylene glycol) ethyl ether acrylaat met zowel di(ethylene glycol) methyl ether acrylaat als tri(ethylene glycol) methyl ether acrylaat werden met succes gemaakt, waarin de fractie van ieder monomeer werd gevarieerd van 0 tot 100 % in zeven stappen. Omdat alle drie de monomeren een zelfde reactiviteit hadden, werden perfect willekeurige copolymeren gevormd. De temperatuur van het troebelingspunt van ieder copolymeer werd bepaald via parallelle turbidimetrie en liet een lineair verband zien met de copolymeer compositie. Dit verband kan gebruikt worden om de fasetransitie van een copolymeer te regelen, wat interessant is voor het gebruik in *in vivo* applicaties

Hoofdstuk 5 beschrijft de synthese van ABA-triblok copolymeren, met een ongeladen middenblok en geladen buitenste blokken, via RAFT polymerisatie. Van de homopolymerisatie van elk monomeer werd eerst een kinetische studie gedaan, waarna kinetische studies van de blok copolymerisaties werden gedaan. Vervolgens werden de triblok copolymeren op grotere schaal gesynthetiseerd, opgezuiverd en gekarakteriseerd. Polymeren met verschillende T_gs en oplosbaarheid werden gebruikt voor de middenblokken, namelijk poly(*n*-butyl acrylaat) als laag T_g hydrofoob polymeer, poly(2-methoxyethyl acrylaat) als laag T_g minder hydrofoob polymeer, polystyreen en poly(cyclohexyl acrylaat) als hoog T_g hydrofobe polymeren en poly(2-hydroxyethyl acrylaat) als wateroplosbaar polymeer. Poly(2-carboxyethyl acrylaat) werd gebruikt als negatief geladen eindroep en poly(2-(dimethylamino)ethyl acrylaat) voor de positief geladen eindgroepen. Ook werd een triblok copolymer met zwitterionische eindgroepen gemaakt. Bijna al deze triblok copolymeren konden met succes en goede controle op grotere schaal gemaakt worden.

De thermische en mechanische eigenschappen van een aantal van deze triblok copolymeren en hun mengsels worden beschreven in Hoofdstuk 6. Triblok copolymeren met tegenovergesteld geladen eindgroepen werden met elkaar gemengd, wat in veel gevallen zorgde voor een fasescheiding tussen de gemengde ionische blokken en de ongeladen blokken. De morfologie van de fasen was afhankelijk van de lengte van de verschillende blokken. De elektrostatische interacties zorgden er, in samenwerking met de fasescheiding, voor dat er supramoleculaire thermoplastische elastomeren werden gevormd uit een mengsel van twee vloeibare polymeren door middel van fysische crosslinking. De triblok copolymeren met poly(*n*-butyl acrylaat) als middenblok en ongeveer 30 % aan geladen groepen resulteerden in een thermoplastisch elastomeer met een cylindrische morfologie en goede fysische eigenschappen. Een hogere concentratie aan geladen groepen of een ongelijke afmeting van het middenblok zorgde voor een minder gestructureerd materiaal met minder goede eigenschappen. Wanneer poly(2-methoxyethyl acrylaat) als middenblok werd gebruikt werd een viskeuze vloeistof, waarin geen fasescheiding werd geobserveerd, verkregen door het mengen van tegenovergesteld geladen triblok copolymeren, wat komt doordat dit polymeer beter mengbaar is met de ionische groepen dan poly(*n*-butyl acrylaat). Een vergelijkbaar resultaat werd verkregen door het mengen van een stervormig geladen homopolymeer met een ABA-triblock copolymeer met poly(*n*-butyl acrylaat) als middengroep, wat waarschijnlijk resulteerde in fasescheiding op macroscopische schaal in plaats van microscopische fasescheiding. Het hogere T_g middenblok poly(cyclohexyl acrylaat) zorgde voor een supramoleculair elastomeer dat een breed rubber plateau heeft bij hogere temperaturen maar erg breekbaar is bij kamertemperatuur. Zwitterionische eindgroepen resulteerden in een rubberachtig materiaal waarvan de eigenschappen sterk afhankelijk waren van de vochtigheid.

In Hoofstuk 7 wordt de bereiding van supramoleculaire hydrogelen van ABA-triblok copolymeren met een wateroplosbaar middenblok en hydrophobe eindgroepen besproken. Het hydrofiele monomeer *N*-acryloyl morpholine werd gecopolymeriseerd met het hydrofobe isobornyl acrylaat via één-pot RAFT polymerisatie met opeenvolgende toevoeging van monomeren in een synthese robot. Hydrofobe interacties tussen de eindgroepen zorgde ervoor dat deze fase-scheiden in grotere hydrofobe domeinen wanner deze in water worden gebracht, wat resulteert in fysieke crosslinking tussen de polymeren. De ontstane hydrogelen werden bestudeerd met reologie en hun zelfhelende vermogen werd aangetoond.

About the author

Lenny obtained a Bachelor of Science in Molecular Sciences from Wageningen University in 2008. During her Master of Science in Molecular Life Sciences she worked on three different research projects. At the Laboratory of Physical Chemistry and Colloid Science of Wageningen University she worked on the encapsulation of lysozyme inside polyelectrolyte complex micelles, under supervision of Saskia Lindhoud and Prof. Martien Cohen Stuart. In the Laboratory of Organic Chemistry at Wageningen University, she synthesized silicon nanoparticles and studied their size-dependent photoluminescence. This project was carried out under supervision of Loes Ruizendaal, Dr. Jos Paulusse and Prof. Han Zuilhof. Lenny gained her first experience in polymer synthesis while working with Dr. Remzi Becer and Prof. Dave Haddleton in the Department of Chemistry at the University of Warwick, where she synthesized thermoresponsive glycopolymers. After obtaining the MSc degree in 2010, she started working on her PhD in the Supramolecular Chemistry Group in March 2011.

Publication list

Included in the thesis:

- L. Voorhaar, M. M. Diaz, F. Leroux, S. Rogers, A. M. Abakumov, G. Van Tendeloo, G. Van Assche, B. Van Mele, R. Hoogenboom, Electrostatic supramolecular thermoplastic materials, submitted
- L. Voorhaar, R. Hoogenboom, One-pot synthesis of amphiphilic diblock and triblock copolymers via high-throughput Cu(0)-mediated polymerization, manuscript in preparation
- L. Voorhaar, K. Van Hecke, G. Vancoillie, Q. Zhang, R. Hoogenboom, High-throughput synthesis of thermoresponsive poly(oligoethylene glycol acrylate) copolymers by RAFT polymerization. In *Controlled Radical Polymerization: Materials*, American Chemical Society **2015**; *Vol. 1188*, pp 63-77.
- L. Voorhaar, S. Wallyn, F. E. Du Prez, R. Hoogenboom, Cu(0)-mediated polymerization of hydrophobic acrylates using high-throughput experimentation. *Polym. Chem.* **2014,** *5*, 4268-4276.

Not included in the thesis:

- Q. Zhang, L. Voorhaar, B. F. Yeşil, R. Hoogenboom, Accurate tuning of polymeric nanoparticles by co-assembly of thermoresponsive polymers and a double hydrophilic thermoresponsive block copolymer, manuscript in preparation
- N. Vanparijs, S. Maji, B. Louage, L. Voorhaar, D. Laplace, Q. Zhang, Y. Shi, W. E. Hennink, R. Hoogenboom, B. G. De Geest, Polymer-protein conjugation *via* a 'grafting to' approach – a comparative study of the performance of protein-reactive RAFT chain transfer agents, *Polym. Chem.* **2015**, *6*, 5602-5614.
- Q. Zhang, L. Voorhaar, B. G. De Geest, R. Hoogenboom, One-Pot Preparation of Inert Well-Defined Polymers by RAFT Polymerization and In Situ End Group Transformation. *Macromol. Rapid Commun.* **2015**, *36*, 1177–1183.
- S. Maji, Z. Zhang, L. Voorhaar, S. Pieters, B. Stubbe, S. Van Vlierberghe, P. Dubruel, B. G. De Geest, R. Hoogenboom, Thermoresponsive polymer coated gold nanoparticles: From MADIX/RAFT copolymerization of N-vinylpyrrolidone and N-vinylcaprolactam to salt and temperature induced nanoparticle aggregation, *RSC Adv.* **2015**, *5*, 42388-42398.
- S. Maji, G. Vancoillie, L. Voorhaar, Q. Zhang, R. Hoogenboom, RAFT Polymerization of 4-Vinylphenylboronic Acid as the Basis for Micellar Sugar Sensors. *Macromol. Rapid Commun.* **2014,** *35*, 214-220.
- B. Louage, Q. Zhang, N. Vanparijs, L. Voorhaar, S. Vande Casteele, Y. Shi, W. E. Hennink, J. Van Bocxlaer, R. Hoogenboom, B. G. De Geest, Degradable Ketal-Based Block Copolymer Nanoparticles for Anticancer Drug Delivery: A Systematic Evaluation. *Biomacromolecules* **2014,** *16*, 336-350.
- S. Slavin, A. H. Soeriyadi, L. Voorhaar, M. R. Whittaker, C. R. Becer, C. Boyer, T. Davis, D. M. Haddleton, Adsorption behaviour of sulfur containing polymers to gold surfaces using QCM-D. *Soft Matter* **2012,** *8*, 118-128.
- Y. Z. Gou, S. Slavin, J. Geng, L. Voorhaar, D. M. Haddleton, C. R. Becer, Controlled Alternate Layer-by-Layer Assembly of Lectins and Glycopolymers Using QCM-D. *ACS Macro Letters* **2012,** *1*, 180-183.
- T. R. Dargaville, R. Forster, B. L. Farrugia, K. Kempe, L. Voorhaar, U. S. Schubert, R. Hoogenboom, Poly(2-oxazoline) Hydrogel Monoliths via Thiol-ene Coupling. *Macromol. Rapid Commun.* **2012,** *33*, 1695-1700.
- S. Lindhoud, L. Voorhaar, R. de Vries, R. Schweins, M. A. C. Stuart, W. Norde, Salt-Induced Disintegration of Lysozyme-Containing Polyelectrolyte Complex Micelles. *Langmuir* **2009,** *25*, 11425-11430.

Acknowledgements

First of all I would like to thank Richard Hoogenboom for accepting me into his (at the time very small) research group, as well as teaching me how to be a good researcher. Obviously I could not have done this work without him.

I would also like to thank everyone in the Supramolecular Chemistry Group for providing a nice work atmosphere, keeping (almost) every piece of equipment running and providing help when necessary. I would like to thank especially Dr. Maji, we worked together and discussed about many different things and I think we learned a lot from each other. Gertjan, Qilu and Victor who were the core of the group when we were first starting and still had to figure everything out on our own, and I think together we really provided the basis for the rest of the group. Bart and Jim & Jim for arranging and fixing many things and providing entertainment during lunchtime. And of course the many other group members we've had over the years who have been nice, helpful, inspiring (and in some cases pretty annoying) colleagues.

I want to thank Jos, Bernhard and Jan for teaching and letting me use their equipment, as well as keeping everything running. My many coauthors, without them I would not have nearly as many well written publications and citations. Maria, Guy and Bruno from the VUB, who helped me understand the materials I made much better.

I also want to thank some of my teammates from KRSG, mainly Katia and Frederique, who helped to keep me sane all these years. My parents, because I would not be here without them. And of course there have been many other people who have been helpful over the years but who I have not mentioned here, thank you to everyone and good luck with everything!